MODELLING THE EFFECTS OF LAND USE ON THE CLIMATE

Steven De Hertog

Thesis submitted in fulfilment of the requirements for the award of the degree of Doctor of Engineering Sciences (Doctor in de Ingenieurswetenschappen)

DEPARTMENT OF HYDROLOGY AND HYDRAULIC ENGINEERING
VRIJE UNIVERSITEIT BRUSSEL

August 2023

Printed by
Crazy Copy Center Productions
VUB Pleinlaan 2, 1050 Brussel
Tel: +32 2 629 33 44
crazycopy@vub.be
www.crazycopy.be

ISBN: 9789464443714
NUR CODE: 930
THEMA: RBPC

PhD Jury Composition

Prof. Dr. Wim Thiery	*Promotor* Department of Hydrology and Hydraulic Engineering Vrije Universiteit Brussel, Belgium
Prof. Dr. Ir. Jiri Nossent	*Secretary* Department of Hydrology and Hydraulic Engineering Vrije Universiteit Brussel, Belgium Flanders Hydraulics, Belgium
Prof. Dr. Philippe Huybrechts	*Chair* Department of Geography Vrije Universiteit Brussel, Belgium
Prof. Dr. Ir. Iris De Graeve	*Vice-Chair* Department of Electrochemical and Surface Engineering Vrije Universiteit Brussel, Belgium
Prof. Dr. Julia Pongratz	*External Examiner* Department of Geography Ludwig-Maximilians-University Munich, Germany Max Planck Institute for Meteorology, Germany
Prof. Dr. Edouard Léopold Davin	*External Examiner* Oeschger Centre for Climate Change Research University of Bern, Switzerland Wyss Acadamy for Nature, Switzerland

Acknowledgements

Within this section I would like to acknowledge the people whom supported and guided me to this point. The process of scientific research nor the life of a scientists happens in a confined space. Even us scientists interact with our environment which helps us grow and reach further than we could have by ourselves. As a safeguard to start with I would like to thank everyone I have had the opportunity to meet during the time frame of this PhD, I will probably not explicitly mention everyone that deserves it here but I truly appreciate the moments I spend at the VUB during the last four years.

Of course I start by thanking my supervisor, Wim Thiery, for giving me the opportunity to go on this journey and do a PhD here at the VUB, I thank you for the excellent guidance, scientific insights and great feedback. As a scientist you have an exceptional drive with a never ending ambition therefore helping to push me to a higher level. As a human, you have an incredible compassion and your good spirits keep even difficult times feasible and make working on a PhD in your group highly enjoyable. I truly appreciated our times here together and can't wait to see how your rocket of a career will continue soaring to new heights.

I was lucky enough to spend this PhD on a European project with wonderful partners in which we had monthly meetings over the last 4 years. I truly appreciated the guidance of Quentin Lejeune who ensured a good flow of the project despite many setbacks and always helped retain a friendly and open atmosphere. I would like to thank the other modellers, Felix Havermann, Suqi Guo, Iris Manola, and Fei Luo for the great and open atmosphere we had and the unbroken spirit even though we had many setbacks, I believe we can be proud of what we achieved in this project. Thanks to all others in the project for the great insights and opportunities to learn from all of your wide reaching expertise. A special thanks goes to Anton Orlov for being an excellent and accessible researcher, it was a true pleasure to work with you and I'm looking forward to continue collaborating.

I would like to thank Philippe Huybrechts for acting as the chair of my jury but also for supervising both my bachelor and master theses. Your critical mindset will always serve as an example of what it means to be a good scientist. I thank Jiri Nossent and Iris De Graeve for the interesting questions during my defense starting discussions I truly enjoyed. Finally I would like to thank Julia Pongratz and Edouard Davin for acting as external examiners.

Your scientific insights are an example to strive towards.

During this time, I had the opportunity to work with an open source community based model. It was unbelievable for me to see the openness and accessibility within the modelling and climate science community and I truly appreciated this. I would like to thank the scientists from National Center for Atmospheric Research for creating and supporting this type of environment with a special thanks to Dave and Peter Lawrence who helped me navigate the complex world of earth system modelling.

Finally I would like to thank some other collaborators Raphael Portmann, Sebastian Schemm, Diego Miralles, and Ruud van der Ent for your expertise and guidance, these collaborations have truly supported my development as a scientist and taught me a different way of approaching the earth system. A special shout out goes to Jessica Keune, I truly appreciated your help and support, your dedication and expertise are exceptional and an example to strive towards.

I don't think I'm exaggerating when I say that I could not have found a better department to do this PhD. I have enjoyed the great atmosphere and friendly colleagues and I am truly grateful to have had the opportunity to work here. A special thanks goes to the colleagues in the Bclimate group for creating a fun and friendly dynamic where we could always support each other both work related and on a personal level. A special thanks to Luke and Yi, we all started our PhDs roughly at the same time and I truly enjoyed the friendship we created along the way. Finally, a special thanks to Inne Vanderkelen, as a senior colleague and a friend you were always there for help and feedback, I strongly believe I would not have been able to achieve this work without your support and encouragement.

A special thanks goes to the HPC support teams of VUB, KULeuven and UGent (yes, I have been using everyone's compute resources). Without the excellent and diligent support teams of the Flemish Super Computing center this work would not have been possible. A specific shout out goes to Alex Domingo Toro from the VUB HPC support team. Thanks for helping with the technical issues of installing an earth system model and having me (a complete linux noob at that time) over at your office to debug together for a full week. Finally I would also like to thank the IT support of VUB with a special thank to Sabine Horstmann for her cheerful and excellent help which always went above and beyond.

I would like to thank my parents for the wonderful and carefree childhood that allowed me to develop into the person I've become today. Many thanks to my sisters Sarah and Nathalie for being there along with me and making our family home into a warm nest. I would like to thank my grand parents for the love and support and especially my grand father for managing to get me to do some sports and actually enjoying it as well (I will start jogging again, I promise). My family's support has been essential for becoming the person I am today. Finally I would like to thank the family Rolain for their kindness and support, with a special thanks to Yves for supporting me when I was struggling with writing my MSc thesis, that early support helped greatly in eventually getting here to write this thesis.

Finally, I would like to give my biggest thanks to Sofie. She supported me every day and made sure I never lost motivation. It was an intense 4 years for us, going through a global pandemic, while living in a single-room apartment in the city center of Brussels, to where we are now. Words cannot describe how important you have been for me throughout this time. Many thanks for being here with me throughout this journey, which I likely would have never even started if it weren't for your support. I love you dearly and hope that I can become the same pinnacle of support for you that you have been for me throughout these years.

Steven De Hertog

Abstract

Land cover and land management changes can alter local, regional, and global climate. This can be by altering the biogeochemical fluxes due to a change in carbon sequestration potential which can alter global greenhouse gas concentrations and therefore global climate. However, it can also be through changes in the physical properties of the surface which in turn alter the energy and water balance and thereby affect regional to local climate. These effects are called the biogeophysical effects and remain poorly constrained, with high uncertainties about both their sign and magnitude. Land cover and land management changes are likely needed towards the future to achieve low-warming future scenarios through land-based mitigation. Therefore, it is of importance that land cover and land management induced climate effects are better understood in order to fully grasp their potential within the context of future mitigation and adaptation. This thesis aims to better constrain the effects of land cover and land management on climate and to illustrate their importance for future mitigation and adaptation potential. To this end, we use Earth System Models that fully asses the climate feedbacks arising from land cover and land management changes.

In the first study, we perform highly idealised simulations of four different types of land cover and land management conversions, (i) cropland expansion, (ii) afforestation, (iii) irrigation expansion and (iv) wood harvesting. These simulations are performed with three different Earth System Models to grasp the inter model uncertainty. The land cover and management changes are performed in a checkerboard pattern (alternating patches of change with patches of no change) to disentangle local from non-local biogeophysical effects. The effects of land cover changes on surface temperature are consistent with observational studies except over certain regions for some Earth System Models. Cropland expansion generally causes a local warming in the tropics and a cooling in boreal latitudes which are consistent across the earth System Models. This pattern was similar but of opposite sign for the local effects of afforestation. The non-local effects, in contrast, are not consistent across the models for cropland expansion (ranging from global cooling to regional warming) while these are consistently a non-local warming for afforestation. Irrigation generally causes a cooling, although the Earth System Models disagree whether this cooling is local or non-local. Wood harvesting was not found to have any clear effects on grid-scale surface temperature. The local surface temperature responses were mostly dominated by changes in turbulent heat fluxes. This analysis overall highlights the importance of separating local

and non-local biogeophysical effects to better understand inter-model differences.

In the second study, we further analyse the idealised Earth System Model simulations for effects on evaporation, precipitation, and vertically integrated moisture flux convergence. We apply a moisture tracking algorithm to assess the effects of land cover and land management on both continental and local moisture recycling. The effects of land cover and land management changes over land are generally consistent across the different Earth System Models. Cropland expansion reduces evaporation, precipitation, and local moisture recycling, while afforestation and irrigation expansion cause the opposite effect. However, the signal does vary strongly in time and space and different patterns emerge within different Earth System Models, which relates to mechanisms dominating the overall change (from global circulation changes to more localised effects). Our results underline the importance of land cover and land management induced effects on moisture fluxes and moisture recycling and highlight some differences across Earth System Models which need to be considered before they can be applied to inform land-based adaptation strategies.

In the third study, we perform future simulations under a 1.5°C-compatible future scenario with one Earth System Model. These simulations are performed under different land cover and land management scenarios which represent two strongly different worlds. The sustainability scenario represents a world which converges socioeconomically and where greenhouse gas pricing and environmental protection is implemented globally. In the inequality scenario, in contrast, such degree of sustainability is only achieved in the wealthier countries while the rest of the world continues under current trends. The results were analysed for global mean temperature, heat stress and downstream socioeconomic impacts such as changes in labour capacity and temperature-related mortality. Achieving a sustainable land cover compared to the inequality scenario is shown to cause a global cooling of ca. 0.3 °C and a clear reduction in heat stress over land. Adverse impacts on humans generally decrease in a world with sustainable land cover change instead of inequality, with notably higher labour capacity and lower heat-related mortality over the tropics. Cold-related mortality, in contrast, rises in some locations such as Northwestern Europe. The adopted land cover and management scenario is crucial for assessing future climate change and should not be neglected within future mitigation and adaptation strategies.

Overall, this thesis advances the current understanding of the effects of land cover and land management changes on climate. We provide an improved understanding of biogeophysical effects by consistently separating local and non-local effects across different Earth System Models and land cover and management conversions specifically for surface temperature. Our results also highlight some remaining uncertainties related to specific Earth System Models, but also to the signal separation approach used which warrant more research. Finally, a second group of simulations illustrates the importance for including land cover and land management change induced climate effects within future land cover scenarios for temperature but also impacts on humans. Land cover and land management induced climate effects should therefore be carefully considered within the design of future land-based mitigation and adaptation pathways.

x

Samenvatting

Veranderingen in landgebruik en landbeheer kunnen het lokale, regionale en mondiale klimaat veranderen. Dit kan gebeuren door wijziging van de biogeochemische stromen als gevolg van een verandering in het koolstofvastleggingspotentieel, waardoor de mondiale broeikasgasconcentraties en derhalve het mondiale klimaat kunnen veranderen. Maar het kan ook gebeuren via veranderingen in de fysische eigenschappen van het oppervlak die op hun beurt de energie- en waterbalans wijzigen en daardoor het regionale en lokale klimaat beïnvloeden. Deze effecten worden de biogeofysische effecten genoemd en blijven slecht gekarakteriseerd, met grote onzekerheden over zowel het teken als de omvang ervan. Veranderingen in landgebruik en landbeheer zijn in de toekomst waarschijnlijk nodig om scenario's met een lage opwarming te behalen. Daarom is het van belang dat er meer inzicht komt in de door landgebruik en landbeheer veroorzaakte klimaateffecten om hun potentieel in het kader van toekomstige mitigatie en adaptatie volledig te begrijpen. Deze thesis heeft tot doel de effecten van landgebruik en landbeheer op het klimaat beter te begrijpen en te beperken en het belang ervan voor toekomstige mitigatie- en adaptatiemogelijkheden te illustreren. Daartoe gebruiken we aardsysteemmodellen die de klimaat effecten van veranderingen in landgebruik en landbeheer volledig in kaart brengen.

In de eerste studie voeren we sterk geïdealiseerde simulaties uit van vier verschillende soorten veranderingen in landgebruik en landbeheer, (i) uitbreiding van akkerland, (ii) bebossing, (iii) uitbreiding van irrigatie en (iv) houtoogst. Deze simulaties worden uitgevoerd met drie verschillende aardsysteemmodellen om de onzekerheid tussen de modellen te begrijpen. De veranderingen in bodembedekking en beheer worden uitgevoerd in een dambordpatroon (afwisselend veranderde en ongewijzigde gebieden) om lokale en niet-lokale biogeofysische effecten van elkaar te scheiden. De effecten van veranderingen in bodembedekking op de oppervlaktetemperatuur komen overeen met waarnemingsstudies, behalve in bepaalde regio's voor sommige aardsysteemmodellen. De uitbreiding van akkerland veroorzaakt over het algemeen een lokale opwarming in de tropen en een afkoeling op boreale breedtegraden, die consistent zijn voor alle aardsysteemmodellen. Voor de lokale effecten van bebossing was dit patroon vergelijkbaar, maar van tegengestelde betekenis. De niet-lokale effecten zijn daarentegen niet consistent in alle modellen voor de uitbreiding van akkerland (variërend van wereldwijde afkoeling tot regionale opwarming), terwijl deze voor bebossing consistent een niet-lokale opwarming zijn. Irrigatie veroorzaakt over het algemeen een afkoeling, hoewel de aardsysteemmodellen het er niet over eens zijn of deze

afkoeling lokaal of niet-lokaal is. Houtoogst bleek geen duidelijke effecten te hebben op de oppervlaktetemperatuu. De lokale respons op de oppervlaktetemperatuur werd meestal gedomineerd door veranderingen in de turbulente warmtefluxen. Uit deze analyse blijkt hoe belangrijk het is lokale en niet-lokale biogeofysische effecten van elkaar te scheiden om de verschillen tussen de modellen beter te begrijpen.

In de tweede studie analyseren we deze geïdealiseerde simulaties van aardsysteemmodellen verder op hun effecten op verdamping, neerslag en verticaal geïntegreerde vochtfluxconvergentie. We passen een vochttraceringsalgoritme toe om de effecten van landgebruik en landbeheer op zowel continentale als lokale vochtrecyclage te beoordelen. De effecten van veranderingen in landgebruik en landbeheer zijn over het algemeen consistent in de verschillende aardsysteemmodellen. Uitbreiding van akkerland vermindert verdamping, neerslag en lokale vochtrecyclage, terwijl bebossing en uitbreiding van irrigatie het tegenovergestelde effect veroorzaken. Het signaal varieert echter sterk in tijd en ruimte en binnen de verschillende aardsysteemmodellen komen verschillende patronen naar voren, die verband houden met mechanismen die de algemene verandering domineren (van veranderingen in de mondiale circulatie tot meer gelocaliseerde effecten). Onze resultaten onderstrepen het belang van door landgebruik en landbeheer geïnduceerde effecten op vochtstromen en vochtrecyclage en wijzen op enkele duidelijke verschillen tussen aardsysteemmodellen waarmee rekening moet worden gehouden voordat deze kunnen worden toegepast om effectief informatie te verstrekken over aanpassingsstrategieën voor toekomstige klimaatverandering.

In de derde studie voeren we met één aardsysteemmodel toekomstsimulaties uit onder een 1,5°-compatibel toekomstscenario. Deze simulaties worden uitgevoerd onder verschillende scenario's voor landgebruik en landbeheer die twee sterk verschillende werelden vertegenwoordigen in termen van sociaal-economische ontwikkeling, niveaus van milieubescherming en omvang van landgebaseerde mitigatie. Het duurzaamheidsscenario vertegenwoordigt een wereld dat sociaal-economisch convergeert en waarin de prijsstelling voor broeikasgassen en milieubescherming wereldwijd worden doorgevoerd. In het ongelijkheidsscenario daarentegen wordt een dergelijke mate van duurzaamheid alleen bereikt in de rijkere landen, terwijl de rest van de wereld de huidige trends blijft volgen. De resultaten werden geanalyseerd voor de wereldgemiddelde temperatuur, hittestress en sociaaleconomische gevolgen zoals veranderingen in arbeidsproductiviteit en temperatuurgerelateerde sterfte. Het verschil tussen een wereld van ongelijkheid en duurzaamheid blijkt een wereldwijde afkoeling van ca. 0,3° en een duidelijke vermindering van de hittestress boven land te veroorzaken. Nadelige gevolgen voor de mens nemen over het algemeen af in een wereld met duurzame veranderingen in landgebruik in plaats van ongelijkheid, met een aanzienlijk hogere arbeidsproductiviteit en een lagere hittegerelateerde sterfte in de tropen. De koudegerelateerde sterfte daarentegen stijgt op sommige plaatsen en vooral boven Noordwest-Europa. Deze resultaten illustreren duidelijk dat het gekozen scenario voor bodembedekking en beheer cruciaal is voor de beoordeling van toekomstige klimaatverandering en niet mag worden verwaarloosd in toekomstige mitigatie- en aanpassingsstrategieën.

In het algemeen bevordert deze thesis het huidige begrip van de effecten van veranderingen in landbedekking en landbeheer op het klimaat. We bieden een beter begrip van biogeofysische effecten door consequente scheiding van lokale en niet-lokale effecten in verschillende aardsysteemmodellen en veranderingen in bodembedekking en beheer, specifiek voor oppervlaktetemperatuur. Onze resultaten brengen ook enkele resterende onzekerheden aan het licht die verband houden met specifieke aardsysteemmodellen, maar ook met de gebruikte methode voor signaalscheiding, dat meer onderzoek rechtvaardigen. Ten slotte illustreert een tweede groep simulaties hoe belangrijk het is om klimaateffecten door veranderingen in landgebruik en landbeheer op te nemen in toekomstige landgebruikscenario's voor de temperatuur, maar ook voor de gevolgen voor de mens. Bij het ontwerp van toekomstige mitigatie- en adaptatiestrategiën op land moet daarom zorgvuldig rekening worden gehouden met de effecten van landgebruik en landbeheer op het klimaat.

List of abbreviations

AFOLU	Agriculture, Forestry and other Land Use
AMOC	Atlantic Meridional Overturning Circulation
CAM	Community Atmosphere Model
CESM	Community Earth System Model
CFT	Crop Functional Type
CMIP	Coupled Model Intercomparison Project
EC-EARTH	European Consortium Earth System Model
ECMWF	European Center for Medium-range Weather Forecasting
ESM	Earth System Model
GHG	Green House Gas
HTESSEL	Hydrology Tiled ECMWF Scheme for Surface Exchanges over Land
IAM	Integrated Assesment Model
IFS	Integrated Forecast System
IPCC	Intergovernmental Panel for Climate Change
JSBACH	Jena Scheme for Biosphere-Atmosphere Coupling in Hamburg
LAMACLIMA	LAnd MAnagement for CLImate Mitigation and Adaptation
LCLMC	Land Cover and Land Management Change
LPJ-GUESS	Lund-Potsdam-Jena General Ecosystem Simulator
LUCID	Land-Use and Climate, IDentification of robust impacts
LUH	Land Use Harmonistaion Project
LUMIP	Land Use Model Intercomparison Project
MCC	Multi-Country Multi-City network
MFC	Moisture Flux Convergence
MPI-ESM	Max Planck Institute Earth System Model
NDC	Nationally Determined Contributions
NIOSH	National Institute for Occupational Safety and Health
OECD	Organisation for Economic Cooperation and Development
PFT	Plant Functional Type
POP	Parallel Ocean Program
RCP	Representative Concentration Pathway
SSP	Shared Socio-economic Pathway
WACCM	Whole Atmopshere Community Climate Model
WAM	Water Accounting Model

Contents

List of Figures

List of Tables

Chapter 1

Introduction

1.1 The role of land in the climate system

Humans have left their mark on the landscape since the Mesopotamian times, when the first humans started settling and farming, converting land to fields to grow crops. The conversion of land from one cover to another (e.g. forest to cropland) or the application of certain management techniques without the change in cover (e.g. irrigation or wood harvesting) have allowed the human species to grow and develop societies encompassing billions of people nowadays (Harari, 2014). Together, these Land Cover and Land Management Changes (LCLMC) are a crucial pathway in which humans affect the Earth system, both throughout human history but also towards the future (Pongratz et al., 2021). Historically, three quarters of the ice-free land has already been exploited by human activities (Luyssaert et al., 2014). Of this, a complete conversion through deforestation, agriculture and urbanization has affected a quarter of the area, while about half of the land has been under some kind of land management (Luyssaert et al., 2014).

The land is interrelated with the atmosphere by exchanging fluxes of energy, water, and chemical compounds including greenhouse gases (GHGs), and therefore plays an important role in the global carbon cycle. Land can act both as a source of carbon (e.g. during forest fires or deforestation) or as a sink of carbon (e.g., tropical forests or permafrost storing and retaining carbon). The potential of the land sink is driven by the uptake of carbon within the biosphere (net biome production) which depends on land storing carbon through plant photosynthesis and releasing carbon through respiration and other losses, such as forest fires (Kirschbaum et al., 2001). Land also plays a crucial role for the emission of other GHGs such as N_2O and CH_4 through agricultural practices (e.g. fertilisation for N_2O and rice paddies or livestock for CH_4). Land cover plays a role in the existence and distribution of aerosols compounds (e.g. mineral dust, black carbon, biogenic volatile organic compounds) which can modulate climate by, for example, changing cloudiness and rainfall patterns (Teuling et al., 2017). The most important processes for land-atmosphere interactions are summarised in Figure 1.1.

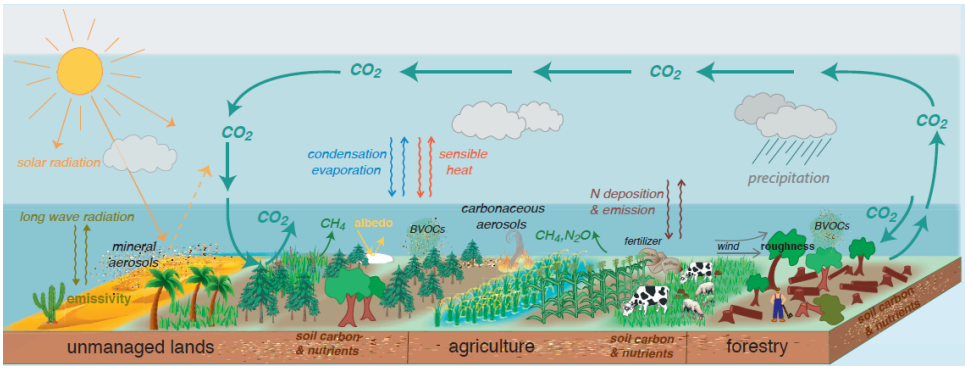

Figure 1.1: Important process for land-atmosphere interactions are shown here. The interaction is determined by surface properties such as albedo and emissivity, which determine longwave and shortwave radiation fluxes, as well as surface roughness, which influences turbulent exchanges of momentum, water and energy. Land also plays a key role in emitting and removing several greenhouse gases but also other components (e.g. aerosols), which can modulate the climate indirectly through changing atmospheric radiation properties or by affecting cloud formation and eventual precipitation. Figure was taken from Chapter 2 of the Intergovernmental Panel on Climate Change (IPCC) Special Report on Climate Change and Land (Jia et al., 2019).

The surface energy balance is a crucial framework for understanding land-atmosphere interactions, and is shown in Equation 1.1. When incoming solar radiation (shortwave SW_{in}) reaches the surface, part of this will be reflected back to the atmosphere (SW_{out}) and the remainder will be absorbed at the surface. This heat can be transferred back to the atmosphere through sensible heat flux (SHF) and – if water is available – latent heat flux (LHF), which is the energy needed for water to evaporate. The remaining heat in the surface can be conducted into the soil through the ground heat flux (G). The surface also radiates longwave outgoing radiation (LW_{out}) depending on its temperature, part of which is reflected back from the atmosphere and returns to the surface (LW_{in}). If the outgoing energy terms are less than incoming radiation terms then the surface will warm leading to an increase in surface temperature, which then causes an increase of LW_{out}. These processes together ensure that energy is conserved at the surface (meaning that the sum of all components is zero).

$$SW_{in} - SW_{out} + LW_{in} - LW_{out} - LHF - SHF - G = 0 \tag{1.1}$$

These energy interactions between the atmosphere and the land are modulated by land surface properties. The reflectivity of a surface (i.e. the proportion of shortwave radiation reflected, also called the albedo) changes strongly depending on its properties. For example, a dark surface like a forest has an albedo between 0.05-0.20 while a bright surface like

fresh snow has albedo values ranging between 0.80-0.95 (Oke, 1987). Surface roughness is another important land surface property as both latent and sensible heat fluxes are turbulent fluxes, meaning they depend on turbulent heat transfer. Hence, land surfaces that are smoother, like grasslands and croplands, will exchange less heat through turbulent energy transfer compared to rougher surfaces, like forests. As the magnitude of the latent heat flux directly determines the amount of evaporation, the energy and water cycles are linked. The surface properties thus modulate how much water can evaporate, which affects atmospheric water vapour content and therefore also cloud formation and rainfall patterns (Bonan, 2015).

All these processes relevant at the land-atmosphere interface also interact with each other causing a variety of feedbacks within the climate system. To fully grasp these effects and the importance and role of the land surface for the climate, it is crucial that these processes and their interactions are represented in models. Earth System Models (ESMs) are a useful tool to grasp these interactions and perform counterfactual simulations to asses the importance or effects of certain changes. In the next section, we review the current knowledge of the effects of land cover and land management changes on the climate using both modelling and observational studies.

1.2 LCLMC-induced climate effects

Over the historic period, LCLMC have been estimated to reduce the global carbon stocks by 116 PgC based on global compilations of carbon stocks for soils (Sanderman et al., 2017) and 447 PgC for vegetation (Erb et al., 2018), which in total accounts for a loss of about half of the world's terrestrial biomass. Large shares of these losses occurred in the pre-industrial period (Canadell et al., 2021) but still remain an important factor to this day (Friedlingstein et al., 2022). These exchanges of chemical fluxes (mostly CO_2, N_2O and CH_4) are called the biogeochemical effects of LCLMC. These biogeochemical effects are generally deemed the most important effects of LCLMC as they affect climate on the global scale by contributing to anthropogenic climate change (Pongratz et al., 2010), with LCLMC being responsible for about 21% of present-day (2010-2019) net anthropogenic GHG (IPCC, 2022). CO_2 emissions are generally caused by agricultural expansion and the consequent deforestation, but can also be through peat drainage or wood harvesting. Erb et al. (2018) showed that over the historical period, land management contributed 42-47% to the reduction of terrestrial carbon stocks with the remaining loss being caused by land cover changes. Emissions of N_2O generally originate from agricultural practices such as nitrogen fertiliser or manure management while CH_4 emissions originate mostly from livestock fermentation or rice cultivation.

LCLMC can also affect the climate through biogeophysical effects which encompasses the effects on water and energy fluxes. These effects can occur when LCLMC affect surface properties, such as albedo or surface roughness, and therefore the exchange of momen-

tum, mass, and energy with the atmosphere (Bonan, 2008; Winckler et al., 2017a; Pongratz et al., 2021). These changes are spatially distinct and depend strongly on the type of conversion (Duveiller et al., 2018). They can play a role locally but can also cause large-scale climate effects when considering LCLMC of sufficient magnitude (e.g. shifting intertropical convergence zone Portmann et al., 2022). Changes in surface albedo, for example after deforestation, can cool the climate as forests (albedo 0.05-0.20) have a lower albedo compared to croplands and grasslands (0.25-0.3 Gao et al., 2005). This increase in albedo causes less shortwave incoming radiation to be absorbed and therefore reduces the surface temperature. This albedo-induced cooling effect is enhanced in boreal latitudes where forests mask snow cover and thus have an additional seasonal cooling effect on the climate. Secondly, evaporative efficiency of different vegetation types has been highlighted as important as some types of land cover, such as forest, have a higher evaporative capacity than other cover types, such as crop- and grasslands (Davin and de Noblet-Ducoudre, 2010). This is due to the deeper roots and higher leaf area of forests compared to crops (Boisier et al., 2012). LCLMC can also affect the roughness, whereby a rougher surface can enhance thermodynamic exchange between the surface and atmosphere and therewith change the partitioning of turbulent heat fluxes compared to a smoother surface. Given the example of deforestation, a forest cover is rougher than grass or cropland and will therefore have larger turbulent heat fluxes (Figure 1.2). Due to the combined effects of evaporative efficiency and roughness changes, evaporation generally decreases as a consequence of deforestation (Duveiller et al., 2018).

These local LCLMC effects can also affect climate elsewhere through advection or large-scale circulation changes (Figure 1.2). In this thesis, we define local biogeophysical effects as the effects induced by LCLMC within the location where LCLMC occurred, while effects occurring over areas where no LCLMC occurred are non-local effects. These local and non-local biogeophysical effects can then cause cascading effects in other components of the climate system. For instance, deforestation-induced warming in the tropics and consequent decreases in evaporation can cause a drying and decrease in precipitation downwind (Spracklen et al., 2018). Consequently, LCLMC can affect the degree of moisture recycling, whereby local evaporation feeds nearby precipitation. This moisture recycling process is important for sustaining tropical forests, especially in Latin-America (Spracklen et al., 2018; Zemp et al., 2014; Staal et al., 2018). Recent observational studies have shown that reforestation can be an effective measure to increase precipitation over Europe (Meier et al., 2021). Over the tropics the amount of in-situ data is limited. However, satellite data suggests that deforestation causes a general decrease in precipitation (Smith et al., 2023).

Modelling studies have also highlighted that LCLMC-induced climatic changes are not limited to lower atmospheric levels and affect the entire atmospheric column via convection and subsidence which can trigger large-scale changes in rainfall and temperature patterns worldwide (Laguë and Swann, 2016; Devaraju et al., 2018; Quesada et al., 2017). For example, Portmann et al. (2022) found that non-local biogeophysical effects of a global afforestation from pre-industrial land cover warms the climate enough to affect global meridional heat transport and global circulation in both oceans and atmosphere.

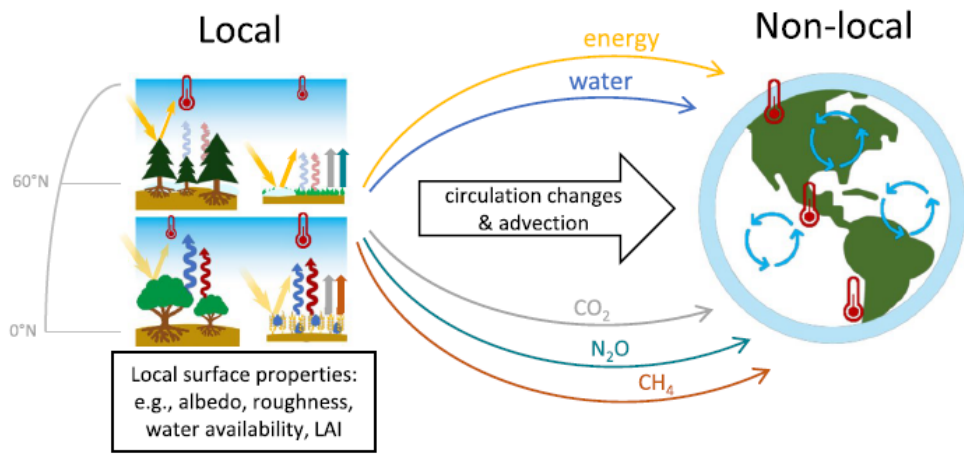

Figure 1.2: Schematic highlighting conceptual framework of local and non-local biogeophysical effects along with the most important processes explained in the text above. Figure was taken from Pongratz et al. (2021).

The effects of LCLMC have been studied through global modelling studies using ESMs. These studies initially focused mainly on deforestation and highlighted an important role of albedo and radiative properties (e.g. Davin and de Noblet-Ducoudre, 2010). However as global observational datasets became available based on in-situ observations (Bright et al., 2017) and remote sensing data (Li et al., 2015; Alkama and Cescatti, 2016; Duveiller et al., 2018), these original model-based findings were challenged. The observational studies highlighted a larger role of roughness-induced changes with less cooling in boreal and intermediate latitudes compared to modelling studies. This discrepancy has been resolved by creating consistent methods for signal separation of local and non-local biogeophysical effects (Winckler et al., 2017a; Chen and Dirmeyer, 2019). Winckler et al. (2019b) showed that when separating local from non-local effects in an ESM, the local effects were consistent with observations. Observational studies often assume a 'space for time' approach which involves comparisons of nearby patches of land with different land cover and assuming the climate effects are similar to a land cover change occurring over time. These approaches typically cancel out any possible non-local effects as the background climate in nearby locations is assumed to average out (Lee et al., 2011). Current consensus on observational data regarding local biogeophysical effects of deforestation encompasses a warming effect in the tropics and most mid-latitude regions dominated by the changes in turbulent heat fluxes, and a cooling in boreal latitudes which is dominated by albedo changes (Duveiller et al., 2018; Pongratz et al., 2021).

Most modelling studies only apply a single ESM, even though early multi-model compar-

isons showed that there is a large spread in the effects of land cover changes within different ESMs (Pitman et al., 2009; De Noblet-Ducoudré et al., 2012; Brovkin et al., 2013). The first model intercomparison project relating to the effects of land cover changes on the climate, the Land Use and Climate, IDentification of robust impacts (LUCID) project, compared present-day to pre-industrial land cover change scenarios but struggled to find clear consistent patterns due to the inter model uncertainties and the differences in implementation of land cover across ESMs (Pitman et al., 2009). Despite improvements in land cover representations, a second model intercomparison focusing on future simulations faced similar issues (Brovkin et al., 2013). To alleviate this, the Land Use Model Intercomparison Project (LUMIP Lawrence et al., 2016) also included a global deforestation experiment which showed a general agreement across ESMs in terms of changes in global mean temperatures (a deforestation-induced global biogeophysical cooling) but also showed strong inconsistencies in regional patterns and energy fluxes (Boysen et al., 2020). As these simulations were fully idealised, non-local effects induced by albedo changes especially over boreal latitudes dominated the global patterns. However, using a single ESM Winckler et al. (2019a) found that local effects could also be strong over certain regions and sometimes even dominate over the non-local signals (e.g. tropics). However, a consistent separation of local and non-local effects within idealised ESM simulations has not yet been performed across multiple ESMs.

Land management change is a relatively new addition to ESMs and therefore studies regarding the effects of management changes on climate are scarce. For example within the phase six of the Coupled Model Intercomparison Project (CMIP6) only three ESMs included a representation of irrigation, which is crucial for modelling climate in heavily irrigated regions such as India (Al-Yaari et al., 2022). Modelling studies have shown that irrigation has a regional cooling effect on climate, especially during heat extremes (Thiery et al., 2017, 2020). However, as irrigation also increases humidity it may effectively increase heat stress despite this cooling effect (Mishra et al., 2020), although the importance of irrigation for heat stress has been questioned recently (Jha et al., 2022). Several studies have suggested remote effects of land management through teleconnections. For example de Vrese et al. (2016) found that Indian irrigation feeds rainfall in Eastern Africa. While irrigation in the Chinese Tarim basin has been linked to the positive mass balance of glaciers within the Karakoram mountain chain in contrast to the blobal trends of negative mass balances due to climate change (de Kok et al., 2018, 2020). Other management practices such as cropland albedo management (Hirsch et al., 2017; Seneviratne et al., 2018; Davin et al., 2014; Lombardozzi et al., 2018) and wood harvesting (Erb et al., 2018) have also been studied for their effects on climate but are generally not fully implemented in ESMs and their climatic effects are therefore less well constrained.

1.3 The role of land in climate change mitigation and adaptation

Land can play a crucial role for both mitigating climate change (i.e. reducing GHGs concentrations) and helping populations adapt to climate change (e.g. through additional cooling from trees). Land especially plays an important role in low-warming scenarios, such as the 1.5 K-compatible scenarios from the Paris Agreement (Roe et al., 2019; Rogelj et al., 2018). Within the 2015 Paris Agreement the ambition was set to limit global warming to "well below 2 K" and additionally to "pursue efforts to limit temperature increase to 1.5 K above pre-industrial levels." (UNFCCC, 2015). However, up until now the submitted Nationally Determined Contributions (NDCs) are falling short of these goals (Meinshausen et al., 2022).

Within this context, land is often considered as a possible avenue of achieving these low-warming targets. The land sector is responsible for 10-12 GtCO_2 emissions which amounts to 21% of present-day (2010-2019) net anthropogenic GHG (IPCC, 2022). This contribution represents the net balance between emissions due to land use changes and carbon sequestered through vegetation growth. As the land sink currently stores up to 30% of anthropogenic emissions since 1850 (Friedlingstein et al., 2022), it is essential to achieve 1.5 K warming goals. In this sense it is not only important to reduce emissions from land use change but also to enhance the land sink which could allow for reaching 'negative emissions' past net zero in the second half of the century (Minx et al., 2018). Approaches to enhance land carbon uptake, such as Bio-Energy Carbon Capture and Storage (BECCS) or afforestation are heavily dependent on land availability and would require large-scale LCLMC, potentially even compromising food production and biosphere functioning (Boysen et al., 2017; Séférian et al., 2018; Heck et al., 2018; Stokstad, 2019; Reid et al., 2020). Despite these issues, large-scale deployments of carbon dioxide removals were included in all but one of the 2 K compatible scenarios and in all 1.5 K scenarios produced by the Integrated Assessment Modelling community (Rogelj et al., 2018). Therefore, substantial LCLMC are deemed likely towards the future. However, in contrast to GHG emissions which generally originate from the Global North, the land use emissions more often originate from the Global South with a large importance of retaining tropical forests and their associated carbon sinks (Humpenöder et al., 2022).

Generally, policies regarding future land-based mitigation only include the biogeochemical effects of LCLMC, with no consideration of their biogeophysical influence. If considered, only local effects are currently facilitated to be included, with no clear pathway on how to consider non-local biogeophysical effects (Pongratz et al., 2021; Duveiller et al., 2020). Moreover, both the magnitude and potential of the biogeochemical effects as the permanence of new forest in a warmer climate are highly uncertain and topics of active research (Fuss et al., 2018; Popp et al., 2017; Curtis et al., 2018). Recent research shows a decreased resilience of forest under climate change (Hartmann et al., 2022; Forzieri et al., 2022) which further constrains the feasibility of future climate pathways that rely heavily

on land-based mitigation.

LCLMC provides potential synergies for both climate mitigation and adaptation, for example a local biogeophysical cooling effect through afforestation added upon the global carbon effects (Jia et al., 2019). Another potential land-based adaptation strategy is through a combined application of small-scale afforestation and irrigation to enhance precipitation recycling locally, which has been shown to be effective over semi-arid regions (Layton and Ellison, 2016; Ellison et al., 2017). At this stage, most research regarding moisture recycling is focused on specific regions while neglecting global feedbacks. As a consequence, there remains a large uncertainty related to the viability of these adaptation approaches and their full climate implications.

Currently, only few ESM studies exist that explicitly assess the effects of LCLMC within future climates (Brovkin et al., 2013; Boysen et al., 2014; Hirsch et al., 2018a) – most ESM studies focus on historical (Pongratz et al., 2010; Pitman et al., 2009; De Noblet-Ducoudré et al., 2012; Boisier et al., 2012) or idealised simulations (Davin and de Noblet-Ducoudre, 2010; Winckler et al., 2017a, 2019a; Boysen et al., 2020; Portmann et al., 2022). Consequently, there exists a large uncertainty regarding the strength of future land-based mitigation potential as well as regarding potential local and non-local biogeophysical effects. The LCLMC-induced climate effects can also lead to further downstream impacts such as effects on human health or economic productivity. However, these impacts are only rarely studied within dedicated LCLMC simulations in ESMs even though they are crucial to understand future adaptation potential of LCLMC.

1.4 Modelling land cover in Earth System Models

In this thesis, we use Earth System Models (ESM) to investigate the effects of LCLMC on the climate. This approach allows to understand the importance of different processes and feedbacks. The key building blocks for this work therefore consist of (i) the ESM simulations, and (ii) the LCLMC information they ingest. First, we introduce the Land Use Harmonisation Project, in which land cover maps are developed for use in ESMs. Second, we provide a general description of ESMs with a focus on their land components. We discuss the three ESMs used in this thesis: the Community Earth System Model (CESM), the Max Planck Institute Earth System Model (MPI-ESM) and the European Consortium Earth System Model (EC-EARTH). We highlight how these different ESMs resolve LCLMC and relevant processes or model structural differences.

1.4.1 Land Use Harmonisation Project

There was a push to harmonise the representation of land cover in a consistent way across different ESMs within the large cycles of simulations (CMIP) prepared for the Intergovernmental Panel on Climate Change (IPCC) reports. This eventually led to the Land Use

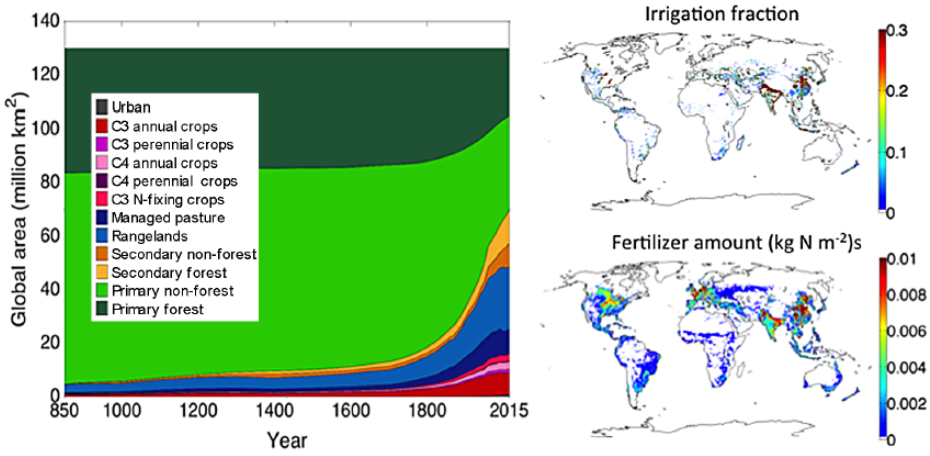

Figure 1.3: Shown are time series of different land cover states included in LUH2 dataset from 850-2015 (left). Fraction of grid cell irrigated in the year 2015 (top right) and amount of fertilizer applied in 2015 (bottom right). Figure was taken from Lawrence et al. (2016).

Harmonisation Project which was first established for CMIP5 (Hurtt et al., 2011) and is currently in its second phase (LUH2) with an updated dataset and higher resolution for CMIP6 (Hurtt et al., 2020). The existence of a harmonised land use dataset across ESMs serves two primary goals: (i) it allows for a more consistent modelling framework between ESMs as all use the same input data and (ii) it minimizes differences at the transitions between historical land use reconstructions and future land use projections (Hurtt et al., 2020). These future land use projections are generally derived from Integrated Assessment Models (IAMs) which are models that based on socioeconomic assumptions can provide policy relevant information. These IAMs can be applied under the different Shared Socioeconomic Pathways (SSPs) to assess what implications certain socioeconomic choices have on a.o. future emissions and land use. The different SSP scenarios used within the latest IPCC reports are each derived within different IAMs (Popp et al., 2017), hence the harmonisation of resulting land use data through LUH2 is crucial as it could lead to artefacts if not harmonised properly.

The LUH2 dataset contains land cover data at 0.25°x0.25° resolution from the time period 850-2100. The land cover data covering the historical period is illustrated in Figure 1.3. It contains fractional land cover descriptions per grid cell for five land use states: cropland, pasture, urban, primary and secondary land. Primary and secondary land are natural areas with the difference that primary land has been unaffected by human disturbances while secondary land is recovering from human disturbances, both can be forest but can also be other natural land (Hurtt et al., 2020). Cropland is disaggregated into five different crop types

based on data from the United Nations Food and Agriculture Organisation as reported in Monfreda et al. (2008). Several land management practices are included in the dataset such as grazing, fertiliser application, and irrigation (Hurtt et al., 2020).

The LUH2 data has been created within the framework of CMIP6 and is an open and accessible tool for the entire community to use both for historical land cover data as well as for future SSP scenarios (Popp et al., 2017). The data can be accessed freely online (`https://luh.umd.edu/index.shtml`). Each ESM has their own ESM-specific tools to translate these LUH2 datasets and its land cover categories into their respective land cover structures.

1.4.2 Earth System Models

ESMs are important tools to help us understand global climate and its response to anthropogenic forcings. They combine a multitude of physical, chemical, and biological processes to simulate both past and future climate. ESMs generally contain submodels for the atmosphere, ocean, land, sea ice, and ice sheets which allows them to simulate important inter linkages and feedback processes. Therefore, they offer a suitable tool to asses human influences on global climate (such as LCLMC). Because of the large amount of processes and interactions between subcomponents, these models tend to be computationally expensive. Therefore, they are generally applied at a relatively coarse spatial resolution of ± 100 km.

Land surface models represent the land component in ESMs. They represent energy, water, and biogeochemical exchanges between the land and atmosphere and simulate biogeophysical as well as biogeochemical effects due to LCLMC (Figure 1.4). Within early climate models, the land components represented a boundary layer for the atmosphere with no interaction components and no explicit representation of vegetation. The approaches to model vegetation in land surface models remain generally relatively simple, with the inclusion of vegetation being limited to one single exchange layer for vegetation canopy (the so-called big leaf approach) and no vertical structure. Land surface models are able to simulate transfer of radiation, momentum, and turbulent exchanges of water and energy (Bonan, 2019). These approaches evolved over time and land surface models started to become increasingly realistic, for instance by including biogeochemical modules that simulate the transfer of carbon and other nutrients (see Figure 1.4C). As the representation of vegetation becomes more realistic, models started to include dynamic vegetation which allows the land surface model to simulate vegetation growth based on the available physical resources (Figure 1.4D), this allows land surface models to move beyond simplified assumptions for key ecosystem processes such as leaf phenology, mortality, and vegetation growth (Bonan, 2019).

To represent land cover within a land surface model, a subgrid land cover hierarchy is defined. A single grid cell is divided in different tiles which can represent various vegetation

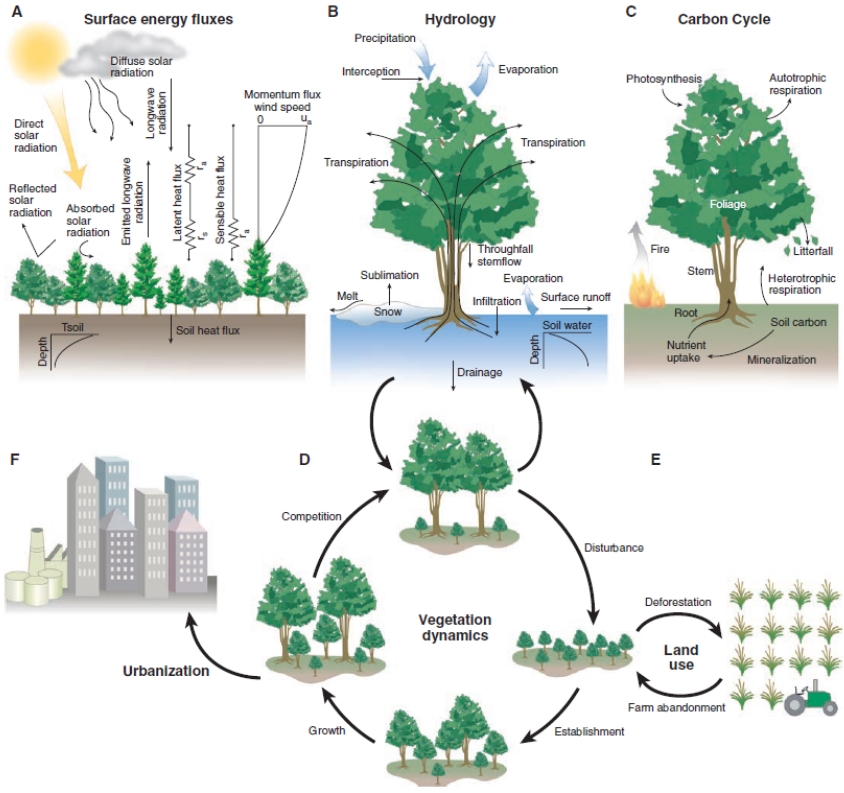

Figure 1.4: Overview of processes resolved within most land surface models, including the surface energy balance (panel A), the terrestrial hydrological cycle (panel B) and the terrestrial carbon cycle (panel C). Some more advanced land surface models also include vegetation dynamics (panel D). land use changes can then be prescribed or dynamic (panel E) and urban areas can also be included (panel F). Figure was taken from Bonan (2008).

types or land cover types (such as bare soil or lakes). This allows for land surface models to represent heterogeneity of land cover types at a finer scale than their native resolution. Different vegetation types can be resolved through Plant Functional Types (PFTs) which are defined as different vegetation types based on functional similarities (e.g. evergreen versus deciduous trees). Not all ESMs explicitly model subgrid heterogeneity and include some assumptions to postprocess subgrid level effects in an implicit way. Each ESM starts from the LUH2 dataset and applies ESM-specific translations to achieve their individual land cover maps in their respective subgrid definitions and on their native spatial grid (Section 1.4.1). Land management representation is still a work in progress in many ESMs and is therefore more often than not excluded from this translation process, despite data on certain management types (such as irrigation and fertilisation) being available in the LUH2 dataset.

Land surface models can be applied within simulations along with the other sub models of ESMs (such as atmosphere and ocean models), in this setup they communicate information (simulated variables such as evaporation or surface runoff) to the other sub models. When all sub components within an ESM are run together the simulations are referred to as fully-coupled simulations. Alternatively, land surface models can also be run separately from the other sub models of an ESM, making the simulations computationally much less expensive. These simulations are then referred to as land-only simulations as they are not coupled to an atmosphere or ocean model, the information that is generally provided from the other submodels then comes from observational data sources or reconstructions (e.g. reanalysis data to replace atmosphere model).

In this thesis, the outputs from three different ESMs are analysed: (i) the Community Earth System Model, (ii) the Max-Planck Institute Earth System Model and (iii) the European Consortium Earth System Model. Below we summarise the structure of these ESMs and highlight important differences in their respective land surface model schemes related to the representation of land cover and land management.

CESM

The Community Earth System Model version 2 (CESM2) is an open-source model hosted and mostly developed at the National Centre for Atmospheric Research but has a large international user base. It simulates the atmosphere, ocean, sea-ice, ice sheets and land and all associated interactions through fluxes and states which are communicated via a coupler (Danabasoglu et al., 2020).

CESM has two atmospheric models, of which the Community Atmosphere Model (CAM) is used within the default configuration. It is often applied at a horizontal resolution of 1° and has 32 levels extending up to 40 km into the atmosphere, which makes that it is not able to fully resolve the stratospheric processes. The second model is the Whole Atmosphere Community Climate Model (WACCM) which uses 70 vertical levels extending up to about 130 km and thus resolves the stratosphere better with more comprehensive atmospheric

chemistry (Danabasoglu et al., 2020). However, as it is more extensive it is also more computationally expensive and therefore less often used in fully-coupled CESM simulations.

The ocean is modelled through the Parallel Ocean Program (POP) which handles the physical ocean flows and processes. It has a horizontal resolution of 1°, similar to the atmosphere model. and up to 60 levels in the vertical going down to depths of 5500 m. The biogeochemical ocean processes are modelled through the Marine Biogeochemistry Library (MARBL) and the ocean waves are modelled through the NOAA WaveWatch-III ocean surface wave prediction model. Sea ice is modelled using CICE while land ice is modelled through the Community Ice Sheet Model (CISM). All these components share fluxes and states with each other though the Common infrastructure for Modelling the Earth (CIME) which serves as a coupler but also as the infrastructure to build and run the model (Danabasoglu et al., 2020).

The Community Land Model (CLM) is used as a land surface scheme within CESM, modelling the terrestrial fluxes and states related to energy, water, and biogeochemical fluxes (Lawrence et al., 2019). River routing is represented through the MOdel for Scale Adaptive River Transport (MOSART). CLM includes an explicit description of sub-grid heterogeneity which is implemented using a nested hierarchy with an individual grid cell constituting of different land units such as vegetated, urban, lake, glacier, and crop fractions. The land cover is prescribed through land cover maps derived from LUH2 and is thus not explicitly modelled within CLM. CLM includes 14 natural PFTs, of which 10 describe forests, 3 describe grasslands and 1 describes bare soil. The crop land unit can be subdivided in up to 8 different crop types. These crop types can exist either on a rainfed patch or an irrigated patch and thus a distinction is made within the crop land unit between different crop types and whether they are irrigated or not, resulting in a total of 16 Crop Functional Types (CFTs) within the model. The grid-scale fluxes are computed through a weighted average of all subgrid specific fluxes per grid cell (Lawrence et al., 2019). Irrigation is explicitly modelled using an irrigation parameterisation, which irrigates depending on water stress of crops. Hence, the model only uses the areal extent of irrigation from LUH2 but computes irrigation amounts itself. Other management practices such as wood harvesting and nitrogen fertilisation are prescribed through the land cover maps.

MPI-ESM

The Max Planck Institute for Meteorology Earth System Model version 1.2 with low resolution configuration (MPI-ESM1.2-LR; hereafter referred to as MPI-ESM) is a fully coupled state-of-the-art ESM that uses the atmospheric component ECHAM6.3 (around 200 km horizontal resolution and 47 atmospheric vertical levels). The atmosphere is coupled via OASIS3-MCT to the ocean dynamic (MPIOM1.6) and ocean biogeochemistry (HAMOCC6) models (around 150 km grid spacing and 40 vertical levels) (Mauritsen et al., 2019).

The land surface model is the Jena Scheme for Biosphere-Atmosphere Coupling in Hamburg (JSBACH3.2), which simulates a total of 12 different PFTs, with 4 forest PFTs (tropical broadleaf evergreen and deciduous trees, extra-tropical evergreen and deciduous trees) and two cropland CFTs (C3 and C4 crops). The spatial fractions are defined by aggregating all natural and crop types from LUH2 and distributing these totals among the different PFTs and CFTs within JSBACH. The pasture and urban categories from LUH2 are aggregated into a pasture land cover type within JSBACH. The model is a dynamic vegetation model but can be constrained to work in a similar way as CLM by prescribing land cover maps. Within the model, subgrid heterogeneity is resolved through the definition of tiles which contain the various PFTs and CFTs. Wood harvesting is implemented within the model but only effects on the biogeochemical fluxes are included with no feedbacks on the modelled water and energy cycles. Irrigation was not yet included in the latest CMIP6 simulations of MPI-ESM but parameterisations for this form of land management have been developed and are included in this thesis (e.g de Vrese et al., 2016; de Vrese and Hagemann, 2018; de Vrese and Stacke, 2020).

EC-EARTH

EC-EARTH is a state-of-the-art Earth system model developed by the EC-Earth consortium (Döscher et al., 2022). Here we use the released version EC-Earth3-Veg (v3.3.3.1). The atmospheric component is the Integrated Forecast System (IFS) developed by the European Centre for Medium-Range Weather Forecasts (ECMWF) that uses the TL255 horizontal grid (± 80 km) and 91 vertical model levels with the top level at 80 km which covers a large range of atmospheric and stratospheric processes. The oceanic component is the Nucleus for European Modelling of the Ocean (NEMO) model (v3.6).

The vegetation model is the Lund-Potsdam-Jena General Ecosystem Simulator (LPJ-GUESS). This model, in contrast to the land surface models in the previous two ESMs, is a dynamic vegetation model which models vegetation extent explicitly. Therefore, only natural land and managed land fractions can be prescribed in LPJ-GUESS. This model computes vegetation dynamics and soil and carbon processes but does not handle the land-atmosphere interactions of water and energy fluxes: this is done within the atmosphere model IFS by a dedicated land surface component, the Hydrology Tiled ECMWF Scheme for Surface Exchanges over Land (HTESSEL) (Döscher et al., 2022).

In LPJ-GUESS, the vegetation dynamics for the land are simulated on 6 stand types, namely Natural, Pasture, Urban, Crop, Irrigated Crop and Peatland. In the Natural stand 10 woody and 2 herbaceous PFTs compete (Smith et al., 2014). On Pasture, Urban, and Peatland fractions, 2 herbaceous species are simulated, conforming to the C3 and C4 photosynthetic pathways. The Crop stands have 5 CFTs, both annual and perennial C3 and C4 crops, and C3 N fixers which is in line with the LUH2 crop categories (Lindeskog et al., 2013). Irrigation is included within LPJ-GUESS but is not yet implemented in IFS and HTESSEL, which implies that irrigation will affect the growth of crops but will not change

water and energy fluxes in this ESM.

Within HTESSEL, land cover is discretised into six different tiles (bare ground, low and high vegetation, intercepted water by vegetation, shaded vegetation, and exposed snow), creating a subgrid hierarchy which is strongly different from the two previous ESMs. The grid-scale fluxes are computed as weighted averages of the different tiles existing in a given grid cell. The subgrid hierarchy defined in HTESSEL allows for only one type of high and low vegetation (forest and crop/shrubs/grasslands, respectively) to exist per grid cell, which is determined by the high and low vegetation type which corresponds to the most dominant fraction within that grid cell as modelled by LPJ-GUESS (Döscher et al., 2022). Due to different processes represented in two separate land surface models in EC-EARTH, some degree of detail is lost in the translation from LPJ-GUESS to HTESSEL. Hence, the atmosphere will interact with a more crude representation of vegetation than what is modelled within LPJ-GUESS.

1.5 Research aims

This thesis aims to advance our understanding of the role of LCLMC on present and future climate conditions. To constrain the uncertainty related to LCLMC-induced climate effects in ESMs, we initially analyse idealised simulations performed with CESM, MPI-ESM, and EC-EARTH. We analyse the climate effects across three ESMs to asses robust patterns for temperature which can be evaluated against observational datasets, but also for moisture fluxes and moisture recycling. Next, we simulate future low-warming scenarios using land cover maps derived from IAMs representing strongly different socio-economic worlds. These simulations are analysed for their effects of LCLMC on the climate to constrain the potential of future land use for future adaptation and mitigation. These overarching research objectives are translated into three separate research goals:

1. **Uncover robust patterns across ESMs for local and non-local biogeophysical effects of LCLMC on temperature [Chapter 2]**.This is done for the biogeophysical effects of idealised changes in afforestation, cropland expansion, irrigation and wood harvesting in three different ESMs. By applying these idealised LCLMC scenarios within several ESMs, we are able to constrain and evaluate their responses to develop a better understanding of the local and non-local biogeophysiscal effects related to different LCLMC practices.

2. **Constrain the response of the atmospheric water cycle to LCLMC in three ESMs [Chapter 3]**. The idealised simulations are analysed with a focus on water fluxes (evaporation and precipitation) and how LCLMC can affect their magnitude. We apply a moisture tracking algorithm to further constrain the implications of LCLMC on both continental and local moisture recycling and to quantify the implications for global water availability.

3. **Assess the impacts of LCLMC in a future low-warming world [Chapter 4]**. We simulate realistic future land use scenarios in a low-warming (Paris Agreement compatible) world under different socioeconomic narratives (Inequality versus sustainability). We analyse the ESM simulations for temperature and humidity changes and investigate how these translate into effects on heat stress. Furthermore, we quantify the economic impacts of LCLMC through changes in labour capacity and health impacts through changes in temperature-related mortality.

1.6 Outline of the thesis

This doctoral thesis is organized based on a series of analyses meant for international peer-reviewed journal articles, either published, in review or in preparation (see page 161 for an overview). The thesis is structured as follows:

In Chapter 2, we analyse the idealised ESM simulations for different LCLMC categories (cropland expansion, afforestation, irrigation expansion, and wood harvesting). The results are first evaluated using observational datasets of global deforestation. Then, a signal separation approach is applied to disentangle the local and non-local effects of LCLMC which are compared across the different ESMs. Finally, we decompose the local effects on surface temperature into the different components of the surface energy balance to constrain the processes causing the local temperature effects.

In Chapter 3, the idealised simulations are analysed for moisture fluxes including evaporation, precipitation and moisture flux convergence to unravel the effects of the different LCLMC on the atmospheric water cycle. A moisture tracking algorithm is applied using subdaily ESM output to quantify the effects of LCLMC on moisture recycling. These effects are analysed using length scales and continental moisture recycling ratios.

In Chapter 4, we analyse future simulations of a low-warming world which we performed with CESM. These simulations compare scenarios with different socio-economic implications (global inequality versus sustainability). The LCLMC-induced climate effects are compared to the combined effects of all other forcings for near-surface temperature and humidity. A metric of heat stress is computed to asses the economic impacts of the LCLMC-induced climate effects on labour capacity. Finally, temperature-related mortality is computed to assess the importance of future LCLMC scenarios for human health.

The key findings of this doctoral research are summarized in Chapter 5, including an outline of future research avenues which could help further the understanding of LCLMC climate interactions and their potential for future mitigation and adaptation.

All ESM simulations analysed in this thesis have been performed within the framework of the LAnd MAnagement for CLImate Mitigation and Adaptation project (LAMACLIMA). I performed the CESM simulations while the data from the MPI-ESM and EC-EARTH simulations were provided by other project partners.

Chapter 2

The biogeophysical effects of idealized land cover and land management changes in Earth System Models

Land cover and land management change (LCLMC) has been highlighted for its critical role in mitigation scenarios. Yet, the climate effect of individual LCLMC options and the local vs. non-local responses are still poorly understood across different Earth System Models (ESMs). We simulate the climatic effects of LCLMC using three ESMs (CESM, MPI-ESM and EC-EARTH). We assess the LCLMC effects using four idealized experiments: (i) a fully afforested world, (ii) a world fully covered by cropland, (ii) a fully afforested world with extensive wood harvesting, and (iv) a full cropland world with extensive irrigation. The local effects of deforestation on surface temperature are largely consistent across the ESMs and the observations, with a cooling in boreal latitudes and a warming in the tropics. However, the energy balance components driving the change in surface temperature show less consistency across the ESMs and the observations. The non-local effects on surface temperature are broadly consistent across ESMs for afforestation, though larger model uncertainty exists for cropland expansion. Irrigation clearly induces a cooling effect, however; the ESMs disagree whether this cooling is local or non-local. Our results overall underline the potential of ensemble simulations to inform decision making regarding future climate consequences of land-based mitigation and adaptation strategies.

This chapter is published as: De Hertog S. J., Havermann F., Vanderkelen I., Guo S., Luo F., Manola I., Coumou D., Davin E. L., Duveiller G., Lejeune Q., Pongratz J., Schleussner C.-F., Seneviratne S. I., Thiery W. (2023) The biogeophysical effects of idealised land cover and land management changes in Earth System Models. Earth System Dynamics, in press.

2.1 Introduction

Land cover change and land management change have been intrinsically connected to human development throughout history. The impact of land cover change and land management change (LCLMC) on the global carbon cycle was estimated at 116 PgC based on global compilations of carbon stocks for soils (Sanderman et al., 2017) and for vegetation as 447 PgC (Erb et al. (2018): a loss of about half of the world's terrestrial biomass), with substantial shares already in the pre-industrial period (Canadell et al., 2021). About 10% of anthropogenic CO2 emissions have been caused by LCLMC over the last decade (Friedlingstein et al., 2022). According to integrated assessment models, LCLMC will play an important role in the near-term future as most low-end warming scenarios assume large-scale deployment of land-based mitigation (Rogelj et al., 2018). However, the effect of changed land cover and management on the climate is still highly uncertain and poorly understood (Mahmood et al., 2014; Pitman et al., 2009; Perugini et al., 2017). For instance, land use policies generally only account for the effects on the carbon balance while largely neglecting the biogeophysical effects (Duveiller et al., 2020). These biogeophysical effects include (i) the effects of land cover and land management change on the surface radiation budget (e.g. a forest is a darker surface than open grass or cropland hence it absorbs more shortwave radiation) (ii) the effects of non-radiative processes like changes in evaporative efficiency and surface roughness, and (iii) the effects induced by atmospheric circulation through altering heat, moisture and momentum transport (Bright et al., 2017; Winckler et al., 2017a; Duveiller et al., 2020). The induced changes in atmospheric circulation are often classified as non-local processes as they typically affect other regions than those where the LCLMC occurred. The effects on surface radiation and surface properties are called local processes, as they are a direct consequence of local LCLMC.

As LCLMC are an often cited approach for local mitigation and adaptation policies (Minx et al., 2018; Perugini et al., 2017), the separation of local and non-local effects can help in reducing current uncertainty in assessments of biogeophysical effects. As non-local effects are a consequence of LCLMC occurring elsewhere, they are generally not a desired effect from specific policies (which tend to have a local scope), but rather an undesired and unintended effect from LCLMC across the globe. In contrast, local effects from LCLMC are directly influenced by local decisions and can be applied more directly in local adaptation and/or mitigation policies. Therefore, the separation between local and non-local effects is beneficial for the implementation of biogeophysical effects related to LCLMC in local mitigation and adaptation policies.

A first set of studies attempted to use Earth System Models (ESMs) to understand the global effects of land cover change, both in idealised (Davin and de Noblet-Ducoudre, 2010; Boysen et al., 2020; Meier et al., 2021) and in more realistic setups (Pitman et al., 2009; Pongratz et al., 2010; Boisier et al., 2012; Ito et al., 2020). However, these studies only show aggregated effects of the biogeophysical processes highlighted above and no direct separation is made between effects caused by local and non-local processes. Some studies extracted the local signals from Earth System Model (ESM) simulations by com-

paring data at tile level (Malyshev et al., 2015) or extracting local signals by comparing neighbouring grid cells with different land cover change rates (Kumar et al., 2013; Lejeune et al., 2017). Nevertheless, these approaches either have a limited spatial coverage (Kumar et al., 2013; Lejeune et al., 2017) or are limited to ESMs with tile level output data (Malyshev et al., 2015). A novel approach by Winckler et al. (2017a), often referred to as the checkerboard approach, separates land cover change signals into local and non-local effects without these limitations. This was done by prescribing a land cover map with grid cells which underwent land cover change and grid cells with the original land cover in a regular pattern (e.g. 1/8, 1/4, etc.). By contrasting this simulation to a reference simulation without land cover change, the local and non-local signals can be separated. However, the simulations performed in Winckler et al. (2017a) are limited to a single ESM (MPI-ESM, Winckler et al. (2017a, 2019a,b,c)). Multi-model studies, like the step-wise deforestation experiment within the Land Use Model Intercomparison Project (LUMIP, Boysen et al. (2020)) report local and non-local effects by comparing results within and beyond the geographical region of deforestation, which, however does not allow for a quantitative separation on the global scale.

A second set of studies investigated the climate effects of land cover change based on observational data. Remote sensing data is used to compare the surface temperature of a forested patch and a patch of open land, both spatially (Duveiller et al., 2018; Li et al., 2015) and temporally (Alkama and Cescatti, 2016). Data from eddy covariance towers providing direct flux measurements (e.g. through FLUXNET) were used to reconstruct the biogeophysical effects of deforestation (Bright et al., 2017). These observational estimates by design exclude the non-local signals which might dominate the response to deforestation, according to recent work applying the alternating LCLMC approach (Winckler et al., 2019b).

Unlike land cover change, the climate effects of land management change, like irrigation and wood harvesting, are less studied. This is remarkable, as observational studies indicate that both land cover change and land management change have an equally important effect on climate variables such as surface temperature (Luyssaert et al., 2014). Moreover land management will be increasingly important towards the future due to land scarcity and the need for intensification as well as the additional pressure on land for carbon dioxide removal (Pongratz et al., 2021). Among land management change options, irrigation has a clear regional cooling effect, especially during warm episodes (Hirsch et al., 2017; Thiery et al., 2017, 2020; Chen and Dirmeyer, 2019; Gormley-Gallagher et al., 2020; Mishra et al., 2020). Despite its recognised imprint on local climate, only a few ESMs simulate irrigation explicitly, with only three ESMs including irrigation in the CMIP6 simulations (Al-Yaari et al., 2022). Wood harvesting has mostly been studied for its biogeochemical effects while the analysis of the biogeophysical effects is still lacking in studies using ESMs. Observational studies, however, indicate an effect of wood harvesting on albedo (Otto et al., 2014) and surface roughness (Nakai et al., 2008). Furthermore, the effect of land management change on atmospheric circulation has been hypothesised, with for instance irrigation-induced cooling causing a delayed onset of the Indian Monsoon (Guimberteau et al., 2012;

Thiery et al., 2017) and modified precipitation patterns in Eastern Africa (de Vrese et al., 2016). Yet, the relative importance of local versus non-local effects induced by land management changes has not been studied so far.

In this study, we quantify the sensitivity of local and non-local climate to LCLMC and investigate the processes contributing to surface temperature changes. We apply the checkerboard approach to idealised simulations in a multi-model framework using three ESMs. Idealised simulations are performed with two land cover change sensitivity experiments (cropland expansion and afforestation), and two land management change sensitivity experiments (irrigation and wood harvest expansion). The simulations represent changes from present-day land cover, and thus provide policy makers with information on potential effects of LCLMC under present-day climate. First, we describe the spatial patterns of the local and non-local effects of surface temperature to the LCLMC sensitivity experiments. Second, we evaluate the local effect in the different ESMs for deforestation against estimates derived from observations and remote sensing (Duveiller et al., 2018; Alkama and Cescatti, 2016; Li et al., 2015; Bright et al., 2017). Finally, we analyse the processes underpinning the local effect of different LCLMC using an energy balance decomposition.

2.2 ESM sensitivity experiments

2.2.1 Participating ESMs

Three state-of-the-art ESMs are used in this study: the Community Earth System Model (CESM), the Max Planck Institute for Meteorology Earth System Model (MPI-ESM), and the European Consortium Earth System Model (EC-EARTH). Here, we provide a brief technical description of each model.

We use CESM version 2.1.3 (hereafter referred to as CESM), an open-source and fully coupled ESM (Danabasoglu et al., 2020). CESM combines the Community Atmosphere Model version 6 (CAM6), the Community Land Model version 5 (CLM5; Lawrence et al., 2019), the Parallel Ocean Program version 2 (POP2), The Community Ice Sheet Model (CISM), the Los Alamos National Laboratory Sea Ice model (CICE), and the Model for Scale Adaptive River Transport (MOSART). CESM has some notable improvements to the previous version (Danabasoglu et al., 2020); for instance, CLM5 includes improvements in the snow and plant hydrology, the lake model, and carbon and nutrient recycling (Lawrence et al., 2019). CLM5 also includes 14 natural Plant Functional Types (PFTs) and 8 Crop Functional Type (CFTs), whereby CFTs can exist either on a rainfed patch or an irrigated patch. The Sub-grid heterogeneity is implemented using a nested hierarchy where an individual grid cell constitutes of different land units such as vegetated, urban, lake, glacier and crop fractions (Lawrence et al., 2019). The CESM simulations were performed at a spatial resolution of 0.90°x1.25°.

The Max Planck Institute for Meteorology Earth System Model version 1.2 with low resolution configuration (MPI-ESM1.2-LR; hereafter referred to as MPI-ESM) is a fully coupled state-of-the-art ESM that uses the atmospheric component ECHAM6.3 and the land component JSBACH3.2 (around 200 km horizontal resolution (T63) and 47 atmospheric vertical levels), which are coupled via OASIS3-MCT to the ocean dynamic (MPIOM1.6) and ocean biogeochemistry (HAMOCC6) models (around 150 km grid spacing and 40 vertical levels). A detailed description of MPI-ESM1.2 can be found in (Mauritsen et al., 2019). A similar setup has been also used within CMIP6/LUMIP, e.g. with studies on biogeophysical effects of deforestation (Boysen et al., 2020) as well as other recent studies on the effects of land use and land cover change on climate (Winckler et al., 2019b,a). JSBACH3.2 simulates in total 12 different plant functional types (PFTs), with 4 forest PFTs (tropical broadleaf evergreen and deciduous trees, extra-tropical evergreen and deciduous trees) and two cropland PFTs (C3 and C4 crops). The MPI-ESM simulations were performed at a spatial resolution of 1.88°x1.88°.

EC-EARTH is a state-of-the-art Earth system model developed by the EC-Earth consortium (Döscher et al., 2022). In this study we use the released version EC-Earth3-Veg (v3.3.3.1). The atmospheric component is the Integrated Forecast System (IFS) developed by the European Centre for Medium Range Weather Forecasts (ECMWF) that uses the TL255 horizontal grid (± 80 km) and 91 vertical model levels with the top level at 0.01 hPa. The oceanic component is the Nucleus for European Modelling of the Ocean (NEMO) model (v3.6). The vegetation model is the Lund-Potsdam-Jena General Ecosystem Simulator (LPJ-GUESS). Note that this is a dynamic vegetation model which does not explicitly solve the energy balance as the previous ESMs did. The atmosphere model IFS has a dedicated land surface component : the Hydrology Tiled ECMWF Scheme for Surface Exchanges over Land (HTESSEL) to handle the surface water and energy fluxes to the atmosphere. In LPJ-GUESS, the vegetation dynamics for the land are simulated on 6 stand types, namely Natural, Pasture, Urban, Crop, Irrigated Crop and Peatland. In the Natural stand 10 woody and 2 herbaceous PFTs compete (Smith et al., 2014). On Pasture, Urban and Peatland fractions 2 herbaceous species are simulated, conforming to the C3 and C4 photosynthetic pathways. The Crop stands have 5 CFTs, both annual and perennial C3 and C4 crops, and C3 N fixers (Lindeskog et al., 2013). The EC-EARTH simulations were performed at a spatial resolution of 0.7°x0.7°.

There are some important differences in how the different ESMs treat land cover. They have a different amount of PFTs which are also defined in different categories. Moreover while in MPI-ESM and CESM land cover is handled within one single sub-model (their respective land surface schemes JSBACH and CLM) and is prescribed, in EC-EARTH there are different models for vegetation dynamics and biogeochemistry (LPJ-GUESS) and for the water and energy cycle (HTESSEL). This implies that for CESM and MPI-ESM the areas which are afforested are assumed to be a physical forest immediately. This is in contrast to EC-EARTH where the dynamic vegetation model determines the physical properties of trees from biomass buildup through vegetation growth. We summarize the most important differences relating to how the ESMs handle land cover in table 2.1. Additionally, in order

Table 2.1: Specifications of how land cover is handled across the different ESMs.

ESM	Land Model	spatial resolution	amount of PFTs	Prescribed land cover
CESM2	CLM5	0.90°x1.25°	14	yes
MPI-ESM1.2	JSBACH3.2	1.88°x1.88°	12	yes
EC-EARTH3-Veg	LPJ-GUESS/HTESSEL	0.7°x0.7°	12	no

to give an idea of the differences in the initial land cover maps, we provide the 2015 forest fractions (evergreen, deciduous and total forest) for all ESMs in section 2.7.1.

2.2.2 Experimental design

We conducted four idealised LCLMC simulations and one reference simulation using the three ESMs. Every simulation has the same set-up, but differs in terms of land cover and land management. As we want to remain independent of any future climate scenarios, the simulations will be performed under present-day (2015) climate forcing. They will cover the entire globe as to inform on where LCLMC might be more or less useful. Four idealised sensitivity experiments are investigated: (i) a fully afforested world (FRST), (ii) a full cropland world (CROP), (iii) a fully afforested world with extensive wood harvesting (HARV), and (iv) a full cropland world with extensive irrigation (IRR). In order to be able to distinguish between the local and non-local effects of these four idealised cases, the LCLMC perturbations are applied following the checkerboard approach of Winckler et al. (2017a) using a checkerboard pattern which is detailed in section 2.1.3, effectively meaning that only half of the grid cells undergo LCLMC. In addition, a control simulation with present-day land cover is performed by every ESM to serve as a reference (hereafter referred to as CTL). The CTL simulation uses the native, present-day land cover map of each ESM, which are all based on the Land Use Harmonization version 2 dataset (LUH2; Hurtt et al., 2020). This implies that each ESM retains its native PFTs. The CTL simulation does not include land management (i.e. irrigation and wood harvesting are set to zero) to have a clear baseline for the sensitivity simulations. In all simulations, anthropogenic forcing (including greenhouse gas and aerosol concentrations) is kept constant at the 2015 conditions. The initial conditions are provided by the CMIP6 historical simulations in 2014 and applied to the different ESMs to conduct model simulations for a period of 160 years. The first 10 years are considered as biogeophysical spin-up and omitted in the analysis. We let the stratospheric aerosols evolve transiently until 2025 based on data from the Scenario Model Intercomparison Project (ScenarioMIP), after which they are kept constant. This was done to ensure that the stratospheric aerosol concentrations in our simulations resemble the mean state of the 21th century. Due to technical constraints in CESM however, the 2025 levels were used from the start of the simulation. The solar forcing is kept at natural oscillations, except for CESM where these are set to a constant value that is chosen equal to the average over the entire simulation period. This is needed to ensure that all ESMs have the same amount of solar energy entering the system over the entire simulation period. Overall, the set-up is designed to represent present-day climatic conditions through model simulations sufficiently long to average out internal variability. All simulations are performed in fully

Table 2.2: Overview of simulation set-up for the ESMs.

Simulation	Land Cover	Land Management
CTL	2015 map	none
CROP	50% crop map, 50% CTL map	none
FRST	50% forest map, 50% CTL map	none
IRR	50% crop map, 50% CTL map	irrigation
HARV	50% forest map, 50% CTL map	wood harvesting (yr 2100 under RCP 8.5)

coupled mode, consistent with the LUMIP protocol (Lawrence et al., 2016), and at each ESM's typical spatial resolution employed for CMIP6 (lat x lon) (MPI-ESM:1.88°x1.88°, CESM:0.90°x1.25°, EC-EARTH:0.7°x0.7°).

The different LCLMC scenarios used in the sensitivity experiments are outlined in Table 2.2. The idealised land cover maps for CESM and MPI-ESM are constructed following the approach described in Davin et al. (2020) using prescribed idealised land cover maps. To create the idealised FRST land cover map, we start from the 2015 land cover map of each model. All PFTs that are neither forest nor bare soil were removed. The remaining forest fractions are increased such that fractions within a grid cell add up to 100 %. As the bare soil fraction is preserved, the resulting land cover map only contains forest PFTs and bare soil. The approach mimics forest expansion across all vegetated, cropland and urban areas but avoids that trees are planted in e.g. desert, high altitude, and tundra regions (Figure 2.1d-f). Note that this approach is only possible for grid cells containing forest PFTs. For grid cells without forest PFTs present, we calculate the latitudinal average (at each ESMs native resolution) of the relative forest PFT distribution consisting of different species. This value is then considered as representative for this latitudinal band and is used to replace all other vegetation in the grid cell. The same approach is followed for constructing the CROP map by keeping the crop fraction constant within a grid cell and removing all non-cropland PFTs (e.g. pasture, bush, forest and grassland; Figure 2.1a-c).

In EC-EARTH, as this version of the model has a dynamic vegetation model (Döscher et al., 2022) a different strategy was chosen. In order to obtain a simulation close to a 100% forest world, the managed vegetation is turned off. Consequently, the fully forested world simulation in EC-EARTH can also contain grasses. For the CROP simulation, the natural land cover is switched off, which forces the model to only grow crops within a grid cell. As in the other ESMs, bare soil fractions were retained, while only vegetated areas and urban areas where considered for land cover change. Note that this difference in implementation of the LCLMC has led to strong differences in the total extent of the LCLMC, most notably regarding the afforestation experiment where EC-EARTH shows little afforestation in contrast to MPI-ESM and CESM (Figure 2.1f). These low amounts of afforestation modelled in the EC-EARTH FRST simulation make that it is less comparable to the other ESMs for this land cover change.

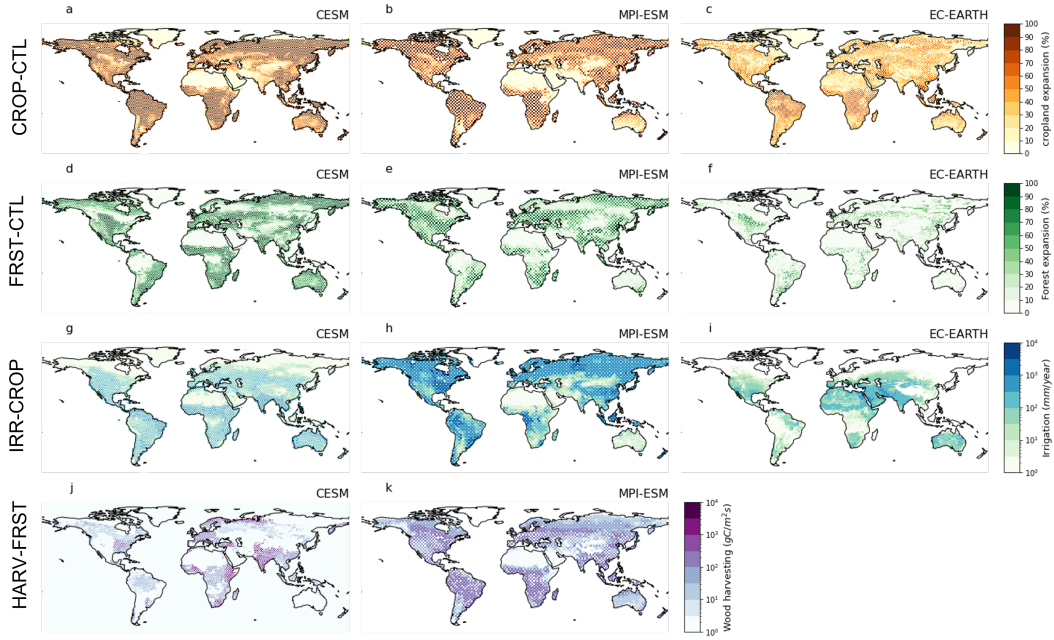

Figure 2.1: Overview of land cover and management changes modelled in the ESM sensitivity experiments. The amount of cropland expansion is shown for the CROP simulation as compared to present-day land cover (CTL) for CESM (a), MPI-ESM (b) and EC-EARTH (c). The amount of afforestation in the FRST simulation as compared to present day land cover (CTL) is shown for CESM (d), MPI-ESM (e) and EC-EARTH (f). Both land cover changes are shown as an area fraction of the land cover in that grid cell. The amount of wood harvest applied in the HARV simulation as compared to the FRST simulation is shown for CESM (g) and MPI-ESM (h) in terms of intensity of harvesting (gC $m^{-2}s^{-1}$). Finally the amount of irrigation is shown as expressed in a discharge (mm $year^{-1}$) for CESM (i), MPI-ESM (j) and EC-EARTH (k). Do note that the color bar is exponential for land management change (g-k) while it is linear for land cover change (a-f).

For the IRR simulation, we apply the same land cover maps as in the CROP simulation, but here, the native irrigation parameterisation of each model is activated and applied at the global scale (Figure 2.1g-i). Although the individual implementations of the irrigation parameterisation differ, all models follow a similar logic. Once a crop suffers a certain amount of water stress (defined differently in the models, see section 2.7.2), this amount is replenished by applying an irrigation flux until the water stress is relieved. In CESM and EC-EARTH, no limit is imposed on water available for irrigation. In MPI-ESM however, water availability is limited by the amount of runoff and drainage in the grid cell.

The amount of wood harvesting is typically a prescribed value in ESMs, often expressed as an amount of biomass carbon extracted from the PFTs. In the HARV simulation, we force the models to use the wood harvest rates specified in the CMIP6 SSP5-8.5 scenario by the end of the century (Figure 2.1j-k). We let the forest grow as in the FRST simulation without harvesting for the first 40 years to build up biomass before prescribing the intensive wood harvest rates. For the remaining 120 years of the simulation, the harvest rates are kept constant. It should be noted that EC-EARTH did not provide this simulation. In MPI-ESM, there is no feedback implemented of this management practice to any atmospheric processes. Therefore, only CESM can be used to investigate the biogeophysical effects due to wood harvesting.

The idealized sensitivity experiments are conducted under present-day climate forcing. The effects of the different LCLMC strategies represent an upper bound on the potential for global mitigation and local adaptation against the current background climate. They should therefore not be perceived as realistic futures. Both CESM and MPI-ESM show extreme land cover changes in the CROP and FRST simulations compared to CTL (Figure 2.1a-f). Overall, the land cover change is stronger in CESM than in MPI-ESM, but the spatial patterns roughly match. Some notable differences include the extent of cropland expansion in Siberia and the amount of afforestation in Australia. Do note that in panels (a) and (b), the amount of cropland expansion (i.e. all conversions to crop) shown is not equivalent to the amount of deforestation (i.e. all conversion from forest to crop) in these simulations as other conversions (e.g. bush and grassland to crop) also occur.

The comparison of land management between CESM and MPI-ESM shows strong differences, despite using a qualitatively consistent implementation across both ESMs. For wood harvesting, the spatial pattern and intensity differ notably. In CESM the wood harvesting is generally more intense locally and less homogeneous across space than in MPI-ESM (Figure 2.1j-k). For irrigation the spatial extent also differs strongly between the models. Most notably, due to the simple irrigation scheme implemented in MPI-ESM (see section 2.7.2), this model shows high irrigation amounts in the boreal latitudes while there is no irrigation occurring in CESM and EC-EARTH at these latitudes (Figure 2.1g-i). Note that within EC-EARTH, irrigation is implemented in the dynamic vegetation model LPJ-GUESS but not within the atmosphere model IFS (due to both models having a separate water cycle). Therefore climate effects within this ESM from irrigation expansion can only occur due to increased vegetation growth as a consequence of the ample water availability (Döscher

et al., 2022).

2.3 Methods

2.3.1 Extraction of local and non-local signals

To disentangle the local and non-local effects due to LCLMC, the checkerboard approach of Winckler et al. (2017a) is applied, which is described here briefly (see Winckler et al. (2017a) for details). The checkerboard approach alternates LCLMC grid cells with grid cells which remain unaltered. This allows for a clean separation of local and non-local effects as the latter only occur over unaltered grid cells while the grid cells where LCLMC did occur represent a combination of both local and non-local effects. In our simulations, 1 out of 2 grid cells are affected by the LCLMC and these cells are spread out in a regular checkerboard pattern. The checkerboard like LCLMC alternation is applied to all simulations except the CTL simulation. This means that for each simulation, only half of the grid cells undergo LCLMC. The remaining unchanged grid cells show the exact same land cover as the CTL simulation. The 150 year-simulation is split into 5 slices of 30 years each. To account for natural variability, we treat each slice as a member of a perturbed initial condition ensemble. A multi-year monthly mean is computed over each of these ensemble members. To extract the local and non-local signals, we subtract a land cover change member (CROP, FRST) from its corresponding CTL member. The resulting signals for grid cells where no land cover change occurred cannot be ascribed to any direct (i.e. local) land cover change effect and can therefore be ascribed entirely to non-local effects caused by LCLMC in other grid cells. We then spatially interpolate (using linear interpolation) these values to get a global map of non-local effects. The differences between both ensemble members for grid cells where land cover change did occur are caused by both local and non-local effects (local effects stem from the land cover change within the grid cell, while non-local effects are caused by land cover change in other grid cells). Hence, these non-local effects are subtracted from the total combined effect to get a local signal. As this local signal can only be calculated over the grid cells where land cover change occurred, we again spatially interpolate this pattern to get a full global map. Finally, the local and non-local signals are summed up to derive the total signal, which corresponds to the signal from an idealised global experiment without the checkerboard-like LCLMC pattern applied. The checkerboard approach is implemented to each model grid at its native resolution. Hence, grid cell sizes vary across the different ESMs. As we have five ensemble members of 30 years for each simulation, we can extract local and non-local signals for each ensemble member, which are then used as a measure of uncertainty coming from natural variability.

The procedure described above can be extended to land management change by using one of the land cover change simulations as a reference simulation instead of the CTL simulation. To extract the signal from irrigation expansion, the IRR simulation is compared

Table 2.3: Overview of observational products available for the different variables considered in the evaluation.(*) This data was first published in 2018 but later extended to cover a larger area in 2020, as the extended dataset is used in this study,we will refer to this dataset as DV20 from hereon. (**) Note that the sensible heat flux was obtained by the closure of the energy balance.

Dataset	Data Type	Available variables
Duveiller et al. (2018, 2020)*	remote sensing	surface temperature, latent heat flux, sensible heat flux**, albedo
Duveiller et al. (2021)	remote sensing	near-surface air temperature
Li et al. (2015)	remote sensing	surface temperature, latent heat flux, albedo
Alkama and Cescatti (2016)	remote sensing	surface temperature, near-surface air temperature
Bright et al. (2017)	flux towers	surface temperature

against the CROP simulation. In case of wood harvesting, the HARV simulation is compared to the FRST simulation.

2.3.2 Evaluation of local signal to deforestation

The modeled responses induced by deforestation are evaluated against products from observational studies. Several studies provide global estimates of the effect of deforestation with remote sensing products (Li et al., 2015; Alkama and Cescatti, 2016; Duveiller et al., 2018) or ground observations (FLUXNET Bright et al., 2017). Only the local signals can be compared here as these observations only capture local effects by design (Winckler et al., 2019a). All four observational studies represent an idealised case where a fully deforested patch of land is compared to a fully forested patch. We therefore use the local signals derived from comparing the CROP to the FRST simulation to evaluate the ESM response to deforestation against these products. It was shown by Winckler et al. (2019a,c) that a comparison between modelled response and these observational estimates is useful to evaluate the performance of ESMs to represent the effects of LCLMC on surface temperature.

The evaluation is also performed for several other variables of interest, including latent heat flux, sensible heat flux, albedo and near-surface air temperature (2 m temperature, tas in CMIP6 nomenclature), however not all of these are available in each dataset (see Table 2.3). The spatial extent of the observational studies varies strongly, therefore the evaluation will be performed along latitudinal bands following Meier et al. (2018) to focus on the global patterns. A description of the different observational datasets used and their spatial maps are provided in section 2.7.3.

2.3.3 Energy balance decomposition for changes in surface temperature

An energy balance decomposition approach is used to decompose the change in surface temperature to its driving surface processes. Here, we use this approach to understand the processes underlying the modelled effects of LCLMC. We use the approach developed by Juang et al. (2007) and modified by Luyssaert et al. (2014) which has often been used in LCLM studies, notably with CLM (Akkermans et al., 2014; Hirsch et al., 2018b; Thiery et al., 2017; Hauser et al., 2019; Vanderkelen et al., 2021). The energy balance equation is shown below.

$$\varepsilon\sigma T_s^4 = (1-\alpha)SW_{in} + LW_{in} - LHF - SHF \tag{2.1}$$

Where ε is the surface emissivity, σ is the Stefan-Boltzmann constant (5.67×10^{-8} W m^{-2} K^{-4}), T_s is the radiative surface temperature as it is directly calculated from surface upwelling longwave radiation, α is the surface albedo, and SW_{in} and LW_{in} are the incoming shortwave and incoming longwave solar radiation, respectively. LHF and SHF are the latent and sensible heat flux, respectively. All fluxes are expressed in W m^{-2}. We take the total derivative to obtain the change in surface temperature, whereby ε can be assumed to be equal to 1 for the application of this equation (Juang et al., 2007; Luyssaert et al., 2014).

$$\Delta T_s = \frac{1}{4\sigma T_s^3}(-SW_{in}\Delta\alpha + (1-\alpha)\Delta SW_{in} + \Delta LW_{in} - \Delta LHF - \Delta SHF) \tag{2.2}$$

Here, we apply the energy balance decomposition only to the local effects derived from the LCLMC signals as these are directly linked to changes in surface properties (Winckler et al., 2017a). While applying this approach, a modest global imbalance of less than 0.1 W m^{-2} is found over all land grid cells for all different cases, indicating the general applicability of the method.

2.4 Results

2.4.1 Evaluation of biogeophysical response to deforestation

We compare observational estimates to the simulated local response of full deforestation (CROP-FRST, i.e. the idealised effect of going from a full forested to a fully cropland world), in order to evaluate the modelled response to deforestation of the different ESMs. The latitudinal response of the average annual local surface temperature for all ESMs are generally within the observational range (Figure 2.2). The latitudinal change in surface temperature is similar to the observational estimates: a warming in the tropics (up to 3 K) and a cooling in the Northern Hemisphere (NH) boreal latitudes (up to -1 K). Only EC-EARTH deviates from this as it shows no cooling in NH boreal latitudes (50°N-80°N) and even shows a warming. CESM simulates a different sign compared to observations in the NH mid-latitudes (30°N-50°N), but performs reasonably well at boreal latitudes. Overall, MPI-ESM matches reasonably well to the observational estimates. In the tropics,

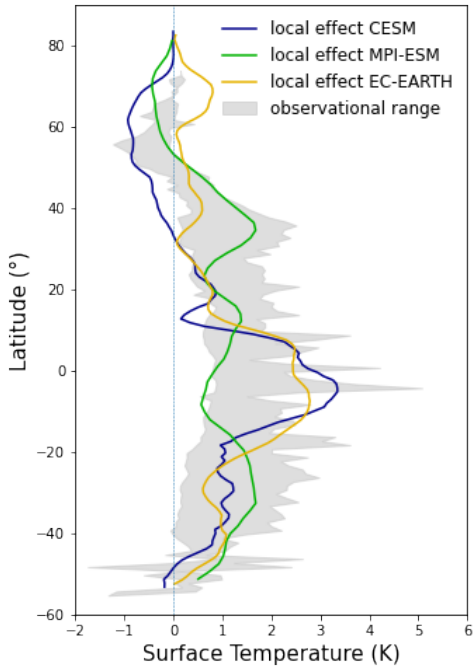

Figure 2.2: Latitudinal evaluation of local surface temperature derived from full deforestation experiments (CROP-FRST) for CESM (blue), MPI-ESM (green) and EC-EARTH (yellow). Note that for all ESMs a running latitudinal mean of 2° was computed. The observational range (grey shade) shows the full range given by four observational estimates (Li et al., 2015; Alkama and Cescatti, 2016; Duveiller et al., 2018; Bright et al., 2017).

MPI-ESM simulates values near the lower bound of the observational range (0.6 K), while CESM and EC-EARTH simulate values near the upper bound (3 K). In general, all models show a reasonable agreement with the observations, both in sign and magnitude over most latitudes; only in the NH mid-latitudes and boreal latitudes the models diverge from the observed range.

Comparing the local effect of deforestation on surface temperature across seasons generally shows a good agreement of MPI-ESM with the observational estimates for the different seasons (Figure 2.3). The CESM simulations lie within the observational range for boreal winter and fall but show a cooling response to deforestation in boreal spring and summer above 30°N, which is in contrast to the observed warming. The EC-EARTH simulations agree well with the observations except for the boreal latitudes where a sustained warming occurs over all seasons except during the boreal summer.

The effect of deforestation on annual local latent and sensible heat fluxes agrees well with

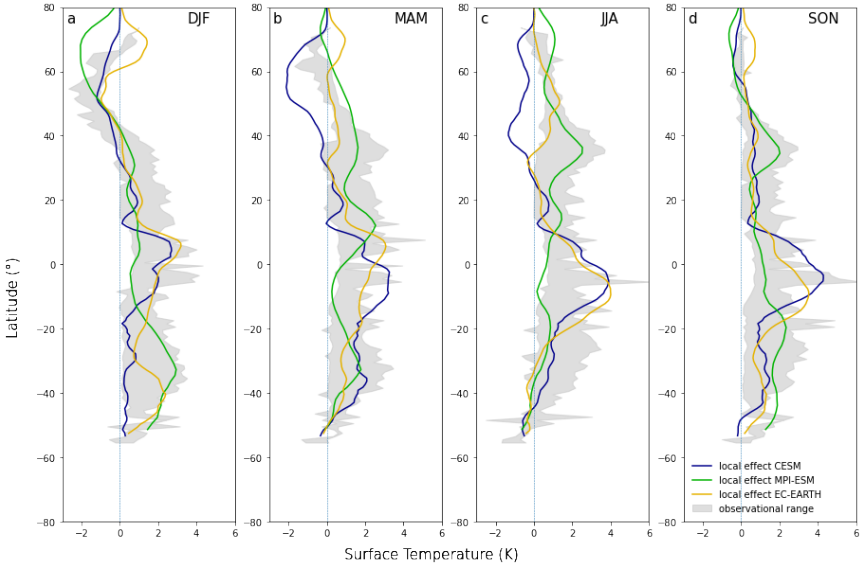

Figure 2.3: Latitudinal evaluation of local surface temperature derived from full deforestation experiments (CROP-FRST) for CESM (blue), MPI-ESM (green) and EC-EARTH (yellow) for different seasons, winter or DJF (December, January, February) in panel a, spring or MAM (March, April, May) in panel b, summer or (June, July, August) in panel c and fall or (September, October, November) in panel d. Note that for all ESMs a running latitudinal mean of 2° was computed. The observational range (grey shade) shows the full range of values spanned by four observational estimates (Li et al., 2015; Alkama and Cescatti, 2016; Duveiller et al., 2018; Bright et al., 2017).

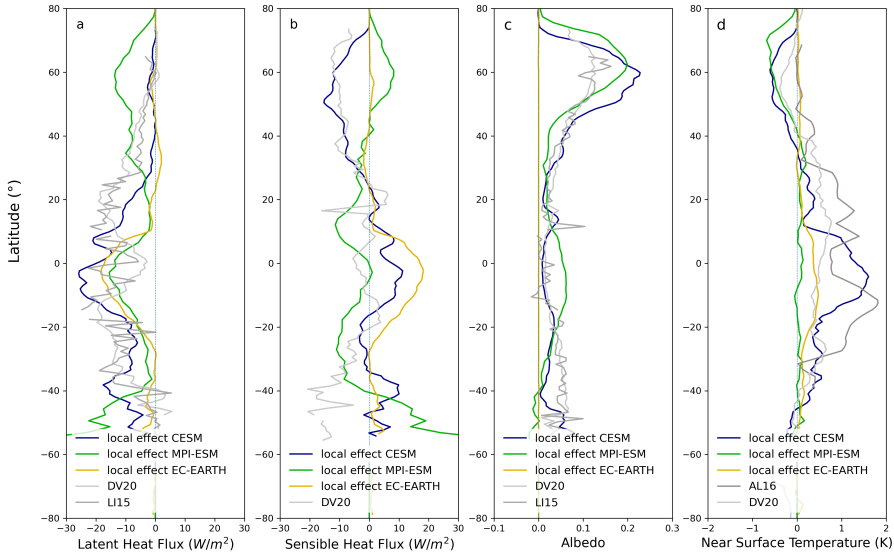

Figure 2.4: Latitudinal evaluation of local energy and climate variables derived from full deforestation experiments (CROP-FRST). The local effect simulated by CESM (blue), MPI-ESM (green) and EC-EARTH (yellow) of latent heat flux (W/m^2) (a) compared to observational estimates by Li et al. (2015); Duveiller et al. (2018) (DV20 and LI15, respectively), of sensible heat flux (W m^{-2}) (b) compared to Duveiller et al. (2018) (DV20), of albedo (-) (c) compared to Li et al. (2015); Duveiller et al. (2018) (LI15 and DV20) and near-surface temperature (K) (d) compared to Alkama and Cescatti (2016); Duveiller et al. (2020) (AL16 and DV20). Note that for all ESMs a running latitudinal mean of 2° was computed.

the observational estimates for all ESMs (Figure 2.4a, b). The latent heat flux is modelled to decrease over most latitudes. MPI-ESM underestimates the magnitude of the latent heat flux signal over most of the subtropics, and shows an overestimation over the boreal latitudes. CESM and EC-EARTH match well to the observations, except at the mid-latitudes where it underestimates the decrease in latent heat flux. EC-EARTH shows no change in latent heat flux except over the tropics where a clear decrease is shown.

Observations show a deforestation-induced decrease in sensible heat flux in the extratropics, a slight increase around 20°N and 20°S and a decrease around the Equator. CESM captures the response in sensible heat flux well in the NH but overestimates it in the tropics and projects an opposite sign over most of the Southern Hemisphere (SH). MPI-ESM underestimates the change over most of the latitudes and shows an increase instead of a decrease at boreal latitudes. Similar to the latent heat flux, EC-EARTH only shows a non-zero effect over the tropics where the model suggests a strong increase. These strong biases in both latent and sensible heat fluxes of MPI-ESM and EC-EARTH do not appear to affect the surface temperature responses. This could partially be explained by opposite signs in the biases of both turbulent heat fluxes, which cancel each other out, as is likely the case over boreal latitudes for MPI-ESM and in the tropics for EC-EARTH.

The deforestation-induced albedo change is especially important at boreal latitudes where it dominates the overall surface temperature response (Davin and de Noblet-Ducoudre, 2010). CESM captures the observed albedo response well, except north of 40°N where it overestimates the albedo change and south of 30°S where it underestimates the albedo change (Figure 2.4c). MPI-ESM shows a similar bias in the SH. It also overestimates the brightening in the tropics and boreal latitudes following deforestation and underestimates the brightening over most mid-latitudes.

The bias in albedo response north of 40°N could be caused by a strong snow masking response in both ESMs, as a snow covered forest is darker than a snow covered cropland. This would also explain the strong cooling in boreal spring and summer seasons in CESM (Figure 2.3b,c) and the bias in annual surface temperature over the mid-latitudes (Figure 2.2). In EC-EARTH the local albedo change is zero (Figure 2.4c), however there is a stronger non-local albedo change (Figure 2.15). The non-local albedo change is near-zero except over boreal latitudes (Figure 2.16). This could be caused by the differences in simulation setup for EC-EARTH where the forest needs to establish throughout the simulation (e.g., biomass and specific land surface properties such as vegetation roughness length, leaf area index and albedo) under the local environmental conditions while in CESM and MPI-ESM some of the specific land surface parameters are immediately established at the start of the simulation. This albedo bias due to differences in simulation setup likely explains the lack of cooling in boreal latitudes in EC-EARTH (Figure 2.3). The results for CESM are in contrast to Meier et al. (2018) who showed that the previous version of CLM (CLM4.5) could reproduce the observed albedo relatively well. However the differences between our results might be due to differences in model setup as CLM was evaluated in land-only mode in Meier et al. (2018) in contrast to the coupled simulations performed here.

The near-surface air temperature is often a preferred metric compared to the surface temperature, as it is more relevant for understanding the perceived temperature and is considered in most policy-relevant metrics including those used to measure global warming (Arias et al., 2021). For local near-surface air temperature change, CESM and EC-EARTH show a response of similar sign to the observations in the SH and tropics. The observations diverge north of 40°N, where the DV20 dataset confirms the cooling which is simulated by CESM and MPI-ESM. In contrast, the AL16 dataset shows no temperature change, which is also the case for EC-EARTH (Figure 2.4d). The near-surface air temperature in MPI-ESM is relatively insensitive to deforestation except north of 40°N as was also shown in (Winckler et al., 2019c). However, it should be considered that near-surface air temperature is a highly contested measure as its definition tends to vary strongly across different ESMs, especially over grid cells or grid cell fractions covered with tall vegetation (Boysen et al., 2020; Winckler et al., 2019c). Therefore, in the remainder of this study, we will focus on the response of LCLMC on surface temperature, while the maps for near-surface air temperature are added in section 2.7.4 for reference.

2.4.2 Local and non-local effects of LCLMC on surface temperature

This section provides an overview of the signal separated effects on surface temperature of the different LCLMC across the different ESMs. We discuss the local, non-local and total effects per LCLMC category. At the end of the section the changes which are consistent across all ESMs are summarized in Table 2.4.

Cropland expansion

As a consequence of cropland expansion (CROP-CTL), CESM shows a strong local cooling over the NH boreal latitudes which extends into most of the NH mid-latitudes (Figure 2.5a). The tropics and subtropics show a strong local warming of up to 4 K over the (deforested) tropical rainforests. MPI-ESM shows a similar pattern to CESM in NH boreal latitudes but with a smaller local cooling which does not extend as far south into the NH mid-latitudes. MPI-ESM also simulates local warming over the tropics, but with a different spatial pattern and magnitude compared to CESM and EC-EARTH. The local signals in EC-EARTH are similar to CESM, showing a strong local warming in the tropics. However, in NH boreal latitudes the signals are mixed, with a cooling over the (deforested) boreal forests and a strong warming over the permafrost covered areas (Siberia, Northern Canada and Alaska). This NH boreal warming is most likely due to the shift in the EC-EARTH simulation from natural land to managed land, leading shorter duration of frozen soils throughout the year which causes a soil warming.

In CESM the local cooling is amplified by a strong non-local cooling over these regions. The non-local effect in MPI-ESM strongly differs from CESM. While CESM simulates a widespread cooling, MPI-ESM shows a weaker but clear warming over the boreal regions, Europe and Eastern USA. The non-local effect in EC-EARTH is mixed with a warming

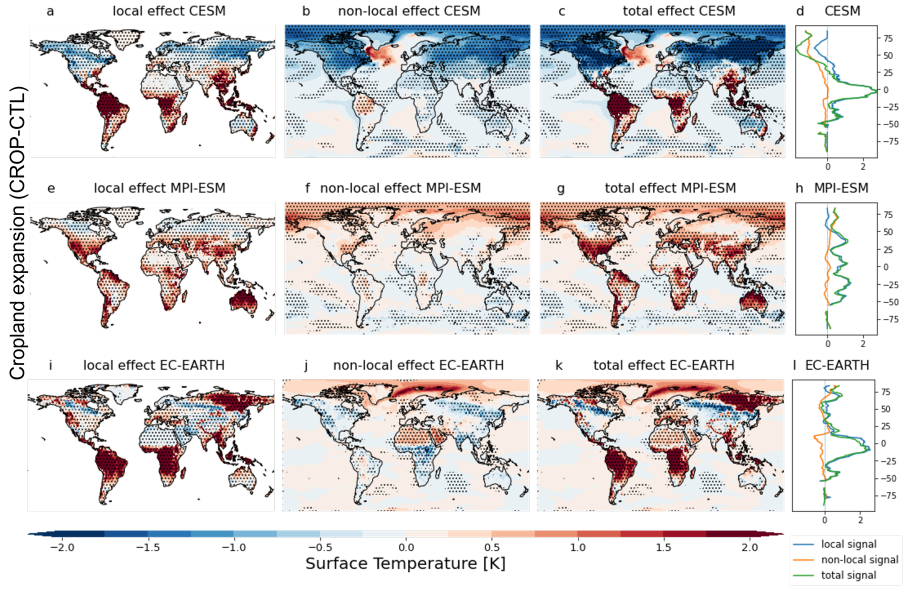

Figure 2.5: Annual mean surface temperature response to cropland expansion (CROP-CTL) of CESM (top row), MPI-ESM (middle row) and EC-EARTH (bottom row). For CESM: the local effect (a), the non-local effect (b) and the total effect (c), the global latitudinal average of the local (blue), non-local (yellow) and total (green) signals (d). (e-h): same as (a-d), but for MPI-ESM. (i-l): same as (a-d), but for EC-EARTH. The stippling on the maps shows grid cells where all 5 ensemble members agree on the sign of change.

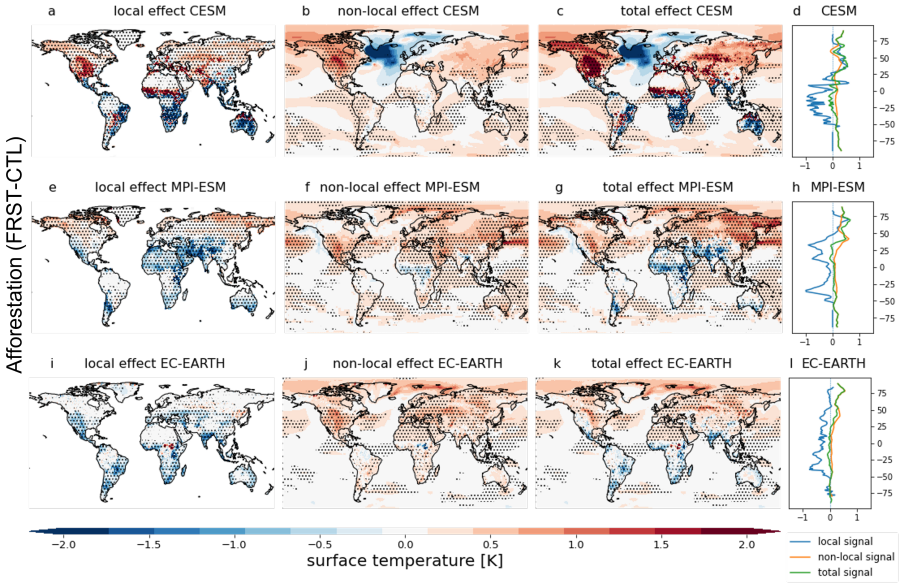

Figure 2.6: Same as Figure 5 but for afforestation (FRST-CTL).

over the Arctic regions and the Sahara, and a cooling in the mid-latitudes and tropics. In all ESMs the local signals dominates the total response in the tropics. The non-local effect also dominates over NH boreal latitudes in CESM and MPI-ESM while in EC-EARTH the pattern differs regionally.

Afforestation

In the afforestation sensitivity experiment (FRST-CTL), the local response is similar to the response in the cropland expansion sensitivity experiment, but shows an opposite sign, as expected (Figure 2.6). A local cooling is simulated over the tropics for all ESMs and a local warming over the boreal latitudes for both MPI-ESM and CESM. The shift from cooling to warming occurs at a higher latitude in MPI-ESM and EC-EARTH compared to CESM. The lack of local boreal warming in EC-EARTH is probably related to the differences in experimental setup and the resulting low amounts of afforestation in this simulation (Figure 2.1f). The non-local effects due to afforestation result in warming for all ESMs, except over the North Atlantic in CESM. This indicates that the non-local effect is dominated by the albedo decrease, which originates from the strong snow masking effect of forest compared to open cropland. This is also indicated by the fact that the non-local warming dominates over the extratropics for all ESMs, in contrast to the local cooling which dominates over the tropics and parts of the subtropics (depending on the ESM).

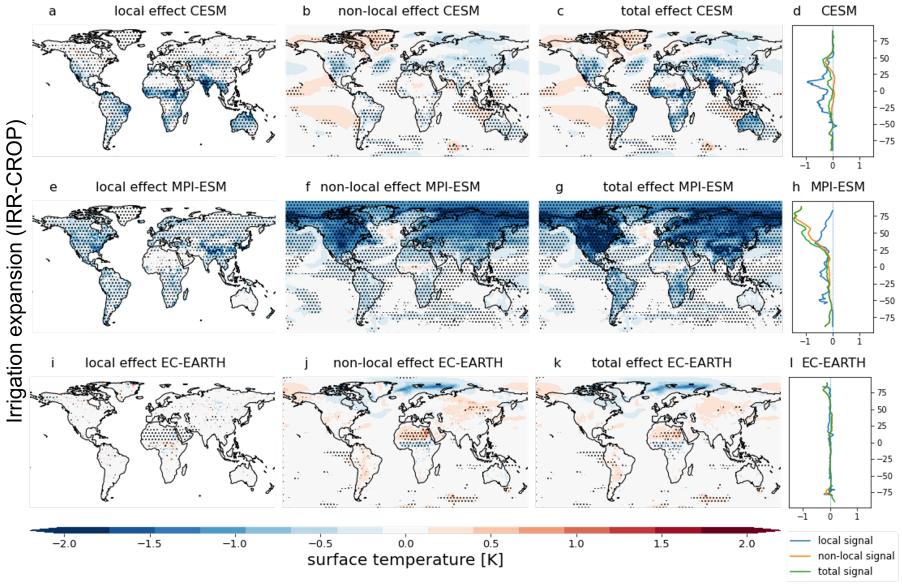

Figure 2.7: Same as Figure 5 but for irrigation expansion in a cropland world (IRR-CROP).

In CESM, this albedo-induced warming causes a cooling blob in the North Atlantic (Figure 2.6b). A similar but opposite pattern is also apparent in the cropland expansion experiment with CESM (Figure 2.5b), but appears as a warming blob with lower magnitude. The same warming blob was also found in the LUMIP deforest-glob experiments by Boysen et al. (2020). A plausible explanation for this dynamic is the different latitudinal effect of the LCLMC option. With a high-latitude hemispheric warming and a slight cooling in low latitudes, the thermodynamic response of the Atlantic Meridional Overturning Circulation (AMOC) would indicate a weakening due to a decrease in the temperature gradient, similar to thermodynamic driven AMOC weakening due to arctic amplification under climate change scenarios (Schleussner et al., 2014). Inversely, global-scale cropland expansion causes non-local cooling except for a localised warming over the North Atlantic. It should be noted, however, that this strong North Atlantic response in CESM is not consistent throughout the entire simulation period despite its high magnitude. The global non-local warming pattern has large implications for future deployment of land-based mitigation strategies, especially for boreal afforestation. However, it should be noted that non-local signals are highly dependent on the spatial pattern as well as the extent of the prescribed land cover change (Winckler et al., 2019b)

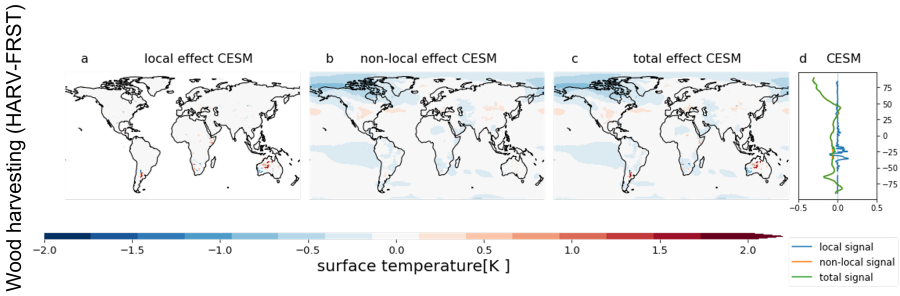

Figure 2.8: Same as Figure 5 but for wood harvest expansion (HARV-FRST). Only results for CESM are shown as MPI-ESM does not simulate biogeophysical effects of wood harvesting and EC-EARTH did not conduct these simulations.

Irrigation expansion

In the idealised irrigation expansion sensitivity experiment (IRR-CROP, i.e. irrigation expansion in a full cropland world), both MPI-ESM and CESM agree on the irrigation-induced reduction in local surface temperature, while irrigation expansion in EC-EARTH does not induce any local effects (Figure 2.7). The very limited local effects in EC-EARTH are caused by a lack of moisture exchange between IFS and LPJ-GUESS, whereby water added in LPJ-GUESS for irrigation does not affect the moisture fluxes in IFS. Hence, in EC-EARTH, irrigation affects crop growth and albedo but does not alter turbulent surface fluxes. In MPI-ESM and CESM, temperature decreases globally due to irrigation expansion, but there are substantial differences in the spatial patterns between the models. These differences partially stem from the large differences in irrigation amounts imposed in the different models (Figure 2.1i-k). EC-EARTH shows some non-local temperature effects but these are small in magnitude and the sign differs across different regions. In CESM, the total signal is dominated by the local response, with only a modest contribution of non-local effects. The non-local irrigation signal in MPI-ESM is generally stronger than the local signal and dominates the total response.

These results corroborate the findings of Thiery et al. (2017) and Chen and Dirmeyer (2019), who found that irrigation has a cooling potential due to an increased latent heat flux over irrigated areas. CESM simulates strong local cooling effects in the subtropics and tropics, while MPI-ESM shows the strongest local cooling in the NH mid-latitudes and less apparent local cooling in the tropics. In CESM, there is a non-local irrigation-induced cooling over the NH mid-latitudes where the local effects are generally small. This indicates that in these latitudes a non-local effect, plausibly due to an increase in cloud cover, dominates the effects of irrigation rather than surface processes like evaporative cooling, which dominate the local effects over the tropics. For MPI-ESM, a strong increase in cloud cover appears to cause the strong non-local cooling (Figure 2.31).

Table 2.4: Summary of local and non-local effects due to the different LCLMC. Each cell indicates where the changes in surface temperature response are consistent in sign.

LCLMC	Local effects	Non-local effects	Total effects
cropland expansion	tropical warming	none	tropical warming
afforestation	tropical cooling	global warming	warming across boreal latitudes and cooling over tropics
irrigation expansion	regional cooling	regional cooling	regional cooling

Wood harvest expansion

The effect of wood harvesting (HARV-FRST) appears to be very small (Figure 2.8). There is generally no local effect and the non-local signal is overall weak and inconsistent in sign across the CESM simulation. The simulated non-local signals may well stem from internal climate variability rather than an actual response to land management change. These results imply that the biogeophysical effects of wood harvesting, as simulated here, are too weak to have a significant imprint in global and local climate conditions at the grid scale in the represented ESMs. This does not imply that the biogeophysical effects cannot play a role locally, but simply suggests that these effects are not strong enough to be discerned at the currently used grid scale level and with the process-detail of current ESMs. An analysis comparing the simulation results at the tile level (within a grid cell) would provide an alternative approach to analyse possible local effects due to wood harvesting.

2.4.3 Energy balance decomposition of the surface temperature changes

Cropland expansion

Using Equation 2.2, the different factors contributing to the response in surface temperature are assessed when aggregated zonally (Figure 2.9) and seasonally (Figure 2.10). In the case of cropland expansion, the warming in the tropics for all ESMs is mostly caused by a strong decrease in latent heat flux, possibly as a consequence of a decreased evaporation capacity (Figure 2.9a and b). The simulated decrease in sensible heat flux in MPI-ESM reduces the heat transport away from the surface, therefore amplifying the warming, while in CESM an increase in sensible heat contributes to a cooling. In MPI-ESM the tropical warming is slightly offset by an albedo increase. In all ESMs, local changes in shortwave and longwave radiation increase the warming signal, however, in EC-EARTH the contribution from enhanced incoming longwave radiation is especially strong, which could indicate that atmospheric properties such as high cloud cover or atmospheric moisture have a strong influence on surface temperature in this model. In CESM over boreal latitudes, the increase in albedo dominates the surface temperature response causing a local cooling which is partly offset by a warming induced by a decrease in sensible heat flux. In MPI-ESM, this boreal albedo effect is much weaker causing no clear local cooling.

In EC-EARTH, the energy balance components do not explain the simulated warming over boreal latitudes, which is most likely related to the fact that EC-EARTH uses the tempera-

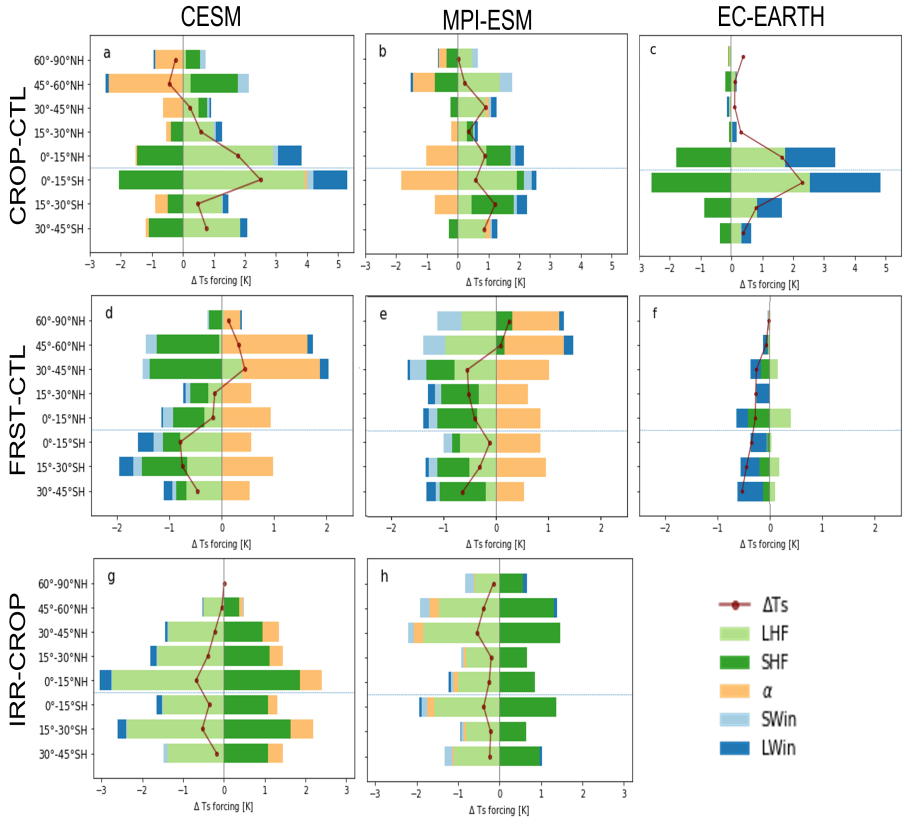

Figure 2.9: The energy balance decomposition of the local surface temperature for the different latitudinal bands. The response to cropland expansion (CROP-CTL) for CESM (a), MPI-ESM (b), and EC-EARTH (c), the response to afforestation (FRST-CTL) for CESM (d), MPI-ESM (e), and EC-EARTH (f) and the response to irrigation expansion (IRR-CROP) for CESM (g) and MPI-ESM (h). EC-EARTH is not shown for irrigation expansion as the local effects are too small for any meaningful analysis.

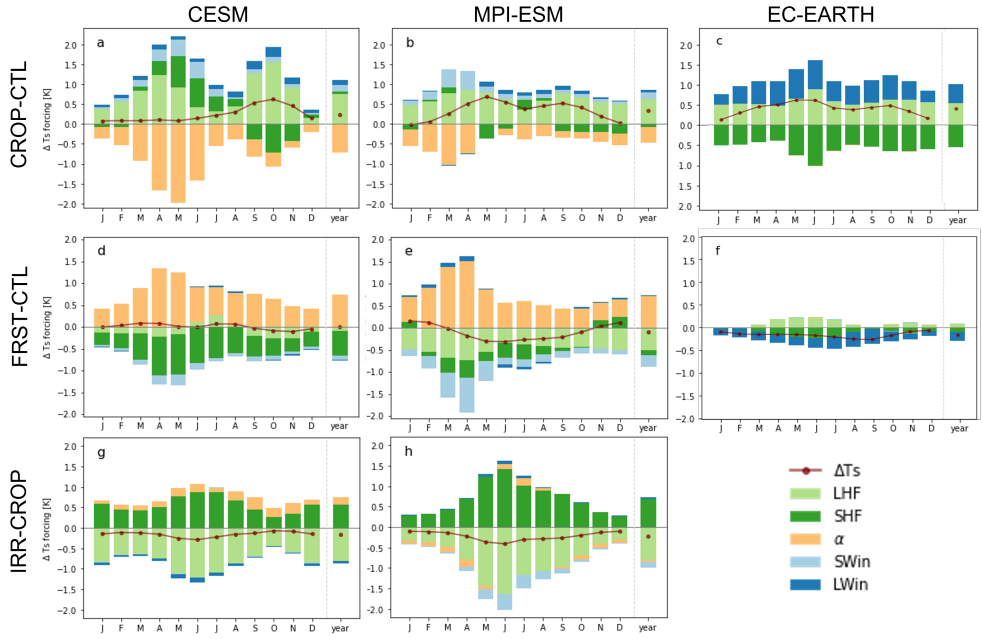

Figure 2.10: Global average seasonal cycle of energy balance decomposition of local surface temperature. The response to cropland expansion (CROP-CTL) for CESM (a), MPI-ESM (b), and EC-EARTH (c), the response to afforestation (FRST-CTL) for CESM (d), MPI-ESM (e), and EC-EARTH (f) and the response to irrigation expansion (IRR-CROP) for CESM (g) and MPI-ESM (h).

ture of the first whole soil layer as surface temperature. As a consequence, other processes that are not related to the surface energy balance (e.g. permafrost thawing) also affect the surface temperature in this model. Finally, contrasting to the other models, the albedo in EC-EARTH does not influence the local surface temperature changes, as there is no change in local albedo (see Figure 2.18).

The cooling effect of albedo due to cropland expansion has a pronounced seasonal response in both MPI-ESM and CESM (Figure 2.10a and b). It is most outspoken during NH spring as a consequence of the reduced snow masking effect. In both MPI-ESM and CESM, the latent heat flux has a strong contribution throughout the year. It shows a seasonality which is most pronounced in CESM, peaking in early spring and fall. The sensible heat flux has a warming effect in CESM throughout most of the year except during the NH fall when it shows a cooling effect. In EC-EARTH the sign of all changes is constant throughout the year. There is a slight seasonal effect for the magnitude of the turbulent heat fluxes and longwave incoming radiation being largest in NH summer and lowest in NH winter. Overall, all ESMs simulate a global surface warming of about 0.3 K due to the local effect of cropland expansion over the year and show a minimal warming in the NH winter.

Afforestation

In the case of afforestation, all models show a reduction of the surface temperature in the SH and tropics (Figure 2.9d,e,f). In MPI-ESM and CESM, this is caused by the cooling effect of increasing turbulent heat fluxes, which is partly counteracted by a warming effect due to an albedo decrease. This albedo effect becomes dominant when moving northward and causes a local warming in CESM starting from the mid-latitudes and in MPI-ESM starting from the boreal latitudes. In EC-EARTH, the cooling is caused by changes in sensible heat flux and incoming longwave radiation, but is counteracted by a decrease in latent heat flux. At boreal latitudes, the albedo-induced warming is partly counteracted by an increase in sensible heat flux in CESM, and by an increase in latent heat flux and a decrease in incoming shortwave radiation in MPI-ESM. The decrease in incoming shortwave radiation might be caused by an afforestation-induced local increase in cloud cover (as shown in Figure 2.26). This would be in line with the theoretical understanding that an increase in latent heat flux causes an increase in low cumuliform clouds (Ban-Weiss et al., 2011). Recent observational results show an afforestation-induced cooling effect related to increased cloud cover (Teuling et al., 2017; Duveiller et al., 2021). However, neither CESM nor EC-EARTH represent this increase in cloud cover, with CESM even showing a slight decrease in cloudiness over boreal latitudes (Figure 2.26).

The albedo-induced effect of afforestation has a clear seasonal peak during NH spring for both MPI-ESM and CESM (Figure 2.10c and d). The turbulent heat fluxes seem to follow a similar seasonality. This indicates that extra-tropical afforestation is dominating the global climate response for these models due to a strong albedo response largely counteracted by the changes in turbulent heat fluxes. In EC-EARTH, a similar seasonal pattern is visible

with larger fluxes in NH summer and smaller fluxes in NH winter as was also the case for cropland expansion. Overall, all models show limited local effects due to afforestation, being quasi 0 K in CESM, -0.15 K in MPI-ESM and 0.2 K in EC-EARTH.

Irrigation expansion

For irrigation, only results for MPI-ESM and CESM are shown as the local surface temperature changes in EC-EARTH are too small for a meaningful decomposition in energy balance components. Both MPI-ESM and CESM show a very different geographic pattern for the irrigation flux (Figure 2.1). However, the models appear to be largely consistent when it comes to the identification of the underlying processes causing the change in surface temperature (Figure 2.9e and f). The increase in latent heat flux dominates the response. This causes a strong cooling which is counteracted by a strong (but weaker) warming effect caused by the decreased sensible heat flux. Surface albedo increases slightly in CESM as wet soils are darker. This change contributes to a rise in surface temperature. MPI-ESM, in contrast, shows a slight decrease in albedo contributing to a lowering of surface temperature. We hypothesise that this albedo decrease in MPI-ESM is a consequence of irrigation causing greener, hence brighter, crops. Longwave and shortwave radiation both give a cooling contribution due to a local increase in cloudiness (Figure 2.31).

The seasonal pattern of irrigation is dominated by the application of irrigation during the dry season (Figure 2.10e and f). As most land is located in the NH, we find the strongest local cooling during NH spring and summer. This seasonal pattern is stronger in MPI-ESM as irrigated croplands extend more northward than in CESM (Figure 2.1g,h). Globally both models predict a slight global cooling effect of around 0.2 K.

2.5 Discussion

2.5.1 Robust patterns in the local response to LCLMC across ESMs

Our results show clear consistencies across CESM, MPI-ESM and EC-EARTH. All three ESMs are able to simulate a response of average annual surface temperature to full deforestation consistent with observational evidence. There remain some clear biases when comparing the ESMs to observations such as a strong albedo response in CESM in the mid-latitudes and a strong (soil-related) warming response in the high latitudes in EC-EARTH. However, general observed patterns such as local cooling over boreal forests and local warming over tropical forests are well captured by the ESMs. The consistency in surface temperature response across ESMs and observations is in stark contrast to the large spread in signals of the turbulent heat fluxes and albedo, which have been highlighted as some of the main driving processes of local temperature change (Davin and de Noblet-Ducoudre, 2010; Winckler et al., 2019c). The energy balance decomposition for the cropland expansion confirms these model biases, which moreover differ across ESMs. For afforestation and cropland expansion, all ESMs show that the tropical response is mainly caused by a

change in turbulent heat fluxes. However, they disagree on how these changes occur. All three ESMs show that local latent heat flux changes determine the surface temperature response in the tropics. However, the role of local sensible heat flux changes differs across ESMs, showing a cooling effect in CESM and EC-EARTH in contrast to MPI-ESM where it has a warming effect. Over boreal latitudes, the albedo dominates the local effect for both cropland expansion and afforestation in CESM and for afforestation in MPI-ESM. EC-EARTH shows that permafrost thawing (unrelated to land cover change) is causing the simulated warming in the cropland expansion experiment. For irrigation expansion, MPI-ESM and CESM consistently show that the increase in latent heat dominates the surface temperature response, causing a local cooling. In the current EC-EARTH setup, there is no coupling of land surface moisture by water fluxes to the atmosphere caused by irrigation are not modelled, hence the only effect on the climate is due to increased growth of crops and respective changes in physical properties.

Although we have harmonised the land cover and management representation across the different models, strong differences remain, most notably in the implementation of irrigation expansion and afforestation (Figure 2.1). This implies that the comparison of the different simulations across ESMs is not perfect and inconsistencies can be caused by disparity in model structure, by spatial differences and differences in extent and implementation of the applied LCLMC. As for afforestation, the differences found here were mainly caused by the differences of implementation of forests in EC-EARTH (where the forest and respective land surface properties change throughout the simulation) compared to CESM and MPI-ESM which start of with a physical forest and its land surface properties. The differences regarding land management are a direct consequence of these implementations being fairly recent in the various ESMs. There is no consistency in the implementation approach for land managements such as irrigation expansion across ESMs, as was also the case in the early land cover change inter-comparison projects (De Noblet-Ducoudré et al., 2012). Over the last decade several improvements were made regarding land cover change to make the ESMs more consistent. For example, using common datasets (Hurtt et al., 2020) and common simulation protocols like the LUMIP experiments under CMIP6 (Lawrence et al., 2016). The same issues that ESMs faced before for land cover change are now apparent for land management change as well. As more ESMs are implementing land management change (Blyth et al., 2021), it is crucial that common datasets and simulation protocols are set up in order to ensure comparability across the various ESMs.

However, despite these limitations our results show that there remain similarities in the LCLMC response in the different ESMs, most notably regarding the local effects. A consensus is emerging regarding the local effects of deforestation/afforestation with a clear cooling/warming at boreal latitudes and a warming/cooling in the tropics, as is in line with observational evidence. The cooling potential of irrigation (both local and non-local) is confirmed by both MPI-ESM and CESM. However, more research is needed to understand the full implications of these biogeophysical effects. The cooling effects induced by irrigation might be offset by the increased humidity and overall induce an increase in heat stress (Mishra et al., 2020). The effects on warm and cold extremes remain to be investigated as

well, but lie beyond the scope of the current study.

Our results highlight the importance of including possible local biogeophysical effects in future land use and land management policies. The current policies underpinning large-scale climate mitigation plans such as the European Green Deal are set up to only take into account the biogeochemical effects of LCLMC strategies such as afforestation. The European Green Deal plans (European Commission, 2020) rely heavily on afforestation as a possible negative emission technology to enhance the land sink by planning to plant up to 3 billion trees within the EU. However, beyond the positive consequences of afforestation on carbon storage, its biogeophysical effects should also be considered in order to plan for (or avoid) side-effects for regional temperature induced by local processes (as shown in Figure 2.6a,e,i). The local biogeophysical effects imply some positive side-effects over specific regions, such as the tropics and mid-latitudes, especially during the summer season; however they could also imply some negative side-effects over the boreal latitudes and part of the mid-latitudes during the winter season. These findings are in line with Windisch et al. (2021) who highlight the existence of various trade-offs between local biogeophysical effects and biogeochemical effects depending on the season and region. These results further strengthen the need for the inclusion of local biogeophysical effects next to biogeochemical effects in order to have an accurate idea of the mitigation potential of forests in LCLMC policies.

2.5.2 Inconsistent non-local effects across ESMs due to idealised cropland expansion

The global non-local cooling in CESM as shown in Figure 2.5 is consistent with the findings of a previous global deforestation simulation using the checkerboard approach performed by Winckler et al. (2019b) with MPI-ESM. However, these results strongly contrast with the non-local response found in MPI-ESM here. Some methodological differences should be noted here: Winckler et al. (2019b) performed a fully idealised deforestation experiment, which is more akin to CROP-FRST comparison in this study than the results of CROP-CTL shown here. It should be noted that for full deforestation (i.e. CROP-FRST) all ESMs (including MPI-ESM) predict a non-local cooling (Figure 2.14), which is consistent with Winckler et al. (2019b). The effect of a cropland expansion (CROP-CTL) in MPI-ESM, which starts from present-day forest extent, results in a clear non-local boreal warming. Two possible mechanisms could explain this counter-intuitive discrepancy between the non-local response of MPI-ESM and CESM in CROP-CTL, in contrast to their consistent results for CROP-FRST: (i) MPI-ESM shows a weaker albedo effect when compared to CESM (Figure 2.5c), additionally (ii), the MPI-ESM model shows a strong decrease in annual boreal cloud cover (see Figure 2.21), which is especially strong in boreal summer (not shown) and could cause an additional warming, possibly offsetting any non-local cooling caused by changes in albedo.

In summary we can state that the non-local effects due to full deforestation presented here are in line with literature (Winckler et al., 2019b). However, the non-local effects display

a larger uncertainty when it comes to the non-local effects of cropland expansion from present day conditions (i.e. CROP-CTL as presented here). It should be noted that due to the strong albedo bias in CESM over NH mid-latitudes (see Figure 2.4d) and the crucial role of albedo in determining the non-local effects, it is probable that the strong non-local cooling shown over CESM is an overestimation.

2.5.3 Non-local biogeophysical response due to land-based mitigation and adaptation

Non-local biogeophysical effects can regionally dominate over local biogeophysical effects. The distinct non-local warming found for afforestation is consistent with the inverse outcome obtained from global deforestation experiments in literature (Winckler et al., 2019b; Davin and de Noblet-Ducoudre, 2010) and is robust across the different ESMs considered here (Figure 2.6b,f,j). However, the strong divergence in outcome from the cropland expansion experiments do show that the albedo effect does not completely control the non-local surface temperature responses. A variety of atmospheric processes affecting the atmospheric moisture balance and large-scale atmospheric dynamics need to be assessed in order to better understand the relevant processes. In CESM a large-scale land cover change even appears to affect global ocean circulation, as was illustrated by the strong AMOC response within this model. It should be noted that this is not a single model feature, as similar AMOC anomalies were visible for two other ESMs in the LUMIP deforestation simulations (Boysen et al., 2020). More research is needed to fully understand the processes that cause the non-local biogeophysical effects related to large-scale land cover change shown here.

Irrigation clearly decreases temperature in both CESM and MPI-ESM, constituting another demonstration that deploying irrigation could entail side-benefits for local temperature reduction especially over agricultural land (Thiery et al., 2017, 2020; Hirsch et al., 2017). These results even suggest that achieving climate benefits could become an objective of irrigation deployment, making it potentially a deliberate adaptation strategy if constraints to its implementation (related for example to water availability or socioeconomic enabling conditions) can be overcome. However, it remains unclear whether the irrigation-induced cooling is predominantly local (induced by turbulent heat fluxes) or non-local (induced by cloud effects), and what the combined effect is of irrigation-induced changes in temperature and humidity patterns on heat stress. Nevertheless, these results help assess the future climate consequences of irrigation expansion. Irrigation has been projected to increase in the future as a means to increase agricultural productivity (van Maanen et al., 2022; Rosa et al., 2020) but it may also aggravate future water stress (Haddeland et al., 2014). It should be noted that irrigation is implemented in a highly idealised way in these simulations, with 2 out of 3 ESMs not being constrained by water limitations. These water limitations should be assessed before irrigation expansion can be considered as a viable adaptation option in any region.

Overall, our results show that future land-based mitigation strategies will need to consider the non-local biogeophysical consequences of LCLMC patterns, as large-scale afforestation is a key strategy in intensive land-based mitigation scenarios (Smith et al., 2015; Humpenöder et al., 2014), especially in those compatible with a 1.5 K world (Roe et al., 2019). In particular, the robust non-local biogeophysical warming from global afforestation presented in this study indicates that future land-based mitigation strategies would lead to an even more extensive unintended warming than the local biogeophysical warming that has been widely reported for boreal regions and the mid-latitudes in winter. More research is needed to bridge the knowledge gaps regarding which regions would be mostly responsible for this non-local warming if afforested and what would be the magnitude of this warming in realistic afforestation scenarios.

2.5.4 Limitations and outlook

The idealised simulations performed in this study give an overview of the potential biogeophysical effects from LCLMC. We were able to separate local and non-local effects due to the application of a checkerboard like LCLMC perturbation to our idealised land cover maps (Figure 2.1). The local effects are only caused by changes occurring within the grid cell. Hence, they represent the most extreme possible outcome of the application of a certain LCLMC within that single grid cell, without accounting for other LCLMC around the globe. In contrast, the non-local signals are a compound response caused by the LCLMC around the globe. These represent an underestimate in magnitude of the non-local effects in a simulation of global LCLMC, as due to the checkerboard pattern, non-local effects are the consequence of LCLMC applied to only half of the grid cells around the globe. As the non-local effects, by design, also capture all internal climate variability they are more uncertain than the local effects presented here. To limit the uncertainty related to climate variability as much as possible, the simulations could be repeated within an ensemble setup. However, such setup would require substantial additional computation and storage resources.

Furthermore it should be noted that the application of the checkerboard approach has some methodological implications, as the resulting local and non-local signals intrinsically contain an interpolation error. Although we tried to minimise this error by using a checkerboard pattern of 1 out of 2 grid cells, this error can still reach up to 0.3 K based on previous simulations with MPI-ESM (Winckler et al., 2017a). Moreover, the approach has limitations due to the size of a grid cell in the different ESMs. The land cover change needed to get a local effect as presented here remains highly unrealistic (around 100 km). As ESMs are becoming computationally more efficient and their resolution gets increased, the validity of this assumption could be tested using higher resolution ESMs.

Some biases exist within the evaluation approach as the modelled surface temperature does not exactly match the radiative surface temperature measured in the observational estimates. For instance, the satellite measurements have an inherent sampling bias as they only measure during cloud free conditions. Also, the different observational estimates

have different and often non-overlapping spatial coverage. Nevertheless, these observational studies using a diversity of approaches show a large consistency among themselves and thus can act as a benchmark for the representation of land cover change within ESMs (Winckler et al., 2019a,b).

The results shown within this paper highlight some clear consistencies across the ESMs, however, often the ESMs tend to show differences as well. For example, more work is needed to improve the representation of irrigation, especially for EC-EARTH and MPI-ESM. As MPI-ESM suffers from unrealistic irrigation amounts, especially in the boreal regions while underestimating the potential irrigation in the subtropics such as India. Furthermore, EC-EARTH is currently not a viable model for a study of the biogeophysical effects of irrigation, as water fluxes from land are not communicated to the atmosphere. This limitation is worth addressing as the implementation of irrigation in ESMs has been shown to make them more realistic over regions of intense irrigation (Al-Yaari et al., 2022). Regarding land cover change, all ESMs still struggle to replicate observed patterns in energy fluxes (Figure 4). CESM has a strong overestimation of the albedo in the intermediate latitudes (30°N-50°N) with clear temperature biases over these regions, an issue which could be considered in future development of this ESM. The afforestation implemented in EC-EARTH in this study could have been improved and made more comparable to the other ESMs by changing the simulation setup. For example by forcing forest to exist from the start of the simulation (as was done in MPI-ESM and CESM) instead of allowing EC-EARTH to model afforestation as default within the dynamic vegetation model LPJ-GUESS.

The simulations presented here are unique as they combine a multi-model approach with a direct separation of local and non-local effects. Further analyses could investigate the effects of LCLMC beyond the seasonal and mean changes in surface properties, heat fluxes, and temperature. These simulations allow to analyse both the transient response of LCLMC-induced biogeochemical effects, and the socioeconomic impact from their biogeophysical effects. The non-local effects presented here can further be analysed to gain a better understanding of the circulation changes induced by the LCLMC. A moisture tracking analysis could be performed to investigate the effects on global precipitation patterns, as previous studies showed that Amazonian deforestation could induce a drying of the region (Lejeune et al., 2015). The local effects diagnosed from these extreme sensitivity experiments could also be used as training data for less computationally expensive statistical models to emulate biogeophysical effects arising from less extreme and more realistic LCLMC scenarios. Overall, we hope that the results of the simulations presented here can help increase the present understanding of LCLMC and build towards a framework that facilitates the inclusion of biogeophysical effects of LCLMC in future policy frameworks.

2.6 Conclusions

In this study, we showed the first results of a new slate of fully-coupled ESM simulations within a multi-model framework targeted at analysing the effects of land cover and land management change (LCLMC). We simulate the global biogeophysical response to (i) cropland expansion (ii) afforestation, (iii) irrigation expansion and (iv) wood harvesting, using the Community Earth System Model (CESM), the Max Planck Institute Earth System Model (MPI-ESM) and the European Consortium Earth System Model (EC-EARTH). We apply the checkerboard approach of Winckler et al. (2017a) to disentangle the local and non-local biogeophysiscal effects.

A model evaluation is performed for a global deforestation scenario using the local effects derived from the ESM simulations and several observational estimates. All ESMs agree well with the observed annual mean surface temperature change. CESM, however, overestimates the albedo in boreal and mid-latitudes, and persistently locates the transition from local warming to local cooling more south compared to the observations. A soil-induced effect in EC-EARTH causes a warming in boreal latitudes. MPI-ESM and EC-EARTH show strong differences in the representation of the turbulent heat fluxes despite their overall agreement with observed surface temperature changes.

The biogeophysical effects of idealised LCLMC are shown to be important and non-negligible to understand the overall climate impact of LCLMC. Deforestation causes a local warming in the tropics and a cooling over boreal latitudes for all ESMs. For afforestation, a clear tropical cooling is consistent across ESMs. The non-local effects carry more uncertainty which may be due to a wider variety of mechanisms at play and due to the strong natural variability intrinsic to atmospheric processes. However, this would require further investigation to be confirmed. All ESMs show a strong non-local warming as a consequence of large-scale afforestation. Irrigation expansion cools the climate both through local and non-local effects, although the contribution of local and non-local effects to this cooling is inconsistent across ESMs. Finally, the effect of extensive wood harvesting is shown to be too small to have a clear imprint on the grid-scale climate.

The driving processes underlying the local surface temperature effects were analysed using an energy balance decomposition technique. The local surface temperature effects of land-cover change (both cropland expansion and afforestation) are dominated by the response in turbulent heat fluxes in the tropics. In the case of afforestation, the albedo is the dominant factor in boreal latitudes for MPI-ESM and CESM. This is also the case for the local effects in the cropland expansion experiment for CESM, in contrast to the MPI-ESM where turbulent fluxes dominate in the boreal latitudes. In EC-EARTH, the boreal surface temperature change could not be explained by the energy balance decomposition, as the boreal warming is caused by processes that are not included in the simplified version of the surface energy balance, such as permafrost thawing. Moreover, the strong influence of incoming longwave radiation indicates that atmospheric properties (such as cloud cover and moisture content) are strongly related to local surface temperature changes. Both CESM and MPI-ESM agree

that the main local surface temperature response due to irrigation is driven by a strong increase in latent heat flux which is only partly counteracted by a decrease in sensible heat flux.

Overall, our results confirm that the biogeophysical effects of LCLMC are an important factor to consider in future land planning strategies, especially as they reveal the robust importance of non-local climate responses in the context of mitigation potential of land cover change. In the case of large-scale afforestation specifically, the non-local response could lead to global-scale unintended warming, in particular over the boreal and mid-latitude regions.

Data and code availability

CESM is an open source model which can be freely downloaded here (`https://www.cesm.ucar.edu/models/cesm2/release_download.html`). The scripts used for the signal separation of the 3 ESMs, the evaluation and the energy balance decomposition can be found on the github page of the hydrology department of VUB (`https://github.com/VUB-HYDR/2022_De-Hertog_etal_ESD`). The data analysed within this study can be found here `https://www.wdc-climate.de/ui/entry?acronym=DKRZ_LTA_1147_ds00001`, the simulation data used in this paper (more than 180 TB for CESM) will be made available through the dkrz, for those interested in using these data please contact the authors.

2.7 Supplementary material

2.7.1 Differences in forest fractions in CTL land cover maps

In Figure 2.11 the fraction of deciduous, evergreen and total forest cover are shown for the 3 ESMs. This is to illustrate the differences in the CTL land cover maps which stem from a different definition of the natural PFTs in each ESM. Although all ESMs are based on the LUH2 dataset we can still see that there are clear differences in the types of forest modelled (evergreen or deciduous) but also in the total amount of forest.

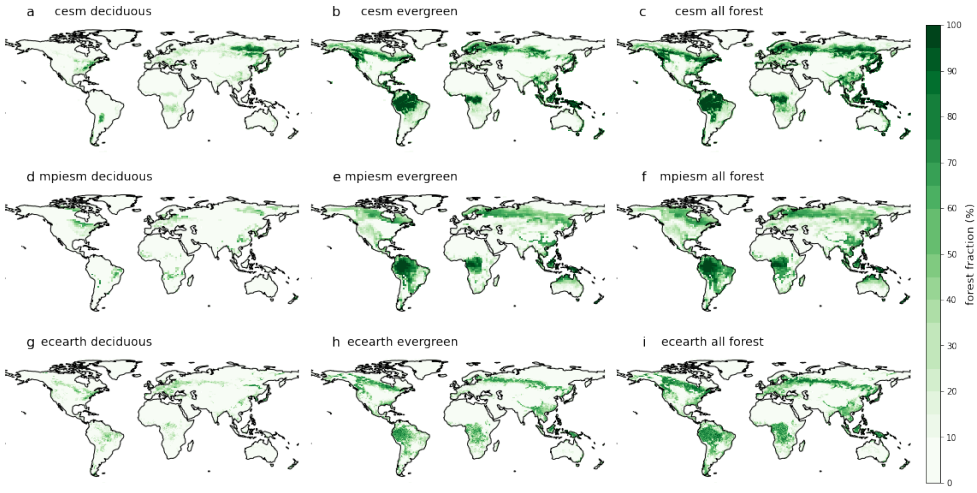

Figure 2.11: Total amount of forest (%) is shown for the 2015 CTL map for each ESM displaying different forest types. The amount of deciduous forest for CESM is shown in panel (a), the amount of evergreen forest in panel (b) and total amount of forest in panel (c). For MPI-ESM the amount of deciduous forest is shown in panel (d), evergreen forest in panel (e) and total amount of forest in panel (f). For EC-EARTH the amount of deciduous forest is shown in panel (g), evergreen forest in panel (h) and total amount of forest in panel (i).

2.7.2 Irrigation implementation in the different ESMs

MPI-ESM:
- soil moisture of first (0 - 0.065 m) and second (0.065 - 0.319 m) soil layer (out of 5) is filled up each time step (20-30 minutes) to field capacity if field capacity was not reached and if enough irrigation water is available in storage.
- irrigation water is stored each time step when the reservoir drops below 0.2 m and filled up with all available water from (surface) runoff and drainage during that time step.

CESM:
-Irrigation is applied daily at the first timestep after 6AM only when the soil moisture over all soil layers containing roots falls below a defined target soil moisture which is defined in order to match present day irrigation. If soil moisture falls below the target soil moisture it is replenished until at the target soil moisture level.
-The water needed for applying irrigation is taken from river water storage, however when this is inadequate to meet water demand it can also be subtracted from the ocean model, therefore no real water availability limit is applied within CLM. -Irrigation is only applied when the crop leaf area >0, i.e. this means that crops are only irrigated when they are in there vegetation state (during the growing season).

EC-EARTH:
-In LPJ-GUESS the amount of irrigation is the deficit a crop plant is experiencing. So if a crop needs an additional amount of water, it is added to the top of the soil column.
-The water comes from nowhere (i.e. unlimited water source).
- The water flux is not communicated to IFS, i.e. irrigation does not affect the surface water fluxes within the atmosphere. The only effect is that an irrigated crop would have a higher leaf area index and cover fraction compared to a non-irrigated crop of the same type.

2.7.3 Surface temperature in observational datasets

The comparison of the ESM data and the different observational datasets has some inconsistencies as was already described before by Winckler et al. (2019b). From Figure 2.12 it is apparent that the different datasets do not have the same spatial coverage. Besides this the calculation of the temperature signal differs across studies. In Alkama and Cescatti (2016) the observed signal is extracted by looking at changes over time in contrast to the other studies where this was extracted by comparing nearby locations during the same timestep. Also different conversion types are considered, in Li et al. (2015) and Duveiller et al. (2020) a generic forest to open land (both crop and grassland) is considered while in Bright et al. (2017) only a forest to grass conversion is considered. In Alkama and Cescatti (2016) apart from forest clearing to grass and crop also windfall events and fires where included in the analysis. Each dataset also covers different time periods although all datasets only include data after the year 2000 (hence representing present day conditions) and the total duration each estimate is based on are similar. All studies provide an estimate of the response of

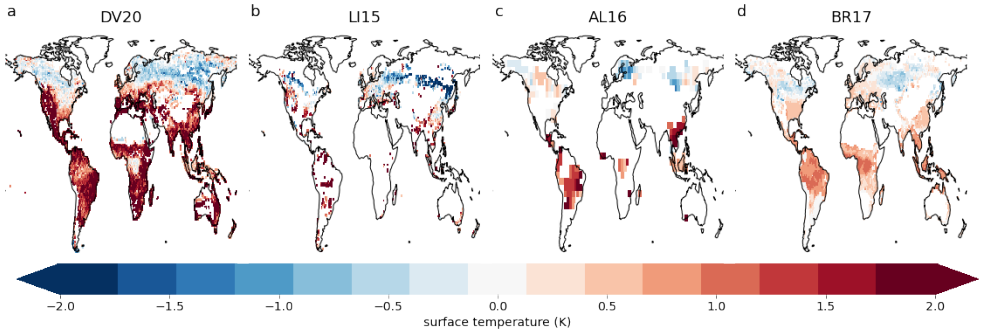

Figure 2.12: Annual mean surface temperature is shown for the used observational datasets. The data from Duveiller et al. (2020) is shown in panel a, from Li et al. (2015) is shown in panel b, from Alkama and Cescatti (2016) is shown in panel c and from Bright et al. (2017) is shown in panel d.

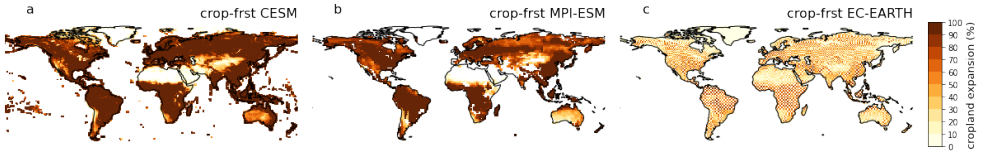

Figure 2.13: Total amount of deforestation (%) is shown for the CROP-FRST signal separated data for CESM in panel (a), MPI-ESM in panel (b) and EC-EARTH (c). Note that the land cover maps are not interpolated for EC-EARTH.

surface temperature to a full deforestation except Alkama and Cescatti (2016) where actual deforestation was considered and which had to be converted to a full deforestation signal by weighting with the deforestation fraction, in order to get robust results only grid cells where selected where more than 1% of actual deforestation had occurred over the analysis period considered. For Bright et al. (2017) only data was provided for conversions from specific forest species, to allow for a consistent comparison to the ESMs these values had to be weighted using the weights of each forest PFT within the specific ESMs. Therefore, an estimate of the Bright et al. (2017) data was created representing the different ESMs there PFT distributions, however, these differed only slightly so an average was taken over all estimates to be compared across all ESMs.

For the creation of the evaluation plots, the signals from the different datasets was calculated over all grid cells where data was available as most have a sufficient amount of grid cells in each latitudinal band. Each dataset was retained at its original resolution for the calculation of the latitudinal averages in order to avoid interpolation errors. The observational data could be directly compared to the output from the CROP-FRST signal separated data as in most grid cells almost a full deforestation occurs as is shown in Figure 2.13. The

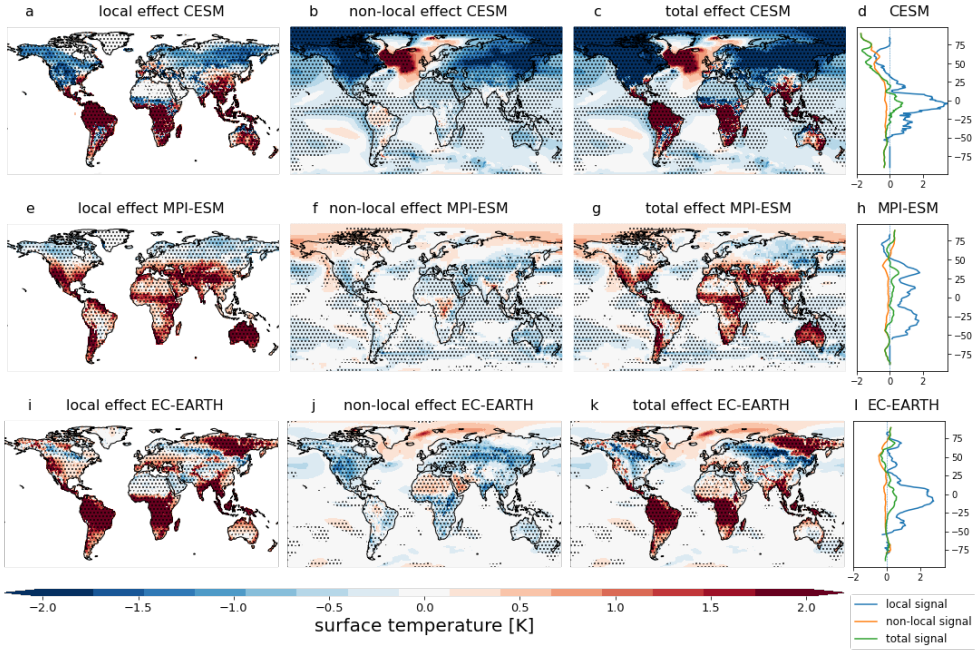

Figure 2.14: Annual mean surface temperature response to full idealised deforestation (CROP-FRST) of CESM, MPI-ESM and EC-EARTH. The local effect in CESM (a), the non-local effect (b) and the total effect (c). The latitudinal average of the local (blue), non-local (yellow) and total (green) signals of CESM (d). (e-h): same as (a-d), but for MPI-ESM. (i-l): same as (a-d), but for EC-EARTH. The stippling on the maps shows grid cells where all 5 ensemble members agree on the sign of change.

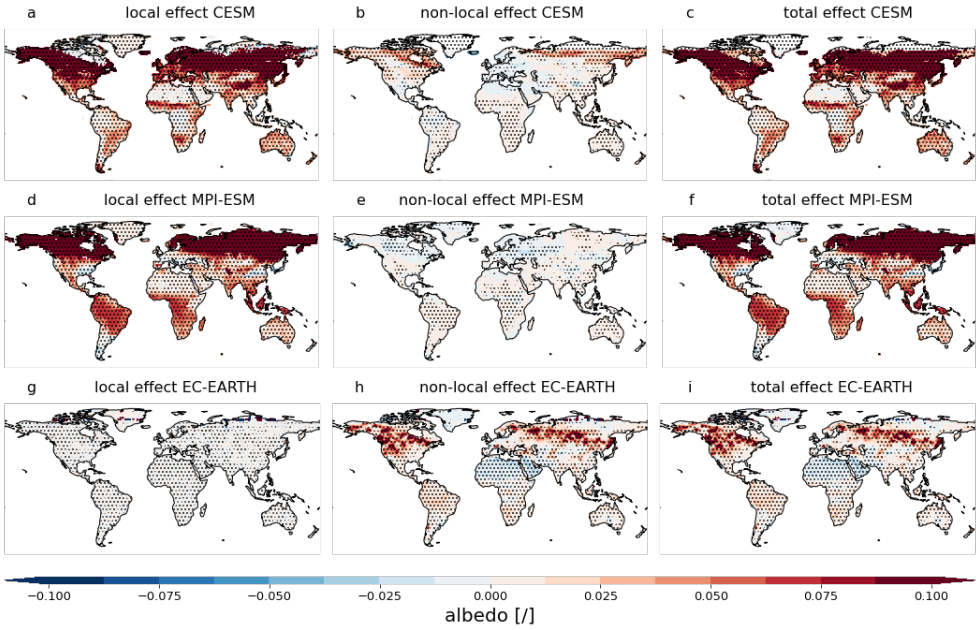

Figure 2.15: Annual mean albedo response to full idealised deforestation (CROP-FRST) of CESM, MPI-ESM and EC-EARTH. The local effect in CESM (a), the non-local effect (b) and the total effect (c). (d-f): same as (a-c), but for MPI-ESM. (g-i): same as (a-c), but for EC-EARTH. The stippling on the maps shows grid cells where all 5 ensemble members agree on the sign of change.

corresponding maps showing the local, non-local and total surface temperature effects are shown in Figure 2.14.

2.7.4 Signal separated albedo response

The albedo response (local, non-local and total) are shown for the CROP-FRST case in Figure 2.15. This clearly illustrates a peculiar feature related to the EC-EARTH model, while albedo change is mainly local (as is the case for MPI-ESM and CESM) it is completely non-local for EC-EARTH. The colorbar range was chosen to clearly show all (even small) changes in albedo. It shows that the albedo change has a dominant local component for CESM and a smaller non-local component, MPI-ESM only shows a local contribution with no non-local effect and EC-EARTH only shows a non-local contribution.
This is further illustrated by Figure 2.16 where the latitudinal averages of the local, non-local and total effects are compared to the observational datasets from Duveiller et al. (2020) and Li et al. (2015). This again illustrates what was mentioned above, i.e. there is no local component of albedo change for EC-EARTH while this is the dominant component for MPI-ESM and CESM. However it also clearly shows that even when total effects are

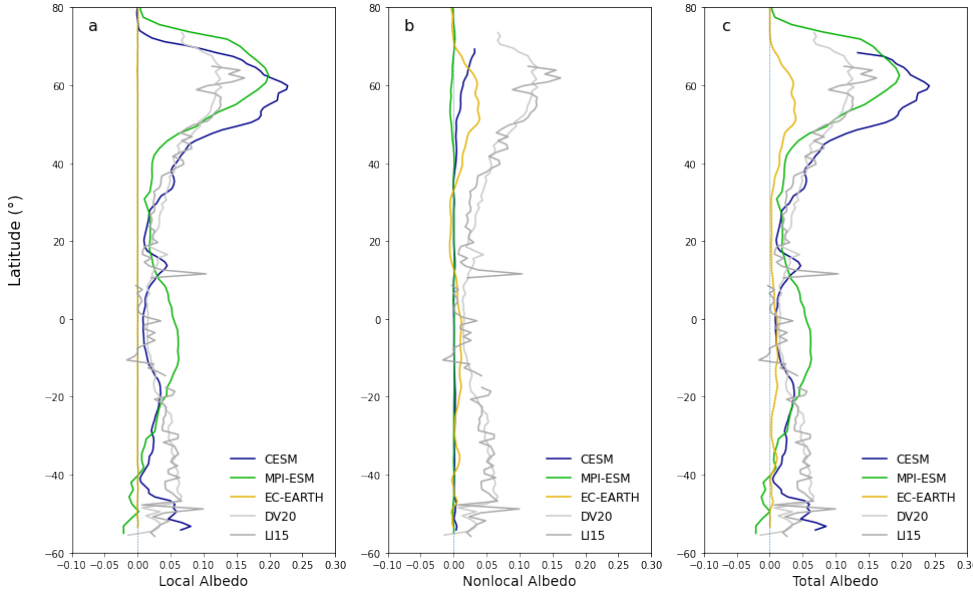

Figure 2.16: Latitudinal evaluation of annual mean albedo derived from full deforestation experiments (CROP-FRST) for CESM (blue), MPI-ESM (green) and EC-EARTH (yellow) with only the local effect shown in panel a, only the non-local effect in panel b, and the total effect in panel c. Note that for all ESMs a running latitudinal mean of 2° was computed. The observational data is shown in grey colours as a reference (Li et al., 2015; Duveiller et al., 2020).

considered EC-EARTH strongly underestimates albedo change compared to the observational datasets. This is especially important in the boreal latitudes where EC-EARTH does show a slight increase in the NH, however this effect is still less than half as strong as the observational datasets indicate. Due to the specific simulation setup used in this study EC-EARTH is not able to grow sufficient amounts of vegetation to cause a clear local albedo effect, only non-local effects are visible for this ESM. In CESM and MPI-ESM this issue does not occur as the land cover change immediately implements a physical forest and the related land surface properties without the need for these to grow. It should be noted that due to this issue, EC-EARTH has undergone less land cover change in the CROP-FRST case compared to the other ESMs as the FRST simulation for this ESM showed very little afforestation amounts (see Figure 2.1) and these forests are only established to a limited extent causing smaller biophysical effects on the atmosphere.

2.7.5 Signal separated response of turbulent heat fluxes, albedo and cloud cover for the different LCLM

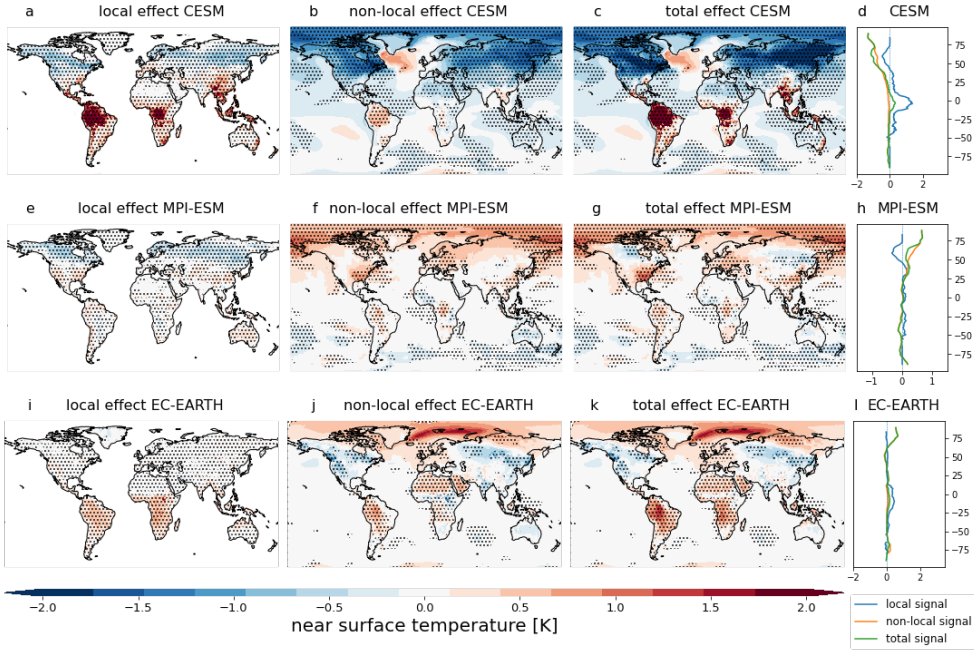

Figure 2.17: Annual mean near-surface temperature response to cropland expansion (CROP-CTL) of CESM, MPI-ESM and EC-EARTH. The local effect in CESM (a), the non-local effect (b) and the total effect (c). The latitudinal average of the local (blue), non-local (yellow) and total (green) signals of CESM (d). (e-h): same as (a-d), but for MPI-ESM. (i-l): same as (a-d), but for EC-EARTH. The stippling on the maps shows grid cells where all 5 ensemble members agree on the sign of change.

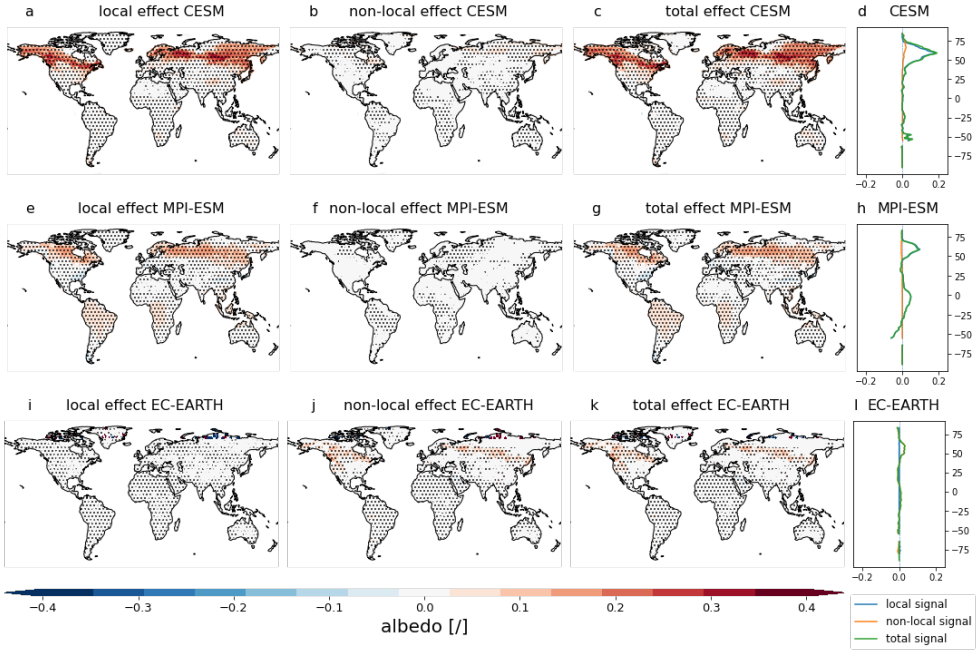

Figure 2.18: Annual mean albedo response to cropland expansion (CROP-CTL) of CESM, MPI-ESM and EC-EARTH. The local effect in CESM (a), the non-local effect (b) and the total effect (c). The latitudinal average of the local (blue), non-local (yellow) and total (green) signals of CESM (d). (e-h): same as (a-d), but for MPI-ESM. (i-l): same as (a-d), but for EC-EARTH. The stippling on the maps shows grid cells where all 5 ensemble members agree on the sign of change.

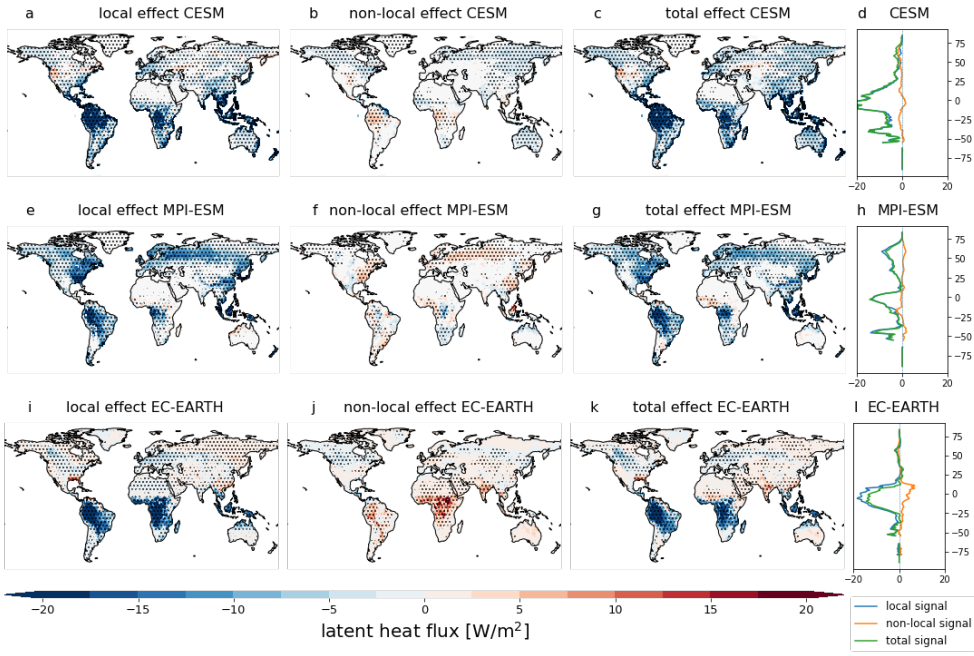

Figure 2.19: Annual mean latent heat flux response to cropland expansion (CROP-CTL) of CESM, MPI-ESM and EC-EARTH. The local effect in CESM (a), the non-local effect (b) and the total effect (c). The latitudinal average of the local (blue), non-local (yellow) and total (green) signals of CESM (d). (e-h): same as (a-d), but for MPI-ESM. (i-l): same as (a-d), but for EC-EARTH. The stippling on the maps shows grid cells where all 5 ensemble members agree on the sign of change.

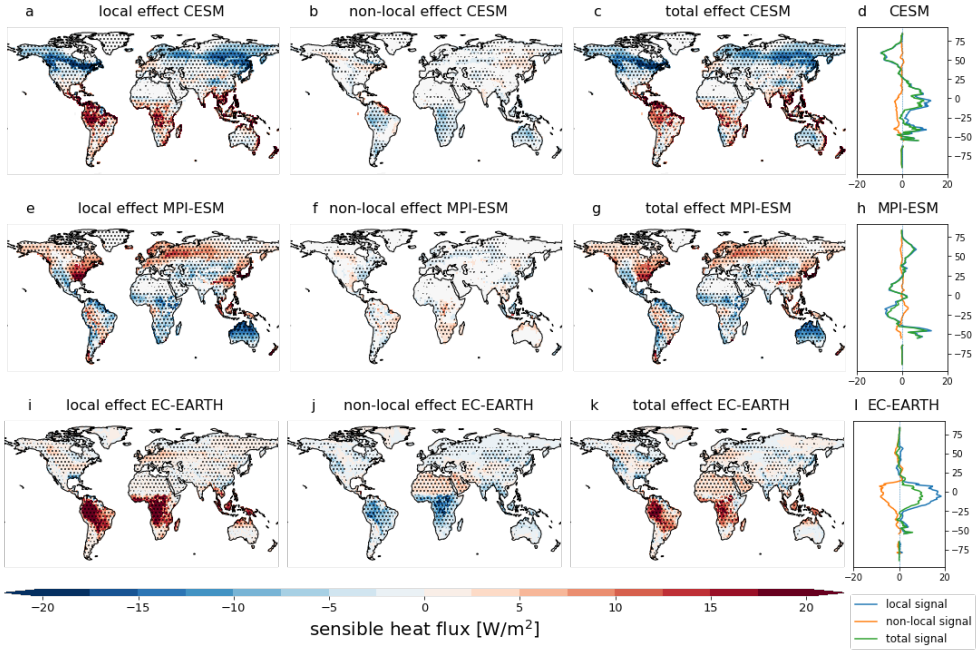

Figure 2.20: Annual mean sensible heat flux response to cropland expansion (CROP-CTL) of CESM, MPI-ESM and EC-EARTH. The local effect in CESM (a), the non-local effect (b) and the total effect (c). The latitudinal average of the local (blue), non-local (yellow) and total (green) signals of CESM (d). (e-h): same as (a-d), but for MPI-ESM. (i-l): same as (a-d), but for EC-EARTH. The stippling on the maps shows grid cells where all 5 ensemble members agree on the sign of change.

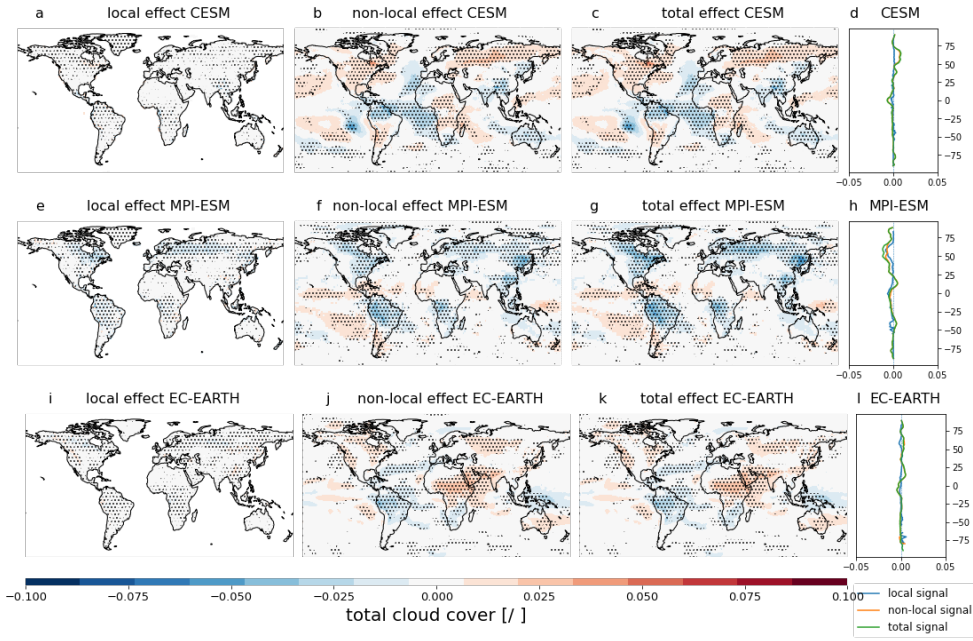

Figure 2.21: Annual mean cloud cover response to cropland expansion (CROP-CTL) of CESM, MPI-ESM and EC-EARTH. The local effect in CESM (a), the non-local effect (b) and the total effect (c). The latitudinal average of the local (blue), non-local (yellow) and total (green) signals of CESM (d). (e-h): same as (a-d), but for MPI-ESM. (i-l): same as (a-d), but for EC-EARTH. The stippling on the maps shows grid cells where all 5 ensemble members agree on the sign of change.

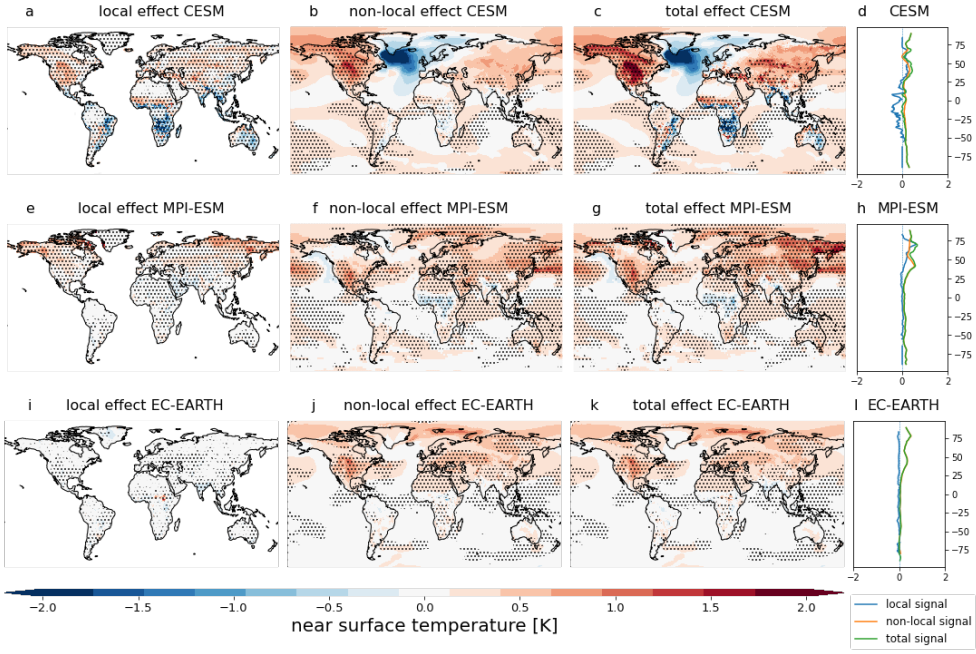

Figure 2.22: Annual mean near-surface temperature response to afforestation (FRST-CTL) of CESM, MPI-ESM and EC-EARTH. The local effect in CESM (a), the non-local effect (b) and the total effect (c). The latitudinal average of the local (blue), non-local (yellow) and total (green) signals of CESM (d). (e-h): same as (a-d), but for MPI-ESM. (i-l): same as (a-d), but for EC-EARTH. The stippling on the maps shows grid cells where all 5 ensemble members agree on the sign of change.

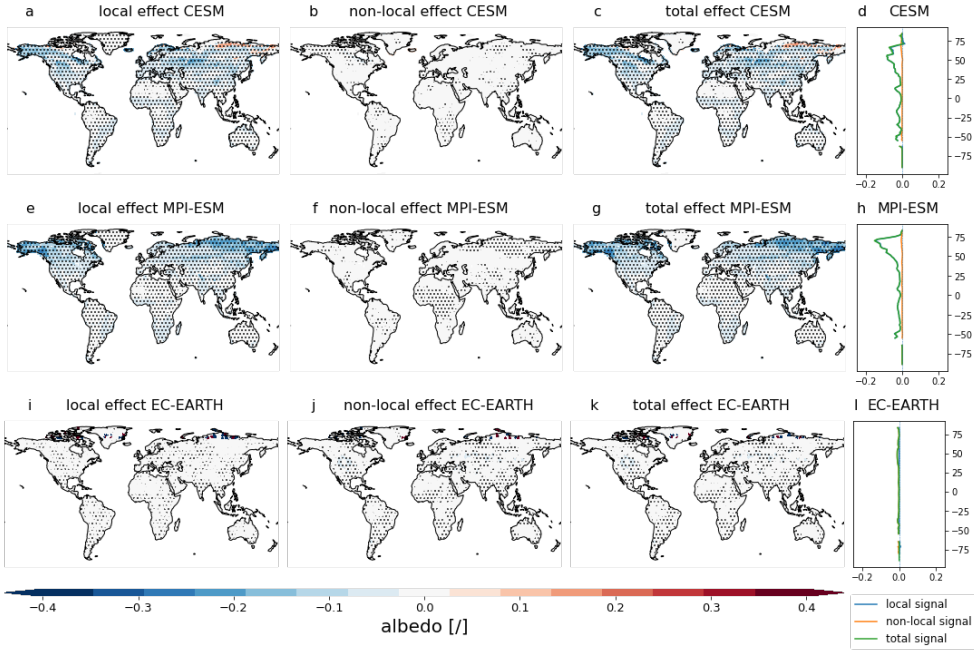

Figure 2.23: Annual mean albedo response to afforestation (FRST-CTL) of CESM, MPI-ESM and EC-EARTH. The local effect in CESM (a), the non-local effect (b) and the total effect (c). The latitudinal average of the local (blue), non-local (yellow) and total (green) signals of CESM (d). (e-h): same as (a-d), but for MPI-ESM. (i-l): same as (a-d), but for EC-EARTH. The stippling on the maps shows grid cells where all 5 ensemble members agree on the sign of change.

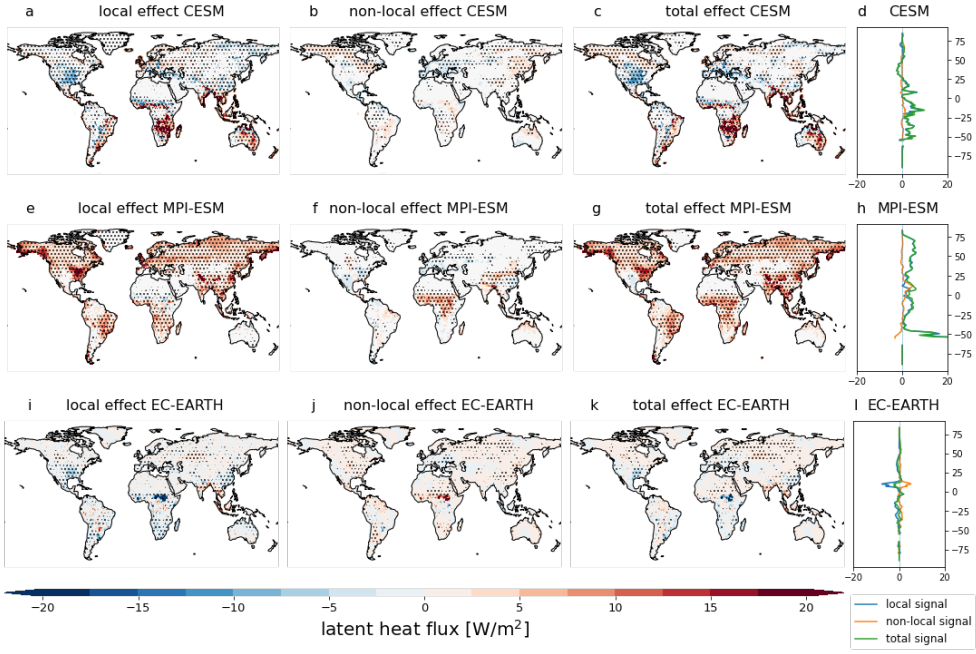

Figure 2.24: Annual mean latent heat flux response to afforestation (FRST-CTL) of CESM, MPI-ESM and EC-EARTH. The local effect in CESM (a), the non-local effect (b) and the total effect (c). The latitudinal average of the local (blue), non-local (yellow) and total (green) signals of CESM (d). (e-h): same as (a-d), but for MPI-ESM. (i-l): same as (a-d), but for EC-EARTH. The stippling on the maps shows grid cells where all 5 ensemble members agree on the sign of change.

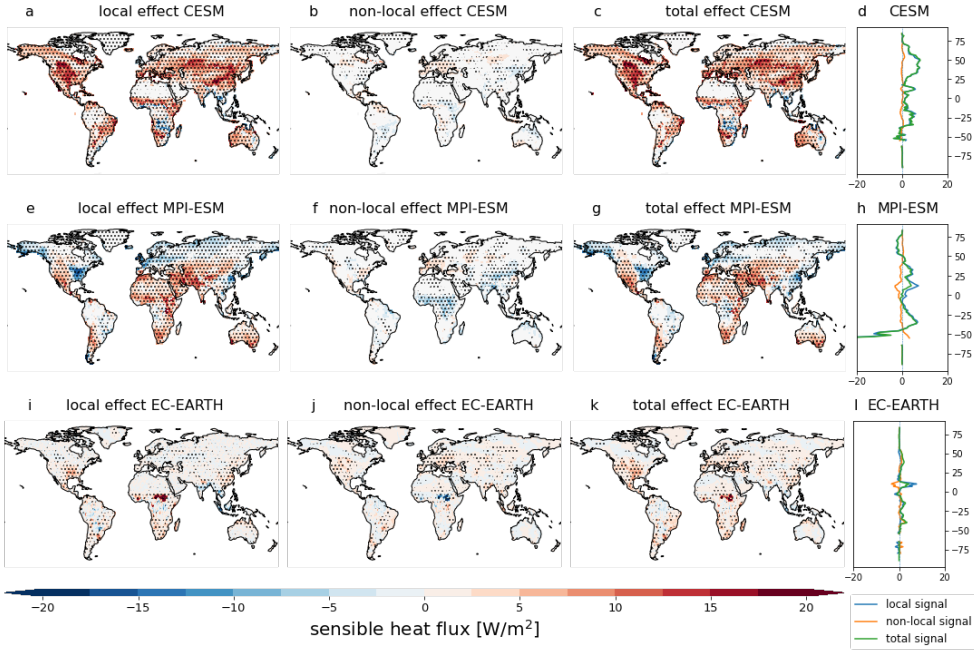

Figure 2.25: Annual mean sensible heat flux response to afforestation (FRST-CTL) of CESM, MPI-ESM and EC-EARTH. The local effect in CESM (a), the non-local effect (b) and the total effect (c). The latitudinal average of the local (blue), non-local (yellow) and total (green) signals of CESM (d). (e-h): same as (a-d), but for MPI-ESM. (i-l): same as (a-d), but for EC-EARTH. The stippling on the maps shows grid cells where all 5 ensemble members agree on the sign of change.

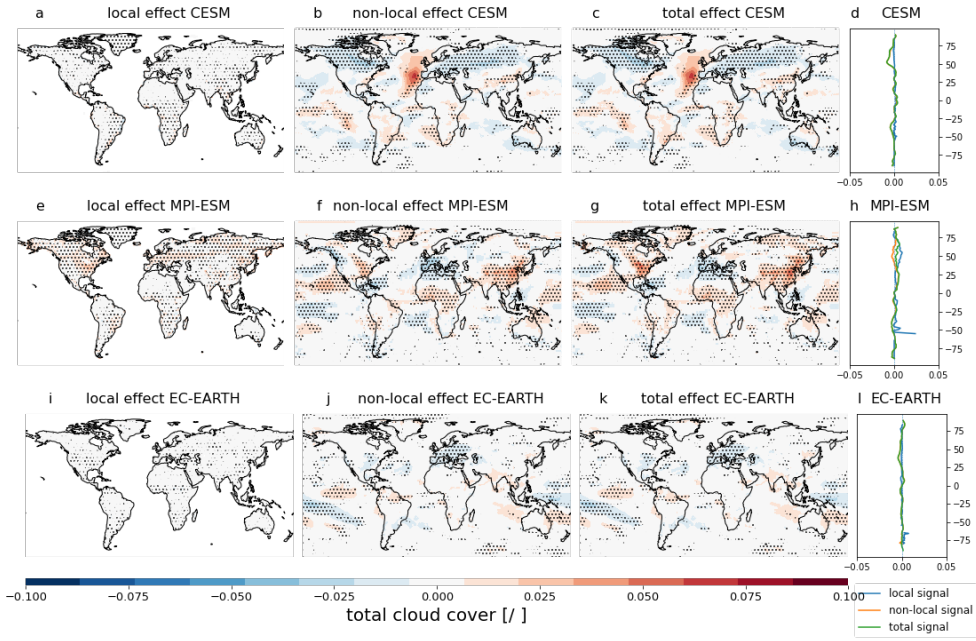

Figure 2.26: Annual mean cloud cover response to afforestation (FRST-CTL) of CESM, MPI-ESM and EC-EARTH. The local effect in CESM (a), the non-local effect (b) and the total effect (c). The latitudinal average of the local (blue), non-local (yellow) and total (green) signals of CESM (d). (e-h): same as (a-d), but for MPI-ESM. (i-l): same as (a-d), but for EC-EARTH. The stippling on the maps shows grid cells where all 5 ensemble members agree on the sign of change.

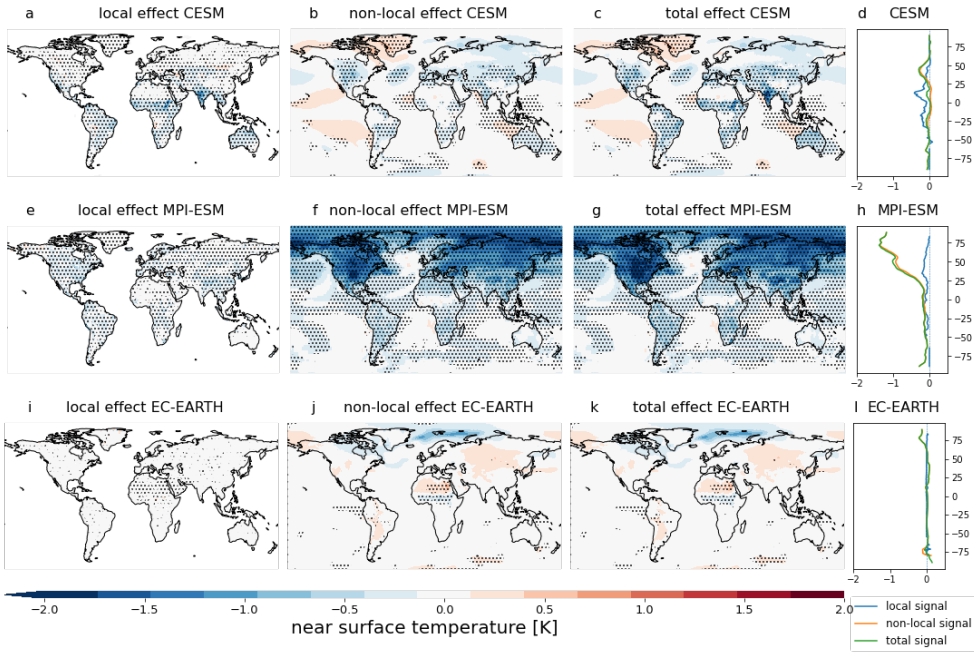

Figure 2.27: Annual mean near-surface temperature response to irrigation expansion (IRR-CROP) of CESM, MPI-ESM and EC-EARTH. The local effect in CESM (a), the non-local effect (b) and the total effect (c). The latitudinal average of the local (blue), non-local (yellow) and total (green) signals of CESM (d). (e-h): same as (a-d), but for MPI-ESM. (i-l): same as (a-d), but for EC-EARTH. The stippling on the maps shows grid cells where all 5 ensemble members agree on the sign of change.

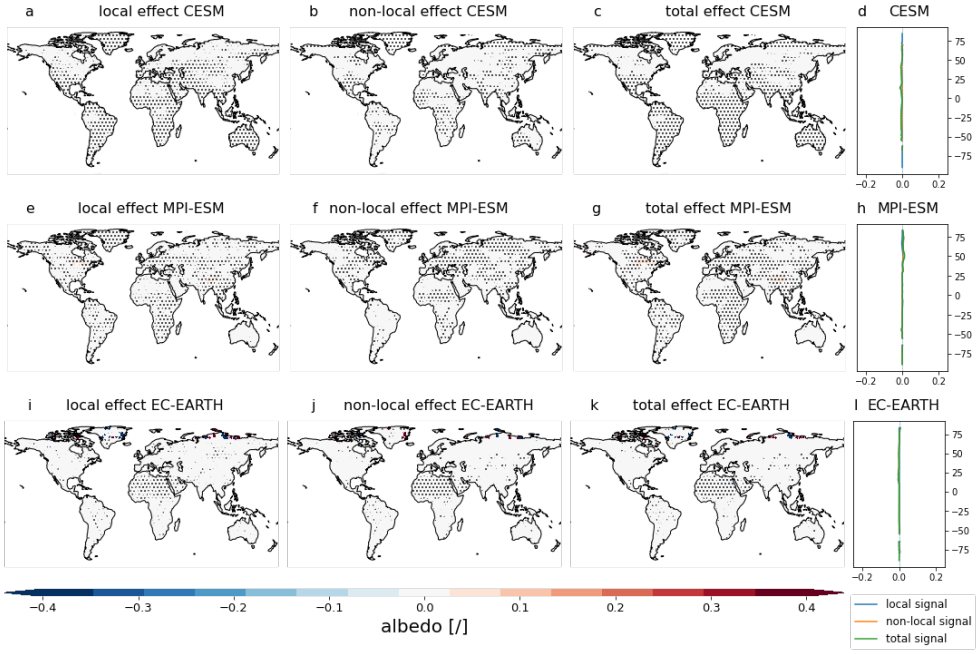

Figure 2.28: Annual mean albedo response to irrigation expansion (IRR-CROP) of CESM, MPI-ESM and EC-EARTH. The local effect in CESM (a), the non-local effect (b) and the total effect (c). The latitudinal average of the local (blue), non-local (yellow) and total (green) signals of CESM (d). (e-h): same as (a-d), but for MPI-ESM. (i-l): same as (a-d), but for EC-EARTH. The stippling on the maps shows grid cells where all 5 ensemble members agree on the sign of change.

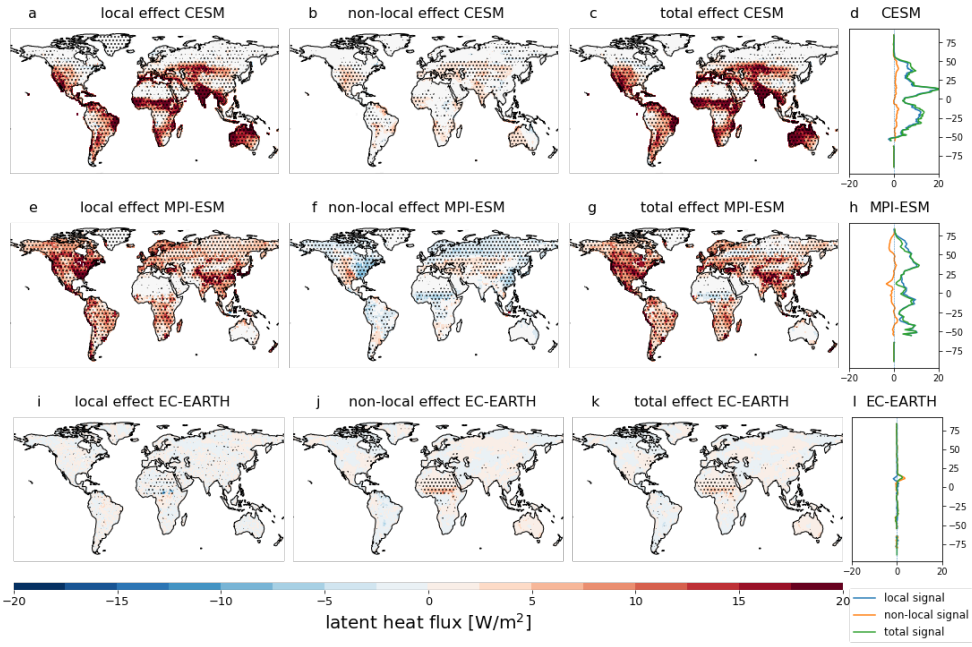

Figure 2.29: Annual mean latent heat flux response to irrigation expansion (IRR-CROP) of CESM, MPI-ESM and EC-EARTH. The local effect in CESM (a), the non-local effect (b) and the total effect (c). The latitudinal average of the local (blue), non-local (yellow) and total (green) signals of CESM (d). (e-h): same as (a-d), but for MPI-ESM. (i-l): same as (a-d), but for EC-EARTH. The stippling on the maps shows grid cells where all 5 ensemble members agree on the sign of change.

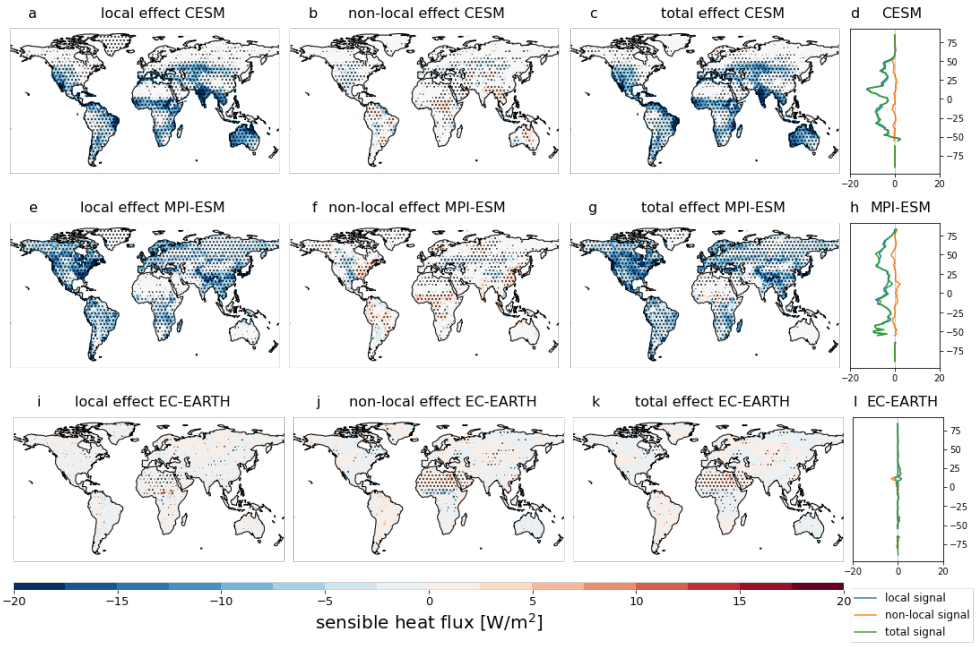

Figure 2.30: Annual mean sensible heat flux response to irrigation expansion (IRR-CROP) of CESM, MPI-ESM and EC-EARTH. The local effect in CESM (a), the non-local effect (b) and the total effect (c). The latitudinal average of the local (blue), non-local (yellow) and total (green) signals of CESM (d). (e-h): same as (a-d), but for MPI-ESM. (i-l): same as (a-d), but for EC-EARTH. The stippling on the maps shows grid cells where all 5 ensemble members agree on the sign of change.

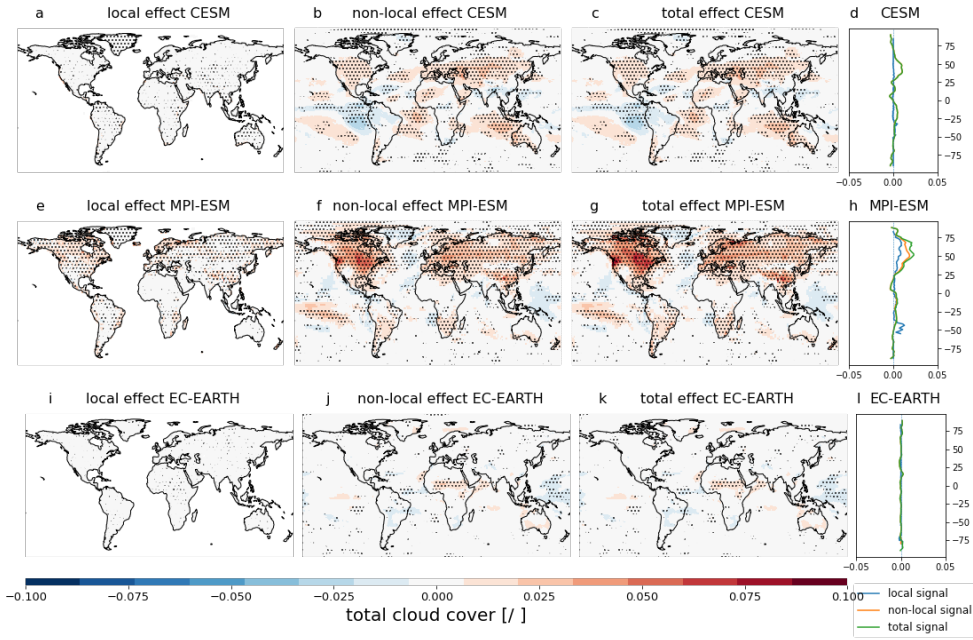

Figure 2.31: Annual mean cloud cover response to irrigation expansion (IRR-CROP) of CESM, MPI-ESM and EC-EARTH. The local effect in CESM (a), the non-local effect (b) and the total effect (c). The latitudinal average of the local (blue), non-local (yellow) and total (green) signals of CESM (d). (e-h): same as (a-d), but for MPI-ESM. (i-l): same as (a-d), but for EC-EARTH. The stippling on the maps shows grid cells where all 5 ensemble members agree on the sign of change.

Chapter 3

Effects of idealised land cover and land management changes on the atmospheric water cycle

Land cover and land management changes (LCLMC) play an important role in land-based mitigation. However, their effects on moisture fluxes and recycling remain uncertain. Here, we analyse the impact of idealised LCLMC scenarios on atmospheric moisture transport in three different ESMs (CESM, MPI-ESM and EC-EARTH). The LCLMC scenarios comprise of a full cropland world, a fully afforested world, and a cropland world with unlimited irrigation expansion. The effects of these LCLMC in the different ESMs are analysed for precipitation, evaporation and vertically integrated moisture flux convergence to understand the LCLMC-induced changes in the atmospheric moisture cycle. Then, a moisture tracking algorithm is applied to assess the effects of LCLMC on moisture recycling at the local (grid cell level) and the global scale (continental moisture recycling). Our results indicate that LCLMC are generally inducing consistent feedbacks on moisture fluxes over land in all ESMs. Cropland expansion causes decreased evaporation and precipitation and reduced local moisture recycling in all ESMs, with the opposite effect for afforestation and irrigation expansion. However, the strength of this influence varies in time and space and across the ESMs and shows a strong dependency on the dominant driver: a dominance of large-scale atmospheric circulation changes against a dominance of local to regional changes in the atmospheric water cycle. Overall, these results show that more research is needed to constrain the uncertainty of these effects within ESMs.

This chapter is currently under review in Earth System Dynamics as: De Hertog S. J., Lopez-Fabara C. E., van der Ent R., Keune J., Miralles D. G., Portmann R., Schemm S., Havermann F., Guo S., Luo F., Manola I., Lejeune Q., Pongratz J., Schleussner C.-F., Seneviratne S. I., Thiery W. (2023) Effects of idealised land cover and land management changes on the atmospheric water cycle. Earth System Dynamics, under review

3.1 Introduction

Currently, about three quarters ($\sim$100 *10^6 km^2) of the ice-free land surface has undergone some kind of anthropogenic land cover or land management change (LCLMC) (Luyssaert et al., 2014; Mbow et al., 2017). All these modifications are important drivers of climate change as they alter the carbon cycle (biogeochemical effects) and affect surface properties, which impact the energy and water balance (biogeophysical effects) (Bonan, 2008; Pongratz et al., 2021, 2010) and feed back on the local to global climate (Winckler et al., 2019b; Boysen et al., 2020; Portmann et al., 2022; De Hertog et al., 2023). Therefore, future LCLMC are increasingly seen as a viable tool for land based mitigation and play a crucial role within low warming emission scenarios (Rogelj et al., 2018; Seneviratne et al., 2018). Hence, exploring and understanding the extent to which LCLMC influence climate has become key to develop effective mitigation and adaptation strategies (Lawrence et al., 2016).

From a biogeophysical perspective, LCLMC lead to changes in the albedo, aerodynamic conductance and the partitioning between the sensible and latent heat flux which has an impact on atmospheric temperature and moisture content (Bowen, 1926; Wang et al., 2009). For example, tropical deforestation is expected to further dry and warm the regional climate (Bonan, 2008; Akkermans et al., 2014; Spracklen et al., 2018). In contrast, irrigation expansion can cause a local to regional cooling and moistening of the atmosphere (Mahmood et al., 2014; Thiery et al., 2017, 2020; Hauser et al., 2019; Tuinenburg et al., 2014). Evaporation, being the link between the surface energy and the water balance (Shukla and Mintz, 1982), modulates the influence of LCLMC on atmospheric conditions (van der Ent et al., 2010; Spracklen et al., 2012). Tracking the origins of precipitation back to evaporation and determining the fraction of terrestrial precipitation that originates from land — here referred to as continental precipitation recycling (van der Ent et al., 2010) — can increase our understanding of the effects of future LCLMC on the climate. On the other hand, the fate of land evaporation can be determined and illustrates the reach of local LCLMC; the fraction of terrestrial evaporation precipitating over land is often referred to as continental evaporation recycling (van der Ent et al., 2010). Even though, it is well established that LCLMC can affect these moisture recycling strengths (Wang-Erlandsson et al., 2018; Benedict et al., 2020) — i.e., the degree to which terrestrial precipitation depends on land evaporation — this is rarely quantified within dedicated ESM studies. Most studies that quantify the effects of LCLMC on the atmospheric moisture cycle focus on the changes in moisture fluxes, but often cannot unravel the role of local and continental moisture recycling in these differences (Tuinenburg et al., 2020; Hoek van Dijke et al., 2022; Baudena et al., 2021; Wunderling et al., 2022; Staal et al., 2018). Those studies that do account for moisture recycling in assessing the effects of LCLMC generally apply reanalysis based recycling ratios (Tuinenburg et al., 2020; Hoek van Dijke et al., 2022; Baudena et al., 2021; Wunderling et al., 2022; Staal et al., 2018) which do not include the two-way feedbacks of circulation changes and the water cycle. By analysing dedicated ESM simulations for LCLMC we are able to address these shortcomings and include the effects of atmospheric circulation changes on moisture recycling.

Idealized or extensive implementations of LCLMC within ESM simulations are used to cope with weather-induced noise that dampens climatic responses (Winckler et al., 2017a; Boysen et al., 2020). Within such simulations, large-scale atmospheric circulation changes have been shown to occur as a consequence of LCLMC (Goessling and Reick, 2011; Boysen et al., 2020; Portmann et al., 2022; Devaraju et al., 2018; Laguë et al., 2019). However, most studies have only focused on one LCLMC type (e.g. Boysen et al., 2020; Laguë et al., 2019; Devaraju et al., 2018)) and only used a single ESM (e.g. Portmann et al., 2022; de Vrese et al., 2016). Further, these studies generally cannot distinguish explicitly between the influence of local processes (directly induced by the LCLMC) and non-local or remote processes (induced by LCLMC elsewhere, including circulation and advection changes). The study of De Hertog et al. (2023) presented a first multi-model intercomparison using three different ESMs and four different LCLMC types in which a clear distinction between local and non-local biogeophysical effects was established through the checkerboard LCLMC implementation as developed by Winckler et al. (2017a). These simulations facilitated the comparison of the climate changes induced by different LCLMC types and to grasp the multi-model uncertainty.

Here, we assess the atmospheric water cycle responses to idealised LCLMC scenarios using global simulations of three different ESMs (De Hertog et al., 2023). The simulations comprise different idealised LCLMC scenarios — from afforestation, over cropland expansion to irrigation expansion — and have been implemented in a checkerboard pattern. The simulation setup and the moisture tracking algorithm and its derived metrics are described below (Section 3.2). We first analyse the ESM output for changes in the atmospheric water cycle including evaporation, precipitation, and atmospheric moisture flux convergence (Section 3.3.1). Second, we analyse the moisture tracking algorithm output to assess the direct effects of LCLMC on moisture recycling and unravel local and remote drivers of the analysed moisture flux changes. This is done on a local scale using the concept of 'length scales' of moisture recycling (Section 3.3.2), and on a continental scale using continental recycling ratios (Section 3.3.3). Finally we highlight the most important findings and implications of this research (Section 3.4 and 3.5).

3.2 Methods

3.2.1 ESM simulations

The ESM simulations analysed here were conducted within the LAnd MAnagement for CLImate Mitigation and Adaptation (LAMACLIMA) project and are presented in detail in De Hertog et al. (2023). In this project, different sensitivity experiments were performed for three ESMs, i.e., the Community Earth System Model version 2.1.3 (CESM), the European Community Earth-System Model 3-Veg v3.3.3.1 (EC-EARTH), and the Max-Planck Institute Earth System Model 1.2 low resolution (MPI-ESM). See De Hertog et al. (2023) for

detailed model descriptions. The experiments comprise four simulations of LCLMC scenarios. One scenario is the control case (hereafter referred to as CTL), which is conducted with a constant land cover corresponding to the year 2015. The three remaining scenarios represent an extreme case of single specific LCLMC, namely afforestation (FRST), cropland expansion (CROP), and irrigation expansion (IRR). Here, irrigation is applied on top of the cropland expansion. Thus, while the impact of afforestation and cropland expansion is always evaluated with respect to the control simulation (i.e., differences are calculated as FRST–CTL and CROP-CTL), the impact of irrigation is evaluated with respect to the cropland expansion simulation (IRR-CROP). All simulations cover a period of 160 years under a present-day climate forcing (corresponding to the year 2015). Note that a simulation including the effects of wood harvesting was also included in De Hertog et al. (2023), however this is not included here as the biogeophysical effects were shown to be too small.

The LCLMC scenarios are generated from the CTL scenario land cover by inducing the LCLMC in a checkerboard-like pattern as presented in Winckler et al. (2017a). The resulting LCLMC is shown in Figure 3.1. This implies that the different LCLMC are implemented in every other pixel (i.e. only 50% of hospitable land grid cells have undergone LCLMC), while all other forcings (i.e. greenhouse gas, stratospheric aerosols,...) remain identical to the initial CTL scenario configurations. Even though, a structured approach was taken to implement the LCLMC in the different ESMs, the geographical extent of irrigation and afforestation differs strongly among different ESMs due to each model's native schemes on irrigation and the transition to forest. This is especially the case for the EC-EARTH afforestation simulation, in which the afforestation simulated was extremely low compared to the other ESMs (Figure 3.1d,e,f). Therefore, the afforestation scenario from EC-EARTH is not considered in this study. Likewise, large discrepancies regarding the simulated irrigation expansion are related to different irrigation parameterisations being implemented in the different ESMs (see section 3.6.2 in De Hertog et al., 2023). Within the model version of EC-EARTH used in this study, irrigation does not cause any biogeophysical feedbacks such that it does not induce any feedbacks on atmospheric moisture. Hence, the irrigation expansion scenario from EC-EARTH is also not considered in this study.

This checkerboard-like implementation of the LCLMC enables a signal separation of the ESM response into local and non-local components (Winckler et al., 2017a; De Hertog et al., 2023). The local effects refer to changes directly induced by the LCLMC within the grid cell while the non-local effects refer to changes induced by LCLMC elsewhere through changes in atmospheric circulation or advection. This separation is only applicable to (near-)surface variables and not to variables representing processes that extend higher into the atmosphere, as there is mixing between different grid cells above the surface. Therefore, the signal separation is not applied to the results for which atmospheric variables were used. Instead, we analyse the ESM output directly which represents an extreme case of LCLMC applied in a checkerboard pattern. For the variables where signal separation can be applied, we provide the figures in section 3.6.1 to support interpretations of these signals. All calculations are applied at each ESM's native spatial resolution (latitude x longitude) (MPI-ESM: 1.88° x 1.88°, CESM: 0.90° x 1.25°, EC-EARTH: 0.7°x

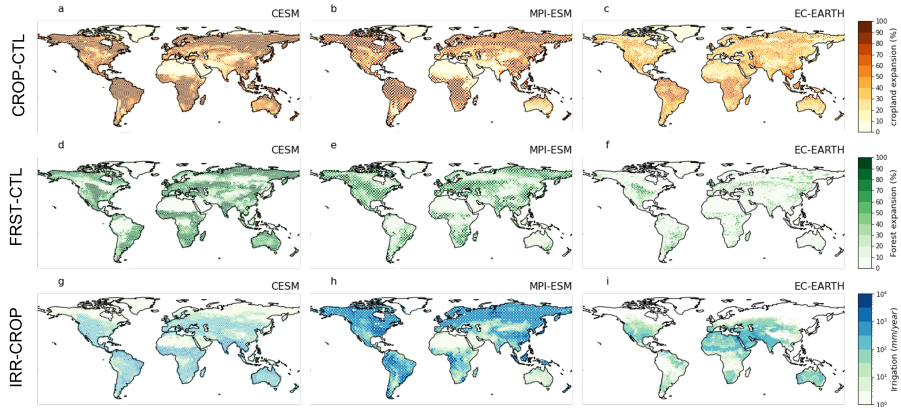

Figure 3.1: Land cover and land management changes as implemented in the three different ESMs. Cropland expansion (CROP-CTL ; a, b, c), afforestation (FRST-CTL ; d, e, f), and irrigation expansion (IRR-CROP ; g, h, i) implemented in CESM, MPI-ESM, and EC-EARTH, respectively. Both, cropland expansion and afforestation, are shown as a change in area fraction (%) while irrigation expansion is shown through the irrigation flux in mm/year.

0.7°).

3.2.2 LCLMC-induced impact on the net water fluxes

To understand the net change in the atmospheric water cycle induced by the different LCLMC, we first analyse their effects on evaporation and precipitation and compare them to the reference simulation of each LCLMC scenario. In addition, the vertically integrated moisture flux convergence (MFC) is computed using the basic principles of conservation of water vapor (Banacos and Schultz, 2005; Cook, 2009; Thiery et al., 2016; Van de Walle et al., 2020), as shown in Eq. 3.1 below.

$$P - E \approx -\frac{1}{g\rho_w} \int_{p_s}^{p\mathrm{TOA}} \left(\vec{\nabla} \cdot q\vec{v}\right) dp \tag{3.1}$$

Where g is the gravitational acceleration [m/s^2], ρ_w is the density of water (1000 kg/m^3), ps and $pTOA$ is the pressure at surface level and top of the atmosphere respectively, q represents the specific humidity of an air parcel [kg/kg], $\vec{v}$ its horizontal wind vector [m/s], P is the precipitation flux per unit area [m/s], E is the surface evaporation flux per unit area [m/s]. $\nabla \cdot (q\vec{v})$ is the atmospheric moisture convergence from the surface to the top of the atmosphere (TOA). The MFC is computed based on 6-hourly data along the available pressure levels of each ESM. For EC-EARTH, only eight atmospheric levels were available,

which is insufficient to compute MFC. Hence, $P-E$ is used as a proxy for the MFC in EC-EARTH. Over land, MFC or $P-E$ are often used a proxy for water availability (Van de Walle et al., 2020; Thiery et al., 2016), and changes of these measures can help understand the impacts of LCLMC on the redistribution of water over land.
The comparison of P, E, and MFC changes with respect to the corresponding reference simulation is performed for the three different LCLMC scenarios, i.e., cropland expansion, afforestation, and irrigation. We focus on annual mean values for the analysis. However, seasonal means (DJF: December, January, February; JJA: June, July, August) are shown in section 3.6.2.

3.2.3 Moisture tracking analysis

To further quantify the direct influence of LCLMC on precipitation and unravel the reach of locally-induced LCLMC on precipitation and water availability, we perform a moisture tracking analysis. Here, we apply the Eulerian moisture tracking model WAM-2layers (van der Ent et al., 2014; Benedict et al., 2020) to identify the origin of precipitation and the fate of evaporation in the ESM simulations and to evaluate the impact of LCLMC-induced evaporation changes on precipitation and water availability. The output of WAM-2layers is then used to compute several metrics relevant to moisture recycling, which can help uncover LCLMC-induced effects within the different ESMs. In this study, we focus on two spatial scales of moisture recycling: (i) local recycling and (ii) continental recycling. Further, as local moisture recycling is defined on the grid-cell area of each ESM, which differs by definition (see section 3.2.1), additional scale-independent metrics are used. Evaporation and precipitation length scales (van der Ent et al., 2010) illustrate the distance that moisture travels on average to or from a given grid cell. In the following, all recycling metrics are presented at annual time scales. Details on the setup of WAM-2layers and the definition of moisture recycling metrics are presented in more detail in the following sections.

WAM-2layers

A moisture tracking algorithm, the Water Accounting Model - 2 layers (WAM-2layers, van der Ent et al. (2014)), is applied to analyse the effects of the different LCLMC on moisture recycling. We use a recent version of this algorithm, which was modified to ingest climate model data with limited vertical levels (Benedict et al., 2020). This moisture tracking algorithm uses an Eulerian approach to solve the atmospheric moisture balance over each grid cell and a specified time step (van der Ent et al., 2014). Model outputs comprise the origins of precipitation or evaporation at the local scale or continental scale depending on which tracking is performed, and facilitate the quantification of local and continental moisture recycling measures (van der Ent et al., 2010; van der Ent et al., 2014, see below). The algorithm has been applied numerous times in recent years for ESM output (Benedict et al., 2020; Guo et al., 2020; Findell et al., 2019; Bosmans et al., 2020). Since for tracking the moisture, the computational power required does not depend on the size

of the region, it is specifically suitable for moisture recycling of climatologies in contrast to the Lagrangian tracking schemes, whose computational demand scales linearly with the size of the region of interest (Van der Ent et al., 2013).
Here, the surface and atmospheric data from all ESM simulations at the original spatial resolution (see section 3.2.1) and the finest temporal resolution (CESM: 6 hours, MPI-ESM: 3 hours for surface variables and 6hr for atmospheric variables, EC-EARTH: 6 hours for surface variables and daily for atmospheric variables) are used as inputs for WAM-2layers. To avoid stability problems related to the numerical discretisation in WAM-2layers (van der Ent et al., 2014), all ESM forcings are linearly interpolated to 15-min time steps. The moisture tracking is applied to the last 30 years within the 160-year simulation period.

Local moisture recycling

Here, two definitions of moisture recycling are used. First, the local precipitation recycling ratio ρ_r, i.e. the fraction of precipitation over a region r that originates from evaporation over the same region (see Eq. 3.2), is calculated. The remaining fraction of precipitation over that region (i.e., $1-\rho_r$) originates from evaporation upwind that is advected into the region r, and can be of either land or oceanic origin. Second, the local evaporation recycling ratio ε_r, i.e. the fraction of evaporation from a region r that falls as precipitation over the same region (see Eq. 3.3), is used. The remaining fraction of local evaporation $(1-\varepsilon_r)$ is transported away from the region and falls downwind of that region as precipitation.
Using the output from WAM-2layers, precipitation over the region r with area A_r, here referred to as P, can be separated into the precipitation originating from the same region (P_r) and the remaining precipitation that originates from upwind regions (P_a), so that $P = P_r + P_a$. Using these outputs, the local precipitation recycling ratio can be calculated as

$$\rho_r = \frac{P_r}{P}. \tag{3.2}$$

Similarly, the local evaporation recycling ratio can be calculated using evaporation from the region r, here referred to as E, and the evaporation that falls as precipitation over the same region (E_r), i.e.

$$\varepsilon_r = \frac{E_r}{E}. \tag{3.3}$$

Both local recycling definitions are subject to the area of the region considered (A_r). Here, local recycling is defined on the area of a grid cell. It is noted that this area varies with latitude per definition and, in addition, varies for the ESM simulations employed here (see section 3.2.1). The differences between local recycling ratios thus need to be interpreted with caution and are not comparable across different data sources or ESMs. To overcome these shortcomings we compute length scales and continental recycling ratios.

Precipitation and evaporation length scales

To assess local moisture recycling independently of the ESM, we compute the length scale of moisture recycling as introduced by van der Ent and Savenije (2011). Length scales

overcome one of the major shortcomings of regional recycling ratios, which are strongly dependent on the shape and scale of the source region they are computed over (van der Ent and Savenije, 2011). Length scales of local moisture recycling are scale-independent and give an indication of a process-based distance over which moisture will travel on average to or from a given grid cell under local hydrological and climatological conditions (van der Ent and Savenije, 2011). Hence they should not be interpreted as actual travel distance, but rather a process based metric of moisture recycling strength using distance units (km). Length scales can be linked to the strength of land–atmosphere feedback and they are comparable to other metrics of land atmosphere feedback (e.g. Seneviratne et al., 2010; Santanello Jr et al., 2018). A short length scale indicates that moisture does not travel far and that local land-atmosphere feedbacks may play a role. On the other hand, a long length scale indicates that moisture originates from far away or travels far once evaporated, and that local recycling is lower. Like local recycling ratios, the length scales can be calculated from a precipitation- or an evaporation-centric perspective (i.e., precipitation recycling ratios λ_ρ or evaporation recycling ratios λ_ε). Here the precipitation length scale represents the process distance for precipitation raining down in a given grid cell and the evaporation length scale represents the process distance evaporation from a given grid cell travels before precipitating. Both length scales (km) can be derived from the local recycling ratios presented above (see section 3.2.3), which are computed at the grid scale level, and the distance travelled along an atmospheric streamline (Dominguez et al., 2006). For the complete derivation of how length scales are defined we refer to van der Ent and Savenije (2011).

Continental moisture recycling

To study the continental contribution to moisture recycling, we compute the continental recycling ratios. Analogous to previous studies (e.g. Brubaker et al., 1993; van der Ent et al., 2010; Gimeno et al., 2012; Findell et al., 2019; Gimeno et al., 2020), we define continental precipitation recycling ratio ρ_c as the fraction of precipitation over land that originates from land evaporation. The precipitation recycling ratio answers the question 'how much of the moisture precipitating over land originates from land?'. The remaining fraction $(1 - \rho_c)$ of the precipitation over land originates from evaporation over oceans. Similarly, continental evaporation recycling ratio ε_c is defined as the fraction of land evaporation that falls as precipitation over land. In contrast to the local recycling ratios, continental recycling ratios refer to the same area, i.e. the area of all continental land regions A_c, which facilitates a direct comparison of recycling ratios between the ESMs with different spatial resolution employed here. Continental evaporation and precipitation are computed by tracking all continental moisture fluxes at the same time, which differs from how this metric is computed in Lagrangian moisture tracking algorithms.

3.3 Results

3.3.1 Changes in atmospheric moisture fluxes due to LCLMC

All ESMs generally show a decrease in evaporation over land due to cropland expansion and an increase in evaporation due to afforestation and irrigation expansion (Figure 3.2). However, some of the ESMs' regional signals deviate from this general pattern. For cropland expansion (Figure 3.2a,d,g), CESM and MPI-ESM simulate a quasi-global decrease in evaporation over all land areas. However, some regions also show an increase such as central U.S. in CESM, as well as East Africa and western Australia in MPI-ESM. The effects over the mid-latitudes exhibit a strong seasonality, with an increase in evaporation in JJA and a decrease in DJF. This impact is clearly visible in CESM and also slightly visible in MPI-ESM (Figure 3.15 and Figure 3.16). In EC-EARTH, the annual patterns are less clear, with a strong decrease in evaporation following cropland expansion over tropical forests and a slight decrease over the mid-latitudes, but a clear increase over subtropical and tropical regions, such as the Sahel, East Africa, India and Australia. Moreover, all models clearly distinguish between feedbacks over deforested grid cells and those that have remained unaltered, following the checkerboard implementation of LCLMC (see section 3.2.1). There are deforested patches that show a distinct decrease in evaporation while the nearby unaltered grid cells instead show a strong increase. This is also confirmed by Figure 3.9 which shows the signal-separated effects of evaporation for the cropland expansion simulations. Using the checkerboard implementation to separate local and non-local effects, EC-EARTH simulates a clear local decrease in evaporation due to cropland expansion, while the non-local effect cause an increase in evaporation over the tropics, resulting in attenuated net effects as shown in Figure 3.2. This dampening effect from non-local feedbacks on locally induced evaporation decreases is also present to a much smaller extent in MPI-ESM in eastern US, the boreal latitudes, and parts of the tropics as well as in CESM in few parts of the tropics (see Figure 3.9).

Regarding afforestation, CESM and MPI-ESM show opposite patterns compared to cropland expansion, with mostly an increase in evaporation (Figure 3.2b,e). However, in CESM the Northern-Hemisphere extra-tropics and the Sahel show a clear increase in annual evaporation due to afforestation, whereby the increase in the extra-tropics is clearly seasonal (JJA) (Figure 3.15 and Figure 3.16). Over the North Atlantic, CESM simulates a widespread and strong decrease of evaporation, which may be linked to the widespread cooling of the North Atlantic in this ESM (De Hertog et al., 2023).

Regarding irrigation expansion, both models (CESM and MPI-ESM) strongly agree on the sign of evaporation change over land and simulate a global increase (Figure 3.2c,f). Differences between both ESMs are mostly related to the extent to which irrigation is applied within the different ESMs (see Figure 3.1). Moreover, in some regions such as the boreal latitudes, the Sahel and Central Europe, MPI-ESM simulates a decrease in evaporation over unaltered grid cells due to the non-local effects induced by irrigation expansion (see Figure 3.11).

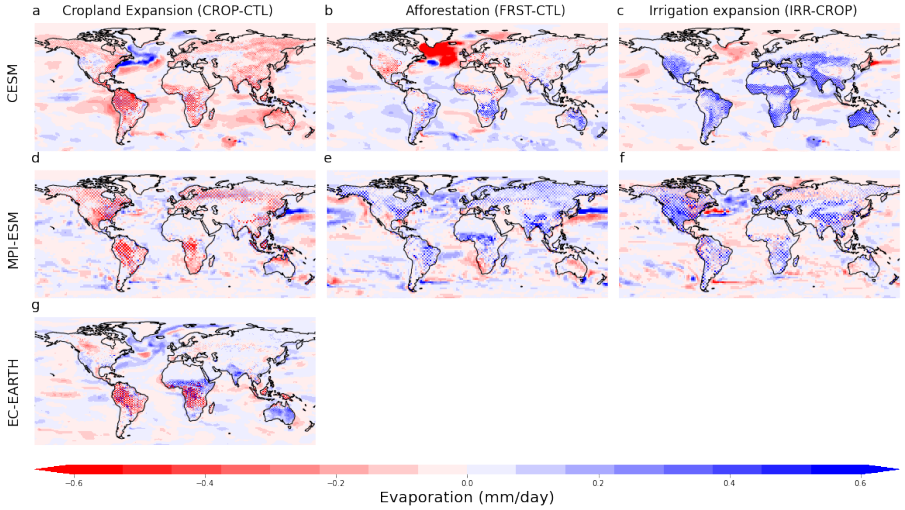

Figure 3.2: The mean annual impacts of land cover and land management changes on evaporation (mm/day), for cropland expansion (CROP-CTL; a,d), afforestation (FRST-CTL; b,e) and irrigation expansion(IRR-CROP; c,f) for CESM and MPI-ESM respectively. Cropland expansion for EC-EARTH is shown in (g).

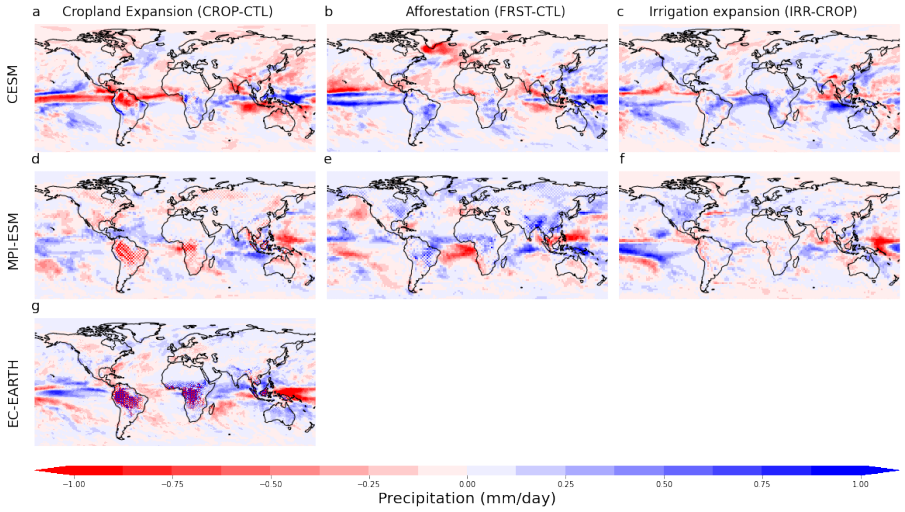

Figure 3.3: The mean annual impacts of land cover and land management changes on precipitation (mm/day), for cropland expansion (CROP-CTL; a,d), afforestation (FRST-CTL; b,e) and irrigation expansion(IRR-CROP; c,f) for CESM and MPI-ESM respectively. Cropland expansion for EC-EARTH is shown in (g).

The effects of LCLMC on precipitation are less distinct across the models, but some regionally consistent patterns emerge (Figure 3.3). Globally, cropland expansion causes a decrease in precipitation while afforestation and irrigation expansion cause an increase. Under the cropland expansion scenario, there is a decrease of precipitation over land in MPI-ESM (Figure 3.3b), mostly generated by locally-induced feedbacks (Figure 3.12). CESM also simulates a decrease of precipitation over most land areas, except for Central America, the Congo basin and Eastern Africa (Figure 3.3a), which are mostly influenced by non-local feedbacks of cropland expansion (Figure 3.12). The patterns of precipitation changes around the tropics in CESM are similar to those found in Portmann et al. (2022). In their study, Portmann et al. (2022) showed that deforestation in CESM is cooling the Northern extra-tropics, which leads to changes in the intensity of the Hadley cell and the position of the intertropical convergence zone, which could also explain the simulated pattern here. In line with CESM, the cropland expansion simulation with EC-EARTH simulate the largest changes in precipitation over the ocean and forest areas within the tropics. However, there is a shift of these changes that is causing less precipitation north of Australia and more precipitation over the tropical Pacific. The strongest feedbacks are again found over the tropical forests, where local feedbacks cause a decrease in precipitation in central South America in all ESMs. However, EC-EARTH also simulates a strong increase of precipitation in neighboring, unmodified grid cells due to non-local feedbacks (Figure 3.12).

Afforestation is causing widespread increases in precipitation over land (Figure 3.3b,e). This increase is quasi-global in MPI-ESM, while in CESM some areas show a precipitation decrease, such as the Indian subcontinent, the Sahel, and Europe. In CESM, the afforestation-induced precipitation differences over the intertropical convergence zone are again similar to those found by Portmann et al. (2022), indicating that shifts of the large-scale circulation determine the precipitation patterns in this ESM. This finding is corroborated by the fact that afforestation-induced feedbacks are again more local in MPI-ESM while the feedbacks simulated by CESM are almost completely non-local (see Figure 3.13).

For the irrigation expansion scenario, all models simulate a global increase in precipitation. In CESM, it is apparent that Southeast Asia is an exception to this pattern and shows a clear reduction of precipitation despite being an area of large-scale irrigation. This finding might be linked to the hypothesis that the regional temperature decreases as a consequence of irrigation expansion (De Hertog et al., 2023), further causing a weakening of the Indian summer monsoon and a decrease of precipitation over large parts of the continent, a feedback mechanism that has also been documented in previous studies (de Vrese et al., 2016; Guimberteau et al., 2012; Thiery et al., 2017). This decrease in precipitation over India is to some extent also present in MPI-ESM, although it is not as strong as in CESM. However, for both ESMs it is clear that the response over this region is mostly non-local (see Figure 3.14) and occurs mainly during JJA (Figure 3.17 and Figure 3.18).
The effects of LCLMCs on MFC show substantial regional difference between CESM and MPI-ESM (Figure 3.4). Overall, the patterns in MFC are highly similar to those seen for precipitation (Figure 3.3) which indicates that these precipitation changes are likely driven by the changes in MFC. Under cropland expansion, the shifts in precipitation bands for

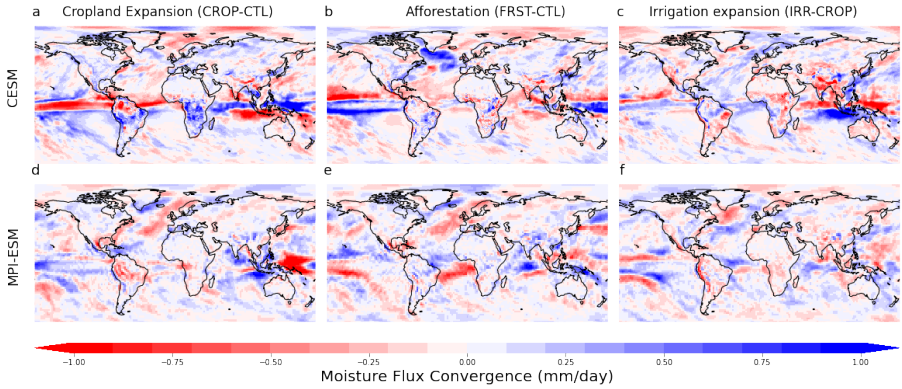

Figure 3.4: The mean annual impacts of land cover and land management changes on Moisture Flux Convergence (MFC) in mm/day, for cropland expansion (CROP-CTL; a,d), afforestation (FRST-CTL; b,e) and irrigation expansion(IRR-CROP; c,f) for CESM and MPI-ESM respectively. For EC-EARTH the P-E plots are available in section 3.6.3.

CESM are likely caused by the effects in MFC over those areas. Decrease in MFC over the Amazon and India, while Central South America and Central Africa show a clear increase in MFC, and consequently an increase in precipitation. In MPI-ESM, there is generally a decrease in MFC as a consequence of cropland expansion (Figure 3.4a,c), which appears to be related to changes in the areas where the largest LCLMC occurred (which confirms the mainly local precipitation changes shown in Figure 4A). In EC-EARTH, we see a general increase of $P-E$, used here as proxy for MFC, over the unaltered patches while the deforested patches show a clear decrease over the tropics (see Figure 3.19g). Regarding afforestation (Figure 3.4b,e), the patterns in MFC are less strong in CESM with an increase over Brazil and parts of East Africa and a decrease over the Sahel and southern Africa. In MPI-ESM, there is generally an increase in MFC over land. Following irrigation expansion (Figure 3.4c,f), there is generally a decrease in MFC over land for both ESMs. This decrease in MFC is especially strong over Southeast Asia in CESM but is also apparent for MPI-ESM and could explain the precipitation decreases shown over this region in Figure 3.3 further confirming the weakened Indian Summer Monsoon hypothesis.

3.3.2 Changes in local precipitation and evaporation length scales due to LCLMC

To unravel the direct impact of LCLMC-induced evaporation changes on the precipitation over land (and the other way around), we evaluate the outputs from WAM-2layers and illustrate local evaporation and precipitation length scales for each model and LCLMC scenario. An overview of consistent patterns for change in moisture fluxes and length scales is shown in Table 3.1. Even in their control simulations, the different ESMs show very different magnitudes of length scales of moisture recycling, both for the precipitation length scale

(Figure 3.5) and the evaporation length scale (Figure 3.6). CESM shows the largest length scales indicating that the importance of local recycling is relatively small. EC-EARTH, in contrast, generally shows very low values of the length scale indicating that local recycling is more important within this ESM. Despite the large differences in magnitude between the length scales of the different ESMs, the spatial patterns are quite similar. The precipitation length scale is smallest over tropical rainforests and mountain ranges (see for example the Tibetan Plateau) indicating that these locations mostly get precipitation from nearby evaporation. These patterns also occur for the evaporation length scale, although here locations with a dry and continental climate such as Siberia and Greenland also show very low values. This implies that evaporation occurring within these locations generally precipitates nearby.

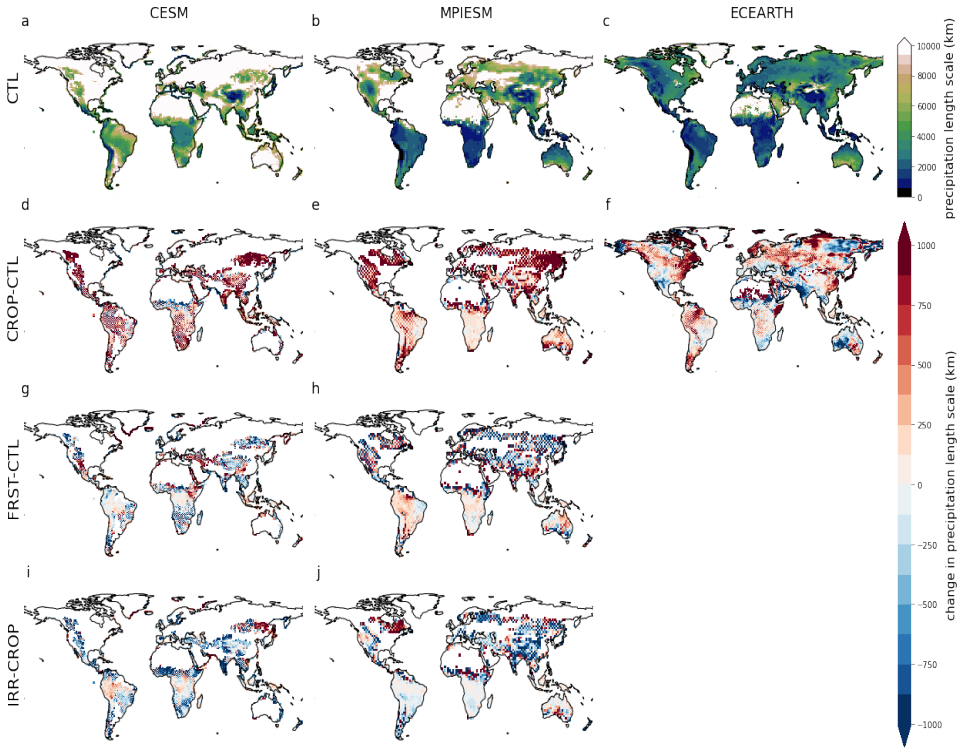

Figure 3.5: The annual mean precipitation length scale (km) for the control (CTL) simulation in CESM (a), MPI-ESM (b) and EC-EARTH (c). The effect of cropland expansion (CROP-CTL) on the annual mean precipitation length scale is shown for CESM (d), MPI-ESM (e) and EC-EARTH (f). The effect of afforestation (FRST-CTL) is shown for CESM (g) and MPI-ESM (h) and finally the effect of irrigation expansion (IRR-CROP) is shown for CESM (i) and MPI-ESM (j). Note that in the difference plots in (d)–(j), the areas with a reference evaporation length scale higher than 10000 km are cropped out.

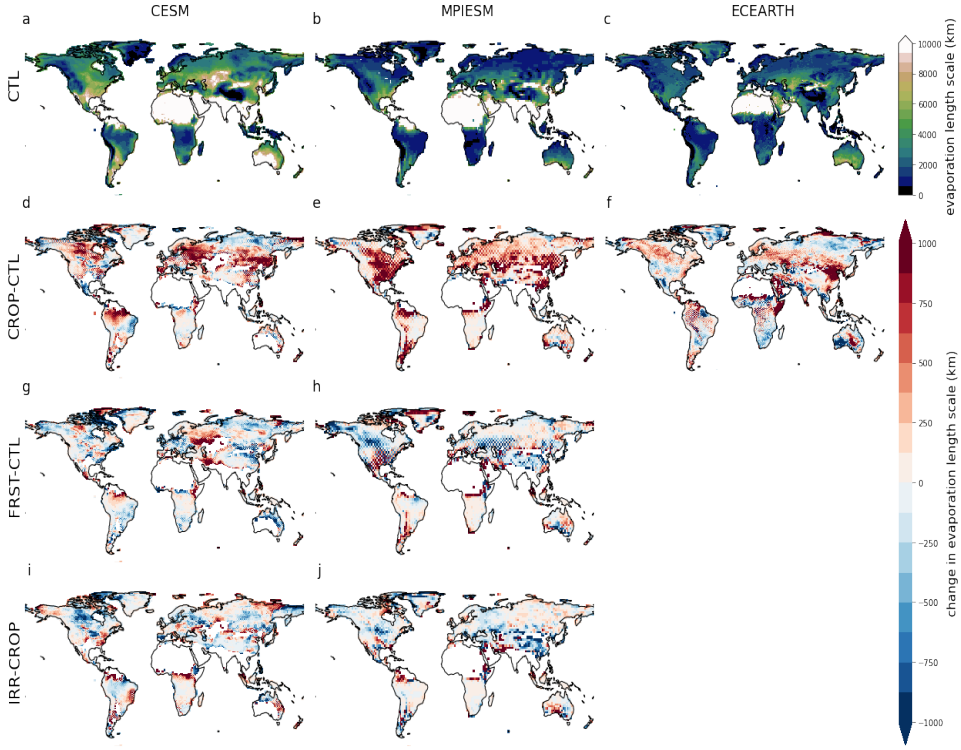

Figure 3.6: The annual mean evaporation length scale (km) for the CTL simulation in CESM (a), MPI-ESM (b) and EC-EARTH (c). The effect of cropland expansion (CROP-CTL) on the annual mean evaporation length scale is shown for CESM (d), MPI-ESM (e) and EC-EARTH (f). The effect of afforestation (FRST-CTL) is shown for CESM (g) and MPI-ESM (h) and finally the effect of irrigation expansion (IRR-CROP) is shown for CESM (i) and MPI-ESM (j). Note that in the difference plots in (d)–(j), the areas with a reference precipitation length scale higher than 10000 km are cropped out.

In general, both the precipitation and evaporation length scale increase as a consequence of cropland expansion (see Figures 3.5d,e,f and 3.6d,e,f). In MPI-ESM, it seems that the Congo Basin is an exception with no clear changes in local recycling occurring there. In EC-EARTH, the patterns are more blurred than in the other ESMs with a decrease in length scales in some regions, such as South Africa and spots over the Central U.S. . However, over regions where the largest cropland expansion occurred (such as Amazon basin and China, see also Figure 3.1), the patterns are consistent with the other ESMs. Over Latin America, a dipole pattern of the change in the evaporation length scale in both EC-EARTH and CESM appears, showing an increase in the West and a decrease in the East. The general increase in length scale due to cropland expansion implies that the LCLMC induces a decrease in local recycling.

Table 3.1: Summary of the effects of moisture fluxes over land due to the different LCLMC. Each cell indicates where the changes in moisture response are consistent in sign.

LCLMC	E	P	λ_ε	λ_ρ
CROP-CTL	decrease over tropics	regional increase/decrease	mostly decrease	mostly increase
FRST-CTL	increase over tropics	increase over tropics	global increase	mostly decrease
IRR-CROP	global increase	global increase	global decrease	global decrease

Afforestation (Figures 3.5g,h and 3.6g,h), induces a pattern that is opposite to the cropland expansion case, with a decrease in length scale for both precipitation and evaporation. However, in some areas, the patterns diverge from the general trend, e.g. afforestation causes an increase of the evaporation length scale over the Amazon in CESM, and an increase of the precipitation length scale over the tropics in MPI-ESM. In general, the changes in both length scales are stronger for the extra-tropics, which is particularly visible for the evaporation length scale. This feedback on the evaporation length scale may be explained by the fact that the tropics are already densely forested in the CTL scenario and thus the additional trees do not alter the local recycling favouring conditions, in contrast to the sparsely forested extra tropics (Figure 3.1).

Regarding irrigation expansion (Figures 3.5i,j and 3.6i,j), the effects on the evaporation length scale are less clear and generally of small magnitude. Irrigation-induced differences show a tendency towards a decreased evaporation length scale, which is rather consistent in MPI-ESM but in CESM this pattern is less clear. The effects on the precipitation length scale in both ESMs are larger and more consistently decreasing due to irrigation expansion. The change in precipitation length scale is small over the tropics due to the small amount of irrigation applied in this region (Figure 3.1). We even observe a slight increase in length scale over the tropical forest in CESM and over some areas in the U.S. in MPI-ESM, which might imply circulation changes in those regions.

3.3.3 Changes in continental moisture recycling due to LCLMC

While there are substantial differences in the local feedbacks of LCLMC on the water cycle, their net impact on water availability over land might be the same. Here, we evaluate how LCLMC impacts E, P and P-E over land, and we identify the direct impact of LCLMC-induced feedbacks on these fluxes via continental moisture recycling (see Section 2.3.4). The values of total annual precipitation (P), continental precipitation (Pc), continental precipitation recycling (ρ_c), evaporation (E), continental evaporation (Ec) and continental evaporation recycling (ε_c) are included in section 3.6.4. Cropland expansion causes a net decrease of evaporation from land in CESM and MPI-ESM, while EC-EARTH

simulates a small net increase of continental evaporation (Figure 3.7a). Through this decrease of evaporation in CESM and MPI-ESM, less moisture is available for continental moisture recycling (dark bars in Figure 3.7a) and for precipitation over oceans (light bars in Figure 3.7a). Analogously, cropland expansion is causing a net decrease of precipitation over land in CESM and MPI-ESM, but a net increase in EC-EARTH, which is due to contrasting signs of change in different parts of the globe (Figure 3.21). In the former two models, the simulated decrease of precipitation mainly results from decreased moisture imports from the ocean (light bars in Figure 3.7b), and only 42% and 26% respectively of the precipitation deficit is estimated to be of continental origin (dark bars in Figure 3.7b).

The effects on evaporation from land due to afforestation are consistent in sign and generally cause an increase for both ESMs. A large part of this increase is available for continental moisture recycling (dark bars in Figure 3.7a) in CESM (48%), but is negligible for MPI-ESM (2%). In MPI-ESM the increase in land evaporation mainly rains out over the oceans (light bars in Figure 3.7a). Evaluated over all land regions, afforestation increases precipitation over land in both MPI-ESM and CESM (Figure 3.7b). The magnitude is much smaller in CESM due to the large spatial heterogeneity in precipitation feedbacks (Figure 3.20), which cancel each other out causing only a small net increase of precipitation over land. For MPI-ESM, there is a large heterogeneity within the signal of change (Figure 3.20), causing diverging contributions of moisture for continental precipitation from ocean and land. Atmospheric circulation changes in this model cause an increase in precipitation of oceanic origin on land, while less precipitation is estimated to be of continental origins.

Regarding irrigation expansion, there is a strong increase of evaporation from land in CESM, of which most rains out over the oceans (light bar in Figure 3.7a), and only a small fraction (17%) is available for continental moisture recycling (dark bar in Figure 3.7a). In MPI-ESM, the effect is smaller due to some areas of decreased recycling (Figure 3.21) but the results still show an overall increase in evaporation of which most rains out over the ocean. For precipitation over land, the effect is not consistent across the ESMs. In CESM there is an increase in precipitation over land of which 34% is available for continental recycling. In contrast, for MPI-ESM there is a global decrease of continental precipitation, of which 12% stems from the precipitation deficit over land.

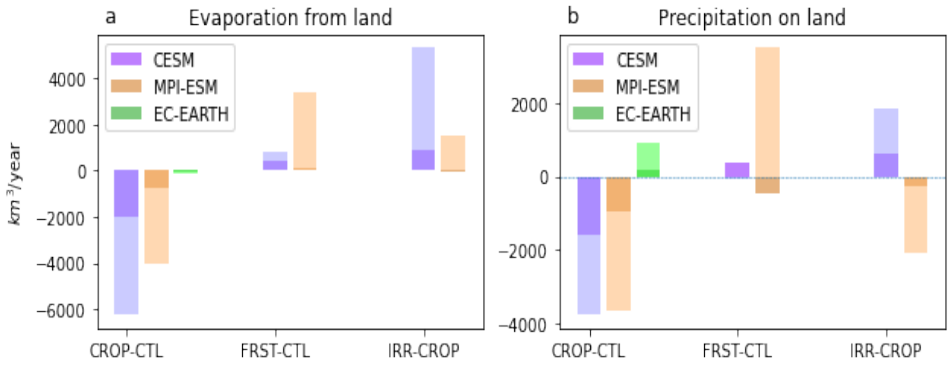

Figure 3.7: The global change in annual mean evaporation (a) and precipitation (b) on land is shown for CESM in blue, MPI-ESM in orange and EC-EARTH in green for cropland expansion (CROP-CTL), afforestation (FRST-CTL) and irrigation expansion (IRR-CROP). The contribution of continental moisture recycling changes is shown in a darker shade of the ESMs respective colours.

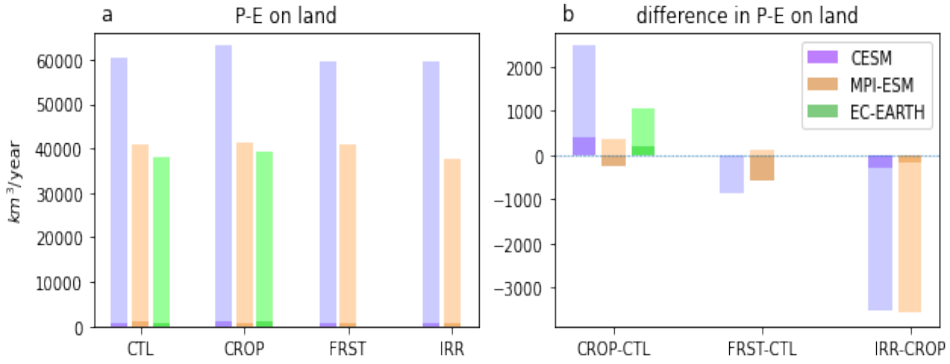

Figure 3.8: The total annual mean P-E on land (a) and change in P-E on land (b) is shown for CESM in blue, MPI-ESM in orange and EC-EARTH in green for cropland expansion (CROP-CTL), afforestation (FRST-CTL) and irrigation expansion (IRR-CROP). The contribution of continental moisture recycling changes is shown in a darker tone of the ESMs respective colours.

Finally, we can quantify the global effects of LCLMC on global water exports from land towards the ocean by analysing the feedbacks on $P-E$. In general, $P-E$ is positive for all three ESMs, being substantially larger in CESM than in MPI-ESM and EC-EARTH (Figure 3.8a), indicating that the land receives more water from the atmosphere, and of oceanic origin, than it provides through evaporation. Both evaporation and precipitation decreases

for MPI-ESM and CESM due to cropland expansion (Figure 3.7), but the decrease in evaporation is larger causing a net surplus of water at the land surface (i.e., $\Delta(P-E) > 0$). There is also a net surplus of water for EC-EARTH although this is mostly due to increased continental precipitation (Figure 3.7). In EC-EARTH and CESM, the contribution due to continental recycling is 16% and 20% respectively (light bars in Figure 3.7 and Figure 3.8b), but the majority comes from changes in oceanic moisture. This differs from MPI-ESM, where less moisture is recycled (dark bar in Figure 3.8b). Afforestation, in turn, is causing a net loss of water at the land surface for both ESMs. CESM simulates an increase in water export from land through an increase of land evaporation that rains out over the ocean (Figure 3.8b). In contrast MPI-ESM shows a slight increase in water availability over land due to oceanic moisture, with the effect of continental moisture changes dominating the global decrease in water availability. Following irrigation expansion, both CESM and MPI-ESM simulate a decrease in water available on land. In both simulations, enhanced evaporation through irrigation from land (see Figure 3.7a) mostly rains out over the ocean (light bars in Figure 3.8b), thus a loss of water on land to the ocean with the contribution of continental recycling being 8% and 5% for CESM and MPI-ESM, respectively.

3.4 Discussion

LCLMC can have substantial effects on atmospheric moisture fluxes and the local and continental recycling of moisture that determine water availability on land. Common patterns emerge from our multi-model analysis, despite strong differences in the implementation of LCLMC and the simulation of the hydrological response in the different ESMs. For cropland expansion, all three ESMs agree that there is a general decrease over land in evaporation and precipitation over most regions as well as a decreased local recycling strength. In contrast, afforestation and irrigation expansion show an opposite pattern of both increased precipitation and evaporation over most regions with enhanced local recycling strength. Here we will discuss some of the discrepancies between the different ESMs and their implications on moisture fluxes and moisture recycling.

3.4.1 Different hydroclimatic responses of ESMs to LCLMC

The effects of LCLMC within the different ESMs have strong regional variations (e.g., Figure 3.2 and Figure 3.3). The differing length scales between ESMs (Figure 3.6 and Figure 3.5) illustrate that different processes dominate within the different ESMs: EC-EARTH shows a stronger importance of local processes in contrast to CESM, where atmospheric circulation seems to dominate the effects. This difference is also clear from the effects on moisture fluxes as EC-EARTH simulates strong mesoscale feedbacks (10 to 100 km), while in CESM global circulation changes appear to dominate. CESM is known to be an ESM with a strong natural variability, as was shown in several other studies (Deser et al., 2012, 2020). It has also been shown to simulate large-scale circulation shifts as a consequence to land cover change (Portmann et al., 2022; Devaraju et al., 2018).
Discrepancies in the CTL length scales estimated for each ESM could also stem from the

different spatial resolutions employed here (CESM:0.90°x1.25°, MPI-ESM:1.88°x1.88° and EC-EARTH:0.7°x0.7°). Although the concept of length scales is independent of the spatial resolution (van der Ent and Savenije, 2011), the capability of ESMs to resolve processes explicitly is resolution-dependent. This implies that certain processes, such as mesoscale convection, are potentially better resolved within EC-EARTH than in CESM and MPI-ESM.

The way LCLMC is implemented in the different ESMs also causes some discrepancies. Some of the ESMs only represent crops by few generic crop types (such as MPI-ESM) while others have different crop types representing different biophysical properties. CESM has eight different crop types representing common crops around the world (Lombardozzi et al., 2020). In CESM, maize has high evaporation rates which might explain why afforestation over the Northern Hemisphere extra-tropics is causing a decrease in evaporation, with particularly strong effects during summer Figure 3.15. The discrepancy between the effects due to afforestation and cropland expansion can be partially explained by a saturation effect, as the effects of adding trees are likely non-linear (Winckler et al., 2017b). For example, in the tropics, extreme deforestation will have larger impacts on the hydrological cycle than adding trees in an already densely forested region. This effect could explain some differences between these simulations such as the smaller precipitation length scale changes in afforestation over the tropics.

The implementation of irrigation also causes substantial differences in climatic responses among the ESMs, as the maps of irrigation extent and amounts differ strongly (Figure 3.1). Both MPI-ESM and CESM show an increase in precipitation, except for the Indian subcontinent where both ESMs show a decrease in precipitation. As there is a cooling over all irrigated areas (De Hertog et al., 2023), there is a lower land–ocean temperature contrast, which reduces convection over land and therefore precipitation (Figure 3.3 and Figure 3.4). This occurs despite the increases in evaporation (Figure 3.2) and enhanced local precipitation recycling (Figure 3.5). Considering all the above, it is likely that the reduced precipitation shown here is caused by a weakened Indian Summer Monsoon as was highlighted by previous studies (Puma and Cook, 2010; de Vrese et al., 2016; **?**; **?**).

3.4.2 Implications of changes in moisture recycling due to LCLMC

LCLMC strongly affects the redistribution of moisture over land in the ESMs. While the absolute length scales of moisture recycling differ among the ESMs, LCLMC-induced changes are consistent across the ESMs, with cropland expansion causing decreased recycling and afforestation and irrigation expansion mostly causing enhanced local recycling (Figure 3.6 and Figure 3.5). The effects of LCLMC on continental recycling and the continental contribution to precipitation over land and evaporation from land are less consistent across ESMs (Figure 3.7 and Figure 3.8), but also geographically more heterogeneous within the ESMs (Figure 3.20 and Figure 3.21). This is due to the complex interactions of local feedbacks with non-local feedbacks, such as advection and circulation changes,

which all affect the redistribution of water globally.

Although the effects of LCLMC on the precipitation and evaporation changes are substantial, they are not as large as previously assumed within literature (Tuinenburg et al., 2020; Hoek van Dijke et al., 2022; Baudena et al., 2021; Wunderling et al., 2022; Staal et al., 2018). This could partially be the case due to the less extensive scenarios considered here (only 50% change due to checkerboard approach). However, differences are expected because most of these studies are based on reanalyses and can only estimate the impact of upwind LCLMC changes on downwind precipitation using constant recycling ratios, neglecting any other feedback. However, to fully capture the impact of LCLMC on moisture recycling, LCLMC ESM simulations should be compared to a control simulation; and the resulting (substantial) differences in recycling ratios show that these feedbacks are not negligible. As LCLMC becomes increasingly relevant as a climate mitigation strategy it is important to include the potential side effects of these strategies on the water cycle. More research is needed to better constrain the effects of LCLMC on moisture recycling in order to support science that can guide future land cover planning.

3.4.3 Circulation effects induced by checkerboard LCLMC implementation

The specific setup of these simulations, with a checkerboard pattern LCLMC, also has limitations and causes some artefacts within the results. This is, for example, illustrated in the patterns of evaporation (Figure 3.2) and precipitation changes (Figure 3.3) from EC-EARTH, especially over the tropics. Due to the scale dependence of the effects of land cover changes on moisture fluxes (Spracklen et al., 2018), mesoscale circulation effects occur in EC-EARTH but do not appear in the other (coarser) ESMs. This checkerboard-like feedback would likely not occur if a full land cover change was simulated instead of the checkerboard implementation of the LCLMC. This implementation could have some important implications, as the non-local effects for EC-EARTH do not represent the effects one would get in a full land cover change simulation, implying that the assumptions behind the checkerboard approach are not met (Winckler et al., 2017a; De Hertog et al., 2023). Moreover, the LCLMC-induced effects on atmospheric circulation and moisture fluxes also affect other climate variables, such as temperature. These checkerboard-induced circulation changes could also explain the differences between the temperature effects found in De Hertog et al. (2023): here, the checkerboard-implementation of cropland expansion in EC-EARTH caused tropical warming, and the simulations from Boysen et al. (2020) with EC-EARTH that simulated full deforestation changes (forest to grass conversion), showed tropical cooling. Further research is required to completely understand the implications of checkerboard-induced climate effects. For example, the LCLMC could be implemented in different densities (1/8, 1/4, 1/2) next to a full deforestation experiment to assess whether these effects are true artefacts of the LCLMC patterns. However, this might imply that the checkerboard approach for signal separation requires a rough spatial implementation to avoid mesoscale circulation feedbacks as seen here for EC-EARTH.

3.5 Conclusions

In this study, we analysed the effects of land cover and land management changes (LCLMC) on the atmospheric water cycle in a slate of idealised simulations (cropland expansion, afforestation and irrigation expansion) performed by three different Earth System Models (ESMs). We showed that the effects on moisture fluxes are substantial with, generally, decreased evaporation and precipitation over land due to cropland expansion and the opposite effects for afforestation and irrigation expansion. However, substantial discrepancies between the different ESMs exist, with EC-EARTH displaying important local recycling and mesoscale circulation effects, while CESM shows a dominance of large-scale atmospheric circulation shifts. These differences can have various causes, such as model parameterisations of crucial processes (e.g., convection) or the extent to which different land cover types are implemented within the ESMs on a global scale. Because some of these effects might have been indirectly influenced by the checkerboard LCLMC pattern used in this study, we advocate for more research to assess the implications of possible checkerboard-induced climate effects and the applicability of this approach for signal separation into local and non-local effects. Despite the strong differences between ESMs, the effects on local recycling are generally consistent in sign, with cropland expansion causing a decreased recycling strength, and afforestation and irrigation expansion generally causing an increased recycling strength. Overall we find that cropland expansion causes a net increase in water availability on land while afforestation and irrigation expansion cause a net decrease. Our simulations show that changes due to atmospheric circulation patterns play an important role in explaining these patterns and should be taken into account when assessing the effects of LCLMC on moisture recycling.

This is the first study – to our knowledge – to explicitly consider moisture recycling when assessing the LCLMC effects on moisture fluxes using multiple ESMs. Our results show that the effects of LCLMC on moisture recycling are substantial both on the local and global scale, with clear implications for water availability on land. The potential effects of LCLMC on the atmospheric water cycle should therefore be considered in future land cover planning.

Data and code availability

The scripts used for the analysis of the moisture fluxes and the adapted version of WAM-2layers can be found on the GitHub page of the Department of Hydrology and Hydraulic Engineering of VUB (`https://github.com/VUB-HYDR/2023_DeHertog_etal_ESD`). The simulation data used in this paper will be made available through the DKRZ, for those interested in using these data until publication please contact the authors.

3.6 Supplementary material

3.6.1 Signal separated plots evaporation and precipitation

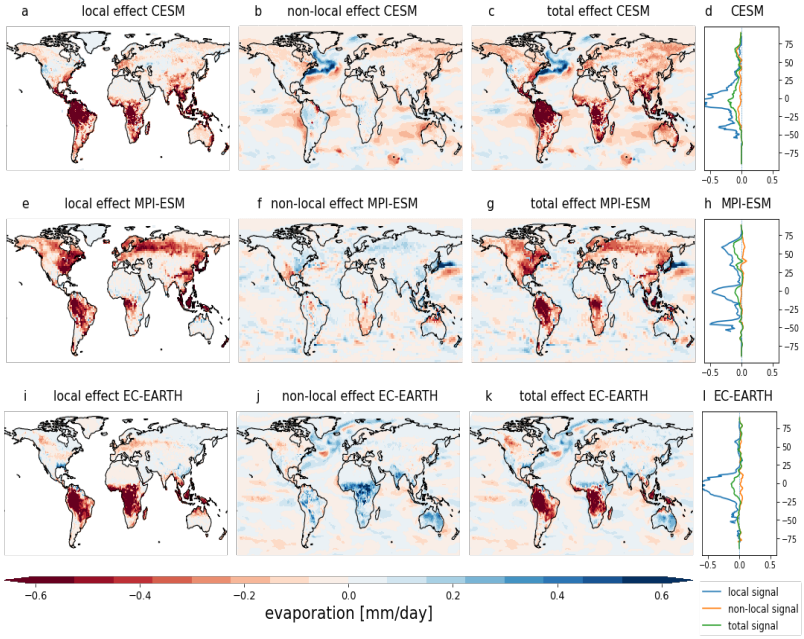

Figure 3.9: Annual mean evaporation response in mm/day to cropland expansion (CROP-CTL) of CESM, MPI-ESM and EC-EARTH. The local effect in CESM (a), the non-local effect (b) and the total effect (c). The latitudinal average of the local (blue), non-local (yellow) and total (green) signals of CESM (d). (e-h): same as (a-d), but for MPI-ESM. (i-l): same as (a-d), but for EC-EARTH. The stippling on the maps shows grid cells where all the sign of change is consistent throughout the simulation.

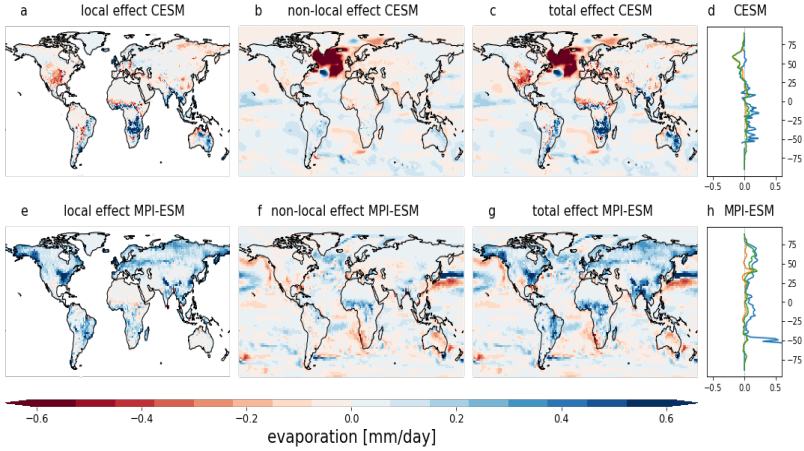

Figure 3.10: Annual mean evaporation response in mm/day to afforestation (FRST-CTL) of CESM and MPI-ESM. The local effect in CESM (a), the non-local effect (b) and the total effect (c). The latitudinal average of the local (blue), non-local (yellow) and total (green) signals of CESM (d). (e-h): same as (a-d), but for MPI-ESM. The stippling on the maps shows grid cells where all the sign of change is consistent throughout the simulation.

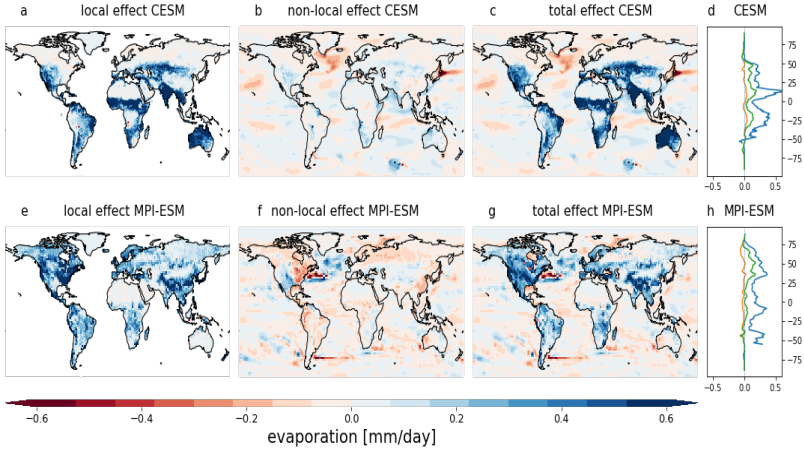

Figure 3.11: Annual mean evaporation response in mm/day to irrigation expansion (IRR-CROP) of CESM and MPI-ESM. The local effect in CESM (a), the non-local effect (b) and the total effect (c). The latitudinal average of the local (blue), non-local (yellow) and total (green) signals of CESM (d). (e-h): same as (a-d), but for MPI-ESM. The stippling on the maps shows grid cells where all the sign of change is consistent throughout the simulation.

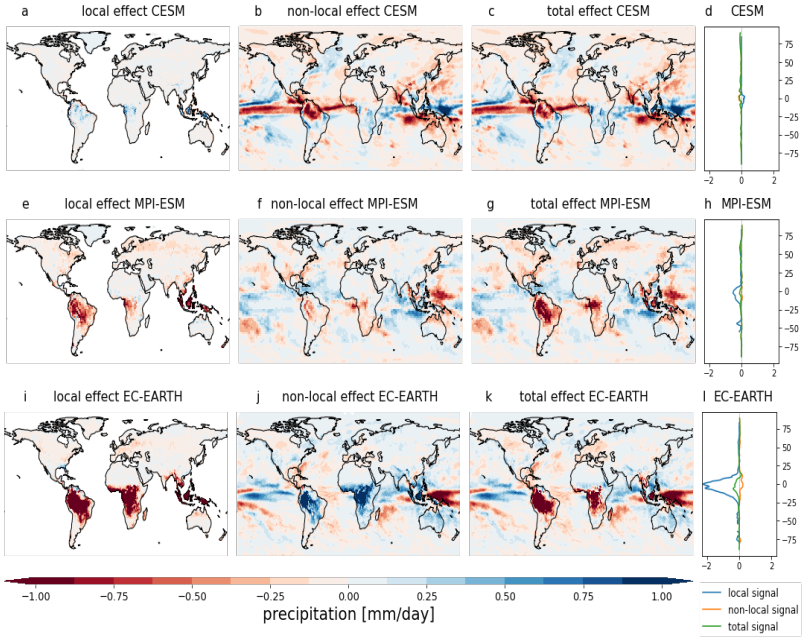

Figure 3.12: Annual mean precipitation response in mm/day to cropland expansion (CROP-CTL) of CESM, MPI-ESM and EC-EARTH. The local effect in CESM (a), the non-local effect (b) and the total effect (c). The latitudinal average of the local (blue), non-local (yellow) and total (green) signals of CESM (d). (e-h): same as (a-d), but for MPI-ESM. (i-l): same as (a-d), but for EC-EARTH. The stippling on the maps shows grid cells where all the sign of change is consistent throughout the simulation.

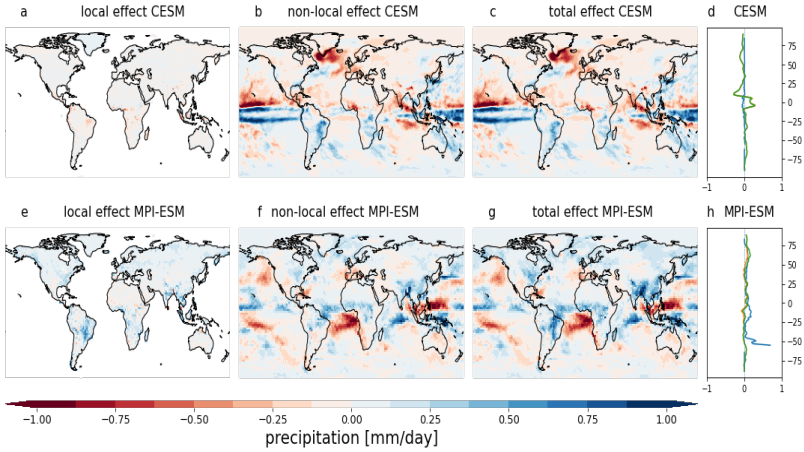

Figure 3.13: Annual mean precipitation response in mm/day to afforestation (FRST-CTL) of CESM and MPI-ESM. The local effect in CESM (a), the non-local effect (b) and the total effect (c). The latitudinal average of the local (blue), non-local (yellow) and total (green) signals of CESM (d). (e-h): same as (a-d), but for MPI-ESM. The stippling on the maps shows grid cells where all the sign of change is consistent throughout the simulation.

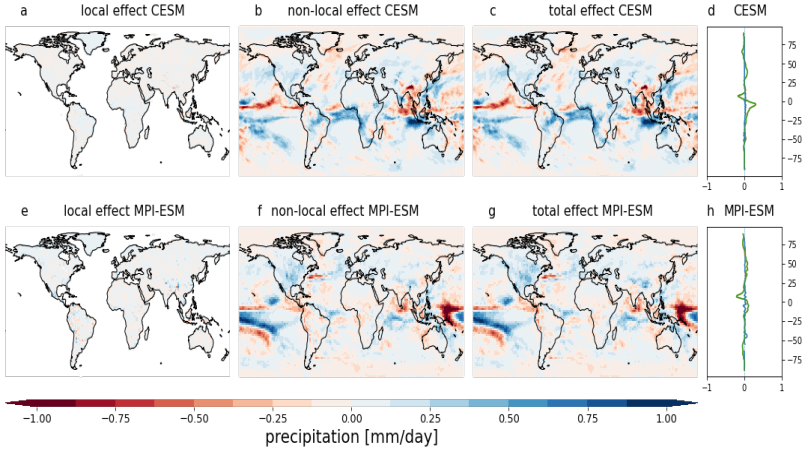

Figure 3.14: Annual mean precipitation response in mm/day to irrigation expansion (IRR-CROP) of CESM and MPI-ESM. The local effect in CESM (a), the non-local effect (b) and the total effect (c). The latitudinal average of the local (blue), non-local (yellow) and total (green) signals of CESM (d). (e-h): same as (a-d), but for MPI-ESM. The stippling on the maps shows grid cells where all the sign of change is consistent throughout the simulation.

3.6.2 Seasonal effects on evaporation and precipitation

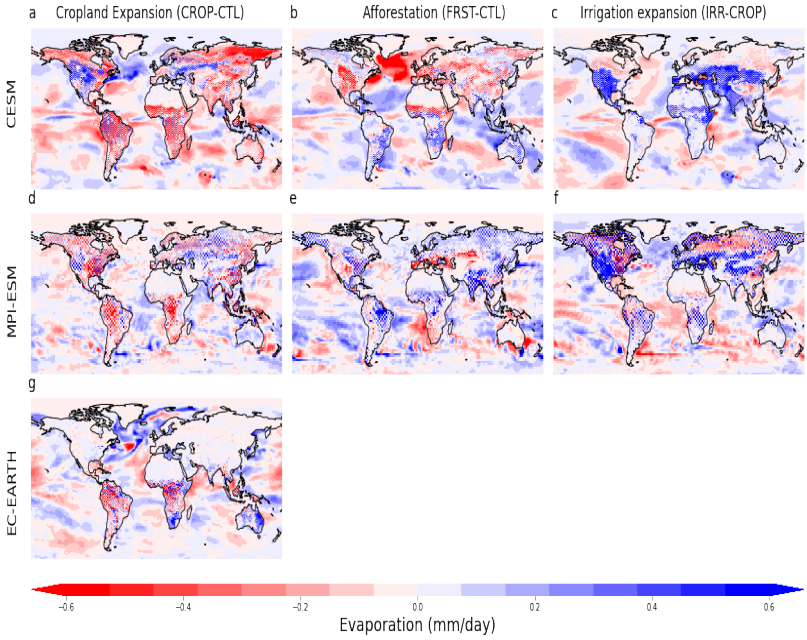

Figure 3.15: The seasonal mean (JJA) effects on evaporation in mm/day as a consequence of cropland expansion (CROP-CTL) in CESM (a), MPI-ESM (d) and EC-EARTH (g), for afforestation (FRST-CTL) in CESM (b) and MPI-ESM (e) and irrigation expansion (IRR-CROP) for CESM (c) and MPI-ESM (f).

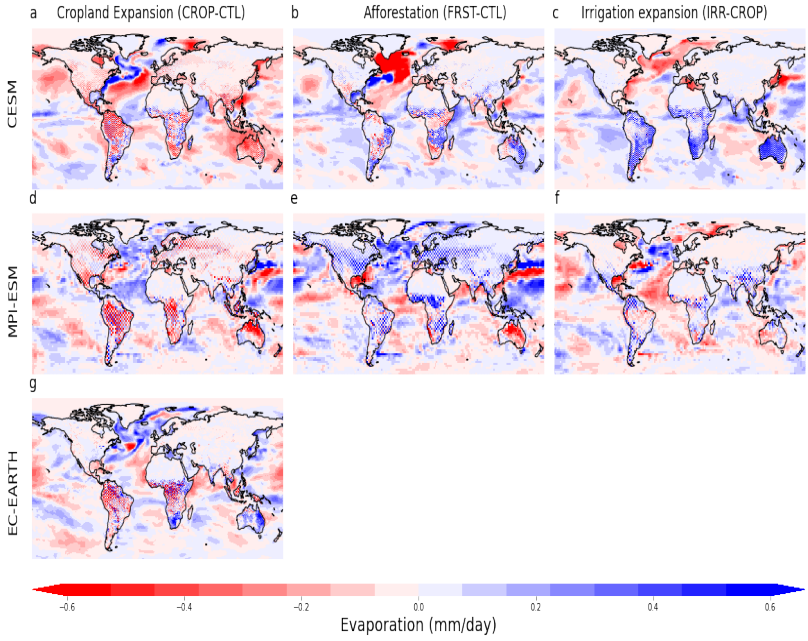

Figure 3.16: The seasonal mean (DJF) effects on evaporation in mm/day as a consequence of cropland expansion (CROP-CTL) in CESM (a), MPI-ESM (d) and EC-EARTH (g), for afforestation (FRST-CTL) in CESM (b) and MPI-ESM (e) and irrigation expansion (IRR-CROP) for CESM (c) and MPI-ESM (f).

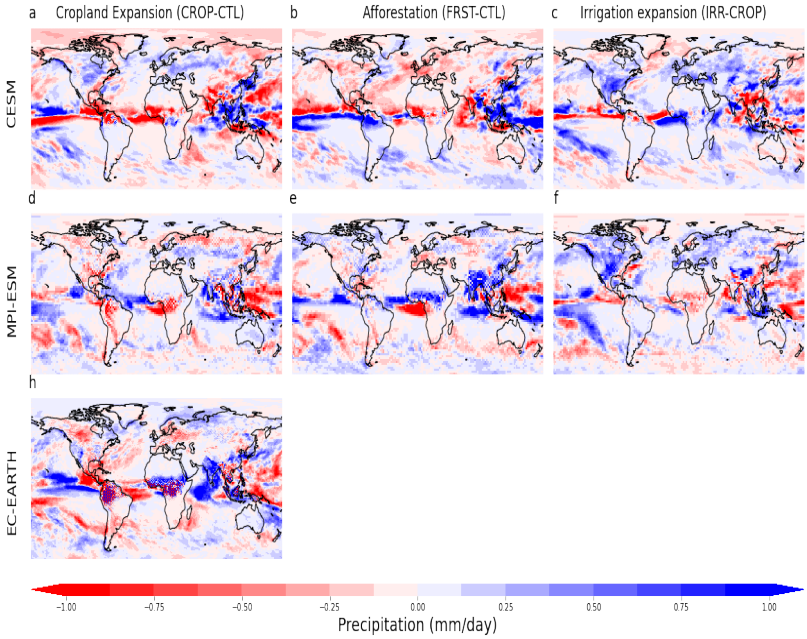

Figure 3.17: The seasonal mean (JJA) effects on precipitation in mm/day as a consequence of cropland expansion (CROP-CTL) in CESM (a), MPI-ESM (d) and EC-EARTH (g), for afforestation (FRST-CTL) in CESM (b) and MPI-ESM (e) and irrigation expansion (IRR-CROP) for CESM (c) and MPI-ESM (f).

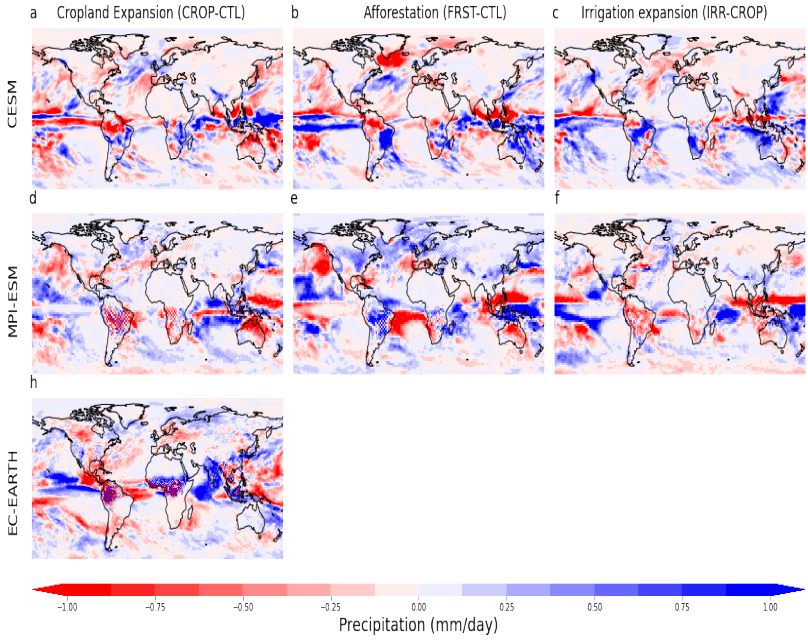

Figure 3.18: The seasonal mean (DJF) effects on precipitation in mm/day as a consequence of cropland expansion (CROP-CTL) in CESM (a), MPI-ESM (d) and EC-EARTH (g), for afforestation (FRST-CTL) in CESM (b) and MPI-ESM (e) and irrigation expansion (IRR-CROP) for CESM (c) and MPI-ESM (f).

3.6.3 P-E as proxy for moisture flux convergence

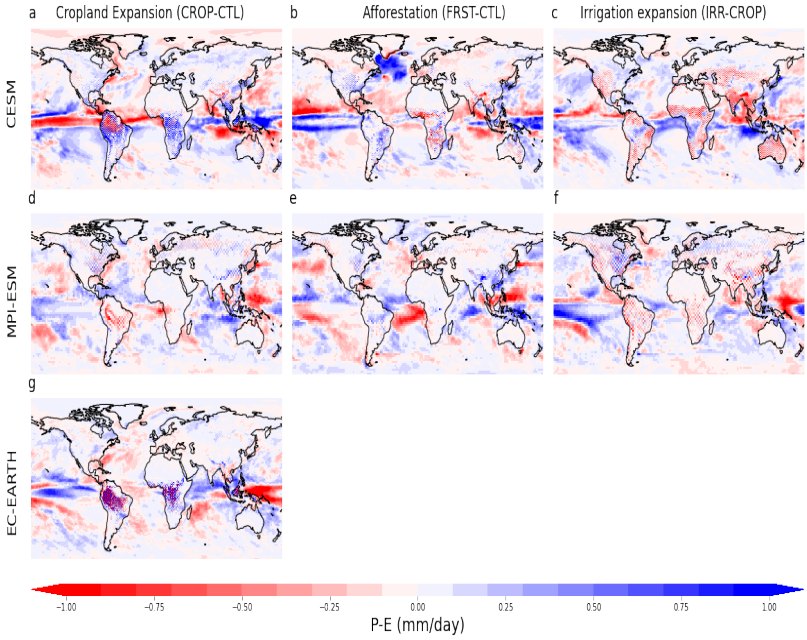

Figure 3.19: The annual mean effects on P-E in mm/day as a consequence of cropland expansion (CROP-CTL) in CESM (a), MPI-ESM (d) and EC-EARTH (g) for afforestation (FRST-CTL) in CESM (b) and MPI-ESM (e) and irrigation expansion (IRR-CROP) for CESM (c) and MPI-ESM (f).

3.6.4 Moisture fluxes of continental origin

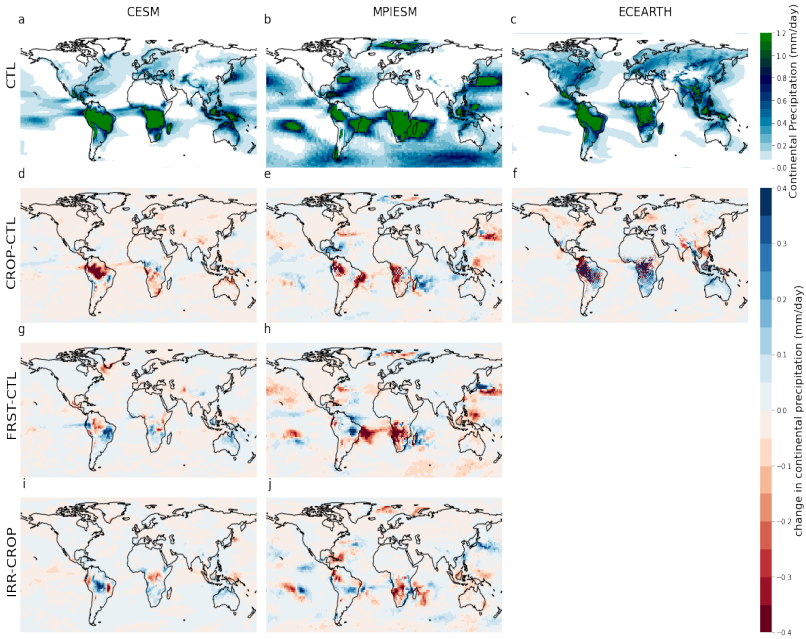

Figure 3.20: The annual mean continental evaporation is shown in mm/day for the CTL simulation in CESM (a), MPI-ESM (b) a,d EC-EARTH (c). The effect of cropland expansion (CROP-CTL) on the annual mean continental evaporation is shown for CESM (d), MPI-ESM (e) and EC-EARTH (f). The effect of afforestation (FRST-CTL) is shown for CESM (g) and MPI-ESM (h) and finally the effect of irrigation expansion (IRR-CROP) is shown for CESM (i) and MPI-ESM (j).

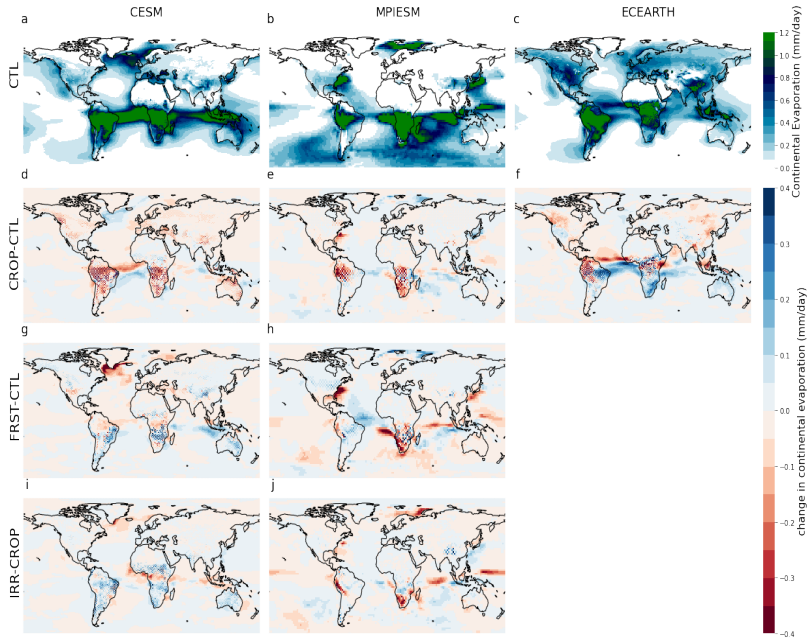

Figure 3.21: The annual mean continental precipitation is shown in mm/day for the CTL simulation in CESM (a), MPI-ESM (b) a,d EC-EARTH (c). The effect of cropland expansion (CROP-CTL) on the annual mean continental precipitation is shown for CESM (d), MPI-ESM (e) and EC-EARTH (f). The effect of afforestation (FRST-CTL) is shown for CESM (g) and MPI-ESM (h) and finally the effect of irrigation expansion (IRR-CROP) is shown for CESM (i) and MPI-ESM (j).

Table 3.2: Summary of annual total values of P, Pc, ρ_c, E, Ec, ε_c for the different simulations and ESMs. The absolute values are given in $km^3/year$.

CESM	P	Pc	ρ_c	E	Ec	ε_c
CTL	4359380	677025	0.155	2519998	659515	0.262
CROP	4244858	628946	0.148	2329935	599010	0.257
FRST	4356876	688149	0.158	2544179	671143	0.264
IRR	4300741	647669	0.151	2492105	626196	0.251
MPI-ESM	P	Pc	ρ_c	E	Ec	ε_c
CTL	3304814	468189	0.141	2065653	434761	0.210
CROP	3193252	438837	0.137	1942738	413053	0.213
FRST	3411430	43719	0.133	2168825	437156	0.201
IRR	3130711	431297	0.138	1988772	410919	0.207
EC-EARTH	P	Pc	ρ_c	E	Ec	ε_c
CTL	3597150	749179	0.208	2437720	72247	0.296
CROP	3625020	754114	0.208	2433458	720834	0.296

Chapter 4

Impacts of future land cover changes on heat stress and human health

In order to achieve the low-warming targets of the Paris agreement large scale and deep emission reductions are required. Within these low-warming scenarios, land-based mitigation is a crucial component to achieve these temperature goals. However, the effects of future land cover and land management changes on climate are poorly constrained and often not considered in the creation of future scenarios by Integrated Assessment Models. Here we show, using fully coupled Earth System Model simulations, that the land use scenario is crucial for assessing climate effects and impacts on humans in future low-warming scenarios. The difference between an inequality and sustainability land use scenario are shown to cause a global cooling of ca. 0.3 K and generally a clear reduction in heat stress over land. Adverse impacts on humans are substantially lower in a world with sustainable land cover change compared to the inequality scenario. Labour capacity is higher over the tropics, while heat-related mortality is reduced globally. Cold-related mortality, in contrast, is increased in some locations, especially over Northwestern Europe. These results clearly illustrate that the adopted LCLMC scenario is crucial and should not be neglected within future mitigation and adaptation strategies.

This chapter is currently in preparation and intended to be submitted as a paper jointly led by De Hertog S.J. and Orlov A.

4.1 Introduction

Land plays a major role in achieving low-warming scenarios in line with the Paris Agreement. In addition to rapid, sustained, and deep fossil fuel emission reductions, all 1.5 K-compatible scenarios include some type of land-based mitigation (Rogelj et al., 2018), such as enhanced carbon sequestration through afforestation, bio-energy plantations. However, Land Cover and Land Management Changes (LCLMC) do not only affect climate through changes in the carbon cycle (biogeochemical effects), but can also affect surface properties which changes the surface energy and water cycles (biogeophysical effects). Within the development of Shared Socioeconomic Pathways (SSPs) by Integrated Assessment Models (IAMs), the climate responses from the implemented Land cover and land management Changes (LCLMC) are generally not fully accounted for. Notably, the biogeophysical effects are neglected, which may lead to a regional over- or underestimation of potential effects of LCLMC (Duveiller et al., 2018; Roe et al., 2019; Seneviratne et al., 2018; Pongratz et al., 2021).

Therefore, it is crucial that the effects of LCLMC on the climate are better constrained. However, Earth System Model (ESM) simulations dedicated to disentangling LCLMC effects on climate generally focus on historical (Pongratz et al., 2010; Pitman et al., 2009; De Noblet-Ducoudré et al., 2012; Boisier et al., 2012) or highly idealised simulation setups (Davin and de Noblet-Ducoudre, 2010; Winckler et al., 2017a, 2019a; Boysen et al., 2020; Portmann et al., 2022; De Hertog et al., 2023) with only few simulations being committed to disentangling LCLMC-induced climate effects under future scenarios (Brovkin et al., 2013; Boysen et al., 2014; Hirsch et al., 2018a). However, as many of the relevant processes are dependent on background climate (Pongratz et al., 2021), dedicated future simulations are required to further constrain and understand the feasibility of low-warming scenarios that are heavily focused on land-based mitigation.

Generally, ESM studies assessing the role of LCLMC on climate only report climate variables such as temperature, but rarely also quantify socioeconomic impacts (e.g. Orlov et al., 2023). However, it is clear that LCLMC-induced climate effects also affect humans. This can be both economically through a reduction in working hours (labour capacity) due to, for example, climate-induced injuries (Fatima et al., 2021) or through an increased risk in mortality due to higher occurrences of extreme temperatures (Gasparrini et al., 2015). While both labour capacity (Orlov et al., 2020) and mortality (Vicedo-Cabrera et al., 2021) will be substantially affected within the different future emission scenarios, it is currently unclear how these indicators will be affected by future LCLMC.

Here we perform and analyse a set of dedicated ESM simulations applying two recently-developed land cover change scenarios representing a world of unequal development and a world of sustainable development (Humpenöder et al., 2022). The simulations are set up under a SSP1-1.9 scenario to asses the importance of these LCLMC-induced effects under a low-warming future. First, we analyse these results for the effects on global and regional mean temperature. Furthermore, we assess the impacts of these LCLMC-induced temper-

ature changes on human beings. This is done by quantifying LCLMC-induced effects on humid heat stress and consequent changes in labour capacity. Finally, we apply the framework from Vicedo-Cabrera et al. (2019) to quantify temperature-related mortality and how these are affected by future land cover changes.

4.2 Methods

4.2.1 Simulation setup

We apply CESM in fully-coupled mode at 0.90°x1.25° spatial resolution. The model is run in emission-driven mode to ensure that the carbon cycle is explicitly resolved (see Section 4.6.1). This ESM has been evaluated for its capacity to model LCLMC-induced temperature effects in several studies (Meier et al., 2018; De Hertog et al., 2023) and has been shown to perform reasonably well for annual average changes in surface temperature.

Four simulations are run and are summarised in Figure 4.1. First, we conduct a short 35-year simulation (presCTL; 1980-2014) which branches of from the *esm-hist* simulations performed within the context of the Coupled Model Intercomparison Project phase 6 (CMIP6). Next, branching of from presCTL, we perform a future simulation (years 2015-2100) under SSP1-1.9 conditions (futCTL). In the futCTL simulation, land cover is kept constant at present-day levels (representing the end of 2014 conditions). Furthermore, two additional simulations are conducted under SSP1-1.9 forcing except for LCLMC which is modelled transiently. These future LCLMC scenarios are derived from the IAM MagPie and were first presented in Humpenöder et al. (2022). They represent two starkly different futures with regard to socioeconomic development, environmental protection, and land-based mitigation. The sustainability scenario (Sust) represents a world where the Agriculture, Forestry and Other Land Use (AFOLU) sector is included in greenhouse prices mechanisms and where there is strict environmental protection. Moreover, the scenario follows the SSP1 economic growth trajectory where due to global economic convergence there is less pressure on land as a consequence of dietary changes and a limited population growth. For the Inequality scenario (Ineq) in contrast, these actions are only taken in countries part of the Organisation for Economic Cooperation and Development (OECD). The rest of world does not implement these actions and follows an SSP4 scenario (meaning high population growth and resource intensive diets) (Humpenöder et al., 2022).

These land cover scenarios are implemented in the ESMs following the same procedure used in CMIP6 (Eyring et al., 2016) by converting them to LUH2 format and then applying the ESM-specific translation into native land cover maps and related Plant Functional Type definitions. For CESM, the eventual land cover changes at the end of the century are shown in Figure 4.2 and the absolute land cover fractions are shown in Figure 4.9. In the sustainability scenario, there is a general decrease in cropland due to population changes and dietary changes. These abandoned croplands are then often afforested, such as across

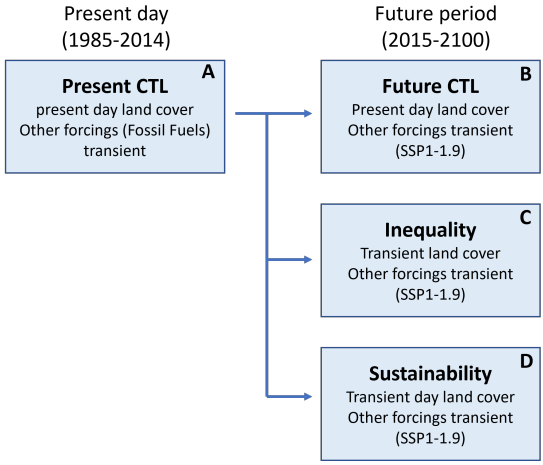

Figure 4.1: Schematic highlighting simulation setup: we perform 2 control simulations, one over the historic period (1985-2014) and one over future period (2015-2100) using SSP1-1.9 forcing, for both land cover is kept constant at the 2014 levels. Two additional simulations are performed applying land cover scenarios from Humpenöder et al. (2022) representing land cover in an unequal world and representing land cover in a sustainable world. For non-LCLMC forcings, the SSP1-1.9 scenario is used.

the US, while there is also afforestation occurring at the expense of grasslands. In the Inequality scenario, there is a strong increase in cropland area at the expense of previously forested and grassland areas, especially in the tropics. In Europe and North America, there is some afforestation even in this scenario. These different socioeconomic scenarios lead to clearly different LCLMC throughout the future period, especially over the tropics.

This simulation setup (Figure 4.1) allows to compare the climate effects between the different future scenarios (Sust-Ineq), while also being able to distinguish the effects of sustainability land cover scenario (Sust-presCTL) and the inequality land cover scenario (Ineq-presCTL) separately. The climate effects as a response to SSP1-1.9 forcing in absence of any LCLMC (futCTL-presCTL) can also be derived and is used as a benchmark for the importance for the LCLMC-induced climate effects. Three ensemble members are run for each of the experiments to average out the influence of natural variability. All climatological variables are analysed as averages over 30-year time slices (1985-2014 for presCTL, 2069-2099 for future experiments) and will be tested for statistical significance using a two-sided Wilcoxon signed rank test of lumped ensemble members at the 0.05 significance level (Wilks, 2006). Additionally, we test for field significance using the false discovery rate to take spatial autocorrelations into account (Lorenz et al., 2016; Vanderkelen et al., 2021).

The version of CESM used here (CESM2.1.3) has never been run under SSP1-1.9 forc-

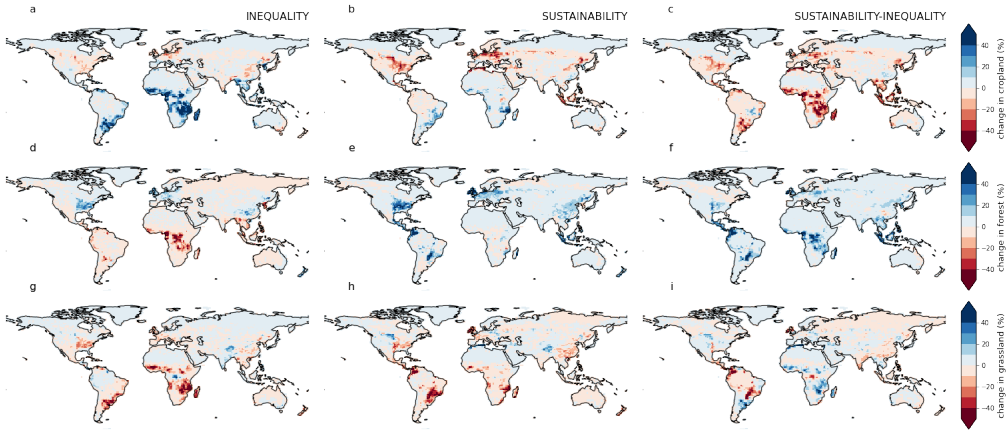

Figure 4.2: Land cover changes implemented in CESM showing the amount of cropland (a-c), forest (d-f) and grassland (g-i) changes as a grid cell fraction (%) within the inequality scenario (a,d,g), sustainability scenario (b,e,h) at the end of the century compared to the 2014 land cover, and between the sustainability and inequality scenarios at the end of the century (c,f,i). The absolute values of the grid cell fractions are shown in supplementary material (Figure 4.9).

ings. This implies that under the default configuration of CESM (using CAM as the atmosphere component) certain forcings are not available for the SSP1-1.9 scenario, as these are generally derived from computationally more expensive simulations using the Whole Atmosphere Community Climate Model (WACCM) (Danabasoglu et al., 2020). The fields which are generally defined from these more complex runs include nitrogen deposition on land and the ocean as well as stratospheric ozone, aerosols, methane oxidation and, tropospheric oxidants. To remain as close as possible to SSP1-1.9 forcing, we use the forcing fields from the nearest scenario available (SSP1-2.6) which uses the same SSP but a different Representative Concentration Pathway (RCP).

4.2.2 Heat stress and impacts on labour capacity

Heat stress is determined by several climatic variables including temperature, relative humidity, incoming solar radiation and wind speed. Several indices have been proposed to quantify heat stress (Buzan et al., 2015; Lemke and Kjellstrom, 2012). Wet Bulb Globe Temperature (WBGT) is the most widely-used metric for quantifying the effects of heat stress on labour capacity (Budd, 2008). As the most accurate and sophisticated approaches for WBGT are computationally expensive, we here use the Environmental Stress Index (ESI) as a substitute for WBGT. Recent studies found that this metric performs reasonably well, especially for annual and seasonal mean values (Kong and Huber, 2022).

$$ESI = 0.63 * T - 0.03 * RH + 0.002 * SW_{in} + 0.0054 * T * RH - \frac{0.073}{0.1 + SW_{in}} \quad (4.1)$$

Where T is near-surface temperature in °C, RH is relative humidity in % and SW_{in} is downwelling shortwave radiation in $\frac{W}{m^2}$. Here 3-hourly output data for temperature, relative humidity and solar incoming radiation are used in order to compute ESI.

To quantify the effects on labour capacity, which is defined as the occupational capacity to safely perform work under heat stress (Dunne et al., 2013), we use the widely-applied metric based on the National Institute for Occupational Safety and Health (NIOSH) standards (Kjellstrom et al., 2009; NIOSH, 1986). These standards describe the frequency and duration of breaks from work required to avoid heat-induced illnesses. Here we use the limits recommended for a 'standard' acclimatised worker of 70 kg. The labour capacity then is quantified as the percentage of a work hour that the worker is able to perform (see Table 4.1). Here we focus on high intensity jobs which are generally performed outside in the sun (such as construction and agriculture). The effects on labour capacity are computed from the ESI heat stress index at the 3-hourly temporal resolution. The 3-hourly ESI values are first linearly interpolated to hourly data and converted to local time, then the effect on labour capacity is the considered as the mean over a 12h work day which is taken from 7 am to 7 pm.

Table 4.1: Recommended rest/work Ratios for ESI Exposure Levels (K) for an average acclimatized worker wearing light clothing, for high work intensive jobs outdoors with a metabolic rate of 400 W.

Rest/work ratios	ESI (K)
0% rest/hour (continuous work)	27
25% rest/hour	27.5
50% rest/hour	29.5
75% rest/hour	31.5
100% rest/hour (no work)	36

Source: Kjellstrom et al. (2009)

4.2.3 Impacts on temperature-related mortality

We use the data from the Multi-Country Multi-City (MCC) Collaborative Research Network which contains health data from a subset of cities (Figure 4.3). From these data estimates of excess mortality due to heat and cold are quantified. Here, excess mortality is defined as the additional mortality relative to the optimal temperature (i.e. temperature with lowest mortality). We use the approach described in detail in Vicedo-Cabrera et al. (2019) and which is summarised here. A time series regression analysis is used to quantify and project mortality impacts related to temperature. This is done by relating mortality to temperature through a location-specific exposure-response function. This response function is

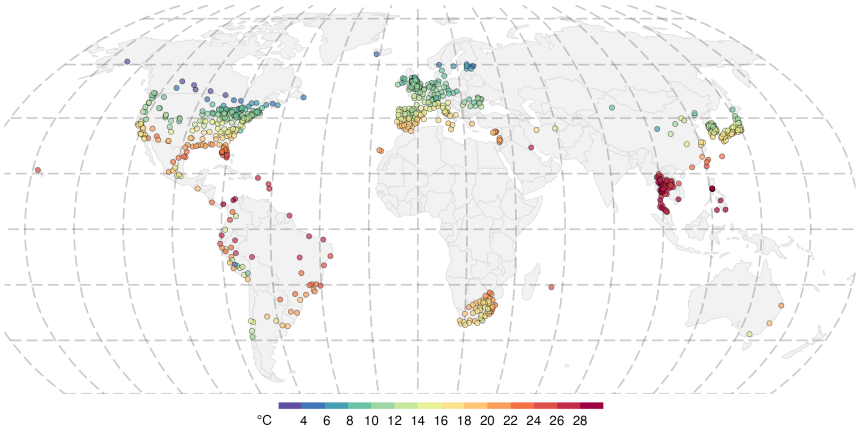

Figure 4.3: Global map indicating cities and corresponding average daily mean temperature for which health data is available to assess the temperature-related mortality. Figure was provided by the MCC network.

generally U shaped meaning that both at very cold temperatures and very hot temperatures mortality spikes.

The ESM temperature data is mapped to each city where data is available using a nearest neighbour approach and then bias-adjusted to match historically observed temperature distribution, using the same approach as used within the Inter-Sectoral Impact Model Intercomparison Project (Lange, 2019). These site-specific downscaled and bias-adjusted temperature data are then used to apply the response function which estimates the effects of the ESM simulations on mortality. The population and vulnerability of the different cities are assumed to remain constant throughout the future hence the only effects on mortality is due to changed temperatures.

For each simulation, the attributable fraction is calculated which represents the absolute value of cumulative excess mortality divided by the location-specific population. The computed attributable fraction can then be compared across scenarios (e.g. Sust-Ineq) to assess the effects on temperature-related mortality of LCLMC-induced climate changes related to the different land cover scenarios.

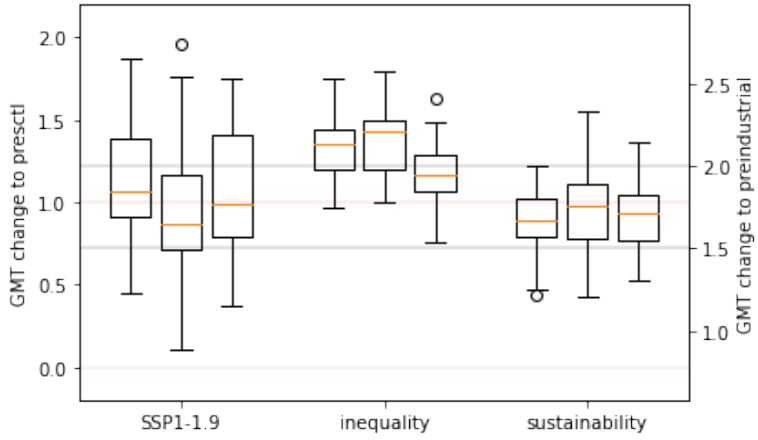

Figure 4.4: Boxplots representing the changes in Global Mean Temperatures (GMT) in ° C within the CESM simulations for the three ensemble members for SSP1-1.9, Inequality and Sustainability scenarios by the end of the century (2069-2099). The left axis highlights the GMT changes compared to mean presCTL while the right axis highlights those against the pre-industrial mean temperature taken from HadCRUT5 (Morice et al., 2021). The black lines indicate the Paris agreement thresholds of 1.5 K and 2 K.

4.3 Results

4.3.1 Climate effects of land cover scenarios

In CESM, the SSP1-1.9 scenario (futCTL-presCTL) causes a global warming of ca. 1 K compared to the 1985-2014 average which equals a 1.75 K warming compared to the pre-industrial period (1850-1900). This indicates that the 1.5 K goal of the Paris agreement is not achieved (Figure 4.4). This warming is global except for the Northern Atlantic ocean and Northwestern Europe, where CESM shows a regional cooling (Figure 4.5). This is a well-known feature within CESM where several simulations with moderate warming amounts show strong changes in Atlantic Meridional Overturning Circulation (AMOC) strength (Portmann et al., 2022; De Hertog et al., 2023; Boysen et al., 2020). The warming is relatively high for an SSP1-1.9 scenario which might be related to this version of CESM being a 'warm' model with a high equilibrium climate sensitivity (i.e. the equilibrium amount of warming after a doubling of CO2) of 5.7 K (Gettelman et al., 2019) which falls outside of the best estimate range of 2.5-4.0 K (Arias et al., 2021). This high climate sensitivity in this CESM version is largely caused by changes in cloud feedbacks over the tropical and Southern oceans (Bacmeister et al., 2020).

The land cover scenarios have a clear effect on global mean temperature, with the inequality scenario (Ineq-futCTL) adding on average 0.3 K [ca. 0.22 K inter-annual variability, here defined as the standard deviation across the three ensemble members] of warming, which

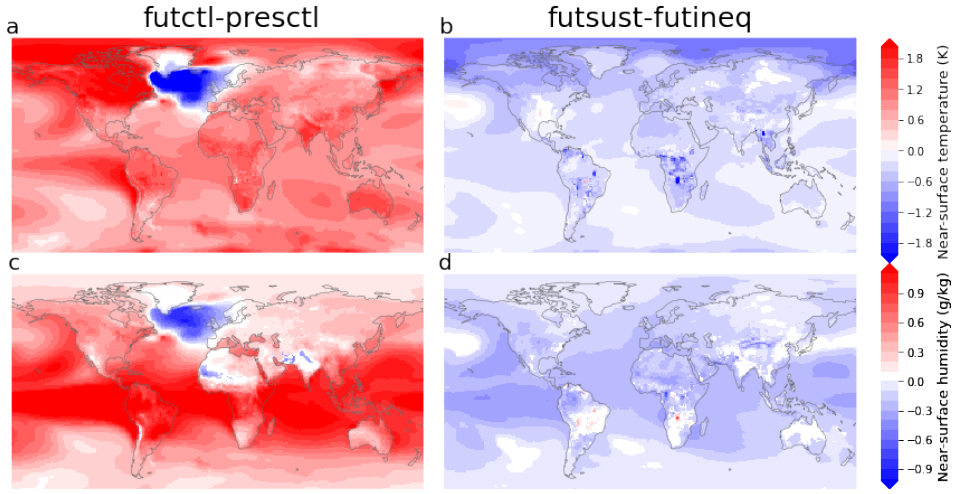

Figure 4.5: Changes in (a) near-surface temperature (K) by the end of the century under the SSP1-1.9 scenario with constant present-day land cover, and (b) between the inequality and sustainability scenarios at the end of the century (2069-2099). (c,d) Same as (a,b) but for near-surface specific humidity (g/kg). Only statistically significant changes are shown (0.05 significance level, two-sided Wilcoxon signed rank test of lumped ensemble members and field significance using the false discovery rate test).

corresponds to 2.05 K of warming relative to the pre-industrial period. Sustainable land cover pathway (Sust-futCTL), in contrast, results a slight decrease in global mean temperature of 0.07 K [ca. 0.22 K] compared to present-day conditions, which yields a warming of 1.68 K above pre-industrial levels. Avoiding the inequality land cover pathway in favor of a sustainability land cover pathway (Sust-Ineq) thus leads to a clear global cooling (Figure 4.5). This is likely due to the biogeochemical effects of the increased afforestation and avoided (mostly tropical) deforestation (Figure 4.2). However, regionally the magnitude of this cooling varies, especially over tropical areas that experience large amounts of deforestation in the inequality scenario (such as Central Africa). These locally stronger effects in temperature are likely linked to local biogeophysical effects. This is also indicated by the large regional differences in turbulent heat flux responses: with a decrease in sensible heat flux and an increase in latent heat flux in most of the areas of enhanced local cooling (Figure 4.10 b,d). This local biogeophysical effect can regionally even be as large as the temperature change induced by SSP1-1.9.

This annual mean cooling is present in all seasons, although some seasonal patterns appear (Figure 4.11). During summer, the biogeochemical cooling is least pronounced with even some slight regional warming due to biogeophysical effects, such as albedo-induced warming over parts of the United States (Figure 4.11c). The local biogeophysical cooling over the tropics is also most pronounced during the summer season although this local cooling

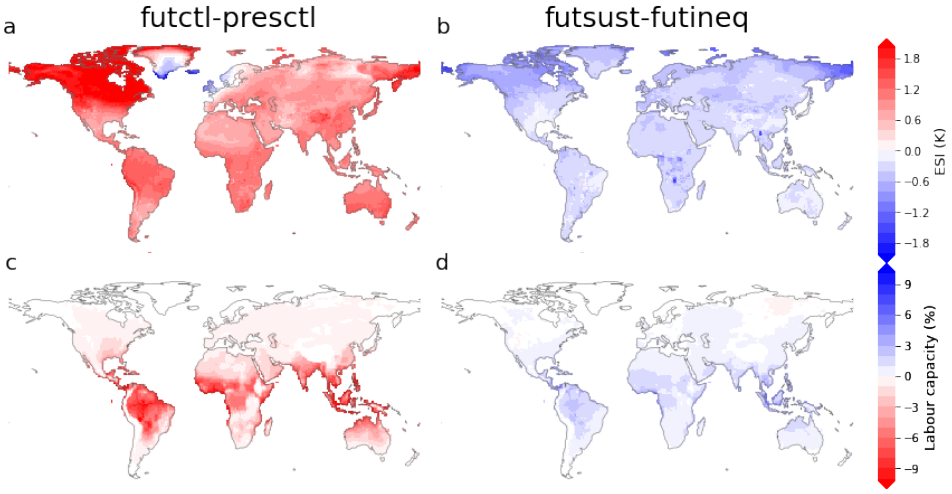

Figure 4.6: Changes in (a) Environmental Stress Index (ESI; K) by the end of the century under the SSP1-1.9 scenario with constant present-day land cover, and (b) between the inequality and sustainability scenarios at the end of the century (2069-2099). (c,d) Same as (a,b) but for Labour capacity in % rest/hour.

effect is also present throughout the rest of the year.

Following the temperature effects, near-surface specific humidity also decreases globally (Figure 4.5d) as a consequence of sustainable land cover pathway instead of the inequality pathway (Sust-Ineq). An exception to this global pattern are regions where the biogeophysical effects are large, such as Southern Africa and Brazil. Here, local latent heat flux increases offset the global decrease in specific humidity locally (Figure 4.5c,d and Figure 4.10). This pattern is apparent in all seasons except for summer and fall in some parts of Southern Africa and Brazil, and over the United States during winter (Figure 4.12). The effect of the the different LCLMC scenarios (Sust-Ineq) on annual precipitation is generally small and not significant, except for a slight increase over parts of Latin America and a mixed signal of regional increases and decreases over Central Africa (Figure 4.13).

4.3.2 Effects on heat stress and labour capacity

Owing to the climate changes under SSP1-1.9 (futCTL-presCTL), the Environmental Stress Index (ESI) increases over global land by 1.2 K. The increase is apparent almost everywhere, except for Northwestern Europe (Figure 4.6). In contrast, the effects of the land cover scenarios (Ineq-Sust) show a global cooling of 0.4 K with spatial patterns strongly consistent with the annual mean temperature changes (Figure 4.5). Except over some areas, such as Southern Brazil, where the decrease in temperature is offset by the increases

in specific humidity. Over areas where forest is preserved or planted, the changes in ESI are substantial and often larger than 50% of the SSP1-1.9 climate change signal.

These effects on ESI can then be translated to changes in labour capacity where the effects of SSP1-1.9 (futCTL-presCTL) clearly show a decrease in labour capacity especially over tropical regions. This spatial pattern is consistent with previous studies of higher warming scenarios (Orlov et al., 2020). The land cover scenarios, in contrast, causes a decrease in ESI and consequently also an increase in labour capacity, albeit of smaller magnitude than the ESI change (Figure 4.6d). The areas of largest ESI decreases do not overlap with areas of increase in labour capacity, because the absolute value of ESI in these regions are often lower than the thresholds affecting labour capacity as defined by the NIOSH standards (see Table 4.1). The areas with largest increases in labour capacity are rather areas which experience high values of absolute ESI, such as Southeastern Asia and the Amazon region. Overall, avoiding the inequality scenario in favour of the sustainability scenario causes a clear increase of labour capacity over the tropics.

4.3.3 Effects on temperature-related mortality

The global temperature effects of the different land cover scenarios also affect temperature-related mortality across a range of cities (Figure 4.7). We find a general decrease in heat-related mortality by the end of the century under the sustainable land cover scenario compared to the inequality scenario, and in some locations also an increase in cold-related mortality (Figure 4.7). These general patterns are in line with the cooling trends shown above (Figure 4.5b). The decreases in heat-related mortality are especially large over the tropics with substantial reductions in countries such as South Africa (up to -4%), Peru and Thailand (up to -7%). In contrast, the increases in cold-related mortality are mostly located in Northwestern Europe with increases up to 2.5% in the United Kingdom. In Northwestern Europe, the increased net mortality – due to an increase in cold-related mortality and no change in heat-related mortality – is in part related to the strong AMOC response in CESM which leads to a cooling under SSP1-1.9 (Figure 4.5a).

The decreases in heat-related mortality under the sustainable land cover change scenario are substantial relative the temperature-related mortality effects under SSP1-1.9 (Figure 4.14). For some countries, such as Thailand and South Africa, the effect of the different LCLMC scenarios is even as large as halve the SSP1-1.9-induced increase in heat-related mortality. Overall, it is clear that temperature-induced mortality can be reduced over most parts of the world when sustainable land cover and the consequent temperature reductions are achieved in favour of inequality land cover.

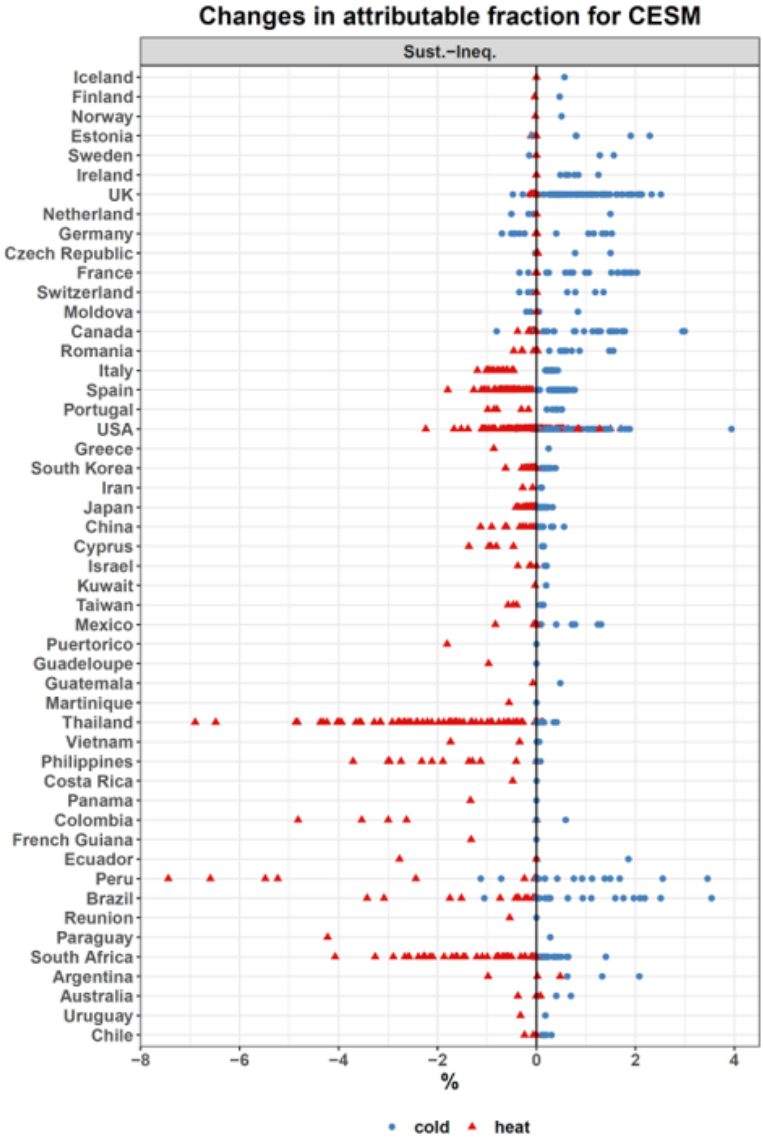

Figure 4.7: Changes by the end of the century (2069-2099) in Attributable Fraction of temperature-related mortality for each country and city under the sustainability LCLMC scenario relative to the inequality scenario. Heat-related mortality changes are indicated as red triangles and cold-related mortality changes as blue circles.

4.4 Discussion

Under a low-warming SSP1-1.9 scenario, the LCLMC scenario substantially affects the global mean temperature and hence the feasibility of the Paris Agreement temperature goals. Within all the simulations presented here, the 1.5 K threshold is breached but in the inequality scenario even the 2 K warming threshold is not achieved. We find that avoiding the inequality land cover pathway in favor of a sustainability land cover pathway as proposed by Humpenöder et al. (2022) leads to a cooler and less moist world (Figure 4.5), thereby reducing heat stress and limiting economic impacts from changing labour capacity (Figure 4.6). Moreover, it reduces the amount of temperature-related mortality substantially over many cities around the world, except over some countries in Northwestern Europe where increases in cold-related mortality cause an increased net mortality (Figure 4.7).

Due to climate change, people in low-income countries will suffer more from impacts than people in high-income countries (Harrington et al., 2018). Here, we show that sustainable future land cover changes can alleviate some of these impacts. In contrast to GHG emission drivers of climate change, which predominantly originate from the wealthier nations, these land cover changes are expected to occur mostly in low-income nations (Humpenöder et al., 2022). However, despite the LCLMC differences between inequality and sustainability scenarios occurring over developing nations, the potential to acquire sustainable land cover and sustainable economic growth is a global burden requiring high levels of collaboration to overcome the financial, technical, and institutional barriers that block sustainable development (IPCC, 2022).

CESM as an ESM has some consistent biases, such as an overestimation of the albedo change following deforestation in boreal latitudes (De Hertog et al., 2023). Another clear feature of this ESM is a strong sensitivity of the AMOC to temperature changes (e.g. Portmann et al., 2022). These features along with the high climate sensitivity of CESM indirectly affect the results. Therefore, it is recommended to extend this work with other ESMs in order to assess model diversity in the effects of these LCLMC scenarios under future climates. Using a multimodel perspective can help uncover robust patterns across ESMs, which can in turn lead to more policy-relevant recommendations (e.g. De Hertog et al., 2023; Boysen et al., 2020).

Generally, when considering the effects on heat stress it is recommended to asses WBGT through the Liljegren method (Liljegren et al., 2008). However, here we opted for the computationally less extensive ESI equation which has been shown to be a valid approximation for annual or seasonal mean values as studied here but does not capture extremes well (Kong and Huber, 2022). Another limitation is that heat stress here is computed from 3 hourly ESM output data, yet as this quantity is highly non linear, it is recommended to calculate these metrics directly within the ESM at the model smallest time step (30 minutes in CESM). Therefore, it is likely that heat stress is underestimated in this study especially for extreme values (Buzan et al., 2015). Furthermore, it should be noted that previous research has indicated that CESM does not capture the diurnal cycle of LCLMC-induced

effects well compared to observational data (Duveiller et al., 2018), which could lead to a misinterpretation of the severity of heat stress (Orlov et al., 2023).

Another limitation for this study is that the NIOSH standards are used as a fixed translation of heat stress effects into labour capacity impacts. However, due to non-linearity in the relation of heat stress and climate, the effects by the end of the century might be stronger than currently reported (Kjellstrom et al., 2018). The NIOSH standards are a safety standard but this does not equal the reality fully (i.e. people can work beyond this point up to a higher physiological limit) this has also been illustrated in empirical studies where the threshold are generally higher than what NIOSH standards describe (Lee et al., 2020, see e.g.). Therefore, the labour capacity effects presented here can be interpreted as an upper bound. Finally only impacts on labour capacity due to humid heat are considered here while effects due to increased/decreased cold are neglected (Orlov et al., 2023).

The results on mortality changes should be interpreted with some caution. First, as our approach assumes constant vulnerability and population, results should not be considered as mortality projections, but rather as an indication of the potential impact of LCLMC on mortality (Vicedo-Cabrera et al., 2018). Second, as the approach depends on a calibration of a temperature-mortality response function build over the historical period, it does not include the effects of climate feedbacks, such as changes in extreme occurrences or hydroclimatic regime shifts, nor the effects of other impacts such as crop failures or sea level rises which may affect human mortality beyond temperature-related mortality. Moreover, as only daily mean temperature is included, it disregards changes in heat stress due to altered evaporation and consequent specific humidity as a consequence of LCLMC (Figure 4.5). Lastly, the results are limited to the sites for which data is available through the MCC network, which omits several locations such as large parts of Africa and lacks some highly populated countries such as India. Yet, previous research has highlighted that many of these locations are especially vulnerable to the effects of both climate change (Harrington et al., 2016, 2018; Russo et al., 2016; Lelieveld et al., 2016; Mazdiyasni et al., 2017) and LCLMC (Thiery et al., 2020; de Vrese et al., 2016; Mishra et al., 2020; Akkermans et al., 2014).

The simulations presented here highlight the importance of climate responses when considering large-scale LCLMC in scenarios. This is the first set of simulations explicitly dedicated to to quantifying the role of land-based mitigation strategies in achieving an SSP1-1.9 scenario. However, this analysis is limited to temperature-induced climate effects and does not cover a full description and interpretation of all processes driving the biogeochemical and biogeophysical LCLMC-induced temperature effects presented here. These simulations could also be analysed for transient responses in order to asses the potential risk of overshoot and how these might be affected by different LCLMC scenarios. In addition, other variables such as soil moisture and atmospheric teleconnections could be considered to further constrain potential impacts categories such as droughts and heat waves. Finally, these simulations can act as training and validation material for computationally light emulators such as MESMER (Beusch et al., 2020; Nath et al., 2022) and the recently developed component for the local biogeophysical effects of land cover changes (Nath et al., 2023,

TIMBER).

4.5 Conclusion

Here we present Earth System Model (ESM) simulations dedicated to disentangling the effects of LCLMC under the low-warming SSP1-1.9 scenario. We use scenarios developed by Humpenöder et al. (2022) which represent two SSP1-1.9-compatible LCLMC pathways but with vastly different socioeconomic assumptions: a sustainable future, where forests are preserved and planted, and a global inequality scenario, where large-scale tropical deforestation occurs due to cropland expansion. These simulations are performed with the Community Earth System Model (CESM) in fully-coupled, emission-driven mode, and designed such that they can disentangle the climatic effects of land cover scenarios towards the end of the century.

We show that avoiding the inequality land cover pathway and achieving the sustainability land cover pathway substantially alters global climate with a global mean temperature decrease of 0.3 K by the end of the century. Due to these global changes in temperature, a reduction in heat stress is visible globally over land of 0.4 K at the end of the century. The LCLMC-induced reduction in heat stress substantially increases labour capacity in tropical regions. Furthermore, temperature-related mortality reduces almost globally, driven by a clear decrease in heat-related mortality and despite an increase in cold-related mortality in some regions.

These results are a clear illustration of the importance of LCLMC-induced climate responses (both biogeochemical and biogeophysical) which are currently only partially considered in the development of SSP scenarios. We show that a sustainable land cover scenario has several benefits both for climate mitigation (global biogeochemical and local biogeophysical cooling) and climate adaptation (reduced economic and health impacts). LCLMC are a crucial component to be considered in the global discussion on climate change and an achievement of LCLMC in line with the sustainability scenario should be considered for future climate policy.

Author contributions

S.J. De Hertog performed the ESM simulations and analysed the climate data. A. Orlov performed the calculations required for assessing the labour capacity and temperature-related mortality. The text for this chapter was written by S.J. De Hertog.

Data and code availability

CESM is an open source model which can be freely downloaded here (`https://www.cesm.ucar.edu/models/cesm2/release_download.html`). The scripts used for this analysis will be made available by the time of submission. The simulation data used in this paper (more than 130 TB for CESM) will be made available through the Deutsches Klimarechenzentrum (DKRZ), for those interested in using these data please contact the authors.

4.6 Supplementary material

4.6.1 Concentration-driven vs. emission-driven simulations

Generally, future simulations assessed in the context of Intergovernmental Panel on Climate Change (IPCC) reports are run in concentration-driven mode, meaning that atmospheric concentrations of CO_2 are used as an input forcing to the ESMs. This is done to increase the consistency across different ESMs as climate is highly sensitive to slight different in CO_2-concentrations. Here, in contrast, we apply emission-driven simulations where CO_2-concentrations are computed (instead of prescribed) within the ESM, by using CO_2-emissions as an input directly. This difference is highlighted within the schematic shown in Figure 4.8. Here we use emission-driven simulations in order to simulate the full land cover climate feedbacks, whereby the strength of the land sink is explicitly modelled and directly affects atmospheric CO_2-concentrations (Jones et al., 2016).

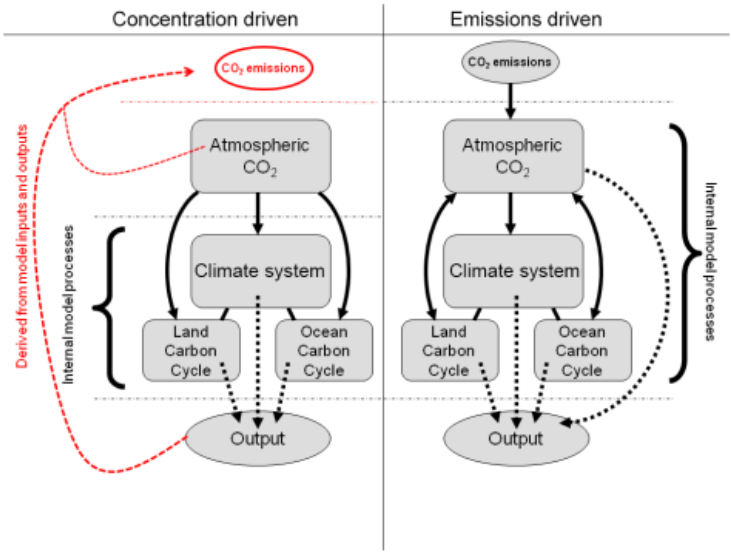

Figure 4.8: Schematic illustrating the difference between concentration-driven simulations (left) and emission-driven simulations (right). Where concentration-driven simulations require inputs derived from other simulations, emission-driven simulations calculate concentrations interactively within the model. Taken from (Jones et al., 2016).

4.6.2 Simulation land cover maps

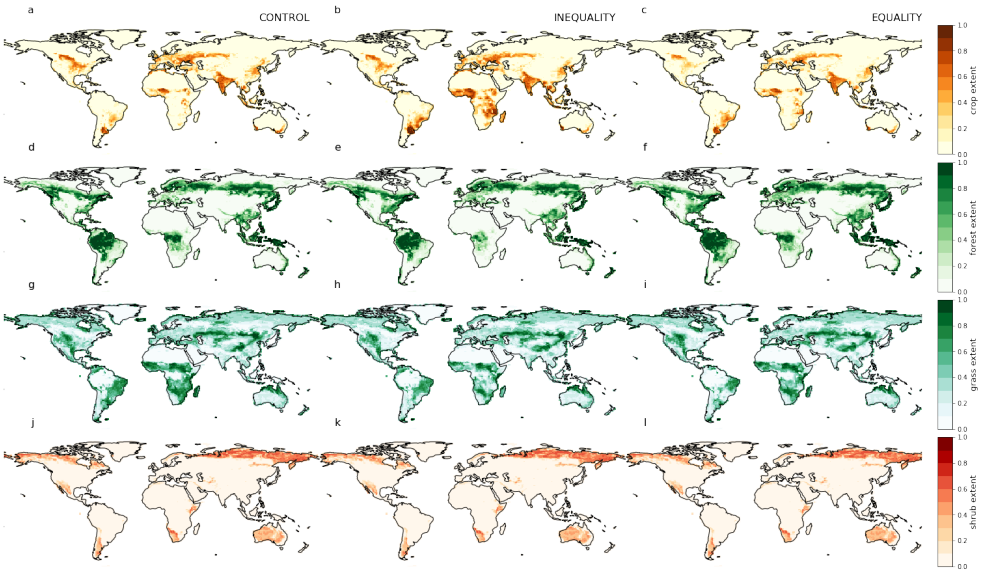

Figure 4.9: Total amount of cropland (a-c), forest (d-f), grassland (g-h) and shrubland (j-l) as a fraction of the grid cell (%) within CESM for the 2014 (CONTROL) land cover (a,d,g,j), for the year 2100 the Inequality scenario (b,e,h,k) and the sustainability scenario (c,f,i,j). As there are limited changes in shrubland in our scenarios, this land cover type is disregarded in the main analysis.

4.6.3 Climate variables

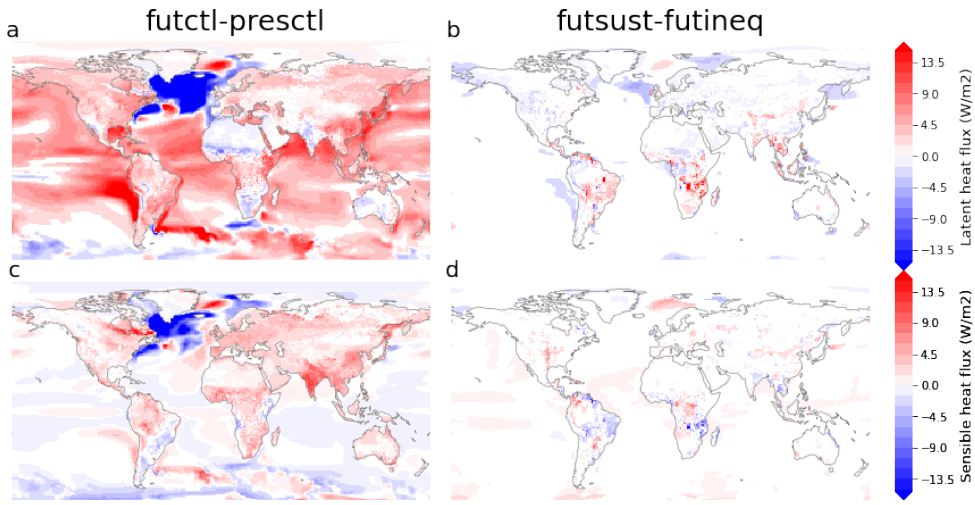

Figure 4.10: Changes in (a) Latent Heat Flux (W/m2) by the end of the century (2069-2099) under the SSP1-1.9 scenario with constant present-day land cover, and (b) between the inequality and sustainability scenarios at the end of the century (2069-2099). (c,d) Same as (a,b) but for Sensible Heat Flux (W/m2). Only statistically significant changes are shown (0.05 significance level, two-sided Wilcoxon signed rank test of lumped ensemble members and field significance using the false discovery rate test).

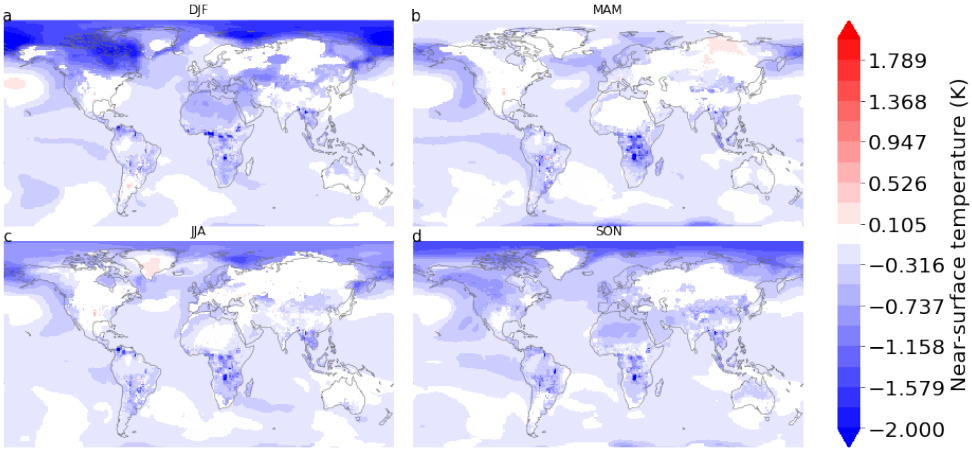

Figure 4.11: Seasonal changes in near-surface temperature changes (K) due to different land cover scenarios (Sust-Ineq) by the end of the century (2069-2099). Boreal Winter (DJF) in panel a, Spring (MAM) in panel b, Summer (JJA) in panel c and fall (SON) in panel d. Only statistically significant changes are shown (0.05 significance level, two-sided Wilcoxon signed rank test of lumped ensemble members and field significance using the false discovery rate test).

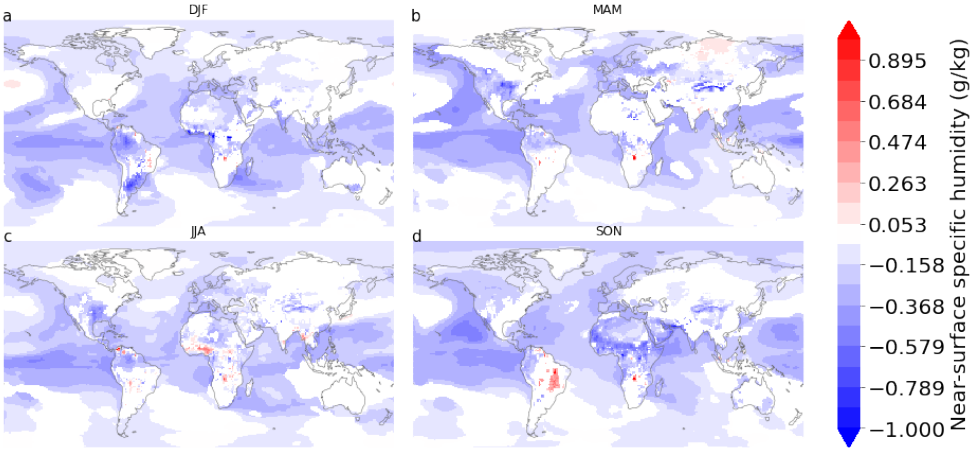

Figure 4.12: Seasonal changes in near-surface specific humidity changes in g/kg due to different land cover scenarios (Sust-Ineq) by the end of the century (2069-2099). Boreal Winter (DJF) in panel a, Spring (MAM) in panel b, Summer (JJA) in panel c and fall (SON) in panel d. Only statistically significant changes are shown (0.05 significance level, two-sided Wilcoxon signed rank test of lumped ensemble members and field significance using the false discovery rate test).

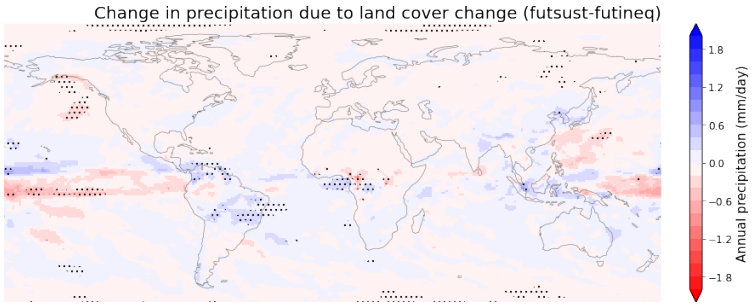

Figure 4.13: Annual average precipitation changes in mm/day due to different land cover scenarios (Sust-Ineq) by the end of the century (2069-2099). Hatching on the map indicates where the signal is statistically significant (0.05 significance level, two-sided Wilcoxon signed rank test of lumped ensemble members and field significance using the false discovery rate test).

4.6.4 temperature-related mortality due to SSP1-1.9

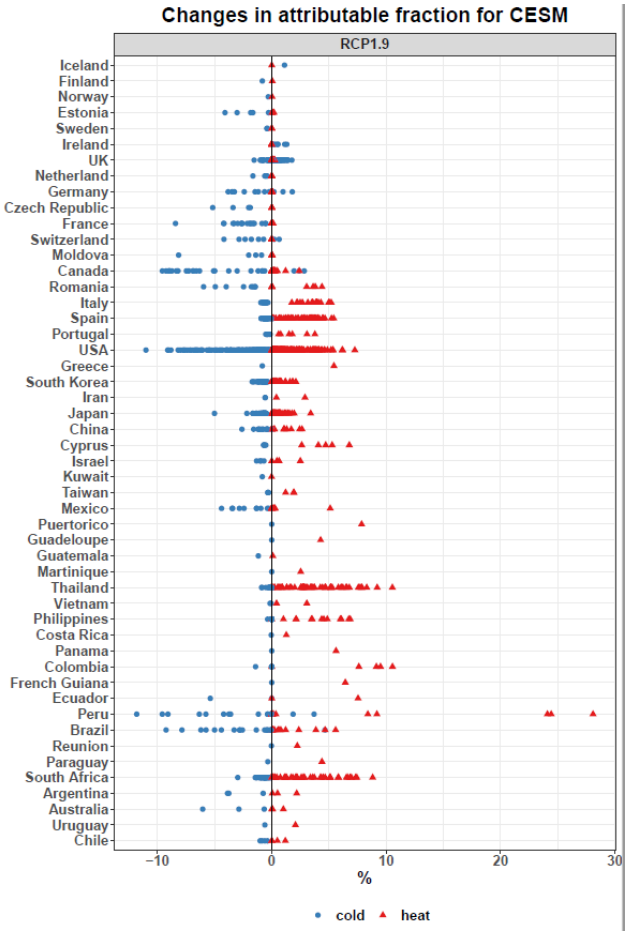

Figure 4.14: Changes in Attributable Fraction of temperature-related mortality for each country and city for the difference in SSP1-1.9 scenario with present-day land cover by the end of the century (2069-2099). With heat-related mortality indicated as red triangles and cold-related mortality as blue circles.

Chapter 5

Conclusion

5.1 Concluding summary

Land Cover and Land Management Changes (LCLMC) have a clear effect on the climate, which depending on the type of LCLMC, region, and scale can differ from a cooling to a warming. However, large-scale LCLMC are likely needed to achieve the goals of the Paris Agreement through some form of land-based mitigation. At this point, a large uncertainty remains related to the potential of enhancing the carbon sink (e.g. afforestation to enhance the biogeochemical effects) as well as the resilience and longevity of these land-based mitigation approaches. Moreover, in most policy and Integrated Assessment Modelling (IAM) modelling approaches, the effects of LCLMC on the energy and water cycle (biogeophysical effects) are fully neglected, potentially overestimating the mitigation potential of certain LCLMC approaches. As we are reaching the stage that land-based mitigation efforts are being initiated (e.g. as part of the European Union's Green Deal), the potential climate effects of LCLMC on the local, regional, and global scales must be better constrained. To achieve this, we need Earth System Models (ESMs) as they are to date the only available tool that can fully encompass the climate effects of LCLMC. However, ESMs often show large discrepancies in climate effects of LCLMC and analyses of their outputs rarely consider variables beyond temperature and precipitation. Therefore, existing studies have limited policy relevance regarding the potential of LCLMC for climate adaptation, even though evidence is clear that LCLMC plays a crucial role at the local scale, for example regarding alleviating heat stress.

In this thesis, we aim to tackle these research needs by further constraining the effects of LCLMC on the climate. We approach this challenge from a multi-model perspective to better grasp the spread of physical representations of the climate system within different ESMs and to uncover robust features. We initially focus on the biogeophysical effects as a high uncertainty remains regarding these effects both in sign and magnitude. In Chapter 2, we apply idealised LCLMC scenarios to assess the sensitivity of the climate system to LCLMC, we separate between local and non-local effects to better understand ESM dif-

ferences. In Chapter 3, we analyse these simulations for moisture fluxes and both local and continental moisture recycling to assess the potential effects of LCLMC on water availability. Finally, in Chapter 4, we apply a future low-warming scenario in CESM with two different land cover scenarios representing vastly different socioeconomic futures. These results are analysed for temperature, heat stress, and impacts on human beings (both economic and health) to illustrate the importance of the future LCLMC scenario for climate mitigation and adaptation. Here, we summarise the key finding from this work and suggest avenues for further research.

The second Chapter introduces an idealised set of simulations intended to better understand and constrain the biogeophysical effects of LCLMC. We simulate the biogeophysical effects for (i) cropland expansion (ii) afforestation, (iii) irrigation expansion and (iv) wood harvesting, using the Community Earth System Model (CESM), the Max Planck Institute Earth System Model (MPI-ESM) and the European Consortium Earth System Model (EC-EARTH). We apply the checkerboard approach to make a clear separation between the local biogeophysical effects, which can be evaluated against observations, and the non-local biogeophysical effects which are due to circulation and advection changes.

We show that the local biogeophysical effects of deforestation on surface temperature in the three Earth System Models (ESMs) are largely consistent with observational data. Nevertheless, some ESMs show clear inconsistencies with observations regionally, such as CESM overestimating albedo-induced cooling in the boreal latitudes and EC-EARTH showing a permafrost thawing-induced warming. The changes in energy fluxes driving these temperature effects are less consistent, although clear patterns emerge for the different LCLMC. Over the tropics, the effects on turbulent energy fluxes dominate for changes in land cover, while in boreal latitudes the role of albedo becomes larger. For irrigation, both temperature and energy fluxes are highly consistent, with the differences across ESMs being more related to spatial pattern of irrigation implementation and whether the effects are local or non-local. However, land management is often still not fully included in ESMs, as illustrated by the disconnected terrestrial and atmospheric water cycle in EC-EARTH, making a study for irrigation effects on climate impossible, and by the lack of biogeophysical feedbacks within MPI-ESM for wood harvesting.

An emergent feature of the simulations is the clear non-local warming in the afforestation experiment, which is consistent across all ESMs. This is in contrast to the wide uncertainty of non-local effects in the cropland expansion experiment, where MPI-ESM shows a warming while CESM shows a cooling and EC-EARTH a mixed signal. The larger uncertainty is likely related due to the wider variety of mechanisms at play and the role of natural variability in the simulated circulation changes. Overall, these results show that the biogeophysical effects have an important and non-negligible effect on the climate and that large fractions of model uncertainty found in previous intercomparison projects (e.g. LUMIP) can be related to non-local effects. Our results further strengthen the consensus that local biogeophysical effects should be included in future land use policies to capture potential trade-offs between biogeochemical and biogeophysical effects (especially in boreal

latitudes). Our analysis further highlights the need for considering potential unintended non-local effects related to future LCLMC.

In the third Chapter, we analyse these idealised LCLMC simulations for the effects on the atmospheric water cycle (evaporation, precipitation and moisture flux convergence). We apply a moisture tracking algorithm to assess the effects of the LCLMC changes on moisture recycling both locally, to quantify changes in strength of land-atmosphere feedbacks, and globally to assess changes in water availability over land. The changes in local moisture recycling are analysed through length scales for evaporation and precipitation to enable comparison of these effects over different grid cell sizes. The global moisture recycling effects are investigated through the concepts of continental evaporation and precipitation recycling ratios.

These results are – to our knowledge – the first time that ESM simulations dedicated to analysing climate effects of LCLMC are analysed for their effects on moisture recycling. We find that the LCLMC scenarios have substantial effects on moisture fluxes and moisture recycling. There is a general decrease in precipitation, evaporation, and local moisture recycling following cropland expansion, while the sign of change is generally opposite for afforestation and irrigation expansion. However, the response patterns diverge spatially and changes in large-scale circulation affect these general trends regionally. Despite these marked consistencies in LCLMC-induced effects across ESMs, there is a clear difference in the processes that dominate moisture recycling within the ESMs, with EC-EARTH generally showing a strong land-atmosphere feedback (small length scales) and CESM showing a higher importance of large-scale circulation changes (large length scales). These large inter-ESM differences warrant further research to better understand these patterns and their implications.

This study highlights the need to investigate the effects on moisture recycling and water availability more explicitly within ESM simulations that implement large-scale and realistic LCLMC scenarios. As afforestation and irrigation are seen as potential avenues for future climate mitigation and adaptation, it is important to constrain the effects this would have on the local and regional water cycle.

This research also uncovered some potential issues with the checkerboard approach. Clear checkerboard-induced circulation patterns occurred in EC-EARTH (due to enhanced mesoscale convection) which would not occur if a full afforestation or deforestation was performed. This indicates that the assumptions underlying the checkerboard approach might not fully hold for this ESM. This feature could potentially limit the applicability of this method on higher resolution climate simulations. Hence, further research with varying ESM spatial resolution or checkerboard patterns is needed to further constrain these implications.

In the fourth Chapter, we present a novel set of simulations where a low-warming 1.5 K-compatible SSP1-1.9 scenario is complemented with different land cover scenarios in CESM.

These land cover scenarios represent strongly different socioeconomic conditions with the sustainability scenarios assuming a converging economic development along with implementation of global greenhouse gas pricing mechanisms for afforestation and strict implementations of environmental protection, which is strongly in contrast to the second scenario where the current unequal economic states are maintained and further enlarged by implementation of all these measures only in OECD countries with the rest of the world continuing as usual. Additional historical and future simulations are performed with constant present-day land cover to clearly separate the effects of LCLMC scenario from other SSP1-1.9 forcings.

These simulations are analysed for their effects on near-surface temperature and specific humidity. The results indicate a global cooling of 0.3 K by the end of the century when following the sustainable land cover pathway instead of the inequality land cover pathway, with regionally larger cooling due to local biogeophysical effects. Humidity generally follows the temperature patterns which leads to a quasi-global decrease in heat stress under sustainability instead of inequality. This causes a reduction in economic impacts through an increased labour capacity over tropical regions as a consequence of the avoided heat stress. In general, heat-related mortality is reduced (especially over the tropics) due to the land cover scenarios while there is also an increase in cold-related mortality especially over Northwestern Europe. These simulations are the first to present the effects of future LCLMC scenarios under a low-warming scenario. They clearly highlight the potential in terms of both mitigation (global cooling) and adaptation (reduction in economic and health impacts) when following a sustainable land cover pathway instead of an inequality pathway. These results clearly illustrate the importance of sustainable development in economically poorer countries as the reduced impacts and temperature effects are largest over the tropics (i.e. where most LCLMC occurs).

In conclusion, the results presented here highlight the large potential of LCLMC for climate mitigation and adaptation, but also clearly identify some issues. Even though some consensus is emerging across ESMs regarding the local biogeophysical effects on surface temperature, large inter-ESM discrepancies remain relating to other aspects such as the water cycle, non-local biogeophysical effects on temperature as well as LCLMC-induced impacts across sectors (e.g. human health) which are currently poorly understood and understudied. Currently, the full range of LCLMC climate feedbacks are still neglected in the development of SSPs, which could lead to over- or underestimation of the potential of LCLMC for climate mitigation. Even though ESMs are the only tools available to the scientific community that fully grasp all process interactions, they are rarely applied to assess possible changes of future LCLMC on adaptation potential (such as water availability or health and economic impacts). This makes that ESMs cannot fulfill their potential role as a tool for advising policy makers on LCLMC planning. In the next section we will therefore look beyond the results of this thesis and draft a way forward to further apply and build on the potential use of ESMs within the context of LCLMC-climate interactions.

5.2 Future research

5.2.1 Ongoing work

The ESM simulations presented in this thesis are part of the LAnd MAnagement for CLImate Mitigation and Adaptation project (LAMACLIMA). Hence, other project partners are still analysing or planning some follow-up analyses on them. First, an analysis is ongoing of the local and non-local biogeochemical effects within the idealised LCLMC simulations (Chapter 2). Second, these simulations will also be used to further extend an emulator in order to also capture the climate effects from irrigation. Third, the results presented in Chapter 4 will be extended. This analysis will be complemented by looking into temperature extremes and extremes in human heat stress. Finally, this analysis will be complemented with additional simulations from MPI-ESM and EC-EARTH using the same simulation setup. This will allow the analysis to move beyond ESM-specific features (e.g. the North-Atlantic warming hole in CESM) and provide more general and robust conclusions regarding the feasibility of the Paris Agreement temperature targets under different land cover scenarios.

5.2.2 Improving the coupling between ESMs and IAMs

A large factor of uncertainty is related to the multitude of models needed to assess land cover scenarios especially for the future. Land cover scenarios are created within IAMs based on socioeconomic assumptions and simplified climate feedbacks, and are then converted to a common format defined within the Land Use Harmonisation Project (LUH2). These common LUH2 land cover maps are then translated via ESM-specific tools to each ESMs native grid and land cover typology. This modelling workflow is required as ESMs, in their current form, cannot model human decision-making needed to assess land cover scenarios. However, at this stage it remains unclear what the implications are of the information lost through the multiple conversions of land cover maps. Even though IAMs and ESMs are fundamentally different models, they share some common outputs which can be linked to land cover such as carbon emission changes related to land cover changes. A consistent assessment of the modelling workflow could prove useful to better understand and constrain potential biases in the representation of land cover within ESMs. Such work can only be achieved by combined efforts from both ESM and IAM communities but could potentially benefit the entire CMIP modelling workflow and therefore help improve the scientific support to policy making.

A simple and easy way to start such a comparison could be through a Land Use Map Model Intercomparison project (another LUM-MIP if you will) where ESMs and IAMs participate and consistently compare the results of land cover maps before and after given transitions such as the IAM to LUH2 or the LUH2 to ESM map transitions. Such a comparison could be relatively easily complemented by some ESM simulations (for example land-only) which would allow to quantify the importance of inconsistencies through errors

in land cover translation process to climate variables such as carbon and temperature. This intercomparison could involve several simulations focusing on both the historical period as future SSP scenarios. The simulations presented in Chapter 4 could serve as an initial test for the validity of these ideas as they are the product of collaboration between scientists from the land use model MagPie and three ESMs – and therefore allow for this intercomparison. It should be emphasized that the collaboration between IAM and ESM modelling groups is crucial in both the execution and setup of such an intercomparison which has the potential to reveal implications in a part of the modelling toolchain which is central to the production of climate information supporting policy makers.

5.2.3 Improving the representation of land surface processes in ESMs

Even though the earliest intermodel comparison projects, performed over a decade ago (LUCID), found that there is a large inconsistency in the representation of Land cover within ESMs and their resulting climate effects (Pitman et al., 2009; De Noblet-Ducoudré et al., 2012), we still find ourselves facing similar issues in the intercomparison presented in this thesis. The increased consistency in temperature response and understanding of the implications of non-local effects shows that the model developments made in past years have clearly paid off, making ESMs representation of land more consistent and realistic. The emergence of global observational datasets allows for a consistent evaluation of land cover implementations. New model developments should be evaluated against such datasets (e.g. Duveiller et al. (2020) for local biogeophysical effects) to assess the ability of ESMs to capture the effects of LCLMC on climate. These evaluations should go beyond land-only simulations and include at least also the atmosphere component as some biases only appear when climate interactions are included (as illustrated within this thesis with the albedo bias over boreal latitudes in CESM despite a good performance in a land-only evaluation study (Meier et al., 2018)).

Within such model evaluation, signal separation approaches have an important role to play as observations by design only capture local effects, while ESM simulations include both local and non-local effects. The checkerboard approach remains a useful signal separation approach, despite the potential issues relating to meso-scale circulation effects (Chapter 3). These issues merit further research which can be tackled by exploring different patterns of LCLMC (instead of a checkerboard a 3/4 or 7/8 LCLMC pattern) or different grid cell resolutions within a specific ESM. Other signal separation approaches such as those presented by Lejeune et al. (2017) can still provide an idea of local effects without the need of a checkerboard like LCLMC pattern implementation (and are currently evaluated against the checkerboard approach within a MSc thesis project).

Future model development is required to further bridge the remaining biases uncovered in this thesis. Several developments are in the pipeline which will further increase the realism of the modelled climate effects due to land cover changes such as the inclusion of biomass heat storage to improve the representation of the effects of land cover on the diurnal cy-

cle (Meier et al., 2019), or the inclusion of transient reservoir and lakes in order to better capture the effects of human behaviour on land cover and thus climate (Vanderkelen et al., 2021). However, several processes are still modelled in a highly simplified way (e.g. tree mortality, wildfires) and some are not even modelled at all (e.g. vegetation growth, nitrogen cycle). Future developments could therefore focus on improving the realism of land cover's representation within ESMs, especially with regard to vegetation processes. The shift from prescribed land cover representation (as used in this thesis for CESM) to dynamic vegetation models embedded in land surface models (e.g. as in EC-EARTH) is an important step to include more realistic land-climate interactions in ESMs.

As the next generation of coupled model simulations (CMIP7) is coming up, we provide a perspective of what should be the focus for dedicated ESM experiments to improve our understanding of the effects of LCLMC on the climate. It is my point of view that for the next phase of LUMIP, the ESM community should step away from idealised simulation set ups, as uncertain non-local biogeophysical effects can strongly affect this picture, and focus more on realistic pathways of land cover including land management practices:

1. **A larger focus on realistic pathways of land cover**. There should be an increased focus on future simulations with a fully coupled setup. This can allow for stronger and more robust science related to the importance of LCLMC scenario within the future period. Information on the potential of land-based mitigation and adaptation is crucial at this stage, and the ESM community needs to provide the information needed for the inclusion of these effects in future decision making. This is where ESMs can be most useful as they are the only tool available to the scientific community that can access the full breadth of climate processes needed to grasp the potential effects of future LCLMC (e.g. by including non-local biogeophysical effects).

2. **A larger focus on land management**. The next crucial step is the inclusion of land management practices in the next phase of LUMIP. Since CMIP6, where only three ESMs included irrigation (Al-Yaari et al., 2022), several ESM have started implementing irrigation and other management practices within their models. Even though the importance of land management has been highlighted for a long time (Luyssaert et al., 2014) the implementation within ESMs has lagged behind. However, we are now finally at a stage where management can be included in large-scale modelling exercises. Irrigation is an obvious target for this with some efforts already ongoing for the historical period specifically (e.g. the IRRMIP project: `https://hydr.vub.be/projects/irrmip`). These type of intercomparisons would allow to asses consistency and assess the need for more complex parameterisations (e.g. in CESM multiple irrigation methods have been implemented (Yao et al., 2022) while most ESMs only model flood irrigation). However, LUMIP should aim beyond just irrigation and also include other management practices such as crop albedo management, wood harvesting, and nitrogen fertilisation.

3. **Consideration of sub-daily output**. A more technical aspect is the data which is

outputted within an intercomparison project, as this constrains the type of potential analyses. LUMIP made a great step forward with the inclusion of subgrid-scale output within the simulation protocols (Lawrence et al., 2016). Here we suggest to complement this with a sub-daily (e.g. 3-hourly output stream) for selected variables, such as precipitation, near-surface temperature and specific humidity. This would allow for a more consistent comparison of the diurnal cycle and heat extremes as well as facilitate the calculation of impact-relevant metrics such as heat stress (Buzan and Huber, 2020), which at this point remain understudied and uncertain.

5.2.4 The potential for land-based mitigation and adaptation

Land-based mitigation is a key tool for achieving low-warming scenarios (Rogelj et al., 2018). However, the research in this thesis highlights some important issues. For example, unintended non-local biogeophysical effects following afforestation could undo any cooling due to an enhanced carbon sink (see Chapter 2). Recent research has highlighted other issues such as longevity and resilience of forest in a future and warmer climate (Fuss et al., 2018; Curtis et al., 2018; Hartmann et al., 2022; Forzieri et al., 2022) which further decreases the viability of afforestation for future mitigation. Ho (2023) highlights that even if all human beings on the planet would plant a tree, assuming these trees would survive and benefit mitigation efforts, it would only make up for 43 hours per year of GHG emission at current trends. Therefore, it is becoming increasingly clear that the mitigation potential of afforestation is highly limited. Future research on LCLMC should shift focus to the adaptation potential of these changes with the climate mitigation potential as a potential co-benefit of future LCLMC rather than the main goal.

To improve the utility of dedicated LCLMC ESM simulations for climate adaptation, we need to extend our analyses from purely climate variables to also include impact categories such as human health, economic impacts, and water availability. Currently, this strand of research is underdeveloped, but there is potential to move fast. In regards to the effects of LCLMC on water availability and moisture recycling, Chapter 3 showed that current approaches to analyse LCLMC-induced effects on moisture based on reanalysis derived recycling ratios (e.g. Tuinenburg et al., 2020) only render an incomplete assessment, as LCLMC-climate feedbacks are completely neglected. Future analysis of dedicated LCLMC simulations can help further constraining these effects by performing moisture tracking analyses on existing or future simulations of realistic future and historical scenarios. However, at this stage more work should go into understanding the strongly different hydrological cycles (illustrated by differing length scales) across ESMs through consistent comparison and evaluation of these metrics to reanalysis-based products. A low-hanging fruit in the applicability of ESMs for climate adaptation is heat stress. ESM-based studies should move beyond reporting effects on temperature and temperature extremes without the inclusion of a moisture dimension. A possible way forward is to include moist heat stress metrics within the default setups of ESM simulations which allows for the calculation of these metrics at the models native time step as was done for CESM (Buzan et al., 2015).

We do not live in the forest. To achieve useful information for impacts on humans, we need to move beyond local biogeophysical effects as reported by observational studies. ESMs are the only tool to date that can capture possible non-local effects and thus the full breadth of the climate effects. The development of an urban tile within ESMs is a promising avenue as this will allow even coarse grid ESMs to provide information at a useful level for climate adaptation. As land-based mitigation efforts are being initiated in Europe and beyond, we need to provide robust scientific information needed for supporting future land use planning.

Bibliography

Akkermans, T., Thiery, W., and Van Lipzig, N. P.: The regional climate impact of a realistic future deforestation scenario in the Congo Basin, Journal of Climate, 27, 2714–2734, 2014.

Al-Yaari, A., Ducharne, A., Thiery, W., Cheruy, F., and Lawrence, D.: The role of irrigation expansion on historical climate change: insights from CMIP6, Earth's Future, 10, e2022EF002 859, 2022.

Alkama, R. and Cescatti, A.: Climate change: Biophysical climate impacts of recent changes in global forest cover, Science, 351, 600–604, https://doi.org/10.1126/science.aac8083, 2016.

Arias, P., Bellouin, N., Coppola, E., Jones, R., Krinner, G., Marotzke, J., Naik, V., Palmer, M., Plattner, G., Rogelj, J., Rojas, M., Sillmann, J., Storelvmo, T., Thorne, P., Trewin, B., Achuta Rao, K., Adhikary, B., Allan, R., Armour, K., Bala, G., Barimalala, R., Berger, S., Canadell, S., Cassou, C., Cherchi, A., Collins, W., Collins, W., Connors, S., Corti, S., Cruz, F., Dentener, F., Dereczynski, C., Di Luca, A., Diongue Niang, A., Doblas-Reyes, F., Dosio, A., Douville, F., Engelbrecht, F., Eyring, V., Fischer, E., Forster, P., Fox-Kemper, B., Fuglestvedt, J., Fyfe, J., Gillett, C., Goldfarb, L., Gorodetskaya, I., Gutierrez, J., Hamdi, R., Hawkins, E., Hewitt, H., Hope, P., Islam, H., Jones, C., Kaufman, D., Kopp, R., Kosaka, Y., Kossin, J., Krakovska, S., Lee, J.-Y., Li, Y., Mauritsen, T., Maycock, T., Meinshausen, M., Min, S.-K., Monteiro, P., Ngo-Duc, T., Otto, F., Pinto, I., Pirani, A., Raghavan, K., Ranasinghe, R., Ruane, A., Ruiz, R., Sallé, R., Samset, B., Sathyendranath, S., Seneviratne, S., Sörensson, S., Szopa, A., Takayabu, I., Tréguier, A., van den Hurk, B., Vautard, R., von Schuckmann, K., Zaehle, S., Zhang, X., and Zickfeld, K.: 2021: Technical Summary. In Climate Change 2021: The Physical Science Basis. Contribution of Working Group I to the Sixth Assessment Report of the Intergovernmental Panel on Climate Change [Masson-Delmotte, V., P. Zhai, A. Pirani, S.L. Connors, C. Péan, S, Cambridge University Press, p. 150, URL `https://www.ipcc.ch/report/ar6/wg1/downloads/report/IPCC_AR6_WGI_TS.pdf`, 2021.

Bacmeister, J. T., Hannay, C., Medeiros, B., Gettelman, A., Neale, R., Fredriksen, H.-B., Lipscomb, W. H., Simpson, I., Bailey, D. A., Holland, M., et al.: CO 2 Increase Experiments Using the CESM: Relationship to Climate Sensitivity and Comparison of CESM1

to CESM2, Journal of Advances in Modeling Earth Systems, 12, e2020MS002 120, 2020.

Ban-Weiss, G. A., Bala, G., Cao, L., Pongratz, J., and Caldeira, K.: Climate forcing and response to idealized changes in surface latent and sensible heat, Environmental Research Letters, 6, https://doi.org/10.1088/1748-9326/6/3/034032, 2011.

Banacos, P. and Schultz, D.: The Use of Moisture Flux Convergence in Forecasting Convective Initiation: Historical and Operational Perspectives, Weather and Forecasting, 20, 351–366, https://doi.org/10.1175/WAF858.1, 2005.

Baudena, M., Tuinenburg, O. A., Ferdinand, P. A., and Staal, A.: Effects of land-use change in the Amazon on precipitation are likely underestimated, Global Change Biology, 27, 5580–5587, 2021.

Benedict, I., van Heerwaarden, C., van der Ent, R., Weerts, A., and Hazeleger, W.: Decline in Terrestrial Moisture Sources of the Mississippi River Basin in a Future Climate, Journal of Hydrometeorology, 21, https://doi.org/10.1175/JHM-D-19-0094.1, 2020.

Beusch, L., Gudmundsson, L., and Seneviratne, S. I.: Crossbreeding CMIP6 Earth System Models with an emulator for regionally optimized land temperature projections, Geophysical Research Letters, 47, e2019GL086 812, 2020.

Blyth, E. M., Arora, V. K., Clark, D. B., Dadson, S. J., De Kauwe, M. G., Lawrence, D. M., Melton, J. R., Pongratz, J., Turton, R. H., Yoshimura, K., and Yuan, H.: Advances in Land Surface Modelling, Current Climate Change Reports, 7, 45–71, https://doi.org/10.1007/s40641-021-00171-5, 2021.

Boisier, J. P., De Noblet-Ducoudré, N., Pitman, A. J., Cruz, F. T., Delire, C., Van Den Hurk, B. J., Van Der Molen, M. K., Mller, C., and Voldoire, A.: Attributing the impacts of land-cover changes in temperate regions on surface temperature and heat fluxes to specific causes: Results from the first LUCID set of simulations, Journal of Geophysical Research Atmospheres, 117, 1–16, https://doi.org/10.1029/2011JD017106, 2012.

Bonan, G.: Ecological climatology: concepts and applications, Cambridge University Press, 2015.

Bonan, G.: Climate change and terrestrial ecosystem modeling, Cambridge University Press, 2019.

Bonan, G. B.: Forests and climate change: forcings, feedbacks, and the climate benefits of forests, science, 320, 1444–1449, 2008.

Bosmans, J., van der Ent, R., Haarsma, R., Drijfhout, S., and Hilgen, F.: Precession- and obliquity-induced changes in moisture sources for enhanced precipitation over the Mediterranean Sea, Paleoceanography and Paleoclimatology, 35, e2019PA003 655, 2020.

Bowen, I. S.: The ratio of heat losses by conduction and by evaporation from any water surface, Physical review, 27, 779, 1926.

Boysen, L. R., Brovkin, V., Arora, V. K., Cadule, P., de Noblet-Ducoudré, N., Kato, E., Pongratz, J., and Gayler, V.: Global and regional effects of land-use change on climate in 21st century simulations with interactive carbon cycle, Earth System Dynamics, 5, 309–319, 2014.

Boysen, L. R., Lucht, W., Gerten, D., Heck, V., Lenton, T. M., and Schellnhuber, H. J.: The limits to global-warming mitigation by terrestrial carbon removal, Earth's Future, 5, 463–474, 2017.

Boysen, L. R., Brovkin, V., Pongratz, J., Lawrence, D. M., Lawrence, P., Vuichard, N., Peylin, P., Liddicoat, S., Hajima, T., Zhang, Y., Rocher, M., Delire, C., Séférian, R., Arora, V. K., Nieradzik, L., Anthoni, P., Thiery, W., Laguë, M. M., Lawrence, D., and Lo, M. H.: Global climate response to idealized deforestation in CMIP6 models, Biogeosciences, 17, 5615–5638, https://doi.org/10.5194/bg-17-5615-2020, 2020.

Bright, R. M., Davin, E., O'Halloran, T., Pongratz, J., Zhao, K., and Cescatti, A.: Local temperature response to land cover and management change driven by non-radiative processes, Nature Climate Change, 7, 296–302, https://doi.org/10.1038/nclimate3250, 2017.

Brovkin, V., Boysen, L., Arora, V. K., Boisier, J., Cadule, P., Chini, L., Claussen, M., Friedlingstein, P., Gayler, V., Van Den Hurk, B., et al.: Effect of anthropogenic land-use and land-cover changes on climate and land carbon storage in CMIP5 projections for the twenty-first century, Journal of Climate, 26, 6859–6881, 2013.

Brubaker, K. L., Entekhabi, D., and Eagleson, P.: Estimation of continental precipitation recycling, Journal of Climate, 6, 1077–1089, 1993.

Budd, G. M.: Wet-bulb globe temperature (WBGT)—its history and its limitations, Journal of science and medicine in sport, 11, 20–32, 2008.

Buzan, J., Oleson, K., and Huber, M.: Implementation and comparison of a suite of heat stress metrics within the Community Land Model version 4.5, Geoscientific Model Development, 8, 151–170, 2015.

Buzan, J. R. and Huber, M.: Moist heat stress on a hotter Earth, Annual Review of Earth and Planetary Sciences, 48, 623–655, 2020.

Canadell, J., Monteiro, P., Costra, M., Cotrim da Cunha, L., Cox, P., Eliseev, A., Henson, S., Ishii, M., Jaccard, S., Koven, C., Lohila, A., Patra, P., Piao, S., Rogelj, J., Syampungani, S., Zaehle, S., and Zickfeld, K.: Climate Change 2021: The Physical Science Basis. Contribution of Working Group I to the Sixth Assessment Report of the Intergovernmental Panel on Climate Change [Masson-Delmotte, V., P. Zhai, A. Pirani, S. L. Connors, C. Pean, S. Berger, N. Caud, Y. Chen, L. Goldfarb, M. I. Gomis, M. Huang, K. Leitzell, E. Lonnoy, J.B.R. Matthews, T. K. Maycock, T. Waterfield, O. Yelekci, R. Yu

and B. Zhou (eds.)], Cambridge University Press, URL https://www.ipcc.ch/report/ar6/wg1/downloads/report/IPCC_AR6_WGI_TS.pdf, 2021.

Chen, L. and Dirmeyer, P. A.: Global observed and modelled impacts of irrigation on surface temperature, International Journal of Climatology, 39, 2587–2600, https://doi.org/10.1002/joc.5973, 2019.

Cook, K.: South American Climate Variability and Change: Remote and Regional Forcing Processes, pp. 193–212, Springer, https://doi.org/10.1007/978-90-481-2672-9_8, 2009.

Curtis, P. G., Slay, C. M., Harris, N. L., Tyukavina, A., and Hansen, M. C.: Classifying drivers of global forest loss, Science, 361, 1108–1111, 2018.

Danabasoglu, G., Lamarque, J. F., Bacmeister, J., Bailey, D. A., DuVivier, A. K., Edwards, J., Emmons, L. K., Fasullo, J., Garcia, R., Gettelman, A., Hannay, C., Holland, M. M., Large, W. G., Lauritzen, P. H., Lawrence, D. M., Lenaerts, J. T., Lindsay, K., Lipscomb, W. H., Mills, M. J., Neale, R., Oleson, K. W., Otto-Bliesner, B., Phillips, A. S., Sacks, W., Tilmes, S., van Kampenhout, L., Vertenstein, M., Bertini, A., Dennis, J., Deser, C., Fischer, C., Fox-Kemper, B., Kay, J. E., Kinnison, D., Kushner, P. J., Larson, V. E., Long, M. C., Mickelson, S., Moore, J. K., Nienhouse, E., Polvani, L., Rasch, P. J., and Strand, W. G.: The Community Earth System Model Version 2 (CESM2), Journal of Advances in Modeling Earth Systems, 12, 1–35, https://doi.org/10.1029/2019MS001916, 2020.

Davin, E. L. and de Noblet-Ducoudre, N.: Climatic impact of global-scale Deforestation: Radiative versus nonradiative processes, Journal of Climate, 23, 97–112, https://doi.org/10.1175/2009JCLI3102.1, 2010.

Davin, E. L., Seneviratne, S. I., Ciais, P., Olioso, A., and Wang, T.: Preferential cooling of hot extremes from cropland albedo management, Proceedings of the National Academy of Sciences, 111, 9757–9761, 2014.

Davin, E. L., Rechid, D., Breil, M., Cardoso, R. M., Coppola, E., Hoffmann, P., Jach, L. L., Katragkou, E., De Noblet-Ducoudré, N., Radtke, K., Raffa, M., Soares, P. M., Sofiadis, G., Strada, S., Strandberg, G., Tölle, M. H., Warrach-Sagi, K., and Wulfmeyer, V.: Biogeophysical impacts of forestation in Europe: First results from the LUCAS (Land Use and Climate across Scales) regional climate model intercomparison, Earth System Dynamics, 11, 183–200, https://doi.org/10.5194/esd-11-183-2020, 2020.

De Hertog, S. J., Havermann, F., Vanderkelen, I., Guo, S., Luo, F., Manola, I., Coumou, D., Davin, E. L., Duveiller, G., Lejeune, Q., Pongratz, J., Schleussner, C. F., Seneviratne, S. I., and Thiery, W.: The biogeophysical effects of idealized land cover and land management changes in Earth system models, Earth System Dynamics, 14, 629–667, https://doi.org/10.5194/egusphere-2023-253, 2023.

de Kok, R. J., Tuinenburg, O. A., Bonekamp, P. N., and Immerzeel, W. W.: Irrigation as a potential driver for anomalous glacier behavior in High Mountain Asia, Geophysical research letters, 45, 2047–2054, 2018.

de Kok, R. J., Kraaijenbrink, P. D., Tuinenburg, O. A., Bonekamp, P. N., and Immerzeel, W. W.: Towards understanding the pattern of glacier mass balances in High Mountain Asia using regional climatic modelling, The Cryosphere, 14, 3215–3234, 2020.

De Noblet-Ducoudré, N., Boisier, J. P., Pitman, A., Bonan, G. B., Brovkin, V., Cruz, F., Delire, C., Gayler, V., Van Den Hurk, B. J., Lawrence, P. J., Van Der Molen, M. K., Müller, C., Reick, C. H., Strengers, B. J., and Voldoire, A.: Determining robust impacts of land-use-induced land cover changes on surface climate over North America and Eurasia: Results from the first set of LUCID experiments, Journal of Climate, 25, 3261–3281, https://doi.org/10.1175/JCLI-D-11-00338.1, 2012.

de Vrese, P. and Hagemann, S.: Uncertainties in modelling the climate impact of irrigation, Climate dynamics, 51, 2023–2038, 2018.

de Vrese, P. and Stacke, T.: Irrigation and hydrometeorological extremes, Climate Dynamics, 55, 1521–1537, https://doi.org/10.1007/s00382-020-05337-9, 2020.

de Vrese, P., Hagemann, S., and Claussen, M.: Asian irrigation, African rain: Remote impacts of irrigation, Geophysical Research Letters, 43, 3737–3745, https://doi.org/10.1002/2016GL068146, 2016.

Deser, C., Knutti, R., Solomon, S., and Phillips, A. S.: Communication of the role of natural variability in future North American climate, Nature Climate Change, 2, 775–779, 2012.

Deser, C., Lehner, F., Rodgers, K. B., Ault, T., Delworth, T. L., DiNezio, P. N., Fiore, A., Frankignoul, C., Fyfe, J. C., Horton, D. E., et al.: Insights from Earth system model initial-condition large ensembles and future prospects, Nature Climate Change, 10, 277–286, 2020.

Devaraju, N., de Noblet-Ducoudré, N., Quesada, B., and Bala, G.: Quantifying the relative importance of direct and indirect biophysical effects of deforestation on surface temperature and teleconnections, Journal of Climate, 31, 3811–3829, https://doi.org/10.1175/JCLI-D-17-0563.1, 2018.

Dominguez, F., Kumar, P., Liang, X.-Z., and Ting, M.: Impact of atmospheric moisture storage on precipitation recycling, Journal of climate, 19, 1513–1530, 2006.

Döscher, R., Acosta, M., Alessandri, A., Anthoni, P., Arsouze, T., Bergman, T., Bernardello, R., Boussetta, S., Caron, L.-P., Carver, G., et al.: The EC-Earth3 earth system model for the coupled model intercomparison project 6, Geoscientific Model Development, 15, 2973–3020, 2022.

Dunne, J. P., Stouffer, R. J., and John, J. G.: Reductions in labour capacity from heat stress under climate warming, Nature Climate Change, 3, 563–566, 2013.

Duveiller, G., Hooker, J., and Cescatti, A.: The mark of vegetation change on Earth's surface energy balance, Nature Communications, 679, https://doi.org/10.1038/s41467-017-02810-8, 2018.

Duveiller, G., Caporaso, L., Abad-Viñas, R., Perugini, L., Grassi, G., Arneth, A., and Cescatti, A.: Local biophysical effects of land use and land cover change: towards an assessment tool for policy makers, Land Use Policy, 91, 104 382, https://doi.org/10.1016/j.landusepol.2019.104382, 2020.

Duveiller, G., Filipponi, F., Ceglar, A., Bojanowski, J., Alkama, R., and Cescatti, A.: Revealing the widespread potential of forests to increase low level cloud cover, Nature Communications, 12, 1–15, https://doi.org/10.1038/s41467-021-24551-5, 2021.

Ellison, D., Morris, C. E., Locatelli, B., Sheil, D., Cohen, J., Murdiyarso, D., Gutierrez, V., Van Noordwijk, M., Creed, I. F., Pokorny, J., et al.: Trees, forests and water: Cool insights for a hot world, Global environmental change, 43, 51–61, 2017.

Erb, K.-H., Kastner, C., Plutzar, W., Bais, A., Carvalhais, N., Fetzel, T., Gingrich, S., Haberl, H., Lauk, C., Niedertscheider, M., Pongratz, J., Thurner, M., and Luyssaert, S.: Unexpectedly large impact of forest management and grazing on global vegetation biomass, Nature, 553, 73–76, 2018.

European Commission: Communication - European Green Deal Investment Plan, European Commission, 2020.

Eyring, V., Bony, S., Meehl, G. A., Senior, C. A., Stevens, B., Stouffer, R. J., and Taylor, K. E.: Overview of the Coupled Model Intercomparison Project Phase 6 (CMIP6) experimental design and organization, Geoscientific Model Development, 9, 1937–1958, 2016.

Fatima, S. H., Rothmore, P., Giles, L. C., Varghese, B. M., and Bi, P.: Extreme heat and occupational injuries in different climate zones: A systematic review and meta-analysis of epidemiological evidence, Environment international, 148, 106 384, 2021.

Findell, K. L., Keys, P. W., van der Ent, R. J., Lintner, B. R., Berg, A., and Krasting, J. P.: Rising temperatures increase importance of oceanic evaporation as a source for continental precipitation, Journal of Climate, 32, 7713–7726, 2019.

Forzieri, G., Dakos, V., McDowell, N. G., Ramdane, A., and Cescatti, A.: Emerging signals of declining forest resilience under climate change, Nature, 608, 534–539, 2022.

Friedlingstein, P., Jones, M. W., O'Sullivan, M., Andrew, R. M., Bakker, D. C., Hauck, J., Le Quéré, C., Peters, G. P., Peters, W., Pongratz, J., et al.: Global carbon budget 2021, Earth System Science Data, 14, 1917–2005, 2022.

Fuss, S., Lamb, W. F., Callaghan, M. W., Hilaire, J., Creutzig, F., Amann, T., Beringer, T., de Oliveira Garcia, W., Hartmann, J., Khanna, T., et al.: Negative emissions—Part 2: Costs, potentials and side effects, Environmental Research Letters, 13, 063 002, 2018.

Gao, F., Schaaf, C. B., Strahler, A. H., Roesch, A., Lucht, W., and Dickinson, R.: MODIS bidirectional reflectance distribution function and albedo Climate Modeling Grid products and the variability of albedo for major global vegetation types, Journal of Geophysical Research: Atmospheres, 110, 2005.

Gasparrini, A., Guo, Y., Hashizume, M., Lavigne, E., Zanobetti, A., Schwartz, J., Tobias, A., Tong, S., Rocklöv, J., Forsberg, B., et al.: Mortality risk attributable to high and low ambient temperature: a multicountry observational study, The lancet, 386, 369–375, 2015.

Gettelman, A., Hannay, C., Bacmeister, J. T., Neale, R. B., Pendergrass, A., Danabasoglu, G., Lamarque, J.-F., Fasullo, J., Bailey, D., Lawrence, D., et al.: High climate sensitivity in the Community Earth System Model version 2 (CESM2), Geophysical Research Letters, 46, 8329–8337, 2019.

Gimeno, L., Stohl, A., Trigo, R. M., Dominguez, F., Yoshimura, K., Yu, L., Drumond, A., Durán-Quesada, A. M., and Nieto, R.: Oceanic and terrestrial sources of continental precipitation, Reviews of Geophysics, 50, 2012.

Gimeno, L., Vázquez, M., Eiras-Barca, J., Sorí, R., Stojanovic, M., Algarra, I., Nieto, R., Ramos, A. M., Durán-Quesada, A. M., and Dominguez, F.: Recent progress on the sources of continental precipitation as revealed by moisture transport analysis, Earth-Science Reviews, 201, 103 070, 2020.

Goessling, H. and Reick, C.: What do moisture recycling estimates tell us? Exploring the extreme case of non-evaporating continents, Hydrology and Earth System Sciences, 15, 3217–3235, 2011.

Gormley-Gallagher, A., Sterl, S., Hirsch, A., Seneviratne, S., Davin, E., and Thiery, W.: Agricultural management effects on mean and extreme temperature trends, Earth System Dynamics Discussions, pp. 1–27, https://doi.org/10.5194/esd-2020-35, 2020.

Guimberteau, M., Laval, K., Perrier, A., and Polcher, J.: Global effect of irrigation and its impact on the onset of the Indian summer monsoon, Climate Dynamics, 39, 1329–1348, 2012.

Guo, L., Van Der Ent, R. J., Klingaman, N. P., Demory, M.-E., Vidale, P. L., Turner, A. G., Stephan, C. C., and Chevuturi, A.: Effects of horizontal resolution and air–sea coupling on simulated moisture source for East Asian precipitation in MetUM GA6/GC2, Geoscientific Model Development, 13, 6011–6028, 2020.

Haddeland, I., Heinke, J., Biemans, H., Eisner, S., Flörke, M., Hanasaki, N., Konzmann, M., Ludwig, F., Masaki, Y., Schewe, J., Stacke, T., Tessler, Z. D., Wada, Y., and Wisser, D.: Global water resources affected by human interventions and climate change, Proceedings of the National Academy of Sciences of the United States of America, 111, 3251–3256, https://doi.org/10.1073/pnas.1222475110, 2014.

Harari, Y. N.: Sapiens: a brief history of humankind, Harper, 2014.

Harrington, L. J., Frame, D. J., Fischer, E. M., Hawkins, E., Joshi, M., and Jones, C. D.: Poorest countries experience earlier anthropogenic emergence of daily temperature extremes, Environmental Research Letters, 11, 055 007, 2016.

Harrington, L. J., Frame, D., King, A. D., and Otto, F. E.: How uneven are changes to impact-relevant climate hazards in a 1.5° C world and beyond?, Geophysical Research Letters, 45, 6672–6680, 2018.

Hartmann, H., Bastos, A., Das, A. J., Esquivel-Muelbert, A., Hammond, W. M., Martínez-Vilalta, J., McDowell, N. G., Powers, J. S., Pugh, T. A., Ruthrof, K. X., et al.: Climate change risks to global forest health: emergence of unexpected events of elevated tree mortality worldwide, Annual Review of Plant Biology, 73, 673–702, 2022.

Hauser, M., Thiery, W., and Seneviratne, S. I.: Potential of global land water recycling to mitigate local temperature extremes, Earth System Dynamics, 10, 157–169, 2019.

Heck, V., Gerten, D., Lucht, W., and Popp, A.: Biomass-based negative emissions difficult to reconcile with planetary boundaries, Nature climate change, 8, 151–155, 2018.

Hirsch, A. L., Wilhelm, M., Davin, E. L., Thiery, W., and Seneviratne, S. I.: Can climate-effective land management reduce regional warming?, Journal of Geophysical Research, 122, 2269–2288, https://doi.org/10.1002/2016JD026125, 2017.

Hirsch, A. L., Guillod, B. P., Seneviratne, S. I., Beyerle, U., Boysen, L. R., Brovkin, V., Davin, E. L., Doelman, J. C., Kim, H., Mitchell, D. M., et al.: Biogeophysical impacts of land-use change on climate extremes in low-emission scenarios: results from HAPPI-Land, Earth's future, 6, 396–409, 2018a.

Hirsch, A. L., Prestele, R., Davin, E. L., Seneviratne, S. I., Thiery, W., and Verburg, P. H.: Modelled biophysical impacts of conservation agriculture on local climates, Global Change Biology, 24, 4758–4774, https://doi.org/10.1111/gcb.14362, 2018b.

Ho, D. T.: World view, Nature, 616, 9, 2023.

Hoek van Dijke, A. J., Herold, M., Mallick, K., Benedict, I., Machwitz, M., Schlerf, M., Pranindita, A., Theeuwen, J. J., Bastin, J.-F., and Teuling, A. J.: Shifts in regional water availability due to global tree restoration, Nature Geoscience, 15, 363–368, 2022.

Humpenöder, F., Popp, A., and Dietrich, J. P.: Investigating afforestation and bioenergy CCS as climate change mitigation strategies, Environmental Research Letters, https://doi.org/10.1088/1748-9326/9/6/064029, 2014.

Humpenöder, F., Popp, A., Schleussner, C.-F., Orlov, A., Windisch, M. G., Menke, I., Pongratz, J., Havermann, F., Thiery, W., Luo, F., et al.: Overcoming global inequality is critical for land-based mitigation in line with the Paris Agreement, Nature Communications, 13, 7453, 2022.

Hurtt, G. C., Chini, L. P., Frolking, S., Betts, R., Feddema, J., Fischer, G., Fisk, J., Hibbard, K., Houghton, R., Janetos, A., et al.: Harmonization of land-use scenarios for the period 1500–2100: 600 years of global gridded annual land-use transitions, wood harvest, and resulting secondary lands, Climatic change, 109, 117–161, 2011.

Hurtt, G. C., Chini, L., Sahajpal, R., Frolking, S., Bodirsky, B. L., Calvin, K., Doelman, J. C., Fisk, J., Fujimori, S., Goldewijk, K. K., Hasegawa, T., Havlik, P., Heinimann, A., Humpenöder, F., Jungclaus, J., Kaplan, J. O., Kennedy, J., Krisztin, T., Lawrence, D., Lawrence, P., Ma, L., Mertz, O., Pongratz, J., Popp, A., Poulter, B., Riahi, K., Shevliakova, E., Stehfest, E., Thornton, P., Tubiello, F. N., van Vuuren, D. P., and Zhang, X.: Harmonization of global land use change and management for the period 850-2100 (LUH2) for CMIP6, vol. 13, Copernicus GmbH, https://doi.org/10.5194/gmd-13-5425-2020, 2020.

IPCC: Climate Change 2022: Mitigation of Climate Change. Contribution of Working Group III to the Sixth Assessment Report of the Intergovernmental Panel on Climate Change [P.R. Shukla, J. Skea, R. Slade, A. Al Khourdajie, R. van Diemen, D. McCollum, M. Pathak, S. Some, P. Vyas, R. Fradera, M. Belkacemi, A. Hasija, G. Lisboa, S. Luz, J. Malley, (eds.)], IPCC, 2022.

Ito, A., Hajima, T., Lawrence, D. M., Brovkin, V., Delire, C., Guenet, B., Jones, C. D., Malyshev, S., Materia, S., McDermid, S. P., Peano, D., Pongratz, J., Robertson, E., Shevliakova, E., Vuichard, N., Wårlind, D., Wiltshire, A., and Ziehn, T.: Soil carbon sequestration simulated in CMIP6-LUMIP models: Implications for climatic mitigation, Environmental Research Letters, 15, https://doi.org/10.1088/1748-9326/abc912, 2020.

Jha, R., Mondal, A., Devanand, A., Roxy, M., and Ghosh, S.: Limited influence of irrigation on pre-monsoon heat stress in the Indo-Gangetic Plain, Nature Communications, 13, 4275, 2022.

Jia, G., Shevliakova, E., Artaxo, P., De Noblet-Ducoudré, N., Houghton, R., House, J., Kitajima, K., Lennard, C., Popp, A., Sirin, A., Sukumar, R., and Verchot, L.: Land–climate interactions. In: Climate Change and Land: an IPCC special report on climate change, desertification, land degradation, sustainable land management, food security, and greenhouse gas fluxes in terrestrial ecosystems [P.R. Shukla, J. Skea, E. Calvo Buendia, V. Masson-Delmotte, H.-O. Pörtner, D.C. Roberts, P. Zhai, R. Slade, S. Connors, R. van Diemen, M. Ferrat, E. Haughey, S. Luz, S. Neogi, M. Pathak, J. Petzold, J. Portugal Pereira, P. Vyas, E. Huntley, K. Kissick, M. Belkacemi, J. Malley, (eds.)]., Cambridge University Press, 2019.

Jones, C. D., Arora, V., Friedlingstein, P., Bopp, L., Brovkin, V., Dunne, J., Graven, H., Hoffman, F., Ilyina, T., John, J. G., et al.: C4MIP–The coupled climate–carbon cycle model intercomparison project: Experimental protocol for CMIP6, Geoscientific Model Development, 9, 2853–2880, 2016.

Juang, J. Y., Katul, G., Siqueira, M., Stoy, P., and Novick, K.: Separating the effects of albedo from eco-physiological changes on surface temperature along a successional chronosequence in the southeastern United States, Geophysical Research Letters, 34, 1–5, https://doi.org/10.1029/2007GL031296, 2007.

Kirschbaum, M., Eamus, D., Gifford, R., Roxburgh, S., and Sands, P.: Definitions of some ecological terms commonly used in carbon accounting, Cooperative Research Centre for Carbon Accounting, Canberra, pp. 2–5, 2001.

Kjellstrom, T., Holmer, I., and Lemke, B.: Workplace heat stress, health and productivity–an increasing challenge for low and middle-income countries during climate change, Global health action, 2, 2047, 2009.

Kjellstrom, T., Freyberg, C., Lemke, B., Otto, M., and Briggs, D.: Estimating population heat exposure and impacts on working people in conjunction with climate change, International journal of biometeorology, 62, 291–306, 2018.

Kong, Q. and Huber, M.: Explicit Calculations of Wet-Bulb Globe Temperature Compared With Approximations and Why It Matters for Labor Productivity, Earth's Future, 10, e2021EF002 334, 2022.

Kumar, S., Dirmeyer, P. A., Merwade, V., Delsole, T., Adams, J. M., and Niyogi, D.: Land use/cover change impacts in CMIP5 climate simulations: A new methodology and 21st century challenges, Journal of Geophysical Research Atmospheres, 118, 6337–6353, https://doi.org/10.1002/jgrd.50463, 2013.

Laguë, M. M. and Swann, A. L.: Progressive midlatitude afforestation: Impacts on clouds, global energy transport, and precipitation, Journal of Climate, 29, 5561–5573, 2016.

Laguë, M. M., Bonan, G. B., and Swann, A. L.: Separating the impact of individual land surface properties on the terrestrial surface energy budget in both the coupled and uncoupled land–atmosphere system, Journal of Climate, 32, 5725–5744, https://doi.org/10.1175/JCLI-D-18-0812.1, 2019.

Lange, S.: Trend-preserving bias adjustment and statistical downscaling<? xmltex\break?> with ISIMIP3BASD (v1. 0), Geoscientific Model Development, 12, 3055–3070, 2019.

Lawrence, D. M., Hurtt, G. C., Arneth, A., Brovkin, V., Calvin, K. V., Jones, A. D., Jones, C. D., Lawrence, P. J., de Noblet-Ducoudré, N., Pongratz, J., et al.: The Land Use Model Intercomparison Project (LUMIP) contribution to CMIP6: rationale and experimental design, Geoscientific Model Development, 9, 2973–2998, 2016.

Lawrence, D. M., Fisher, R. A., Koven, C. D., Oleson, K. W., Swenson, S. C., Bonan, G., Collier, N., Ghimire, B., van Kampenhout, L., Kennedy, D., Kluzek, E., Lawrence, P. J., Li, F., Li, H., Lombardozzi, D., Riley, W. J., Sacks, W. J., Shi, M., Vertenstein, M., Wieder, W. R., Xu, C., Ali, A. A., Badger, A. M., Bisht, G., van den Broeke, M., Brunke, M. A., Burns, S. P., Buzan, J., Clark, M., Craig, A., Dahlin, K., Drewniak, B., Fisher, J. B., Flanner, M., Fox, A. M., Gentine, P., Hoffman, F., Keppel-Aleks, G., Knox, R., Kumar, S., Lenaerts, J., Leung, L. R., Lipscomb, W. H., Lu, Y., Pandey, A., Pelletier, J. D., Perket, J., Randerson, J. T., Ricciuto, D. M., Sanderson, B. M., Slater, A., Subin, Z. M., Tang, J., Thomas, R. Q., Val Martin, M., and Zeng, X.: The Community

Land Model Version 5: Description of New Features, Benchmarking, and Impact of Forcing Uncertainty, Journal of Advances in Modeling Earth Systems, 11, 4245–4287, https://doi.org/10.1029/2018MS001583, 2019.

Layton, K. and Ellison, D.: Induced precipitation recycling (IPR): A proposed concept for increasing precipitation through natural vegetation feedback mechanisms, Ecological Engineering, 91, 553–565, 2016.

Lee, S.-W., Kim, I.-G., Kim, H.-M., Lee, D.-G., Lee, H.-C., and Choi, G.: Spatio-temporal patterns of the minimum rest time for outdoor workers exposed to summer heat stress in South Korea, International Journal of Biometeorology, 64, 1755–1765, 2020.

Lee, X., Goulden, M. L., Hollinger, D. Y., Barr, A., Black, T. A., Bohrer, G., Bracho, R., Drake, B., Goldstein, A., Gu, L., et al.: Observed increase in local cooling effect of deforestation at higher latitudes, Nature, 479, 384–387, 2011.

Lejeune, Q., Davin, E. L., Guillod, B. P., and Seneviratne, S. I.: Influence of Amazonian deforestation on the future evolution of regional surface fluxes, circulation, surface temperature and precipitation, Climate Dynamics, 44, 2769–2786, https://doi.org/10.1007/s00382-014-2203-8, 2015.

Lejeune, Q., Seneviratne, S. I., and Davin, E. L.: Historical land-cover change impacts on climate: Comparative assessment of LUCID and CMIP5 multimodel experiments, Journal of Climate, 30, 1439–1459, https://doi.org/10.1175/JCLI-D-16-0213.1, 2017.

Lelieveld, J., Proestos, Y., Hadjinicolaou, P., Tanarhte, M., Tyrlis, E., and Zittis, G.: Strongly increasing heat extremes in the Middle East and North Africa (MENA) in the 21st century, Climatic Change, 137, 245–260, 2016.

Lemke, B. and Kjellstrom, T.: Calculating workplace WBGT from meteorological data: a tool for climate change assessment, Industrial Health, 50, 267–278, 2012.

Li, Y., Zhao, M., Motesharrei, S., Mu, Q., Kalnay, E., and Li, S.: Local cooling and warming effects of forests based on satellite observations, Nature Communications, 6, https://doi.org/10.1038/ncomms7603, 2015.

Liljegren, J. C., Carhart, R. A., Lawday, P., Tschopp, S., and Sharp, R.: Modeling the wet bulb globe temperature using standard meteorological measurements, Journal of occupational and environmental hygiene, 5, 645–655, 2008.

Lindeskog, M., Arneth, A., Bondeau, A., Waha, K., Seaquist, J., Olin, S., and Smith, B.: Implications of accounting for land use in simulations of ecosystem carbon cycling in Africa, Earth System Dynamics, 4, 385–407, 2013.

Lombardozzi, D., Bonan, G., Wieder, W., Grandy, A., Morris, C., and Lawrence, D.: Cover crops may cause winter warming in snow-covered regions, Geophysical Research Letters, 45, 9889–9897, 2018.

Lombardozzi, D. L., Lu, Y., Lawrence, P. J., Lawrence, D. M., Swenson, S., Oleson, K. W., Wieder, W. R., and Ainsworth, E. A.: Simulating agriculture in the Community Land Model version 5, Journal of Geophysical Research: Biogeosciences, 125, e2019JG005 529, 2020.

Lorenz, R., Pitman, A., and Sisson, S. A.: Does Amazonian deforestation cause global effects; can we be sure?, Journal of Geophysical Research: Atmospheres, 121, 5567–5584, 2016.

Luyssaert, S., Jammet, M., Stoy, P. C., Estel, S., Pongratz, J., Ceschia, E., Churkina, G., Don, A., Erb, K., Ferlicoq, M., et al.: Land management and land-cover change have impacts of similar magnitude on surface temperature, Nature Climate Change, 4, 389–393, 2014.

Mahmood, R., Pielke Sr, R. A., Hubbard, K. G., Niyogi, D., Dirmeyer, P. A., McAlpine, C., Carleton, A. M., Hale, R., Gameda, S., Beltrán-Przekurat, A., et al.: Land cover changes and their biogeophysical effects on climate, International journal of climatology, 34, 929–953, 2014.

Malyshev, S., Shevliakova, E., Stouffer, R. J., and Pacala, S. W.: Contrasting local versus regional effects of land-use-change-induced heterogeneity on historical climate: Analysis with the GFDL earth system model, Journal of Climate, 28, 5448–5469, https://doi.org/10.1175/JCLI-D-14-00586.1, 2015.

Mauritsen, T., Bader, J., Becker, T., Behrens, J., Bittner, M., Brokopf, R., Brovkin, V., Claussen, M., Crueger, T., Esch, M., Fast, I., Fiedler, S., Fläschner, D., Gayler, V., Giorgetta, M., Goll, D. S., Haak, H., Hagemann, S., Hedemann, C., Hohenegger, C., Ilyina, T., Jahns, T., Jimenéz-de-la Cuesta, D., Jungclaus, J., Kleinen, T., Kloster, S., Kracher, D., Kinne, S., Kleberg, D., Lasslop, G., Kornblueh, L., Marotzke, J., Matei, D., Meraner, K., Mikolajewicz, U., Modali, K., Möbis, B., Müller, W. A., Nabel, J. E., Nam, C. C., Notz, D., Nyawira, S. S., Paulsen, H., Peters, K., Pincus, R., Pohlmann, H., Pongratz, J., Popp, M., Raddatz, T. J., Rast, S., Redler, R., Reick, C. H., Rohrschneider, T., Schemann, V., Schmidt, H., Schnur, R., Schulzweida, U., Six, K. D., Stein, L., Stemmler, I., Stevens, B., von Storch, J. S., Tian, F., Voigt, A., Vrese, P., Wieners, K. H., Wilkenskjeld, S., Winkler, A., and Roeckner, E.: Developments in the MPI-M Earth System Model version 1.2 (MPI-ESM1.2) and Its Response to Increasing CO2, Journal of Advances in Modeling Earth Systems, 11, 998–1038, https://doi.org/10.1029/2018MS001400, 2019.

Mazdiyasni, O., AghaKouchak, A., Davis, S. J., Madadgar, S., Mehran, A., Ragno, E., Sadegh, M., Sengupta, A., Ghosh, S., Dhanya, C., et al.: Increasing probability of mortality during Indian heat waves, Science advances, 3, e1700 066, 2017.

Mbow, H.-O. P., Reisinger, A., Canadell, J., and O'Brien, P.: Special Report on climate change, desertification, land degradation, sustainable land management, food security, and greenhouse gas fluxes in terrestrial ecosystems (SR2), Ginevra, IPCC, 2017.

Meier, R., Davin, E. L., Lejeune, Q., Hauser, M., Li, Y., Martens, B., Schultz, N., Sterling, S., and Thiery, W.: Research Collection, Biogeosciences, 15, 4731–4757, URL `https://doi.org/10.3929/ethz-a-010025751`, 2018.

Meier, R., Davin, E. L., Swenson, S. C., Lawrence, D. M., and Schwaab, J.: Biomass heat storage dampens diurnal temperature variations in forests, Environmental research letters, 14, 084 026, 2019.

Meier, R., Schwaab, J., Seneviratne, S. I., Sprenger, M., Lewis, E., and Davin, E. L.: Empirical estimate of forestation-induced precipitation changes in Europe, Nature Geoscience, 14, 473–478, https://doi.org/10.1038/s41561-021-00773-6, 2021.

Meinshausen, M., Lewis, J., McGlade, C., Gütschow, J., Nicholls, Z., Burdon, R., Cozzi, L., and Hackmann, B.: Realization of Paris Agreement pledges may limit warming just below 2 C, Nature, 604, 304–309, 2022.

Minx, J. C., Lamb, W. F., Callaghan, M. W., Fuss, S., Hilaire, J., Creutzig, F., Amann, T., Beringer, T., De Oliveira Garcia, W., Hartmann, J., Khanna, T., Lenzi, D., Luderer, G., Nemet, G. F., Rogelj, J., Smith, P., Vicente Vicente, J. L., Wilcox, J., and Del Mar Zamora Dominguez, M.: Negative emissions - Part 1: Research landscape and synthesis, Environmental Research Letters, 13, https://doi.org/10.1088/1748-9326/aabf9b, 2018.

Mishra, V., Ambika, A. K., Asoka, A., Aadhar, S., Buzan, J., Kumar, R., and Huber, M.: Moist heat stress extremes in India enhanced by irrigation, Nature Geoscience, 13, 722–728, https://doi.org/10.1038/s41561-020-00650-8, 2020.

Monfreda, C., Ramankutty, N., and Foley, J. A.: Farming the planet: 2. Geographic distribution of crop areas, yields, physiological types, and net primary production in the year 2000, Global biogeochemical cycles, 22, 2008.

Morice, C. P., Kennedy, J. J., Rayner, N. A., Winn, J., Hogan, E., Killick, R., Dunn, R., Osborn, T., Jones, P., and Simpson, I.: An updated assessment of near-surface temperature change from 1850: The HadCRUT5 data set, Journal of Geophysical Research: Atmospheres, 126, e2019JD032 361, 2021.

Nakai, T., Sumida, A., Daikoku, K., Matsumoto, K., van der Molen, M. K., Kodama, Y., Kononov, A. V., Maximov, T. C., Dolman, A. J., Yabuki, H., Hara, T., and Ohta, T.: Parameterisation of aerodynamic roughness over boreal, cool- and warm-temperate forests, Agricultural and Forest Meteorology, 148, 1916–1925, https://doi.org/10.1016/j.agrformet.2008.03.009, 2008.

Nath, S., Lejeune, Q., Beusch, L., Seneviratne, S. I., and Schleussner, C.-F.: MESMER-M: an Earth system model emulator for spatially resolved monthly temperature, Earth System Dynamics, 13, 851–877, 2022.

Nath, S., Gudmundsson, L., Schwaab, J., Duveiller, G., De Hertog, S. J., Guo, S., Havermann, F., Luo, F., Manola, I., Pongratz, J., Seneviratne, S. I., Scleussner, C.-F., Thiery,

W., and Lejeune, Q.: TIMBER v0. 1: a conceptual framework for emulating temperature responses to tree cover change, Geoscientific Model Development, 2023.

NIOSH: Criteria for a recommended standard: Occupational exposure to hot environments, National Institute for Occupational Safety and Health, 1986.

Oke, T.: Boundary Layer Climates, Methuen & Co, Ltd, London,, 1987.

Orlov, A., Sillmann, J., Aunan, K., Kjellstrom, T., and Aaheim, A.: Economic costs of heat-induced reductions in worker productivity due to global warming, Global Environmental Change, 63, 102 087, 2020.

Orlov, A., De Hertog, S., Havermann, F., Guo, S., Luo, F., Manola, I., Thiery, W., Lejeune, Q., Pongratz, J., Humpenöder, F., et al.: Changes in land cover and management affect heat stress and labor capacity, Earth's Future, 11, e2022EF002 909, 2023.

Otto, J., Berveiller, D., Bréon, F. M., Delpierre, N., Geppert, G., Granier, A., Jans, W., Knohl, A., Kuusk, A., Longdoz, B., Moors, E., Mund, M., Pinty, B., Schelhaas, M. J., and Luyssaert, S.: Forest summer albedo is sensitive to species and thinning: How should we account for this in Earth system models?, Biogeosciences, 11, 2411–2427, https://doi.org/10.5194/bg-11-2411-2014, 2014.

Perugini, L., Caporaso, L., Marconi, S., Cescatti, A., Quesada, B., De Noblet-Ducoudré, N., House, J. I., and Arneth, A.: Biophysical effects on temperature and precipitation due to land cover change, Environmental Research Letters, 12, https://doi.org/10.1088/1748-9326/aa6b3f, 2017.

Pitman, A. J., De Noblet-Ducoudré, N., Cruz, F. T., Davin, E. L., Bonan, G. B., Brovkin, V., Claussen, M., Delire, C., Ganzeveld, L., Gayler, V., Van Den Hurk, B. J., Lawrence, P. J., Van Der Molen, M. K., Müller, C., Reick, C. H., Seneviratne, S. I., Strengen, B. J., and Voldoire, A.: Uncertainties in climate responses to past land cover change: First results from the LUCID intercomparison study, Geophysical Research Letters, 36, 1–6, https://doi.org/10.1029/2009GL039076, 2009.

Pongratz, J., Reick, C., Raddatz, T., and Claussen, M.: Biogeophysical versus biogeochemical climate response to historical anthropogenic land cover change, Geophysical Research Letters, 37, 2010.

Pongratz, J., Schwingshackl, C., Bultan, S., Obermeier, W., Havermann, F., and Guo, S.: Land Use Effects on Climate: Current State, Recent Progress, and Emerging Topics, Current Climate Change Reports, https://doi.org/10.1007/s40641-021-00178-y, 2021.

Popp, A., Calvin, K., Fujimori, S., Havlik, P., Humpenöder, F., Stehfest, E., Bodirsky, B. L., Dietrich, J. P., Doelmann, J. C., Gusti, M., et al.: Land-use futures in the shared socio-economic pathways, Global Environmental Change, 42, 331–345, 2017.

Portmann, R., Beyerle, U., Davin, E., Fischer, E. M., De Hertog, S., and Schemm, S.: Global forestation and deforestation affect remote climate via adjusted atmosphere and ocean circulation, Nature Communications, 13, 1–11, 2022.

Puma, M. and Cook, B.: Effects of irrigation on global climate during the 20th century, Journal of Geophysical Research: Atmospheres, 115, 2010.

Quesada, B., Devaraju, N., de Noblet-Ducoudré, N., and Arneth, A.: Reduction of monsoon rainfall in response to past and future land use and land cover changes, Geophysical Research Letters, 44, 1041–1050, 2017.

Reid, W. V., Ali, M. K., and Field, C. B.: The future of bioenergy, Global change biology, 26, 274–286, 2020.

Roe, S., Streck, C., Obersteiner, M., Frank, S., Griscom, B., Drouet, L., Fricko, O., Gusti, M., Harris, N., Hasegawa, T., Hausfather, Z., Havlík, P., House, J., Nabuurs, G. J., Popp, A., Sánchez, M. J. S., Sanderman, J., Smith, P., Stehfest, E., and Lawrence, D.: Contribution of the land sector to a 1.5 °C world, Nature Climate Change, 9, 817–828, https://doi.org/10.1038/s41558-019-0591-9, 2019.

Rogelj, J., Shindell, D., Jiang, K., Fifita, S., Forster, P., Ginzburg, V., Handa, C., Kheshgi, H., Kobayashi, S., Kriegler, E., et al.: Mitigation pathways compatible with 1.5 C in the context of sustainable development, IPCC, pp. 93–174, 2018.

Rosa, L., Chiarelli, D. D., Sangiorgio, M., Beltran-Peña, A. A., Rulli, M. C., D'Odorico, P., and Fung, I.: Potential for sustainable irrigation expansion in a 3 °c warmer climate, Proceedings of the National Academy of Sciences of the United States of America, 117, 29 526–29 534, https://doi.org/10.1073/pnas.2017796117, 2020.

Russo, S., Marchese, A. F., Sillmann, J., and Immé, G.: When will unusual heat waves become normal in a warming Africa?, Environmental Research Letters, 11, 054 016, 2016.

Sanderman, J., Hengl, T., and Fiske, G. J.: Soil carbon debt of 12,000 years of human land use, Proceedings of the National Academy of Sciences, 114, 9575–9580, 2017.

Santanello Jr, J. A., Dirmeyer, P. A., Ferguson, C. R., Findell, K. L., Tawfik, A. B., Berg, A., Ek, M., Gentine, P., Guillod, B. P., Van Heerwaarden, C., et al.: Land–atmosphere interactions: The LoCo perspective, Bulletin of the American Meteorological Society, 99, 1253–1272, 2018.

Schleussner, C. F., Levermann, A., and Meinshausen, M.: Probabilistic projections of the Atlantic overturning, Climatic Change, 127, 579–586, https://doi.org/10.1007/s10584-014-1265-2, 2014.

Séférian, R., Rocher, M., Guivarch, C., and Colin, J.: Constraints on biomass energy deployment in mitigation pathways: the case of water scarcity, Environmental Research Letters, 13, 054 011, 2018.

Seneviratne, S. I., Corti, T., Davin, E. L., Hirschi, M., Jaeger, E. B., Lehner, I., Orlowsky, B., and Teuling, A. J.: Investigating soil moisture–climate interactions in a changing climate: A review, Earth-Science Reviews, 99, 125–161, 2010.

Seneviratne, S. I., Wartenburger, R., Guillod, B. P., Hirsch, A. L., Vogel, M. M., Brovkin, V., van Vuuren, D. P., Schaller, N., Boysen, L., Calvin, K. V., et al.: Climate extremes, land–climate feedbacks and land-use forcing at 1.5 C, Philosophical Transactions of the Royal Society A: Mathematical, Physical and Engineering Sciences, 376, 20160 450, 2018.

Shukla, J. and Mintz, Y.: Influence of land-surface evapotranspiration on the Earth's climate, Science, 215, 1498–1501, 1982.

Smith, B., Wårlind, D., Arneth, A., Hickler, T., Leadley, P., Siltberg, J., and Zaehle, S.: Implications of incorporating N cycling and N limitations on primary production in an individual-based dynamic vegetation model, Biogeosciences, 11, 2027–2054, 2014.

Smith, C., Baker, J., and Spracklen, D.: Tropical deforestation causes large reductions in observed precipitation, Nature, 615, 270–275, 2023.

Smith, P., Davis, S. J., Creutzig, F., Fuss, S., Minx, J., Gabrielle, B., Kato, E., Jackson, R. B., Cowie, A., Kriegler, E., Vuuren, D. P. V., Rogelj, J., Ciais, P., Milne, J., Canadell, J. G., McCollum, D., Peters, G., Andrew, R., Krey, V., Shrestha, G., Friedlingstein, P., Gasser, T., Grübler, A., Heidug, W. K., Jonas, M., Jones, C. D., Kraxner, F., Littleton, E., Lowe, J., Moreira, J. R., Nakicenovic, N., Obersteiner, M., Patwardhan, A., Rogner, M., Rubin, E., Sharifi, A., Torvanger, A., Yamagata, Y., Edmonds, J., and Yongsung, C.: Biophysical and economic limits to negative CO2 emissions, Nature Climate Change, 6, https://doi.org/10.1038/nclimate2870, 2015.

Spracklen, D., Baker, J., Garcia-Carreras, L., and Marsham, J.: The effects of tropical vegetation on rainfall, Annual Review of Environment and Resources, 2018.

Spracklen, D. V., Arnold, S. R., and Taylor, C.: Observations of increased tropical rainfall preceded by air passage over forests, Nature, 489, 282–285, 2012.

Staal, A., Tuinenburg, O. A., Bosmans, J. H., Holmgren, M., van Nes, E. H., Scheffer, M., Zemp, D. C., and Dekker, S. C.: Forest-rainfall cascades buffer against drought across the Amazon, Nature Climate Change, 8, 539–543, 2018.

Stokstad, E.: Bioenergy not a climate cure-all, panel warns, 2019.

Teuling, A. J., Taylor, C. M., Meirink, J. F., Melsen, L. A., Miralles, D. G., Van Heerwaarden, C. C., Vautard, R., Stegehuis, A. I., Nabuurs, G.-J., and de Arellano, J. V.-G.: Observational evidence for cloud cover enhancement over western European forests, Nature communications, 8, 1–7, 2017.

Thiery, W., Davin, E. L., Seneviratne, S. I., Bedka, K., Lhermitte, S., and van Lipzig, N. P.: Hazardous thunderstorm intensification over Lake Victoria, Nature communications, 7, 1–7, 2016.

Thiery, W., Davin, E. L., Lawrence, D. M., Hirsch, A. L., Hauser, M., and Seneviratne, S. I.: Present-day irrigation mitigates heat extremes, Journal of Geophysical Research, 122, 1403–1422, https://doi.org/10.1002/2016JD025740, 2017.

Thiery, W., Visser, A. J., Fischer, E. M., Hauser, M., Hirsch, A. L., Lawrence, D. M., Lejeune, Q., Davin, E. L., and Seneviratne, S. I.: Warming of hot extremes alleviated by expanding irrigation, Nature Communications, 11, 1–7, https://doi.org/10.1038/s41467-019-14075-4, 2020.

Tuinenburg, O., Hutjes, R., Stacke, T., Wiltshire, A., and Lucas-Picher, P.: Effects of irrigation in India on the atmospheric water budget, Journal of Hydrometeorology, 15, 1028–1050, 2014.

Tuinenburg, O. A., Theeuwen, J. J., and Staal, A.: High-resolution global atmospheric moisture connections from evaporation to precipitation, Earth System Science Data, 12, 3177–3188, 2020.

UNFCCC: Adoption of the Paris Agreement [Report No. FCCC/CP/2015/L.9/Rev.1], United Nations Framework Convention on Climate Change (UNFCCC), URL `http://unfccc.int/resource/docs/2015/cop21/eng/l09r01.pdf`, 2015.

Van de Walle, J., Thiery, W., Brousse, O., Souverijns, N., Demuzere, M., and Lipzig, N.: A convection-permitting model for the Lake Victoria Basin: evaluation and insight into the mesoscale versus synoptic atmospheric dynamics, Climate Dynamics, 54, 1779–1799, https://doi.org/10.1007/s00382-019-05088-2, 2020.

van der Ent, R. and Savenije, H.: Length and time scales of atmospheric moisture recycling, Atmospheric Chemistry and Physics, 11, 1853–1863, 2011.

Van der Ent, R., Tuinenburg, O., Knoche, H.-R., Kunstmann, H., and Savenije, H.: Should we use a simple or complex model for moisture recycling and atmospheric moisture tracking?, Hydrology and Earth System Sciences, 17, 4869–4884, 2013.

van der Ent, R., Wang-Erlandsson, L., Keys, P. W., and Savenije, H.: Contrasting roles of interception and transpiration in the hydrological cycle–Part 2: Moisture recycling, Earth System Dynamics, 5, 471–489, 2014.

van der Ent, R. J., Savenije, H. H., Schaefli, B., and Steele-Dunne, S. C.: Origin and fate of atmospheric moisture over continents, Water Resources Research, 46, 1–12, https://doi.org/10.1029/2010WR009127, 2010.

van Maanen, N., Andrijevic, M., Rosa, L., and Lejeune, Q.: Scenarios of sustainable irrigation expansion in the 21st century, Environmental Research Letters, pp. 1–17, URL `https://www.researchsquare.com/article/rs-296540/latest.pdf`, 2022.

Vanderkelen, I., Lipzig, N. P. M., Sacks, W. J., Lawrence, D. M., Clark, M. P., Mizukami, N., Pokhrel, Y., and Thiery, W.: Simulating the Impact of Global Reservoir Expansion on the Present-Day Climate, Journal of Geophysical Research: Atmospheres, 126, https://doi.org/10.1029/2020jd034485, 2021.

Vicedo-Cabrera, A. M., Guo, Y., Sera, F., Huber, V., Schleussner, C.-F., Mitchell, D., Tong, S., Coelho, M. d. S. Z. S., Saldiva, P. H. N., Lavigne, E., et al.: Temperature-related mortality impacts under and beyond Paris Agreement climate change scenarios, Climatic change, 150, 391–402, 2018.

Vicedo-Cabrera, A. M., Sera, F., and Gasparrini, A.: Hands-on tutorial on a modeling framework for projections of climate change impacts on health, Epidemiology (Cambridge, Mass.), 30, 321, 2019.

Vicedo-Cabrera, A. M., Scovronick, N., Sera, F., Royé, D., Schneider, R., Tobias, A., Astrom, C., Guo, Y., Honda, Y., Hondula, D., et al.: The burden of heat-related mortality attributable to recent human-induced climate change, Nature climate change, 11, 492–500, 2021.

Wang, J., Chagnon, F., Williams, E., Betts, A., Rennó, N., Machado, L., Bisht, G., Knox, R., and Bras, R.: Impact of deforestation in the Amazon Basin on cloud climatology, Proceedings of the National Academy of Sciences of the United States of America, 106, 3670–4, https://doi.org/10.1073/pnas.0810156106, 2009.

Wang-Erlandsson, L., Fetzer, I., Keys, P., Ent, R., Savenije, H., and Gordon, L.: Remote land use impacts on river flows through atmospheric teleconnections, Hydrology and Earth System Sciences, 22, 4311–4328, https://doi.org/10.5194/hess-22-4311-2018, 2018.

Wilks, D.: On "field significance" and the false discovery rate, Journal of applied meteorology and climatology, 45, 1181–1189, 2006.

Winckler, J., Reick, C. H., and Pongratz, J.: Robust identification of local biogeophysical effects of land-cover change in a global climate model, Journal of Climate, 30, 1159–1176, 2017a.

Winckler, J., Reick, C. H., and Pongratz, J.: Why does the locally induced temperature response to land cover change differ across scenarios?, Geophysical Research Letters, 44, 3833–3840, 2017b.

Winckler, J., Lejeune, Q., Reick, C. H., and Pongratz, J.: Nonlocal effects dominate the global mean surface temperature response to the biogeophysical effects of deforestation, Geophysical Research Letters, 46, 745–755, 2019a.

Winckler, J., Lejeune, Q., Reick, C. H., and Pongratz, J.: Nonlocal Effects Dominate the Global Mean Surface Temperature Response to the Biogeophysical Effects of Deforestation, Geophysical Research Letters, 46, 745–755, https://doi.org/10.1029/2018GL080211, 2019b.

Winckler, J., Reick, C. H., Luyssaert, S., Cescatti, A., Stoy, P. C., Lejeune, Q., Raddatz, T., Chlond, A., Heidkamp, M., and Pongratz, J.: Different response of surface temperature and air temperature to deforestation in climate models, Earth System Dynamics, 10, 473–484, https://doi.org/10.5194/esd-10-473-2019, 2019c.

Windisch, M. G., Davin, E. L., and Seneviratne, S. I.: Prioritizing forestation based on biogeochemical and local biogeophysical impacts, Nature Climate Change, 11, 867–871, https://doi.org/10.1038/s41558-021-01161-z, 2021.

Wunderling, N., Staal, A., Sakschewski, B., Hirota, M., Tuinenburg, O. A., Donges, J. F., Barbosa, H. M., and Winkelmann, R.: Recurrent droughts increase risk of cascading tipping events by outpacing adaptive capacities in the Amazon rainforest, Proceedings of the National Academy of Sciences, 119, e2120777 119, 2022.

Yao, Y., Vanderkelen, I., Lombardozzi, D., Swenson, S., Lawrence, D., Jägermeyr, J., Grant, L., and Thiery, W.: Implementation and evaluation of irrigation techniques in the Community Land Model, Journal of Advances in Modeling Earth Systems, 14, 2022.

Zemp, D., Schleussner, C.-F., Barbosa, H., Van der Ent, R., Donges, J. F., Heinke, J., Sampaio, G., and Rammig, A.: On the importance of cascading moisture recycling in South America, Atmospheric Chemistry and Physics, 14, 13 337–13 359, 2014.

List of Outputs

Peer reviewed articles in scientific journals - as first author

Publications in preparation and submitted for review are listed in grey.

1. **De Hertog S. J.**, Havermann F., Vanderkelen I., Guo S., Luo F., Manola I., Coumou D., Davin E.L., Duveiller G., Lejeune Q., Pongratz J., Schleussner C.-F., Seneviratne S.I., Thiery, W. (2023) The biogeophysical effects of idealised land cover and land management changes in Earth System Models. Earth System Dynamics. in press.

2. **De Hertog S. J.**, Lopez Fabara C. E., van der Ent R., Keune J., Miralles D.G., Portmann R., Schemm S., Havermann F., Guo S., Luo F., Manola I., Lejeune Q., Pongratz J., Schleussner C.-F., Seneviratne S.I., Thiery W. (2023) Effects of idealised land cover and land management changes on the atmospheric water cycle. Earth System Dynamics. in review.

3. **De Hertog S. J., Orlov A.**, Mistry M., Havermann F., Guo S., Manola I., Coumou D., Lejeune Q., Pongratz J., Schleussner C.-F., Menke I., Humpenöder F., Popp A., Lawrence P., Chini L., Hurtt G.C., Seneviratne S.I., Thiery W. (2023) The importance of future land cover scenarios for human health. in preparation for submission.

Peer reviewed articles in scientific journals - as contributing author

1. Portmann R.,Beyerle U., Davin E.L., Fischer E.M., **De Hertog S.J.**, Schemm S. (2022). Global forestation and deforestation affect remote climate via adjusted atmosphere and ocean circulation. Nature Communications, 13, 5569.

2. Orlov A.,**De Hertog S.J.**, Havermann F., Guo S., Luo F., Manola I., Thiery W., Lejeune Q., Pongratz J., Humpenöder F., Windisch M., Nath S., Popp A., Schleussner C.-F. (2023). Changes in Land Cover and Management Affect Heat Stress and Labour Capacity. Earth's Future, 11, 2909.

3. Nath S.,Gudmundsson L., Schwaab, J., Duveiller G., **De Hertog S.J.**, Guo S., Havermann F., Luo F., Manola I., Pongratz J., Seneviratne S. I., Scleussner C.-F., Thiery W., Lejeune Q. (2023). TIMBER v0.1: a conceptual framework for emulating temperature responses to tree cover change. Geoscientific Model Development, in press.

Presentations at conferences and workshops

1. European Geo-sciences Union Meeting, April 2023. The importance of land cover scenarios for human health.

2. European Geo-sciences Union Meeting, May 2022. The effects of land cover and land management changes on the atmospheric water cycle.

3. Study day on 'Belgian contributions to Earth Sciences in a Changing World', May 2022. The effects of land cover and land management changes on the atmospheric water cycle.(poster presentation)

4. Land Model & Biogeochemistry Working Group Winter Meeting, February 2022. The biogeophysical effects of idealised land cover and land management changes in Earth System Models. (online presentation)

5. American Geo-sciences Union Meeting, December 2021. The biogeophysical effects of idealised land cover and land management changes in Earth System Models.(online presentation)

6. Aspen Global Change Institute Workshop on Linking Human and Earth System Models, July 2021, The biogeophysical effects of idealised land cover and land management changes in Earth System Models.(poster presentation)

7. European Geo-sciences Union Meeting, April 2021. The biogeophysical effects of idealised land cover and land management changes in Earth System Models.(online presentation)

8. International Environmental Modelling and Software Society, September 2020. Idealised land cover and land management simulations in Earth System Models.(online presentation)

9. European Geo-sciences Union Meeting, May 2020. Idealised land cover and land management simulations in Earth System Models.(online presentation)